July 2016

Bioengineered Platforms to Study Carcinoma Cell Response to Drug Treatment

Thuy V. Nguyen

BIOENGINEERED PLATFORMS TO STUDY CARCINOMA CELL RESPONSE TO DRUG TREATMENT

A Dissertation Presented

by

THUY VINH LUONG NGUYEN

Submitted to the Graduate School of the
University of Massachusetts Amherst in partial fulfillment
of the requirements for the degree of

DOCTOR OF PHILOSOPHY

May 2016

Department of Chemical Engineering

BIOENGINEERED PLATFORMS TO STUDY CARCINOMA CELL RESPONSE TO DRUG TREATMENT

A Dissertation Presented

by

THUY VINH LUONG NGUYEN

Approved as to style and content by:

_____

Shelly R. Peyton, Chair

_____

Neil Forbes, Member

_____

Ryan Hayward, Outside Member

_____

John Klier, Department Head
Department of Chemical Engineering

DEDICATION

To my Father, my Mother, and my Sister,

Your love and support made this possible

ACKNOWLEDGEMENTS

First, I am very grateful to my graduate advisor, Dr. Shelly Peyton, for taking me in as her first graduate student even though I did not have any previous biology knowledge. Dr. Peyton has been a great advisor and mentor, and I would like to thank her for her tremendous support throughout my time in graduate school. She has always been willing to help me when I need her, such as reviewing my abstracts for conferences, giving me feedback on my presentations, reviewing my manuscripts, etc. Her passion for science was very inspiring to me and the other students in lab. Being the first graduate student in her lab is a challenging and fantastic experience, and I have gained great experience through the journey. The training in her lab has changed me in many ways, and I have been excited to see myself improving over the years in many areas, including technical skills, presenting and public speaking skills, organizational skills, most importantly, being a better research scientist. She has been very reliable and always giving me honest and constructive advice to improve my weaknesses and my research. For all of this, I am extremely grateful to have a mentor and advisor like Dr. Peyton.

I am very grateful to my colleagues in Dr. Peyton's lab, especially past members: Dr. William Herrick, Dannielle Ryman, and current members: Dr. Samuel Polio, Dr. Maria Gencoglu, Dr. Katie Bittner, Lauren Barney, Lauren Jansen, Alyssa Schwartz, Elizabeth Brooks, and Sualyneth Galarza, as well as the great undergraduates whom I had the opportunity to mentor (Marianne Sleiman, Timothy Moriarty, and Danielle LaValley). I thank each of them for their tremendous support such as technical suggestions, writing and presenting critiques, technical assistance and collaborations. I have enjoyed our conversations regarding research and life and our sharing of fun

moments in the lab and at conferences. Besides, Dannielle, Lauren B., Lauren J., Alyssa, and Elizabeth have always kept me in check with everything in lab. Will, Lauren B., Alyssa, and Elizabeth have helped me place orders or allowed me to use their procards to order materials for my research. I also thank many other undergraduates that I have interacted with (Tyler Vlass, Erinn Dandley, Prateek Katti, Maxsimillyan Nowak, Aidan Gilchrist, Michael Grunwald, Shayna Nolan, Thomas McCarthy, and John MacMunn); my interactions with them have made my experience in the Peyton lab memorable. I hope to stay in touch with everyone for many years to come.

I would like to thank the members of my thesis committee, Dr. Neil Forbes and Dr. Ryan Hayward for their support. They spent time to discuss with me about my research progress and challenged me to think outside the box. My meetings with them were very informative and enlightening.

I am grateful to the University of Massachusetts Amherst, especially the department of Chemical Engineering, for the financial support. I would like to thank Dr. Barry Siadat and Mrs. Afsaneh Siadat for their generous donation, which has funded my stipend and fees for the last couple years of my graduate study. I also would like to acknowledge other funding sources such as the National Institute of Health and the Materials Research Science and Engineering Center.

I also would like to thank the Chemical Engineering departmental staff members: Marie Wallace, Amity Lee-Bradley, Anshalee Guarnieri and Lauren O'Brien. I appreciate their hard work to ensure my on-time payment, supply ordering, travel reimbursement, and other related paperwork.

Finally, I would like to thank my family for their continuing support, love, and encouragement. Specifically, I am very grateful to my parents and sister for their financial and emotional support. My parents have given me a great financial support from buying me a brand new car to paying for my meal plans and airline tickets to visit home. They have always tried to make sure that I have a comfortable life and everything that I need to pursue my passions. My sister has always been a huge part of my life. Whether it was her phone calls or fun text messages showing her cat and dogs, little things like those have kept me sane when my work life got crazy.

ABSTRACT

BIOENGINEERED PLATFORMS TO STUDY CARCINOMA CELL RESPONSE TO DRUG TREATMENT

MAY 2016

THUY VINH LUONG NGUYEN

B.S., GEORGIA INSTITUTE OF TECHNOLOGY

M.S., GEORGIA INSTITUTE OF TECHNOLOGY

PH.D., UNIVERSITY OF MASSACHUSETTS AMHERST

Directed by: Professor Shelly R. Peyton

The tumor extracellular matrix (ECM) plays an important role in facilitating tumor growth and mediating tumor cells' resistance to drugs. However, during drug development, potential chemotherapeutics are screened in plastic plates, which lack relevant ECM physicochemical cues. In order to improve drug development process, this dissertation includes the development of relevant 2D and 3D biomaterial systems that can be used to study carcinoma cell response to drug treatment.

A novel poly(ethylene glycol)-phosphorylcholine (PEG-PC) high-throughput biomaterial platform was developed to study how the ECM mechanochemical properties affect cancer cells' response to drug. The PEG-PC biomaterial is optically transparent, has a mechanical range from 1 to 10,000 kPa in Young's modulus, and allows easy coupling of cell adhesive proteins. When testing several breast and liver cancer cell lines

on PEG-PC gels that had different stiffnesses and integrin-binding sites, there was a significant increase in drug resistance with increasing substrate stiffness. It was found that this stiffness-induced drug resistance was independent of Rho-ROCK and EGFR signaling, but co-administration of a β_1 integrin antibody, or an inhibitor to JNK, with sorafenib effectively eliminated the stiffness-mediated sorafenib resistance. Finally, 3D hydrogel systems, poly(N-isopropylacrylamide)-PEG (PNIPAAm-PEG) and PEG-Maleimide, were utilized to create multi-cellular spheroids to study drug resistance in 3D. Both SkBr3s and MDA-MB-231s were tested with sorafenib, lapatinib, temsirolimus, and doxorubicin across varying moduli and geometry (plastic, 2D and 3D hydrogels, spheroid) in different medium conditions. For some drugs, the change in platform or medium was found to have the largest effect on the variation of the IC-50 than the change in modulus. Specifically, the IC-50s varied the most when SkBr3s were treated with sorafenib and temsirolimus and when MDA-MB-231s were treated with sorafenib and lapatinib. However, when treated with doxrorubicin, the IC-50s of both cell types were similar across all platforms. These results demonstrate the utility of tailored biomaterial systems to address basic questions related to tumor microenvironment and drug resistance in cancer, and highlight the importance of incorporating relevant ECM factors into drug testing.

TABLE OF CONTENTS

Page

LIST OF TABLES

Table Page

LIST OF FIGURES

CHAPTER 1

INTRODUCTION

1.1 The Impact Of Cancer On Human Health

In the U.S., the Centers for Disease Control (CDC) and the National Cancer Institute (NCI) reported more than 1 million cases of invasive cancers and more than 574,000 cancer-related deaths for each of the year between 1999 and 2011 [1]. In 2015, the number of new cancer cases are projected to be 1.7 million with breast and prostate cancer as the most dominant types of cancer for women and men, respectively [2]. These two types of cancer have been the top two of cancer incidence (Figure 1.1) and are projected to remain at the same place in 2030 [3]. Currently, the overall cost of cancer care is projected to be $173 billion in 2020, an increase of 39% from 2010 [4]. In addition to the high cost of cancer treatment, cancer patients usually suffer devastating side effects from chemotherapy and radiation. Those side effects include: reduction in bone density, cardiotoxicity, cognitive deficits, distress, fatigue, infertility, pain, and pulmonary dysfunction [5]. Furthermore, cancer survivors usually suffer the fear of cancer recurrence (FCR), which is a major psychological problem that results in anxiety and depression; these psychological issues can deeply affect their quality of life and relationships [6,7].

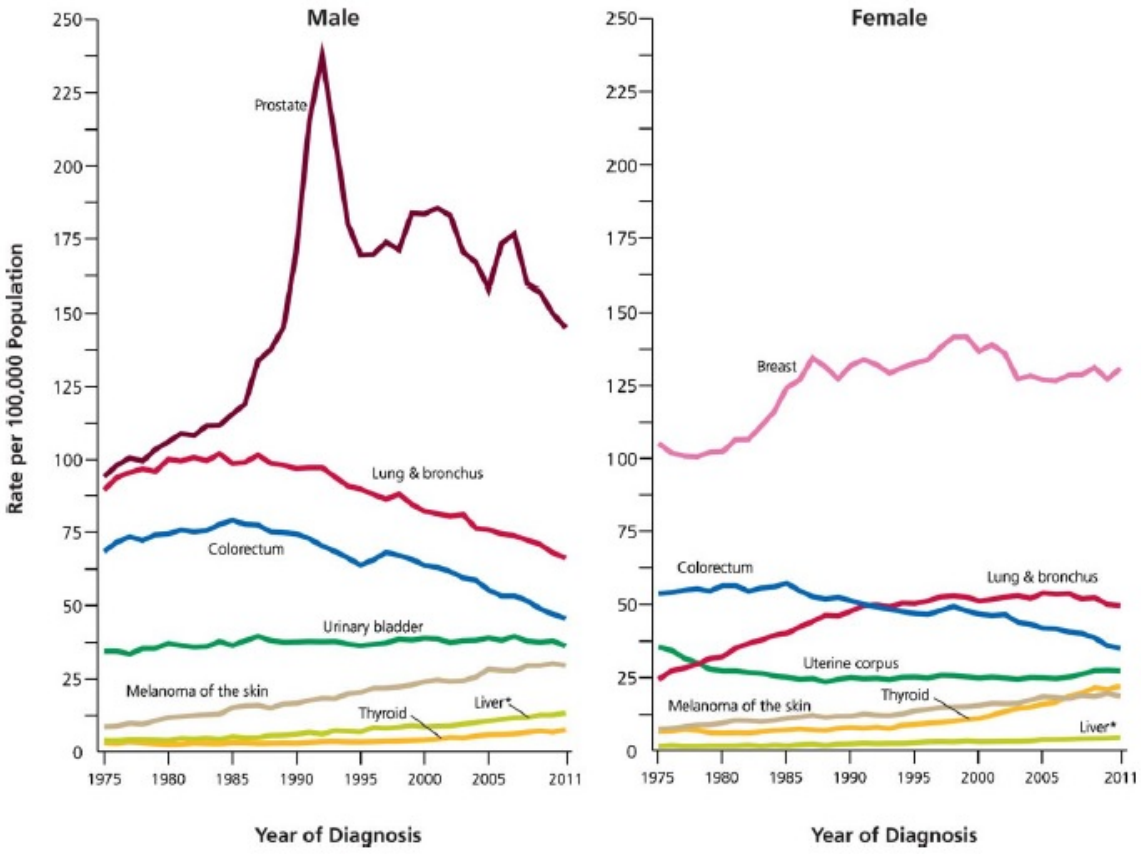

Figure 1.1 Trends in incidence rates for selected cancer by sex (U.S. 1975 - 2011). Prostate cancer has the highest incidence rate for male whereas breast cancer incidence rate is the highest for female. Figure adapted with permission from [2]. © 2012American cancer society, Inc.

1.2 The Biology Of Cancer

A tumor develops as a result of unregulated cell growth. Cancerous tumors are those that are capable of metastasizing to distal tissues to form secondary tumors. A healthy cell has to go through many stages to acquire progressive transformation to a highly malignant cell [8,9]. This multiple step process includes the capability of sustaining growth factor supply through autocrine or paracrine signaling, continuing to divide indefinitely, reprogramming of cellular metabolism to sustain unlimited growth,

being insensitive to anti-growth signals, evading apoptosis and immune destruction, maintaining angiogenesis, invading local tissue and metastasizing to distal tissues. Two characteristics that allow normal cells to develop these hallmark capabilities are genetic mutations that alter many intracellular regulatory pathways and inflammation of the tissue microenvironment that promotes tumor growth [9].

Although genetic mutation is one of the key factors for tumor development, a single mutated gene is not enough to drive cancer cell growth. However, certain inherited mutated genes can put a person at higher risk to develop cancers. Women who carry BRCA1 and BRCA2 mutations have higher risks of having breast and ovarian cancers [10]. For example, by the age of 70, the risks of having breast cancer are 71% and 84% for BRCA1 and BRCA2 carriers, respectively [10]. However, inherited mutations in APC and DNA mismatch repair (MMR) genes only account for 4 - 6% of colorectal cancer (CRC) incidence in patients with family history of CRC [11]. In many cancers, multiple mutations are required for tumor cells to acquire growth advantage, and the majority of those are somatic mutations, which develop during a person's lifetime. For instance, the development of CRC starts with mutations in the APC gene, which results in early adenoma; then subsequent mutations in K-RAS, p53, SMAD4 lead to cancer [12,13]. Thousands of somatic mutations in protein kinases, which are molecular targets of many current therapies, have been identified in many human cancers [14,15]. However, only a portion of these mutations are considered to be 'driver' mutations, which confer growth advantage, whereas the others are considered to be 'passenger' mutations, which do not confer growth advantage [15].

Besides genetic mutations, inflammation in the tissue microenvironment can give rise to cancer development. Infection and chronic inflammation can create a microenvironment that fosters cancer cell proliferation, survival and invasion [16]. For instance, human papillomavirus (HPV) infection can result in oropharyngeal squamous cell carcinomas [17], head and neck squamous cell carcinomas [18], and cervical cancer [19]. Chronic hepatitis B or C virus (HBV or HCV) infection often leads to long-term inflammation and development of liver fibrosis and cirrhosis [20–22] followed by hepatocellular carcinoma [23]. Chronic infection can trigger the release of many pro-inflammatory cytokines/chemokines (TNF-α, TGF-β1, etc) that can recruit many immune cells (neutrophils, monocytes, macrophages, mast cells, etc) that infiltrate the tissue in order to fight against the infection [16]. If the infection is chronic, the long-term presence of these cells can trigger a continuous production of cytokines, cytotoxic mediators (reactive oxygen species or ROS), and soluble mediators of cell killing (TNF-α, interleukins, and interferons) [16]. ROS can cause DNA damage and mutations, and many of these chemokines can cause epigenetic alterations and promote tumor cell growth, angiogenesis, and metastasis [16,24,25]. The presence of ROS and inflammatory cytokines can activate local cells to modify the extracellular matrix and release many factors that are in favor of tumor development and exacerbate the tissue inflammation [26,27].

1.3 Drug Resistance In Cancer

1.3.1 Adaptive drug resistance

Adaptive drug resistance is the ability of a cell to adapt to treatment after initial exposure. Tumor cells can become resistant to drugs by increasing efflux, increasing mutations, activating cell survival pathways, inactivating death signaling pathways, enabling DNA-damage repair, and triggering autophagy (Figure 1.2) [28].

In order to change the rate of drug efflux, cancer cells upregulate expression of P-glycoproteins transporters that can detect and pump out cytotoxic molecules such as doxorubicin or taxol as they cross the plasma membrane [29]. For drugs that require receptors or transporters to enter the cells, selective resistant cells harbor mutations that alter the function of these transporters, thus eliminating the intracellular drug uptake [29].

Kinase inhibitors have become more popular in cancer treatment due to their lower side-effects than conventional cytotoxic chemotherapy [30]. Cancer cells can acquire adaptive resistance to many kinase inhibitors by activating receptor tyrosine kinases (RTKs) and their downstream signaling pathways to enhance survival. For instance, activations of MET and AXL receptors were identified as mechanisms for resistance to trastuzumab and lapatinib in HER2-overexpressing breast cancer cells [31,32]. EGFR and PI3K/Akt activation promoted resistance of hepatocellular carcinoma cells to sorafenib [33,34]. Triple-negative breast cancer cells that were treated with a MEK inhibitor resulted in a rapid kinome reprogramming in which multiple RTKs and downstream signaling pathways were activated to induce drug resistance [35]. In melanoma, activation of the Akt pathway could mediate resistance to BRAF inhibitor [36]. Squamous cancer cells can resist gefitinib, an EGFR inhibitor, by increasing

phosphorylation of IGFR, thus activating PI3K/Akt to enhance cell growth [37]. Moreover, cancer cells can also develop adaptive resistance to kinase inhibitors through mutations that can change kinase binding domains, thus avoiding inhibitor binding [30]. Chronic myelogeneous leukaemia (CML) tumor cells can amplify BCR-ABL genes to compensate for the loss of Bcr-Abl, which is inhibited by imatinib [38].

Besides increasing survival pathways, cancer cells can also regulate apoptotic pathways through expression of anti-apoptotic molecules in Bcl-2 family such as Bcl-2 and Bcl-XL [39,40]. Loss of function of pro-apoptotic molecules such as Bax and Bak can lead to complete resistance to the powerful chemotherapeutic drug cisplatin [41]. Overexpression of Bcl-2 and downregulation of Bax/Bak is present in many types of cancers [42]. In addition, the epithelial-to-messenchymal (EMT) transition can trigger a cancer-stem-cell-like phenotype and mediate drug resistance [43].

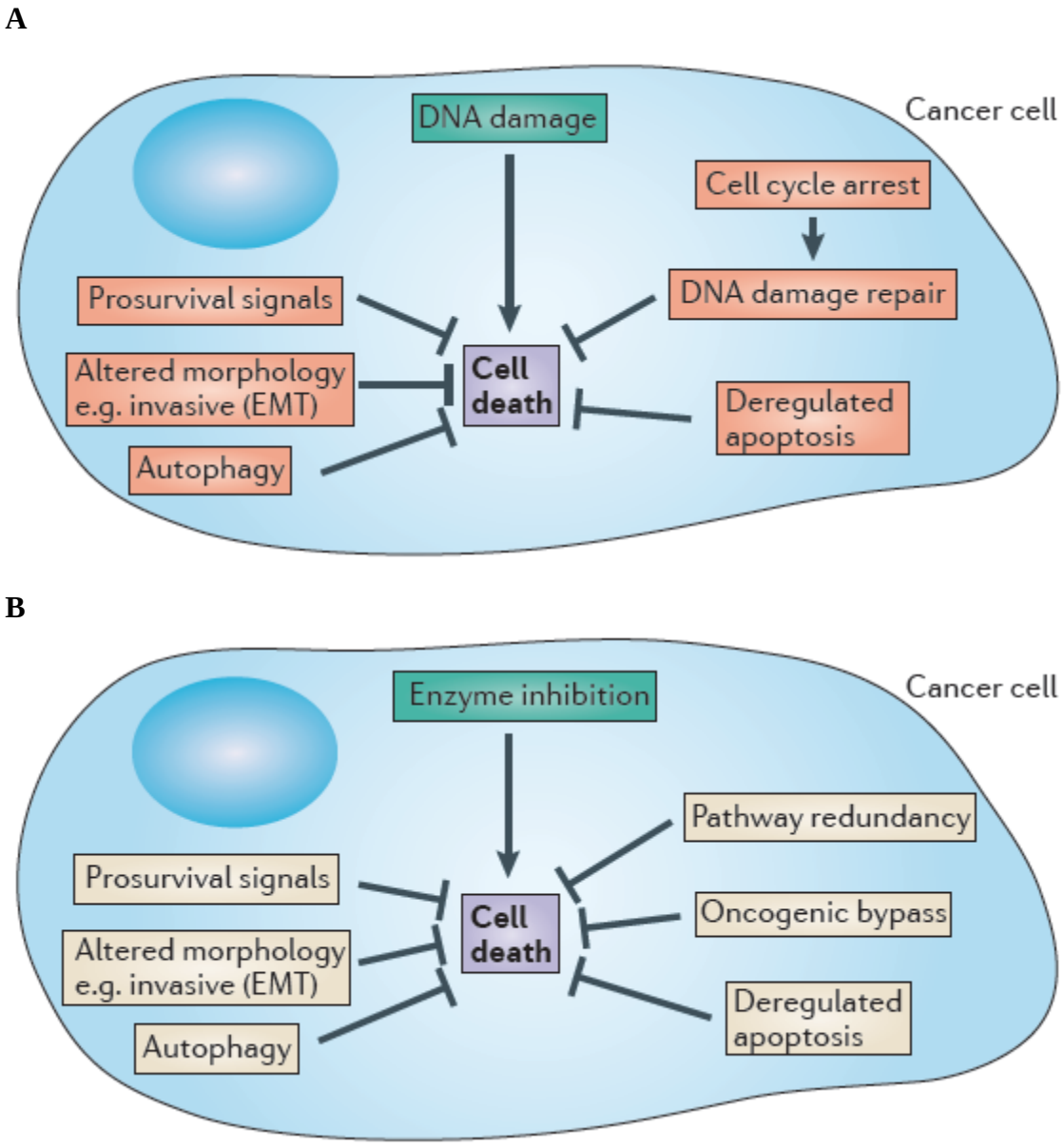

Figure 1.2 Schematic of different mechanisms of acquired drug resistance. Cancer cells can resist to **(A)** chemotherapeutic drugs that trigger DNA damages and **(B)** targeted drugs that inhibit kinase activities through multiple intracellular changes. Figure adapted with permission from [28]. © 2013 MacMillan Publishers Inc.

1.3.2 Microenvironment-induced resistance

The tumor microenvironment is known to play an important role in providing a niche to nurture the growth of cancer cells and mediate signals that allow them to survive chemotherapeutic treatment [44]. Cancer cells can receive signals from the tumor microenvironment through mechanical (ECM stiffening) and biochemical cues (Figure 1.3).

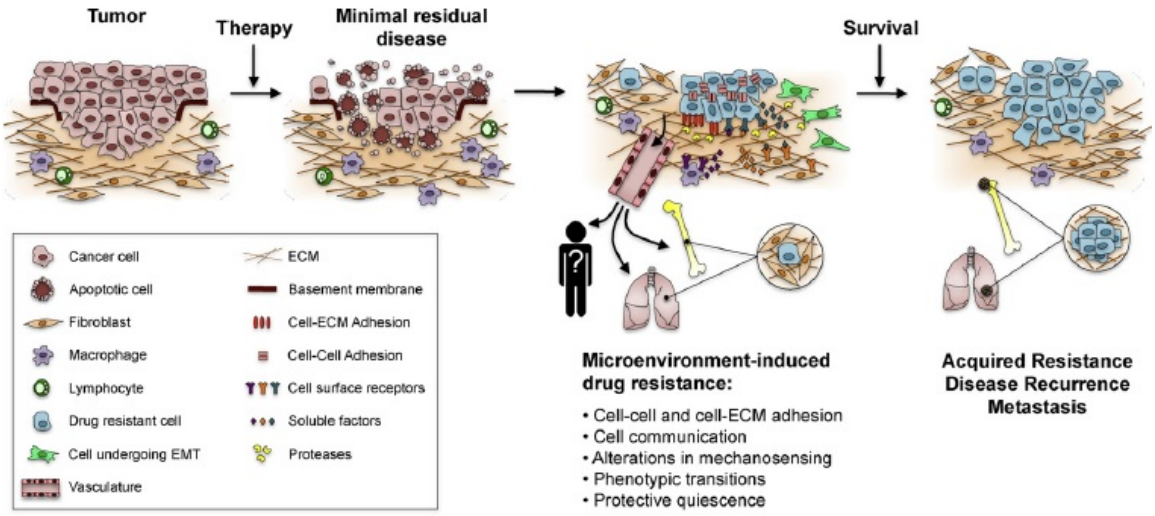

Figure 1.3 Tumor microenvironment and cancer development. The interaction between tumor cells and the microenvironment are important in regulating cancer cells' response to drugs. Figure adapted with permission from [45]. © 2012 Elsevier, Inc.

1.3.2.1 Extracellular matrix stiffening and cancer progression

During tumor progression, stromal fibroblasts, which differentiate into myofibroblasts [46], and cancer-associated fibroblasts (CAF) [47], remodel the ECM by breaking down the basement membrane and depositing fibril forming collagens [48–50]. The increase in crosslinked fibrous collagens results in tissue stiffening [50–52], which stimulates cancer cell proliferation [52,53], invasion and intravasation [54–56], disrupts

cell-cell adhesion [57], and alters sensitivity to growth factors [58], while simultaneously limiting the diffusion of therapeutic agents into the tumor [59].

Mechanotransduction is the process through which cells convert mechanical stimuli to biochemical signals that can subsequently regulate cellular function. Mechanotransduction is mediated through integrin binding of cells to ECM proteins. Integrins are heterodimers composed of α- and β-subunits. Different heterodimerizations of α- and β-subunits are required when the cells bind to different ECM proteins [60]. Binding of integrins to ECM proteins can mediate many different downstream signaling pathways such as PI3K/Akt and Ras/Raf/ERK to promote cell survival and proliferation or Rho/ROCK to alter cell motility (Figure 1.4) [61], and integrin binding can also induce the drug resistance of cancer cells to other chemotherapeutic drugs [62]. Expression of α_6 [63], β_1 [64–68], and β_6 [69] are known to induced chemoresistance in breast and colon cancers. Hence, a change in adhesive ECM proteins in the tissue microenvironment can confer resistance to chemotherapeutics via integrin-mediated signaling. ECM stiffening due to matrix crosslinking can induce integrin clustering, which leads to the formation of focal adhesions [70]. There are 180 proteins associated with focal adhesions; many of these are cytoskeletal proteins and signaling proteins such as kinases, phosphatases, and regulators of GTPases [71]. Therefore, focal adhesions play a role as cellular mechanosensors that transduce signals from the ECM to regulate cell behavior. The Rho GTPase family contains many key regulators of the actin cytoskeleton. The most well-studied members of the family are Rho, Rac1, and cdc42, which control the formation of stress fibers, lamellipodia, and filopodia, respectively [72]. Both Rho and Rac1 are required for the formation of focal adhesions [73]. The formation of focal adhesions can

also activate focal adhesion kinase (FAK), which intensifies both the oncogene HER2-mediated PI3K and ERK signaling pathways, to promote malignant transformation [52,53,70]. Activated FAK also promotes 3D invasiveness and facilitates cytoskeletal remodeling dynamics and contractile force generation [74].

Furthermore, stiffening of tumor tissue leads to the compression of blood vessels, which limits the delivery chemotherapeutic agents and the access of immune cells to kill tumor cells [75]. Hypoxic environments can also select for a subpopulation of cells that can survive harsh environments, thus they tend to be resistant to chemotherapeutics and radiation [75–77].

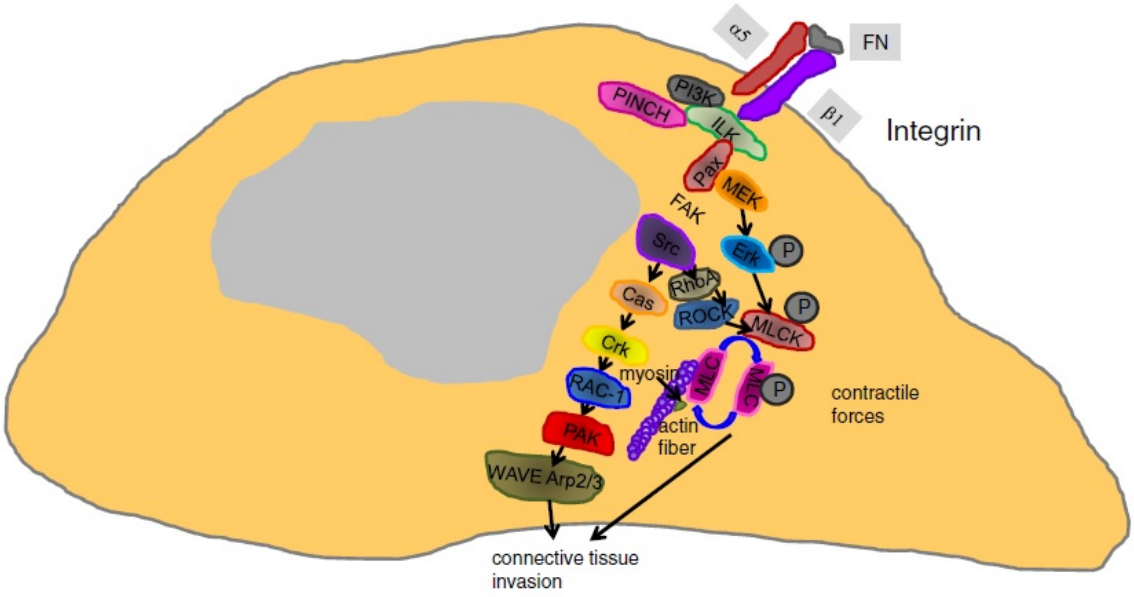

Figure 1.4 Representative downstream signaling pathways that can be mediated through integrin binding. FN: Fibronectin, PI3K: Phosphoinositide 3-kinase, ILK: Integrin-linked kinase, Pax: paxillin, MEK: Mitogen-activated protein kinase kinase, ERK: Extracellular signal-regulated kinase, MLCK: Myosin light-chain kinase, MLC: Myosin light chain, Cas: Crk associated substrate, RAC-1: Ras-related C3 botolinum toxin substrate 1, PAK: p21 protein-activated kinase 1, WAVE: Wiskott-Aldrich syndrome family protein. Figure adapted with permission from [74]. © 2013 IOP publishing Ltd.

1.3.2.2 Biochemical factors and cancer progression

Within tumor tissue, multiple biochemical cues, which are pre-existing or made by tumor cells and other cell types, can mediate survival signals to tumor cells. These biochemical cues are growth factors, cytokines, and other factors that are released from different cell types in the tumor microenvironment. Interactions of tumor cells with these biochemical cues are known to enhance their proliferation, survival and invasion [78–80].

Certain stromal growth factors mediate cell proliferation in the presence of otherwise powerful chemotherapeutic drugs. For example, hepatocyte growth factor (HGF) can impart resistance to vemurafenib in melanoma [81,82], and TGF-β can induce the expansion of cancer stem-like cells, which are responsible for chemotherapy-resistance and relapse [83]. These growth factors are generally thought to be released by local stromal fibroblasts, which upon DNA-damage from treatments with a combination of mitoxantrone and docetaxel or radiation, stimulate prostate cancer cell proliferation and invasion through β-catenin signaling [84]. Cancer cells can also produce matrix metalloproteinases (MMP) to break down the ECM, which allows them to invade the local tissues for metastasis [85,86]. This ECM breakdown also allows cancer cells to access to matrix-bound growth factors such as EGF and TGF-β [78].

In addition to soluble growth factors, the presence of cytokines and other cellular secreted factors play a role in cancer cell drug resistance and invasion. The inflammatory tumor microenvironment recruits many immune cells such as macrophages, dendritic cells, T cells, and natural killer cells, and these infiltrated immune cells are the major source of cytokine production [87]. Some cytokines have an anti-tumor effect whereas some promote tumor development [24,88]. Interleukin 8 (IL-8) is known to mediate

breast cancer cell migration and invasion [89,90]. IL-8 and VEGF autocrine signaling can induce EMT, which results in drug resistance, and invasiveness [91]. IL-6, IL-17, and IL-23 are also known to enhance tumor progression [24]. IL-4 was also found to mediate drug resistance in colon cancer stem cells [92]. Tumors grown from drug resistant cells, which had characteristics of cancer stem cells, were found to have elevated levels of cytokines, angiogenic and growth factors such as VEGF, bFGF, IL-6, IL-8, HGF, PDGF-BB, G-CSF, and SCGF-β [93].

1.4 Biomaterial Platforms For Cancer Studies

1.4.1 The cost of drug development

Part of the incredible cost of cancer care is due to the high price tag of cancer drugs. It costs over $1 billion to bring a new drug to the market, and the success rate is approximately 10% [94]. The major reason for this low overall success rate and unimaginable cost is due to the limitation of preclinical cancer models, which are not predictive of human outcomes [94]. Typically, a drug development process will start with the identification of a biologically relevant target that drives the disease progression, then followed by a high-throughput screening of many small molecules or biologics. The molecules that emerge from the high-throughput screening are further optimized and tested on relevant animal models before entering clinical trials. However, many compounds that show efficacy during high-throughput screening do not show similar results when subsequently tested *in vivo* on animals or humans. This highly inefficient *in vitro* high-throughput screening increases not only the cost but also the drug development time, which is approximately 14 years on average (Figure 1.5) [95]. Currently, the high-

throughput screening is usually performed with cells on plastic plates. Given the important roles of the ECM's mechanochemical signals in regulating cancer cell growth and their drug response as discussed earlier, it is critical to have an *in vitro*, high-throughput biomaterial drug- testing platform that can capture these relevant mechanochemical cues.

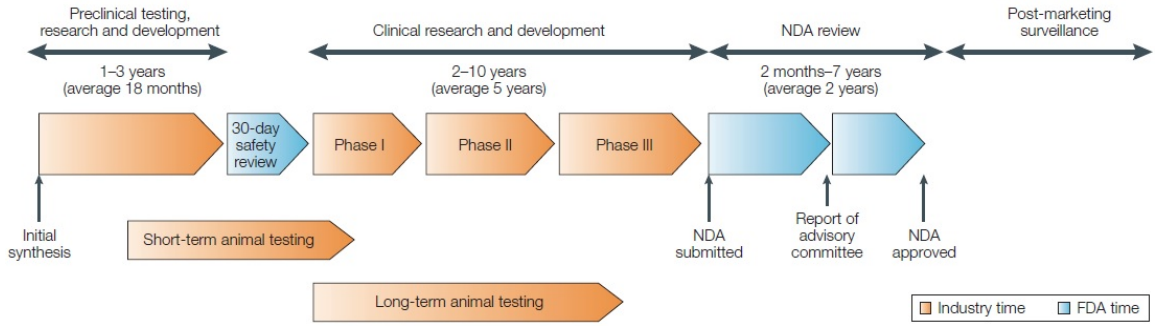

Figure 1.5 An outline of the standard drug development pipeline. Figure adapted with permission from [95]. © 2004 MacMillan Publishers Inc.

1.4.2 Hydrogels for mimicking tumor microenvironment

Hydrogels are porous hydrophilic materials. Due to their hydrophilicity and biocompatibility, hydrogels are widely used for many biomedical applications from drug delivery to tissue engineering [96], such as how cell and matrix interaction governs stem cell fate on 2D [97] and in 3D [98]. In addition, hydrogels have been used as platforms to study many biological phenomena in human diseases, such as cell migration [99] in 2D [100–102] and 3D [103–105], cellular response to drug treatment in ovarian cancer [106] and melanoma [107].

Hydrogels are typically derived from natural or synthetic polymers. Common natural polymers include hyaluronic acid, chitosan, collagen, fibrin, agarose, alginate [108]. Some of the natural polymers such as collagen, fibrin, and hyaluronic acid are

components of mammalian ECM, thus they also contain many integrin binding sites for cell adhesion. On the other hand, chitosan, alginate, and agarose are polysaccharides-derived from other natural sources (algae, chitin, etc), and they do not contain integrin binding sites. Natural polymers can be physically crosslinked to form hydrogels. Depending on the type of polymer, different methods can be utilized to induce physical crosslinking such as warming/cooling the polymer solution, mixing polyanion with polycation or with mutivalent ions of opposite charge, and changing pH [96]. However, hydrogels formed from these natural polymers are degradable over time through different mechanisms [108], and it is not possible to independently control the amount of binding sites and the material mechanical property. Increasing or decreasing the number of adhesive sites also increases or decreases the mechanical stiffness since the mechanical properties of these hydrogel are dependent on protein concentration. Therefore, some groups have spurred the development of natural- polymer hydrogels that allow independent control of binding sites and mechanical property. For example, hyaluronic acid can be modified with methacrylate and maleimide functional groups, and these functional groups can be chemically crosslinked by DL-dithiothreoitol (DTT) or Ultra Violet radiation [109,110].

In contrast, synthetic polymer hydrogels allow independent control over mechanical and adhesive properties. Synthetic hydrogels are derived from derivatives of synthetic polymers such as poly(hydroxyethyl methacrylate) (PHEMA), poly- (ethylene glycol) (PEG), poly(vinyl alcohol) (PVA), poly(ethylene oxide) (PEO), polyacrylamide (PAAm), etc [108]. Polymerization methods include chain-growth polymerization through free-radical polymerization and step-growth polymerization through Michael-

addition reactions [111]. Since synthetic polymers do not contain cell binding sites like natural polymers, peptides or full-length proteins that mediate cell adhesion need to be incorporated into the gels. Therefore, the mechanical properties can be modified through changing of polymer concentration or cross-link density without affecting the number of cell binding site. Hydrogel surfaces can be functionalized with cell binding peptides or full-length proteins following different bioconjugate methods such as azide-alkyne "click" chemistry [112]. In three dimensions, both cell binding peptides or degradable peptides can be incorporated into the hydrogel system [111,113,114]. Therefore, the ability to incorporate specific binding or degradable peptides in a controllable manner allows synthetic hydrogel to be tailored for a specific study. For example, both RGD cell binding peptide and MMP-degradable crosslinkers were incorporated into 3D hydrogel systems to study how matrix stiffness affects the progression of glioblastoma [115], and an in situ fluorogenic MMP sensor peptide was used to investigate how drug treatment influences MMP activity of metastatic melanoma cells in three dimensions [116]. RGD is the binding site of fibronectin, and many other cell binding peptides from other proteins are also identified [62].

In addition, composite hydrogels that are made from both natural and synthetic polymers have been used in many studies. For instance, composite hydrogels of PEG and collagen were used as scaffolds for immune cells [117] and pancreatic cancer cells [118]. Hybrid PEG-based hydrogels can also be created by combining PEG polymers with the recombinant proteins containing both fibrinogen and collagen binding sites [119].

1.5 Hypothesis

As depicted in Figure 1.3, the tumor microenvironment plays an important role in promoting the growth of cancer cells and mediating resistance to chemotherapeutics. The change in the ECM properties during disease progression results in mechanical and biochemical changes that profoundly affect cell behaviors via alterations in intracellular signaling (Figure 1.4). Since many novel targeted drugs have been designed to inhibit specific intracellular pathways as a mechanism to stop cancer cell growth, it is not well understood how both mechanical and biochemical changes can lead to alterations in downstream intracellular signaling pathways that ultimately hamper the effectiveness of targeted drugs. **I hypothesize that cancer cells become resistant to chemotherapeutics via interaction with the physicochemical cues from the tumor ECM (Figure 1.6).** The research presented in this dissertation aims to elucidate the mechanisms by which the tumor ECM contributes to drug resistance in both 2D and 3D. Testing this hypothesis requires the development of a high-throughput platform, which can capture the ECM mechanochemical properties, to facilitate the drug screening process. These 2D and 3D platforms were made with synthetic hydrogels that allow tunable mechanical properties and easy functionalization of full-length ECM proteins or short peptides that contain binding sites found in natural ECM proteins. Anti-cancer drugs were tested with cells seeded on the hydrogel surface or encapsulated within the hydrogels. Furthermore, the intracellular signaling that is mediated by the interactions with these 2D and 3D platforms were examined.

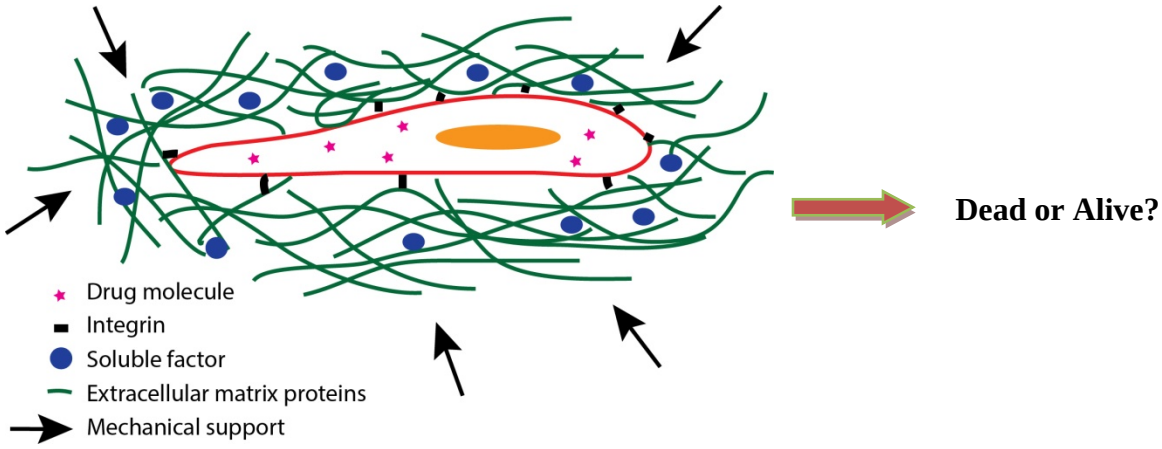

Figure 1.6 An outline of governing hypothesis.

1.6 Objectives For Dissertation

I hypothesize that the mechanical and biochemical properties of the ECM can influence cancer cell response to chemotherapeutics. The research presented in this dissertation were outlined as specific aims in Figure 1.7.

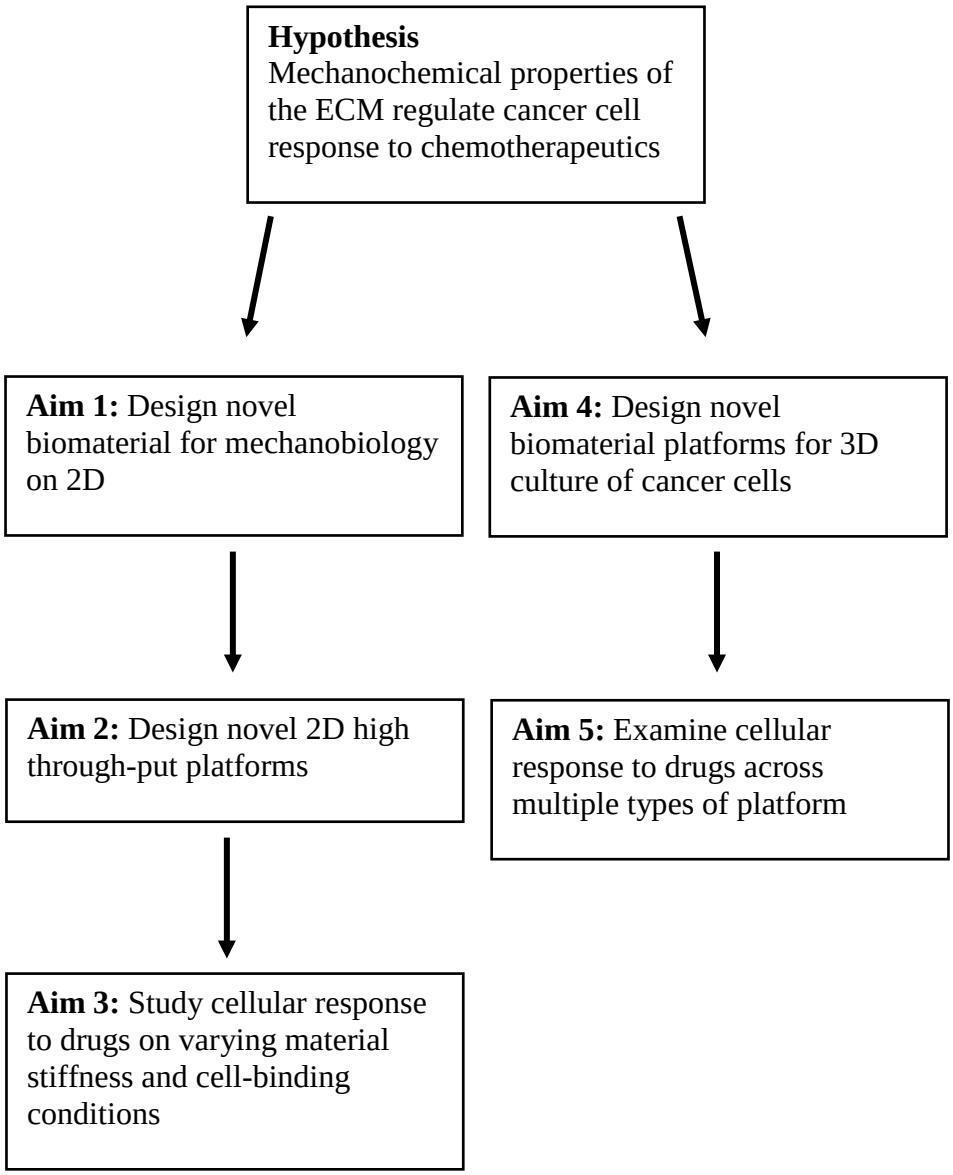

Figure 1.7 Objectives for Dissertation. Chapter 2 describes aim 1, where the novel PEG-PC biomaterial was created for mechanobiology. Chapter 3 describes aim 2, where high-throughput platforms were designed from PEG, PEG-PC, and PAA, and cell response to drug was examined as a function of integrin binding. Chapter 4 describes aim 3, where cancer cell response to sorafenib was studied across varying conditions. Finally, chapter 4 describes aims 4 and 5, where both PNIPAAm-PEG and PEG-MAL were used as platforms for 3D culture, and cell response to drug was studied with different platforms.

1.7 Significance

The mechanical and biochemical cues from the ECM regulate many cellular behaviors including proliferation, differentiation, and migration. However, how these physicochemical cues together affect cell response to chemotherapeutics is not well understood. The research presented in this dissertation addresses this question at the sub-cellular level across varying geometries, material properties, and cell-binding ligands. Insights gained from this research will not only provide better understanding of cell-matrix and drug interactions, but also aid in future design of biomaterials to study many other diseases. The novel PEG-PC gel developed from this research has a mechanical range that matches or exceeds any previously reported hydrogel system and can be served as an ideal platform for future studies in regenerative medicine and disease mechanisms. The high-throughput biomaterial platforms created from this research are promising predictive tools for future drug screening, and help to facilitate the process of drug development.

1.8 References

[1] U.S.C.S.W. Group. United States Cancer Statistics: 1999-2011 Incidence and Mortality Web-based Report. Atlanta U.S. Dep. Heal. Hum. Serv. Centers Dis. Control Prev. Natl. Cancer Inst. 2014.

[2] R.L. Siegel, K.D. Miller, A. Jemal. Cancer Statistics, 2015. CA Cancer J Clin. 2015. 65: 5–29.

[3] L. Rahib, B.D. Smith, R. Aizenberg, A.B. Rosenzweig, J.M. Fleshman, L.M. Matrisian. Projecting cancer incidence and deaths to 2030: The unexpected burden of thyroid, liver, and pancreas cancers in the united states. Cancer Res. 2014. 74: 2913–2921.

[4] A.B. Mariotto, K. Robin Yabroff, Y. Shao, E.J. Feuer, M.L. Brown. Projections of the cost of cancer care in the United States: 2010-2020. J. Natl. Cancer Inst. 2011. 103: 117–128.

[5] R. Siegel, C. Desantis, K. Virgo, K. Stein, A. Mariotto, T. Smith, et al. Cancer Treatment and Survivorship Statistics , 2012. CA. Cancer J. Clin. 2012. 62: 220–241.

[6] J. V. Crist, E. a. Grunfeld. Factors reported to influence fear of recurrence in cancer patients: A systematic review. Psychooncology. 2013. 22: 978–986.

[7] S. Simard, B. Thewes, G. Humphris, M. Dixon, C. Hayden, S. Mireskandari, et al. Fear of cancer recurrence in adult cancer survivors: A systematic review of quantitative studies. J. Cancer Surviv. 2013. 7: 300–322.

[8] D. Hanahan, R.A. Weinberg. The Hallmarks of Cancer. Cell. 2000. 100: 57–70.

[9] D. Hanahan, R. a Weinberg. Hallmarks of cancer: the next generation. Cell. 2011. 144: 646–74.

[10] E. Levy-Lahad, E. Friedman. Cancer risks among BRCA1 and BRCA2 mutation carriers. Br. J. Cancer. 2007. 96: 11–15.

[11] C.D. Heinen. Genotype to phenotype: Analyzing the effects of inherited mutations in colorectal cancer families. Mutat. Res. - Fundam. Mol. Mech. Mutagen. 2010. 693: 32–45.

[12] E.R. Fearon, B. Vogelstein. A genetic model for colorectal tumorigenesis. Cell. 1990. 61: 759–767.

[13] K. Kawada, S. Hasegawa, T. Murakami, Y. Itatani, H. Hosogi, M. Sonoshita, et al. Molecular mechanisms of liver metastasis. Int. J. Clin. Oncol. 2011. 16: 464–72.

[14] Z. Kan, B.S. Jaiswal, J. Stinson, V. Janakiraman, D. Bhatt, H.M. Stern, et al. Diverse somatic mutation patterns and pathway alterations in human cancers. Nature. 2010. 466: 869–873.

[15] C. Greenman, P. Stephens, R. Smith, G.L. Dalgliesh, C. Hunter, G. Bignell, et al. Patterns of somatic mutation in human cancer genomes. Nature. 2007. 446: 153–158.

[16] L.M. Coussens, Z. Werb. Inflammation and cancer. Nature. 2002. 420: 860–867.

[17] M.L. Gillison, T. Broutian, R.K.L. Pickard, Z. Tong, W. Xiao, L. Kahle, et al. Prevalence of Oral HPV Infection in the United States, 2009-2010. Yearb. Pediatr. 2013. 2013: 10–12.

[18] M.L. Gillison, X. Castellsagué, A. Chaturvedi, M.T. Goodman, P. Snijders, M. Tommasino, et al. Eurogin Roadmap: Comparative epidemiology of HPV infection and associated cancers of the head and neck and cervix. Int. J. Cancer. 2013. 134: 497–507.

[19] J.R. Carter, Z. Ding, B.R. Rose. HPV infection and cervical disease: A review. Aust. New Zeal. J. Obstet. Gynaecol. 2011. 51: 103–108.

[20] L. Castéra, J. Vergniol, J. Foucher, B. Le Bail, E. Chanteloup, M. Haaser, et al. Prospective comparison of transient elastography, Fibrotest, APRI, and liver biopsy for the assessment of fibrosis in chronic hepatitis C. Gastroenterology. 2005. 128: 343–350.

[21] F. Vizzutti, U. Arena, R.G. Romanelli, L. Rega, M. Foschi, S. Colagrande, et al. Liver stiffness measurement predicts severe portal hypertension in patients with HCV-related cirrhosis. Hepatology. 2007. 45: 1290–7.

[22] S. Lotersztajn, B. Julien, F. Teixeira-Clerc, P. Grenard, A. Mallat. Hepatic fibrosis: molecular mechanisms and drug targets. Annu. Rev. Pharmacol. Toxicol. 2005. 45: 605–28.

[23] C. Cha, R.P. Dematteo. Molecular mechanisms in hepatocellular carcinoma development. Best Pract. Res. Clin. Gastroenterol. 2005. 19: 25–37.

[24] S.I. Grivennikov, F.R. Greten, M. Karin. Immunity, Inflammation, and Cancer. Cell. 2010. 140: 883–899.

[25] F. Balkwill, A. Mantovani. Inflammation and cancer: Back to Virchow? Lancet. 2001. 357: 539–545.

[26] A.Y. Hui, S.L. Friedman. Molecular basis of hepatic fibrosis. Expert Rev. Mol. Med. 2004. 5: 1–23.

[27] J.D. Yang, I. Nakamura, L.R. Roberts. The tumor microenvironment in hepatocellular carcinoma: current status and therapeutic targets. Semin. Cancer Biol. 2011. 21: 35–43.

[28] C. Holohan, S. Van Schaeybroeck, D.B. Longley, P.G. Johnston. Cancer drug resistance: an evolving paradigm. Nat. Rev. Cancer. 2013. 13: 714–26.

[29] M.M. Gottesman. Mechanism of Cancer Drug Resistance. 2002.

[30] J. Zhang, P.L. Yang, N.S. Gray. Targeting cancer with small molecule kinase inhibitors. Nat. Rev. Cancer. 2009. 9: 28–39.

[31] D.L. Shattuck, J.K. Miller, K.L.C. Iii, C. Sweeney. Met Receptor Contributes to Trastuzumab Resistance of Her2-Overexpressing Breast Cancer Cells. 2008. 1471–1478.

[32] L. Liu, J. Greger, H. Shi, Y. Liu, J. Greshock, R. Annan, et al. Novel Mechanism of Lapatinib Resistance in HER2-Positive Breast Tumor Cells : Activation of AXL. 2009. 1363089: 6871–6879.

[33] Z. Ezzoukhry, C. Louandre, E. Trécherel, C. Godin, B. Chauffert, S. Dupont, et al. EGFR activation is a potential determinant of primary resistance of hepatocellular carcinoma cells to sorafenib. Int. J. Cancer. 2012. 131: 2961–9.

[34] K. Chen, H. Chen, W. Tai, W. Feng, C. Hsu, P. Chen, et al. Activation of Phosphatidylinositol 3-Kinase / Akt Signaling Pathway Mediates Acquired Resistance to Sorafenib in Hepatocellular Carcinoma Cells. 2011. 337: 155–161.

[35] J.S. Duncan, M.C. Whittle, K. Nakamura, A.N. Abell, A. a Midland, J.S. Zawistowski, et al. Dynamic reprogramming of the kinome in response to targeted MEK inhibition in triple-negative breast cancer. Cell. 2012. 149: 307–21.

[36] D. Perna, F.A. Karreth, A.G. Rust, P.A. Perez-mancera, M. Rashid. BRAF inhibitor resistance mediated by the AKT pathway in an oncogenic BRAF mouse melanoma model. 2014. 1–10.

[37] M. Guix, A.C. Faber, S.E. Wang, M.G. Olivares, Y. Song, S. Qu, et al. Acquired resistance to EGFR tyrosine kinase inhibitors in cancer cells is mediated by loss of IGF-binding proteins. 2008. 2609–2619.

[38] H. Daub, K. Specht, A. Ullrich. Strategies to overcome resistance to targeted protein kinase inhibitors. Nat. Rev. Drug Discov. 2004. 3: 1001–10.

[39] U. Sartorius, P. Krammer. Upregulation of BCL-2 is involved in the mediation of chemotherapy resistance in human small cell lung cancer cell lines. 2002. 592: 584–592.

[40] D. Decaudin, S. Geley, T. Hirsch, M. Castedo, P. Marchetti, A. Macho, et al. Bcl-2 and Bcl-X L Antagonize the Mitochondrial Dysfunction Preceding Nuclear Apoptosis Induced by Chemotherapeutic Agents Bcl-2 and Bcl-XL Antagonizethe Mitochondrial DysfunctionPrecedingNuclear Apoptosis Induced by Chemotherapeutic Agents1. 1997. 62–67.

[41] W. Qian, J. Salamoun, J. Wang, V. Roginskaya, B. Van Houten, P. Wipf. The combination of thioxodihydroquinazolinones and platinum drugs reverses platinum resistance in tumor cells by inducing mitochondrial apoptosis independent of Bax and Bak. Bioorg. Med. Chem. Lett. 2015. 25: 856–863.

[42] Y. Pommier, O. Sordet, S. Antony, R.L. Hayward, K.W. Kohn. Apoptosis defects and chemotherapy resistance: molecular interaction maps and networks. Oncogene. 2004. 23: 2934–49.

[43] a Singh, J. Settleman. EMT, cancer stem cells and drug resistance: an emerging axis of evil in the war on cancer. Oncogene. 2010. 29: 4741–51.

[44] L. a Hazlehurst, T.H. Landowski, W.S. Dalton. Role of the tumor microenvironment in mediating de novo resistance to drugs and physiological mediators of cell death. Oncogene. 2003. 22: 7396–402.

[45] A.L. Correia, M.J. Bissell. The tumor microenvironment is a dominant force in multidrug resistance. Drug Resist. Updat. 2012. 15: 39–49.

[46] L. Rdnnov-jessen, O.W. Petersen, V.E. Koteliansky, M.J. Bissell. The Origin of the Myofibroblasts in Breast Cancer. 1995. 95: 859–873.

[47] K.H.T. Paraiso, K.S.M. Smalley. Fibroblast-mediated drug resistance in cancer. Biochem. Pharmacol. 2013. 85: 1033–41.

[48] E.S. Radisky, D.C. Radisky. Stromal induction of breast cancer: inflammation and invasion. Rev. Endocr. Metab. Disord. 2007. 8: 279–87.

[49] S. Faouzi, B. Le Bail, V. Neaud, L. Boussarie, J. Saric, P. Bioulac-sage, et al. Myofibroblasts are responsible for collagen synthesis in the stroma of human hepatocellular carcinoma: an. 1999. 275–284.

[50] M.F. Insana, C. Pellot-Barakat, M. Sridhar, K.K. Lindfors. Viscoelastic imaging of breast tumor microenvironment with ultrasound. J. Mammary Gland Biol. Neoplasia. 2004. 9: 393–404.

[51] A. Samani, J. Zubovits, D. Plewes. Elastic moduli of normal and pathological human breast tissues: an inversion-technique-based investigation of 169 samples. Phys. Med. Biol. 2007. 52: 1565–76.

[52] K.R. Levental, H. Yu, L. Kass, J.N. Lakins, M. Egeblad, J.T. Erler, et al. Matrix crosslinking forces tumor progression by enhancing integrin signaling. Cell. 2009. 139: 891–906.

[53] M.J. Paszek, N. Zahir, K.R. Johnson, J.N. Lakins, G.I. Rozenberg, A. Gefen, et al. Tensional homeostasis and the malignant phenotype. Cancer Cell. 2005. 8: 241–54.

[54] M. Egeblad, M.G. Rasch, V.M. Weaver. Dynamic interplay between the collagen scaffold and tumor evolution. Curr. Opin. Cell Biol. 2010. 22: 697–706.

[55] J. Condeelis, J.W. Pollard. Macrophages: obligate partners for tumor cell migration, invasion, and metastasis. Cell. 2006. 124: 263–6.

[56] A. Haage, I.C. Schneider. Cellular contractility and extracellular matrix stiffness regulate matrix metalloproteinase activity in pancreatic cancer cells. FASEB J. 2014. 1–11.

[57] S. Kumar, V.M. Weaver. Mechanics, malignancy, and metastasis: the force journey of a tumor cell. Cancer Metastasis Rev. 2009. 28: 113–27.

[58] J.-H. Kim, A.R. Asthagiri. Matrix stiffening sensitizes epithelial cells to EGF and enables the loss of contact inhibition of proliferation. J. Cell Sci. 2011. 124: 1280–7.

[59] P.A. Netti, D.A. Berk, M.A. Swartz, A.J. Grodzinsky, R.K. Jain. Role of Extracellular Matrix Assembly in Interstitial Transport in Solid Tumors Role of Extracellular Matrix Assembly in Interstitial Transport in Solid Tumors 1. 2000. 2497–2503.

[60] J.D. Humphries, A. Byron, M.J. Humphries. Integrin ligands at a glance. J. Cell Sci. 2006. 119: 3901–3.

[61] R.O. Hynes. Integrins : Bidirectional , Allosteric Signaling Machines In their roles as major adhesion receptors , integrins. 2002. 110: 673–687.

[62] a. E. Berman, N.I. Kozlova, G.E. Morozevich. Integrins as a potential target for targeted anticancer therapy. Biochem. Suppl. Ser. B Biomed. Chem. 2012. 6: 205–210.

[63] X.H. Yang, L.M. Flores, Q. Li, P. Zhou, F. Xu, I.E. Krop, et al. Disruption of laminin-integrin-CD151-focal adhesion kinase axis sensitizes breast cancer cells to ErbB2 antagonists. Cancer Res. 2010. 70: 2256–63.

[64] F. Aoudjit, K. Vuori. Integrin signaling inhibits paclitaxel-induced apoptosis in breast cancer cells. Oncogene. 2001. 20: 4995–5004.

[65] N. Cordes, C.C. Park. Beta1 Integrin As a Molecular Therapeutic Target. Int. J. Radiat. Biol. 2007. 83: 753–60.

[66] C.C. Park, H. Zhang, M. Pallavicini, J.W. Gray, F. Baehner, C.J. Park, et al. Beta1 integrin inhibitory antibody induces apoptosis of breast cancer cells, inhibits growth, and distinguishes malignant from normal phenotype in three dimensional cultures and in vivo. Cancer Res. 2006. 66: 1526–35.

[67] E.S. Yao, H. Zhang, Y.-Y. Chen, B. Lee, K. Chew, D. Moore, et al. Increased beta1 integrin is associated with decreased survival in invasive breast cancer. Cancer Res. 2007. 67: 659–64.

[68] P.B. dos Santos, J.S. Zanetti, A. Ribeiro-Silva, E.I.C. Beltrão. Beta 1 integrin predicts survival in breast cancer: a clinicopathological and immunohistochemical study. Diagn. Pathol. 2012. 7: 104.

[69] S. Liu, J. Wang, W. Niu, E. Liu, J. Wang, C. Peng, et al. The β6-integrin-ERK/MAP kinase pathway contributes to chemo resistance in colon cancer. Cancer Lett. 2013. 328: 325–34.

[70] H. Yu, J.K. Mouw, V.M. Weaver. Forcing form and function: biomechanical regulation of tumor evolution. Trends Cell Biol. 2011. 21: 47–56.

[71] T. Geiger, R. Zaidel-Bar. Opening the floodgates: proteomics and the integrin adhesome. Curr. Opin. Cell Biol. 2012. 24: 562–8.

[72] a. Hall. Rho GTPases and the Actin Cytoskeleton. Science (80-.). 1998. 279: 509–514.

[73] N. a Hotchin, a Hall. The assembly of integrin adhesion complexes requires both extracellular matrix and intracellular rho/rac GTPases. J. Cell Biol. 1995. 131: 1857–65.

[74] C.T. Mierke. The role of focal adhesion kinase in the regulation of cellular mechanical properties. Phys. Biol. 2013. 10: 065005.

[75] R.K. Jain, J.D. Martin, T. Stylianopoulos. The role of mechanical forces in tumor growth and therapy. Annu. Rev. Biomed. Eng. 2014. 16: 321–46.

[76] W.R. Wilson, M.P. Hay. Targeting hypoxia in cancer therapy. Nat. Rev. Cancer. 2011. 11: 393–410.

[77] P. Carmeliet, R.K. Jain. Molecular mechanisms and clinical applications of angiogenesis. Nature. 2011. 473: 298–307.

[78] L. a Liotta, E.C. Kohn. The microenvironment of the tumour-host interface. Nature. 2001. 411: 375–9.

[79] T.L. Whiteside. The tumor microenvironment and its role in promoting tumor growth. Oncogene. 2008. 27: 5904–12.

[80] K. Pietras, A. Ostman. Hallmarks of cancer: interactions with the tumor stroma. Exp. Cell Res. 2010. 316: 1324–31.

[81] T.R. Wilson, J. Fridlyand, Y. Yan, E. Penuel, L. Burton, E. Chan, et al. Widespread potential for growth-factor-driven resistance to anticancer kinase inhibitors. Nature. 2012. 487: 505–9.

[82] R. Straussman, T. Morikawa, K. Shee, M. Barzily-Rokni, Z.R. Qian, J. Du, et al. Tumour micro-environment elicits innate resistance to RAF inhibitors through HGF secretion. Nature. 2012. 487: 500–4.

[83] N.E. Bhola, J.M. Balko, T.C. Dugger, M.G. Kuba, V. Sánchez, M. Sanders, et al. TGF- β inhibition enhances chemotherapy action against triple-negative breast cancer. 2013. 123.:

[84] Y. Sun, J. Campisi, C. Higano, T.M. Beer, P. Porter, I. Coleman, et al. Treatment-induced damage to the tumor microenvironment promotes prostate cancer therapy resistance through WNT16B. Nat. Med. 2012. 18: 1359–68.

[85] M.J. Duffy, T.M. Maguire, A. Hill, E. Mcdermott, N.O. Higgins, S. Vincent. Metalloproteinases : role in breast carcinogenesis , invasion and metastasis. 2000.

[86] A. Köhrmann, U. Kammerer, M. Kapp, J. Dietl, J. Anacker. Expression of matrix metalloproteinases (MMPs) in primary human breast cancer and breast cancer cell lines: New findings and review of the literature. BMC Cancer. 2009. 9: 188.

[87] W. Lin, M. Karin. A cytokine-mediated link between innate immunity , inflammation , and cancer. J. Clin. Investig. 2007. 117: 1175–1183.

[88] G. Dranoff. Cytokines in cancer pathogenesis and cancer therapy. Nat. Rev. Cancer. 2004. 4: 11–22.

[89] S.-H. Park, J.-H. Kim, D.-H. Lee, J.-W. Kang, H.-H. Song, S.-R. Oh, et al. Luteolin 8-C-β-fucopyranoside inhibits invasion and suppresses TPA-induced MMP-9 and IL-8 via ERK/AP-1 and ERK/NF-κB signaling in MCF-7 breast cancer cells. Biochimie. 2013. 95: 2082–2090.

[90] K. Wu, S. Katiyar, A. Li, M. Liu, X. Ju, V.M. Popov, et al. Dachshund inhibits oncogene-induced breast cancer cellular migration and invasion through suppression of interleukin-8. Proc. Natl. Acad. Sci. U. S. A. 2008. 105: 6924–6929.

[91] S. Desai, S. Laskar, B.N. Pandey. Autocrine IL-8 and VEGF mediate epithelial-mesenchymal transition and invasiveness via p38/JNK-ATF-2 signalling in A549 lung cancer cells. Cell. Signal. 2013. 25: 1780–91.

[92] M. Todaro, M.P. Alea, A. Scopelliti, J.P. Medema, G. Stassi. IL-4-mediated drug resistance in colon cancer stem cells. Cell Cycle. 2008. 7: 309–313.

[93] V. Levina, A.M. Marrangoni, R. DeMarco, E. Gorelik, A.E. Lokshin. Drug-selected human lung cancer stem cells: Cytokine network, tumorigenic and metastatic properties. PLoS One. 2008. 3.:

[94] W.N. Hait. Anticancer drug development: the grand challenges. Nat. Rev. Drug Discov. 2010. 9: 253–254.

[95] M. Dickson, J.P. Gagnon. Key factors in the rising cost of new drug discovery and development. Nat. Rev. Drug Discov. 2004. 3: 417–29.

[96] a S. Hoffman. Hydrogels for biomedical applications. Ann. N. Y. Acad. Sci. 2001. 944: 62–73.

[97] A.J. Engler, S. Sen, H.L. Sweeney, D.E. Discher. Matrix elasticity directs stem cell lineage specification. Cell. 2006. 126: 677–89.

[98] T.P. Kraehenbuehl, P. Zammaretti, A.J. Van der Vlies, R.G. Schoenmakers, M.P. Lutolf, M.E. Jaconi, et al. Three-dimensional extracellular matrix-directed cardioprogenitor differentiation: systematic modulation of a synthetic cell-responsive PEG-hydrogel. Biomaterials. 2008. 29: 2757–66.

[99] H.-D. Kim, S.R. Peyton. Bio-inspired materials for parsing matrix physicochemical control of cell migration: a review. Integr. Biol. (Camb). 2012. 4: 37–52.

[100] S.R. Peyton, A.J. Putnam. Extracellular matrix rigidity governs smooth muscle cell motility in a biphasic fashion. J. Cell. Physiol. 2005. 204: 198–209.

[101] W.G. Herrick, S. Rattan, T. V. Nguyen, M.S. Grunwald, C.W. Barney, A.J. Crosby, et al. Smooth Muscle Stiffness Sensitivity is Driven by Soluble and Insoluble ECM Chemistry. Cell. Mol. Bioeng. 2015.

[102] G. Maheshwari, G. Brown, D. a Lauffenburger, a Wells, L.G. Griffith. Cell adhesion and motility depend on nanoscale RGD clustering. J. Cell Sci. 2000. 113 (Pt 1: 1677–86.

[103] S.R. Peyton, C.B. Raub, V.P. Keschrumrus, A.J. Putnam. The use of poly(ethylene glycol) hydrogels to investigate the impact of ECM chemistry and mechanics on smooth muscle cells. Biomaterials. 2006. 27: 4881–93.

[104] J.E. Leslie-Barbick, J.J. Moon, J.L. West. Covalently-immobilized vascular endothelial growth factor promotes endothelial cell tubulogenesis in poly(ethylene glycol) diacrylate hydrogels. J. Biomater. Sci. Polym. Ed. 2009. 20: 1763–79.

[105] C.M. Kraning-Rush, S.P. Carey, M.C. Lampi, C. a Reinhart-King. Microfabricated collagen tracks facilitate single cell metastatic invasion in 3D. Integr. Biol. (Camb). 2013. 5: 606–16.

[106] D. Loessner, K.S. Stok, M.P. Lutolf, D.W. Hutmacher, J. a Clements, S.C. Rizzi. Bioengineered 3D platform to explore cell-ECM interactions and drug resistance of epithelial ovarian cancer cells. Biomaterials. 2010. 31: 8494–506.

[107] E.Y. Tokuda, J.L. Leight, K.S. Anseth. Modulation of matrix elasticity with PEG hydrogels to study melanoma drug responsiveness. Biomaterials. 2014. 35: 4310–4318.

[108] N. a. Peppas, J.Z. Hilt, a. Khademhosseini, R. Langer. Hydrogels in Biology and Medicine: From Molecular Principles to Bionanotechnology. Adv. Mater. 2006. 18: 1345–1360.

[109] S.R. Khetani, S.N. Bhatia. Engineering tissues for in vitro applications. Curr. Opin. Biotechnol. 2006. 17: 524–31.

[110] B. Ananthanarayanan, Y. Kim, S. Kumar. Elucidating the mechanobiology of malignant brain tumors using a brain matrix-mimetic hyaluronic acid hydrogel platform. Biomaterials. 2011. 32: 7913–23.

[111] J. Patterson, M.M. Martino, J. a. Hubbell. Biomimetic materials in tissue engineering. Mater. Today. 2010. 13: 14–22.

[112] J.F. Lutz, Z. Zarafshani. Efficient construction of therapeutics, bioconjugates, biomaterials and bioactive surfaces using azide-alkyne “click” chemistry. Adv. Drug Deliv. Rev. 2008. 60: 958–970.

[113] G.H. Underhill, P. Galie, C.S. Chen, S.N. Bhatia. Bioengineering methods for analysis of cells in vitro. Annu. Rev. Cell Dev. Biol. 2012. 28: 385–410.

[114] L.G. Griffith. Emerging design principles in biomaterials and scaffolds for tissue engineering. Ann. N. Y. Acad. Sci. 2002. 961: 83–95.

[115] C. Wang, X. Tong, F. Yang. Bioengineered 3D Brain Tumor Model To Elucidate the Effects of Matrix Stiffness on Glioblastoma Cell Behavior Using PEG-Based Hydrogels. 2014.

[116] J.L. Leight, E.Y. Tokuda, C.E. Jones, A.J. Lin, K.S. Anseth. Multifunctional bioscaffolds for 3D culture of melanoma cells reveal increased MMP activity and migration with BRAF kinase inhibition. Proc. Natl. Acad. Sci. 2015. 112: 201505662.

[117] A.N. Stachowiak, D.J. Irvine. Inverse opal hydrogel-collagen composite scaffolds as a supportive microenvironment for immune cell migration. J. Biomed. Mater. Res. A. 2008. 85: 815–28.

[118] C.S. Ki, T.-Y. Lin, M. Korc, C.-C. Lin. Thiol-ene hydrogels as desmoplasia-mimetic matrices for modeling pancreatic cancer cell growth, invasion, and drug resistance. Biomaterials. 2014. 35: 9668–77.

[119] S.C. Rizzi, J. a Hubbell. Recombinant protein-co-PEG networks as cell-adhesive and proteolytically degradable hydrogel matrixes. Part I: Development and physicochemical characteristics. Biomacromolecules. 2005. 6: 1226–38.

CHAPTER 2

SYNTHESIS OF PEG-PC BIOMATERIAL SYSTEM AND MECHANICAL/STRUCTURAL CHARACTERIZATION

2.1 Abstract

Both synthetic and natural biomaterial platforms are commonly used as mimics of *in vivo* tissues for *in vitro* studies in mechanobiology. These biomaterial platforms can be tailored to capture many aspects of the *in vivo* ECM, therefore studies conducted using these platforms are potentially more predictive of *in vivo* outcomes than traditional tissue culture plastic plates. Synthetic biomaterials allow the mechanical and adhesive properties to be tuned independently, as opposed to natural biomaterials. In response to the needs of new synthetic biomaterials with improved properties, a new class of hydrogels was created by combing PEG and phosphorylcholine (PC). The resulting hydrogels have an extremely wide range of tunable mechanical properties, with small mesh sizes and high optical transparency. As a proof of concept, the stiffness sensing of multiple cell lines on the hydrogels was studied through quantification of focal adhesion properties. This novel PEG-PC biomaterial can be useful for many applications in studying mechanobiology.

2.2 Introduction

Both naturally derived polymers and chemically synthetic polymers are widely used as biomaterial platforms to support cell culture in two and three dimensions (2D, 3D). The two most common naturally derived materials are collagens and matrigel. Both of these materials contain native binding sites for cell adhesion; however, it is not possible to independently control the amount of binding sites and the material mechanical property, i.e. increasing or decreasing the number of adhesive sites also increases or decreases the mechanical stiffness. On the other hand, synthetic polymer hydrogels allow independent control over mechanical and adhesive properties. The two most commonly used synthetic hydrogels are made from either polyacrylamide (PAA) or poly(ethylene glycol) (PEG) polymers. The PAA hydrogel was the first popularized biomaterial used in mechanobiology studies. However, these gels have limited mechanical range and are not suitable for three-dimensional (3D) studies. PEG-based hydrogels have a modulus of 20-500 kPa [1,2], and can be engineered to contain specific hydrolytic [3,4] or enzymatic degradable sites [5] for 3D cell culture. Both PEG and PAA can be coupled with short peptides or full-length proteins of interest.

Phosphorylcholine is a zwitterion that locates at the outer membrane of the cells, providing an inert surface for many biological reactions [6]. 2-methacryloyloxyethyl phosphorylcholine (MPC) is a monomer containing a phospholipid polar group. Co-polymers that incorporated MPC were shown to suppress clot formation and reduce platelet adhesion due to its anti-protein adsorption property, which is a result of enhancing surface hydrophilicity [7]. MPC co-polymers were also shown to be more anti-protein adsorptive than poly[2-hydroxyethyl methacrylate (HEMA)] due to larger free

water fraction on the surface [7]. Therefore, inclusion of a PC zwitterion group into a PEG hydrogel can potentially create a more hydrophilic biomaterial and prevent the proteins from culture serum to passively adsorb to the hydrogel surface and influence cell behavior.

Ishihara and co-workers investigated the mechanical property of MPC polymer hydrogels, which were cross-linked either with N,N'- methylenebisacrylamide (BIS) or 2-(methacryloyloxy)ethyl-[N-(2-methacryloyloxy)ethyl]phosphorylcholine (MMPC). They found that MMPC showed higher cross-linking reactivity with MPC than BIS, therefore improving the tensile property of the material [8]. This result suggests that incorporation of PC groups into a hydrogel network can potentially increase the mechanical properties. MPC monomers can be incorporated into a hydrogel network following free-radical polymerization [9] or Michael addition [10]. The work in this chapter describes the creation of a novel "PEG-PC" hydrogel by co-polymerizing MPC with PEG dimethacrylate (PEGDMA) following free-radical polymerization. The resulting PEG-PC hydrogels have a mechanical range that spans four orders of magnitude (1-10,000 kPa), which matches or exceeds any previously reported hydrogel system, and have an improved anti-protein adsorption property compared to PEGDMA hydrogels [9]. Here, the bulk mechanical properties of PEG-PC hydrogels are measured using a compression test in which the hydrogels, in the absence of cells, are deformed at a constant strain rate.

2.3 Materials And Methods

2.3.1 PEG-PC hydrogel formation

2-methacryloyloxyethyl phosphorylcholine (Sigma-Aldrich) (MPC) was dissolved in phosphate buffered saline (PBS) to make a final concentration of 0.6 M (17 wt %). PEGDMA (average Mn 750, Sigma-Aldrich, St. Louis, MO), varied between final concentrations of 7.4 mM and 0.7 M (0.5−55 wt %), was added into the MPC solution to create various PEG-PC polymer hydrogel precursor solutions. Solutions were degassed for 30 s with nitrogen and sterilized using a 0.2 μm syringe filter (Thermo Fisher Scientific, Waltham, MA). Depending on the desired format, two different free radical initiators were used for polymerization. To cure under UV light, 0.8 wt % Irgacure 2959 (BASF, Ludwigshafen, Germany) was added, and gel formation was induced with a Spectroline High-Intensity UV Lamp at 365 nm (Model no. SB-100P, Westbury, NY), 3.5 in. from the gel for 7 min. To form hydrogels in the absence of UV light, 0.05 wt % ammonium persulfate (APS) and 0.125 vol % tetramethylethylenediamine (TEMED, Bio-Rad Laboratories, Hercules, CA) were added, and gels were polymerized under nitrogen for 10 min.

2.3.2 Hydrogel mechanical and structural characterization

PEG-PC hydrogel cylinders for mechanical compression testing were formed in 5-mm Teflon molds and swelled in PBS for 48 h. Post swelling, hydrogel dimensions were measured with digital calipers, and mechanical compression tests were performed with a TA Instruments (New Castle, DE) AR-2000 rheometer at a 2 μm/s strain rate. The Young's modulus (E) for each hydrogel was calculated by plotting the measured normal force between 0 and 4% strain and dividing the slope of the best-fit linear regression by

the hydrogel cross-sectional area. The Young's modulus was obtained for 4 or more hydrogels for each PEGDMA concentration. To determine an approximate average mesh size as a function of PEGDMA cross-linker content with constant PC content, hydrogels were swelled in PBS for 48 h, then weighed, fully lyophilized, and weighed again. The average mesh size, ξ, of the PEG-PC hydrogels was determined as a function of PEGDMA cross-linker concentration according to the Flory theory as modified by Canal and Peppas:

$$\xi = \upsilon_{2,s}^{-\frac{1}{3}}(\bar{r}^2)^{1/2}$$

where $\upsilon_{2,s}$ is the swollen volume fraction of polymer and $(\bar{r}^2)^{1/2}$ is the average end-to-end distance of the PEGDMA cross-linker.

2.3.3 Making gels on coverslips and protein functionalization

18 mm glass coverslips (Thermo Fisher Scientific, Waltham, MA) were plasma treated (Harrick Plasma, Ithaca, NY) and subsequently methacrylate-silanized with 2 vol% 3-(trimethoxysilyl) propyl methacrylate (Sigma-Aldrich, St. Louis, MO) in 95% ethanol (adjusted to pH 5.0 with glacial acetic acid) for 5 min, washed 3 times with 100% ethanol, and dried at 120 °C for 15 min. To make thin PEG-PC hydrogels with even heights and suitable for microscopy, 80 μL PEG-PC hydrogels were polymerized with APS and TEMED between a methacrylated-silanized coverslip and an untreated coverslip for 20 min on the bench. After polymerization, the hydrogels were allowed to swell in PBS, and the non-treated coverslips were removed easily with fine forceps.

The gel surfaces can be coupled with the heterobifunctional cross-linker, which contains a highly amine-reactive functional group for covalent linkage to a variety of integrin-binding proteins. Two heterobifunctional cross-linkers used were sulfo-

SANPAH (ProteoChem, Denver, CO) and acrylate-poly(ethylene glycol)-succinimidyl valerate (PEG-SVA; Laysan Bio, Arab, AL). With sulfo-SANPAH, swollen gels on coverslips were transferred to 12-well tissue culture dishes and treated with sulfo-SANPAH (0.3 mg/mL in pH 8.5 HEPES buffer) under UV light for 15 min, rinsed twice with HEPES buffer, and followed immediately by incubation with proteins overnight. With PEG-SVA, the cross-linker was added to the PEG-PC prehydrogel solution at 0.11 wt %. This method incorporates an amine reactive group into the bulk of the hydrogel instead of isolating the reaction at the surface like sulfo-SANPAH. The protein used was type I collagen (rat tail, Life Technologies), recombinant human collagen III (FibroGen, San Francisco, CA), and human plasma fibronectin (EMD Millipore, Billerica, MA). Protein solution was made in sterile PBS and adjusted to pH 3 to prevent collagen gelation. Post protein reaction, hydrogels were washed 3 times with sterile PBS with shaking and then UV sterilized for 60 min before cell seeding.

2.3.4 Cell culture

All supplies were purchased from Life Technologies (Carlsbad, CA) unless otherwise noted. Human breast cancer cell lines (MDA-MB-231 and SkBr3) were generous gifts from Dr. Shannon Hughes at the Massachusetts Institute of Technology, and were cultured in Dulbecco's Modified Eagle's Medium (DMEM) supplemented with 10% fetal bovine serum (FBS) and 1% penicillin-streptomycin (P/S) at 37ºC and 5% CO_2. Human hepatocellular carcinoma (HCC) cells (HEP3Bs, American Type Culture Collection, Manassas, VA) were cultured in modified Eagle's medium (MEM) supplemented with 10% FBS and 1% P/S at 37ºC and 5% CO_2. Human aortic smooth

muscle cells (HASMCs) were cultured in DMEM supplemented with 1% P/S and smooth muscle growth supplement (SMGS).

2.3.5 Immunofluorescent imaging and focal adhesion quantification

Hydrogels with Young's moduli of 18, 26, 165, and 400 kPa were made and subsequently coupled with 10 μg/cm^2 collagen I. Cells were seeded at a density of 10,000 cells/cm^2 in serum-free medium and allowed to adhere for 48 hours. Cells were rinsed two times with warm PBS, fixed with 4% formaldehyde, permeabilized with Tris-buffered saline (TBS) containing 0.5% Triton X-100 (Promega), and blocked with AbDil (2 wt.% BSA in TBS with 0.1% Triton X-100, TBS-T). F-actin was labeled with Alexa Fluor 555-conjugated phalloidin for 1 h. Vinculin was labeled with a monoclonal mouse anti-vinculin antibody (Sigma-Aldrich) for 1 h, followed by an anti-mouse FITC secondary antibody (Jackson ImmunoResearch Laboratories, West Grove, PA) for 1 h. Cell nuclei were labeled with DAPI (MP Biomedicals, Santa Ana, CA) for 5 min. Cells were thoroughly washed between labeling steps with TBS-T. Each sample was treated with ProLong Gold antifade reagent for 5 min before imaging on a Zeiss Axio Observer Z1 microscope with a 63x oil immersion objective (Carl Zeiss AG, Oberkochen, Germany), and images were compiled in ImageJ (NIH, Bethesda, MD).

2.3.6 Quantification of protein adsorption

A modified ELISA [11] was used to quantify non-specific protein adsorption. The fully swollen hydrogels were incubated with 10 mg/mL bovine serum albumin (BSA; Sigma) for 20 h at 37 °C. The gels were subsequently incubated with a primary antibody to BSA (Life Technologies) and a secondary antibody conjugated to horseradish peroxidase (HRP; Abcam, Cambridge, U.K.) in PBS for 90 min. The gels were washed 5

times with PBS between each incubation. The gels were then incubated with 0.1 mg/mL 3,3′,5,5′-tetramethylbenzidine (TMB; Sigma) and 0.06% hydrogen peroxide (Fisher) in 0.1 M sodium acetate (pH 5.5; Sigma) for 1 h at room temperature with shaking. Then an equal volume of 1 M sulfuric acid (Sigma) was added, and the absorbance at 450 nm was measured with a ELx800 absorbance microplate reader (BioTek).

2.3.7 Statistical Analysis

Statistical analysis was performed using Prism v5.04 (GraphPad Software, La Jolla, CA). Statistical significance was evaluated by either using unpaired Student's t tests (with Welch's correction as necessary) or one-way analysis of variance (ANOVA) with a Tukey post-test. Data are reported as mean ± standard deviation. $p \leq 0.05$ is denoted with *, ≤ 0.01 with **, and ≤ 0.001 with ***; $P > 0.05$ is considered not significant ("ns").

2.4 Results

2.4.1 PEG-PC hydrogels have a wide range of Young's Moduli

PEG-PC hydrogels were synthesized by combining various concentration of PEGDMA with 0.6M PC (17 wt %) followed by free-radical polymerization (Figure 2.1). The photopolymerized PEG-PC hydrogels have a tunable mechanical range over 4 orders of magnitude of Young's moduli, from 0.9 ± 0.2 kPa at 7.4 mM (0.5 wt %) PEGDMA to 9300 ± 900 kPa at 0.7 M (55 wt %) PEGDMA (Figure 2.2).

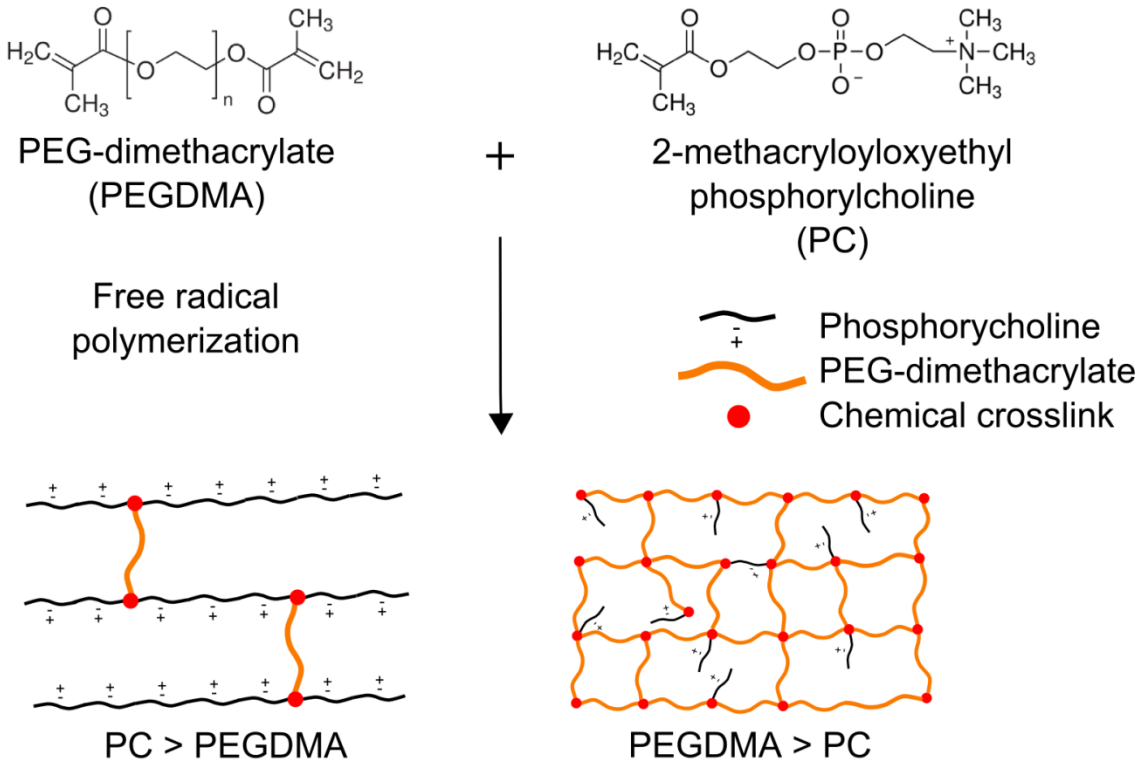

Figure 2.1 Schematic of PEG-PC hydrogel structure. PEG-PC hydrogels were prepared by addition of PEGDMA and PC followed by free-radical polymerization. At low PEGDMA concentrations, the network structure is dominated by PEGDMA-cross-linked linear PC polymers, whereas the network structure is dominated by PEGDMA with sparsely distributed PC groups at very high PEGDMA concentrations. Figure adapted with permission from [9]. © 2013 American Chemical Society.

When APS and TEMED are used as initiators for polymerization, there were minor differences in Young's modulus compared to using Irgacure for the same PEGDMA concentration (Figure 2.3A). This trend was consistent at low concentrations of PEGDMA. When comparing the gel fractions between the two polymerization methods, polymerizing with Irgacure is less efficient, and the resulting gels had larger mesh sizes and were softer (Figure 2.3B).

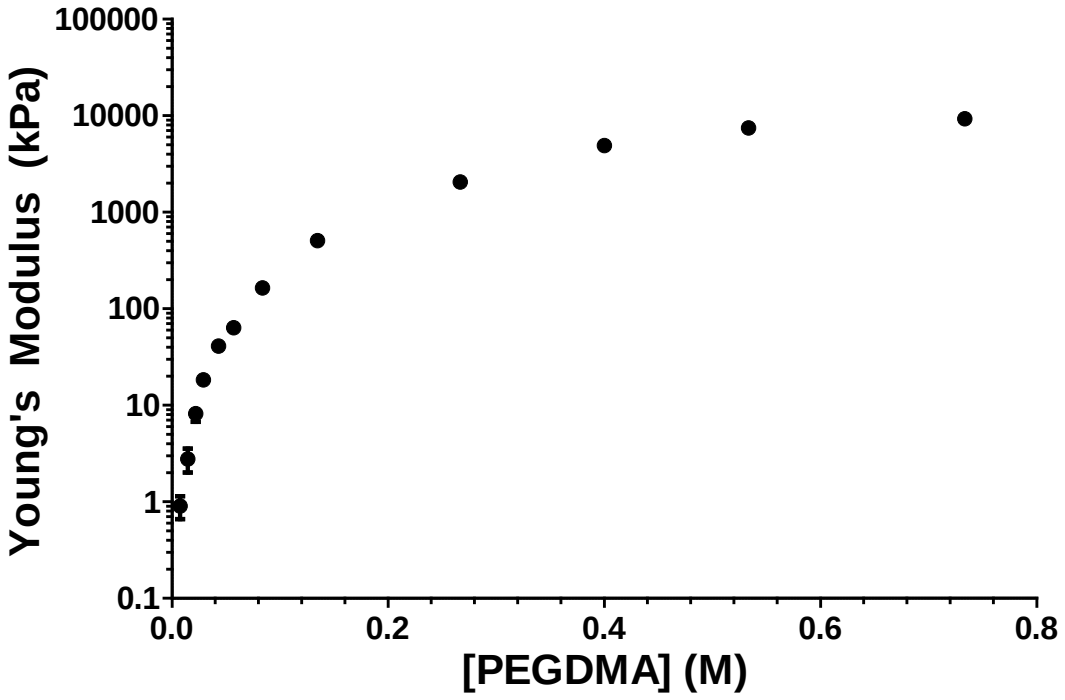

Figure 2.2 Young's modulus of PEG-PC. Young's modulus, E, of PEG-PC hydrogels as a function of PEG cross-linker concentration from 7.4 mM to 0.7 M. PC was held at 17 wt % (0.6 M). Error bars are standard deviations. Each adjacent pair is significantly different as determined by an unpaired Student's t test with $p < 0.001$ or better. Figure adapted with permission from [9]. © 2013 American Chemical Society.

A

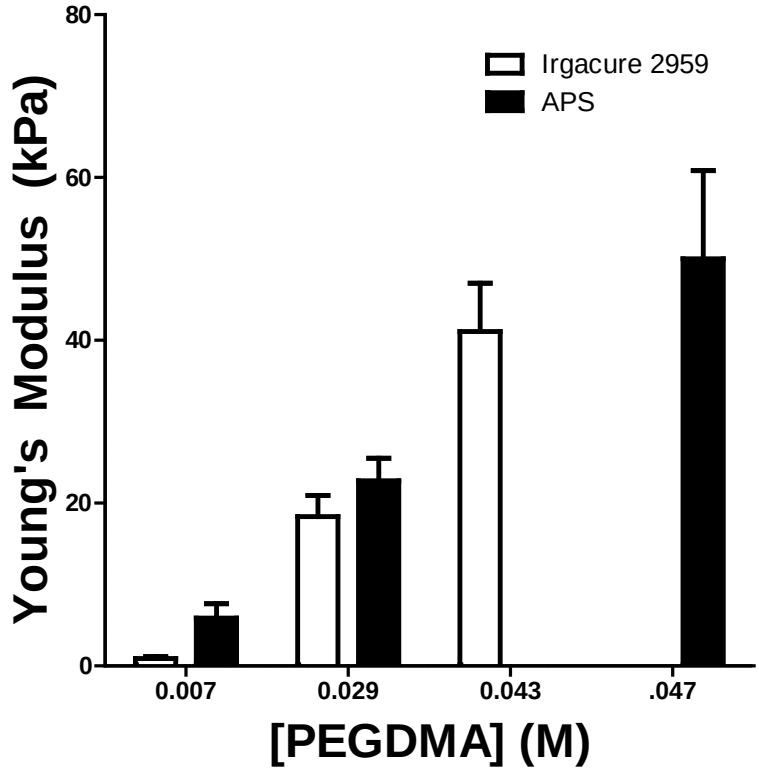

B

[PEGDMA] (M)	0.007	0.029	0.043	0.047
IRG, E (kPa)	0.9 ± 0.2	18 ± 3	41 ± 6	
IRG, ξ (Å)	53 ± 4	35 ± 2	33 ± 5	
IRG, %poly	96 ± 6	108 ± 5	94 ± 2	
APS, E (kPa)	5.9 ± 1.8	23 ± 3		50 ± 11
APS, ξ (Å)	41 ± 1	29 ± 4		29 ± 0.4
APS, %poly	111 ± 5	100 ± 3		105 ± 2

Figure 2.3 The mesh sizes and Young's modulus of PEG-PC following polymerization with Irgacure and APS/TEMED. The mesh sizes and Young's modulus varies between two different methods of polymerization, Irgarcure and APS/TEMED, at low PEGDMA concentrations. **(A)** Young's modulus of hydrogels polymerized with APS/TEMED are much higher compared to polymerization with Irgacure at low PEGDMA concentrations. **(B)** Hydrogels polymerized with APS/TEMED have smaller mesh sizes and higher percentage of polymerization. Figure adapted with permission from [9]. © 2013 American Chemical Society.

2.4.2 PEG-PC have small mesh sizes and structural dependent swelling

When the amount of PEGDMA cross-linker increases from 7.4 mM to 0.7 M, the mesh size decreases from 5.3 ± 0.4 nm to 0.95 ± 0.01 nm (Figure 2.4). However, the expected strong correlation between mesh size and Young's modulus was found only over a partial range of cross-linker concentrations: from 7.4 to 135 mM PEGDMA (Pearson's $R = -0.8383$, $p < 0.05$) and from 0.3 to 0.7 M PEGDMA (Pearson's $R = -0.9572$, $p < 0.05$). Interestingly, these behaviors separate where the weight percent of PC and PEGDMA are equal in the gel. This finding suggests a hydrogel structural change, from one dominated by methacrylic PC polymer that is cross-linked by PEGDMA to one dominated by a PEG polymer, which is also cross-linked by PEGDMA, with PC pendant groups (Figure 2.1). The percentage of PBS uptake was calculated from the masses of the fully swollen hydrogels and pre-swelling hydrogels (right after polymerization). Due to the hydrophilicity of the PC groups, PEG-PC can swell in PBS at all cross-linker concentrations, and there are also two different swelling regimes that are separated at the point where the hydrogel structural change occurs (Figure 2.5).

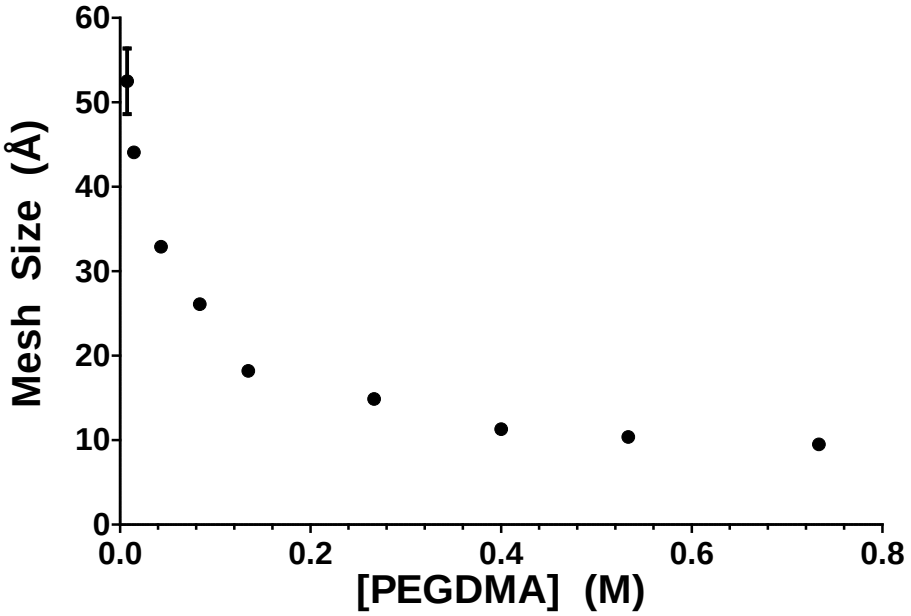

Figure 2.4 The average mesh sizes of PEG-PC hydrogels (PC at 0.6 M) as a function of PEG cross-linker concentration. Error bars are standard deviations (N ≥ 4). Figure adapted with permission from [9]. © 2013 American Chemical Society.

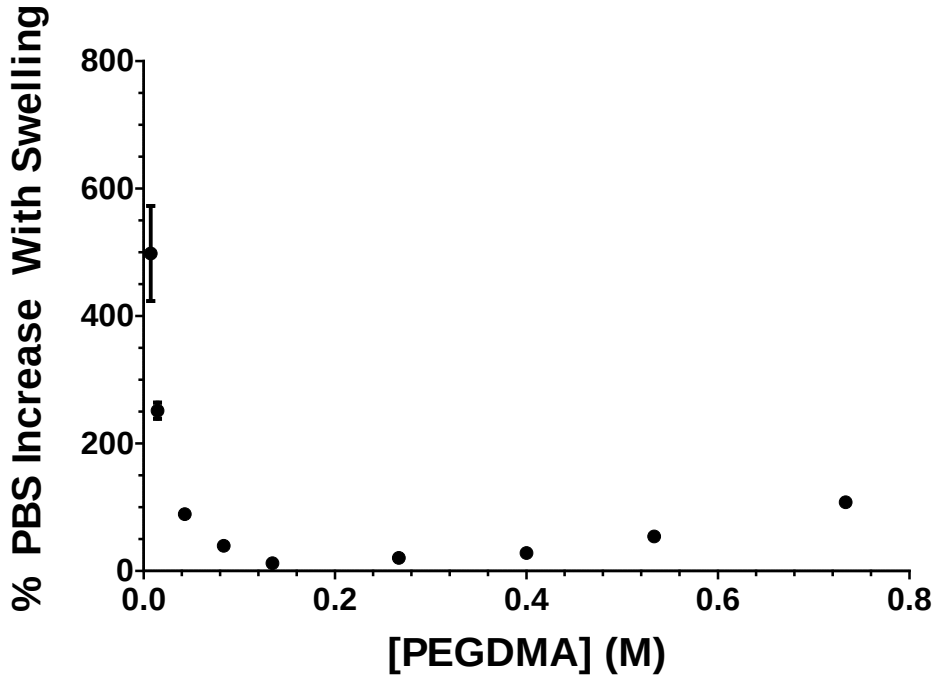

Figure 2.5 PEG-PC swelling behavior. PEG-PC swelling behavior in PBS, which is maintained at even very high cross-linker concentrations. Figure adapted with permission from [9]. © 2013 American Chemical Society.

2.4.3 PC groups reduce non-specific adsorption of proteins to PEG gel

Collagen I, which was covalently coupled to the hydrogel surface by using sulfo-SANPAH, was detected by immunofluorescence, whereas no collagen I was detected on gel surfaces without the use of sulfo-SANPAH (Figure 2.6). These results demonstrate qualitatively that PEG-PC hydrogels are non-fouling to protein adsorption. To determine quantitatively whether incorporation of the hydrophilic PC groups enhanced resistance to protein adsorption to PEGDMA, bovine serum albumin (BSA) was allowed to adsorb to the surface of PEGDMA only (0.145 M) and PEG-PC (0.6 M PC and 0.054 M PEGDMA) hydrogels that had the same Young's modulus, and an ELISA was performed. There was a small amount of BSA detected on PEGDMA hydrogel surface, but not with the PEG-PC hydrogel (Figure 2.7A). When the PEGDMA concentration was kept constant at 0.084 M whereas PC was varied from 0.15 to 0.6 M, the BSA adsorption decreased with increasing PC content (Figure 2.7B).

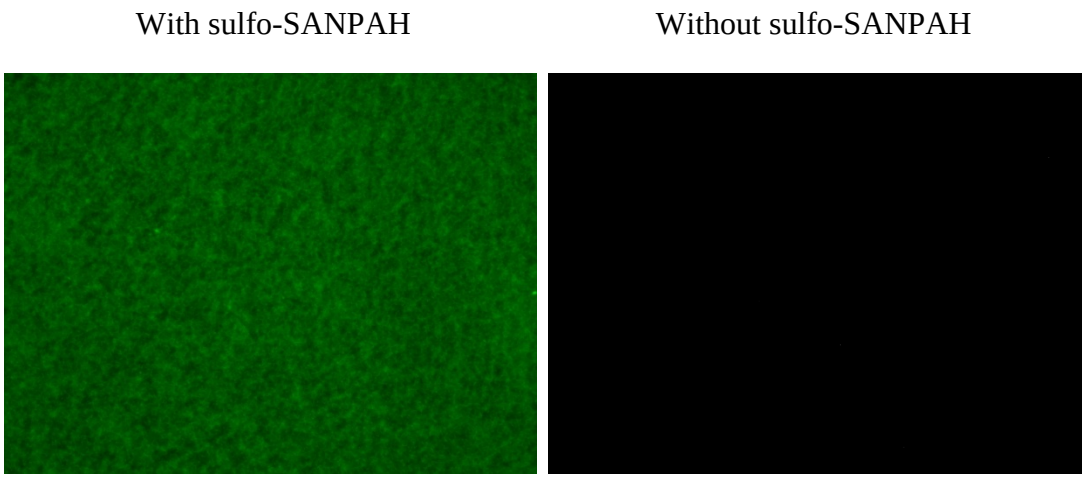

Figure 2.6 Proteins can be coupled to PEG-PC surface in a controllable manner. Collagen I is covalently coupled to the gel surface by using sulfo-SANPAH.

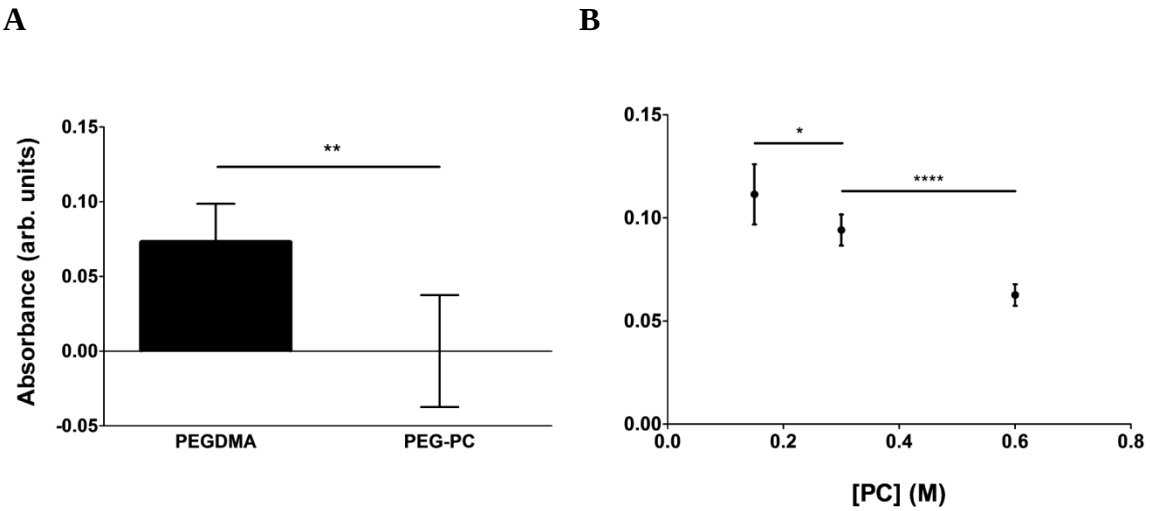

Figure 2.7 PEG-PC hydrogels are non-fouling. **(A)** No BSA was detected on the PEG-PC hydrogels compared to PEGDMA hydrogels that have similar modulus. **(B)** Adsorbed BSA at a constant PEGDMA concentration decreases with increasing PC content, demonstrating the ability of PC to prevent fouling. Figure adapted with permission from [9]. © 2013 American Chemical Society.

2.4.4 PEG-PC hydrogels are suitable for mechanobiology studying of various cell types

PEG-PC hydrogels were polymerized and covalently attached on glass coverslips. Integrin-binding ECM proteins were covalently coupled to the hydrogel surface in order to induce cell adhesion and spreading (Figure 2.8). The two methods used to couple ECM proteins were sulfo-SANPAH and PEG-SVA (Figure 2.9). When neither of the heterobifunctional cross-linker was used, a minimal cell attachment and spreading was observed as indicated in Figure 2.9A with HASMCs (bottom left) and HEP3Bs (bottom right). This result demonstrates that PEG-PC hydrogels are non-fouling, resistant to non-specific cell attachment, and useful for studies in which parsing the roles of integrin-binding versus mechanical properties is desired. Many different cell types can also attach and spread out on PEG-PC gels with different stiffnesses (Figure 2.10).

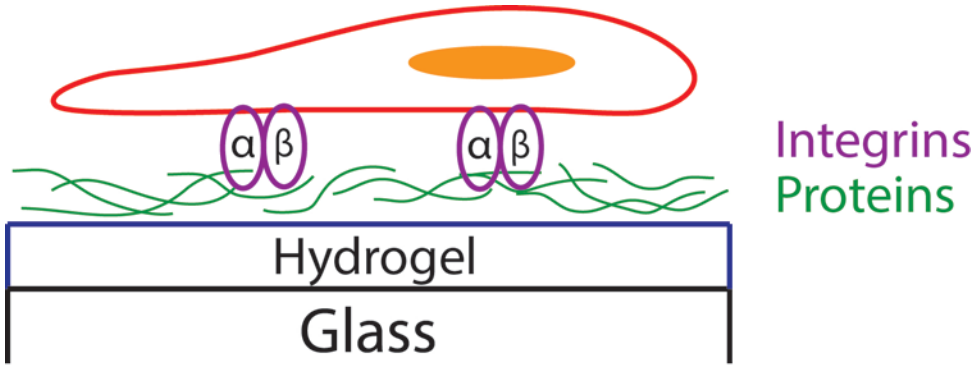

Figure 2.8 Schematic of cell attachment to PEG-PC hydrogel via integrin binding.

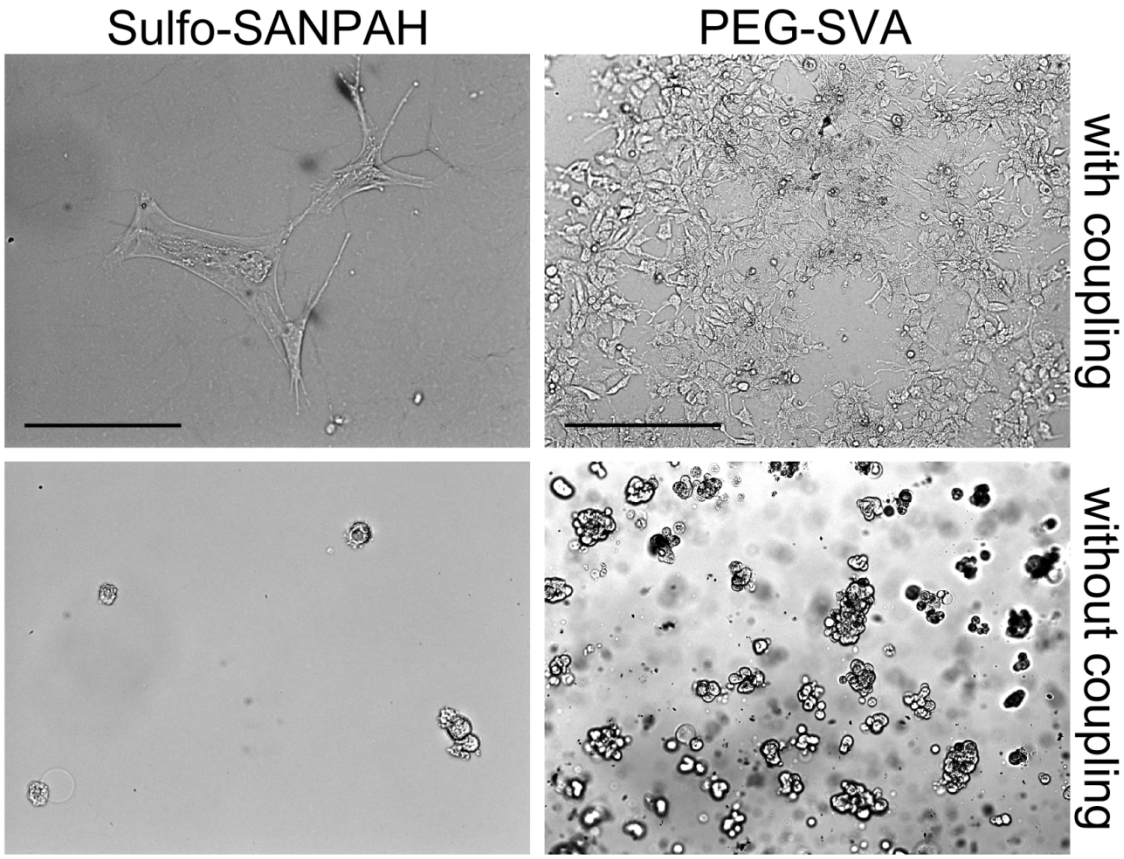

Figure 2.9 Cell adhesion can be controlled through protein coupling. (Left) HASMCs on PEG-PC (170 kPa) with (top) or without (bottom) sulfo-SANPAH and collagen I at 10 μg/cm^2; scale bar is 100 μm. (Right) HEP3B cells on PEG-PC (8.3 kPa) with (top) or without (bottom) PEG-succinimidyl valerate (PEG-SVA) and 65% collagen III, 23% collagen I, and 2% fibronectin at 5 μg/cm^2; scale bar is 200 μm. Figure adapted with permission from [9]. © 2013 American Chemical Society.

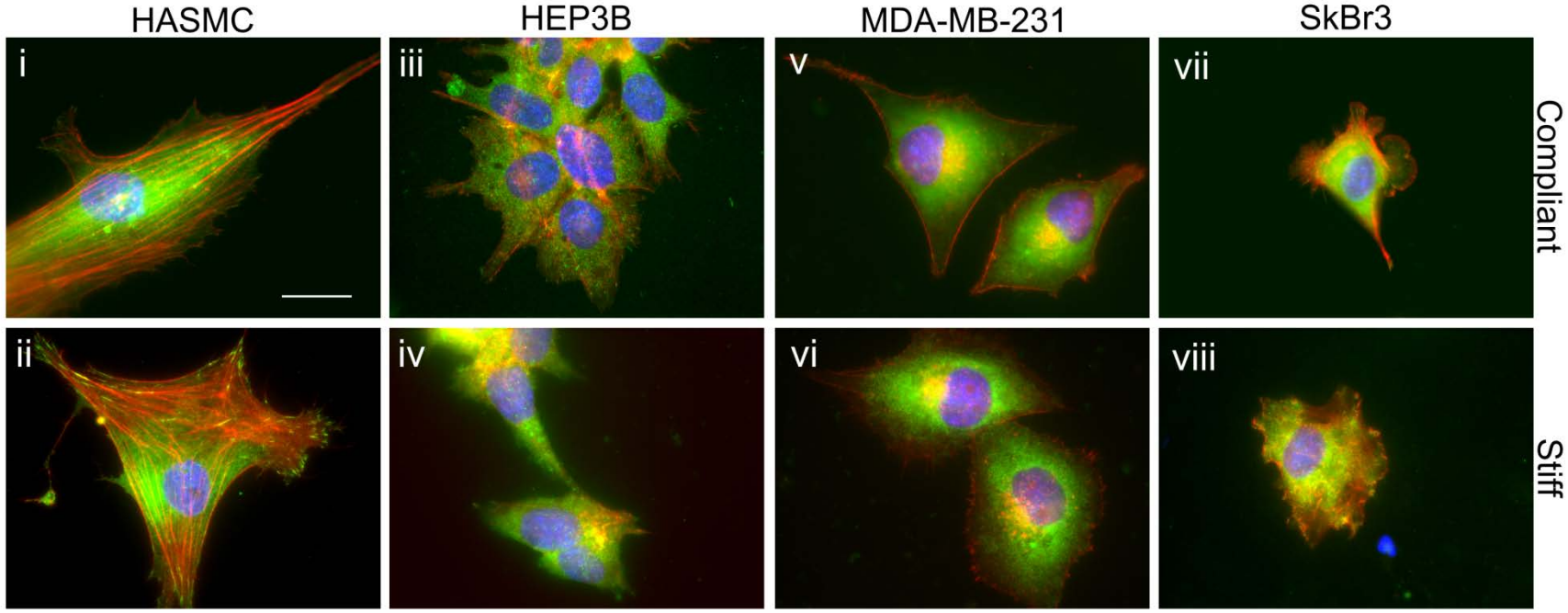

Figure 2.10 Modulus and integrin-binding on PEG-PC gels controls cell morphology. (i, ii) HASMCs on PEG-PC (compliant = 3 and stiff = 170 kPa, respectively, except for SkBr3 for which stiff = 400 kPa) with collagen I. Vinculin = green, F-actin = red, and Nucleus = blue. (iii, iv) HEP3Bs. (v, vi) MDA-MB-231s. (vii, viii) SkBr3s. Scale bar is 20 μm. Figure adapted with permission from [9]. © 2013 American Chemical Society.

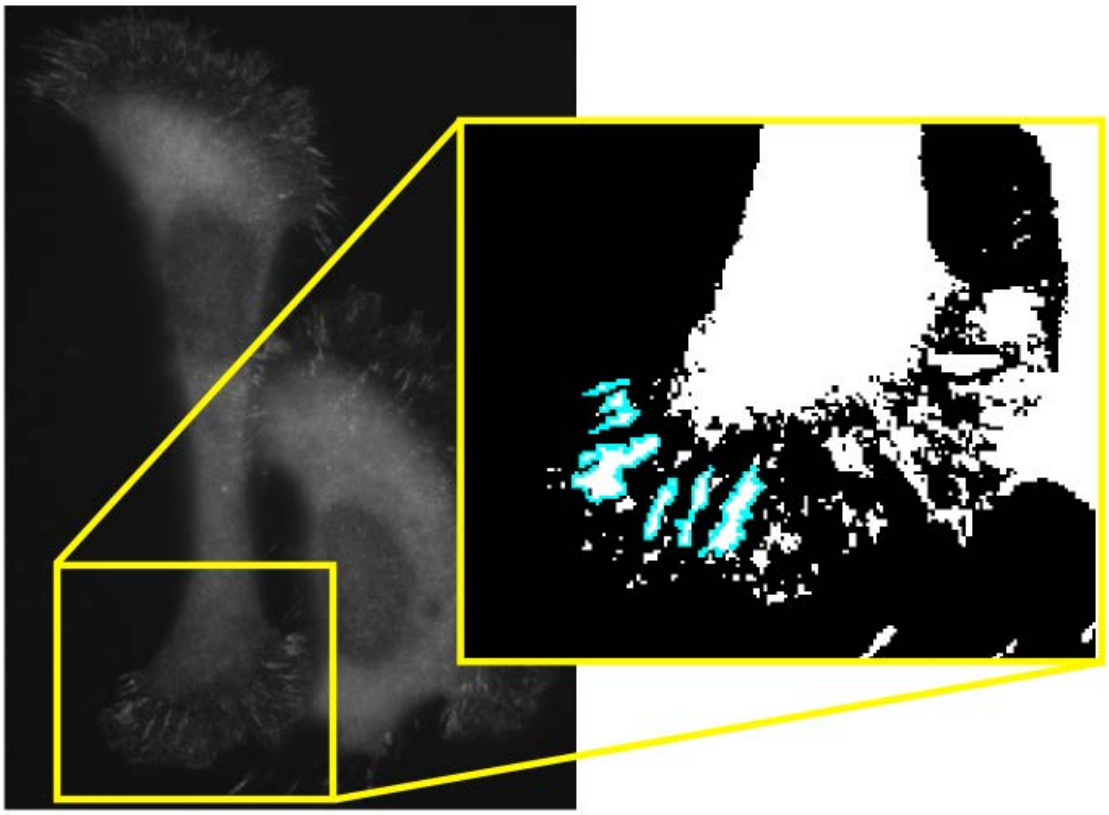

Figure 2.11 Image thresholding and focal adhesion tracing. Image thresholding and focal adhesion tracing (labeled vinculin) were performed in ImageJ. Figure adapted with permission from [9]. © 2013 American Chemical Society.

In order to demonstrate that cells sense differences in the stiffness of PEG-PC hydrogels, the number of focal adhesions, their areas, and shapes were quantified. Liver cancer (HEP3B) and two breast cancer cell lines (SkBr3 and MDA-MB-231) were cultured for 48 h on PEG-PC gels of varying stiffness, coupled with 10 μg/cm^2 collagen I. The cells were then fixed and stained for vinculin, which co-localizes with focal adhesions. ImageJ was used to quantify the focal adhesions (Figure 2.11). HEP3Bs had significantly fewer focal adhesions per cell on the 165 and 400 kPa gels compared the 18 kPa gels, whereas the amount of focal adhesions of the other cell lines did not show any significant difference with respect to stiffness (Figure 2.12A). Focal adhesion area decreased with Young's modulus in SkBr3 and 231 cells (areas on the stiffest PEG-PC

were reduced approximately 37% and 45% from the softer PEG-PC hydrogels, $p < 0.05$ and $p < 0.01$, respectively), and interestingly, HEP3B focal adhesion area is biphasic (area on 26 kPa PEG-PC is 65% larger than on 18 and 165 kPa, $p < 0.01$) (Figure 2.12B). SkBr3 was the only cell line that had focal adhesion elongation decreases with increasing stiffness (Figure 2.12C). These results demonstrate the ability of PEG-PC hydrogel mechanical properties to tune cytoskeletal organization and reveal that mechanosensitivity is cell line specific. The proliferation of these cell lines on the same stiffnesses and the Spearman correlation between the proliferation and focal adhesion were also quantified. There was not any correlation between proliferation and focal adhesion area or elongation (Figure 2.13).

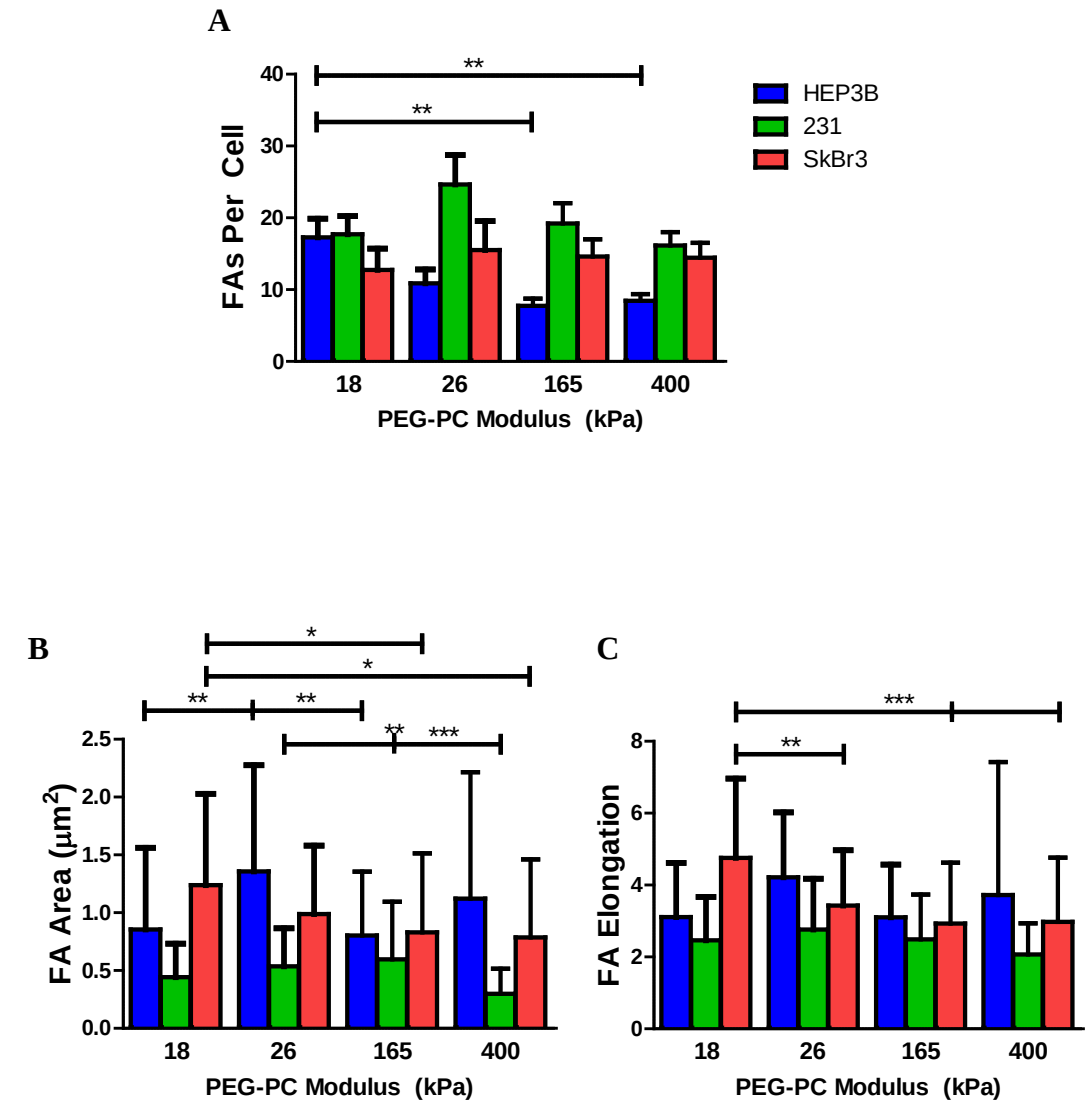

.

Figure 2.12 Focal adhesion characterization. PEG-PC modulus control of focal adhesions is cell-specific. Average number of focal adhesions (FA) counted per cell **(A)**, average focal adhesion area **(B)**, and average focal adhesion elongation **(C)** as a function of PEG-PC modulus. Figure adapted with permission from [9]. © 2013 American Chemical Society.

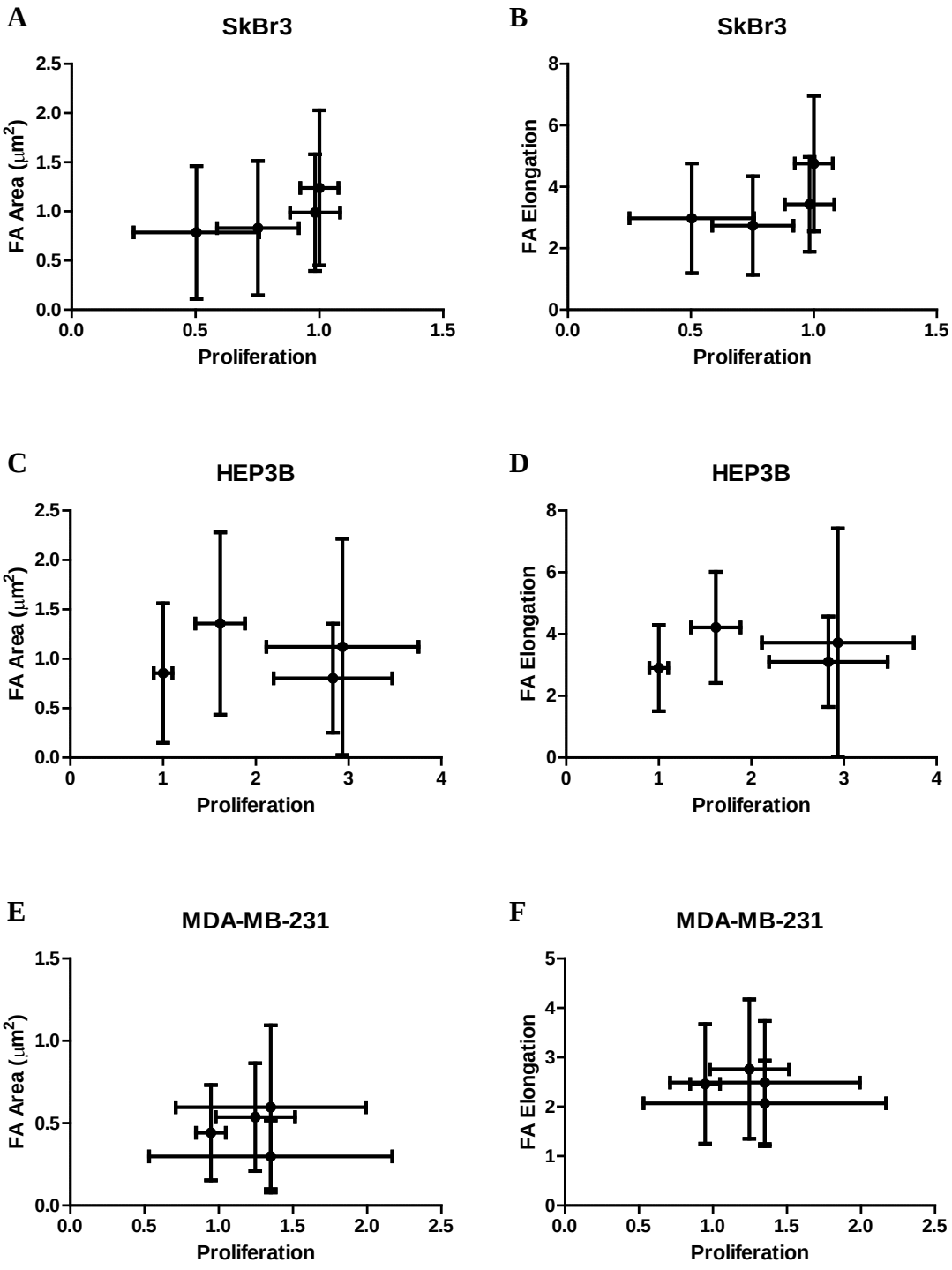

Figure 2.13 Correlation between focal adhesion and proliferation. There is not any correlation between proliferation and area or shape of focal adhesions. Correlation between proliferation and focal adhesion area of **(A)** SkBr3, **(C)** HEP3B, **(E)** MDA-MB-231. Correlation between proliferation and focal adhesion elongation of **(B)** SkBr3, **(D)** HEP3B, **(F)** MDA-MB-231.

2.5 Discussion

With 17 wt % (0.6 M) of PC, polymerization of PEG-PC hydrogels can be achieved with the amount of PEGDMA cross-linker as low as 7.4 mM, which results in 0.9 kpa hydrogels, and the hydrogel stiffness can be expanded up to 9,300 kPa at 0.7 M of PEGDMA (Figure 2.14). PEG-PC hydrogels can also be polymerized with lower concentrations of PC combined with higher concentrations of PEGDMA such as with 13.5 wt % PC (Figure 2.15) and 8 wt % PC (Figure 2.16). However, the hydrogels only remain transparent with an addition of PEGDMA cross-linker up to 0.3 M, whereas PEGDMA only hydrogels are opaque at low PEGDMA and become more transparent as the cross-linker concentration increases (Figure 2.17).

[PEGDMA] (M)	0.007	0.015	0.022	0.029	0.043	0.057	0.084	0.135	0.30	0.40	0.50	0.70
[PEGDMA] (wt.%)	0.55	1.1	1.6	2.2	3.2	4.3	6.3	10.1	20	30	40	55
E (kPa)	0.9	2.8	8.2	18	41	64	170	500	2060	4900	7500	9300
SD (kPa)	0.2	0.8	1.5	2.6	5.9	3.7	22	74	66	350	80	920
N	7	6	9	6	6	4	5	8	4	6	3	6

Figure 2.14 Young's modulus of PEG-PC. Increasing the PEGDMA also increases the Young's Modulus. The PC content was held at 17 wt. % (0.6 M). Figure adapted with permission from [9]. © 2013 American Chemical Society.

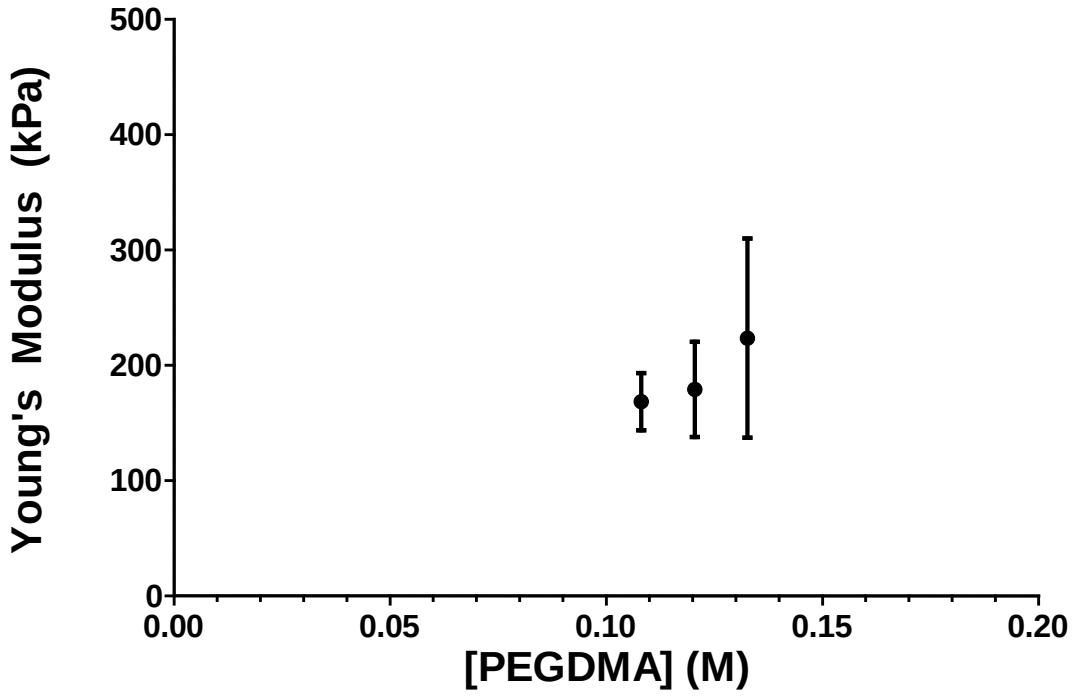

Figure 2.15 Young's modulus of PEG-PC at 0.5 M PC. Young's modulus, E, of PEG-PC hydrogels as a function of PEG cross-linker concentration from 108 mM to 133 mM. PC was held at 13.5 wt. % (0.5 M). Error bars are standard deviations.

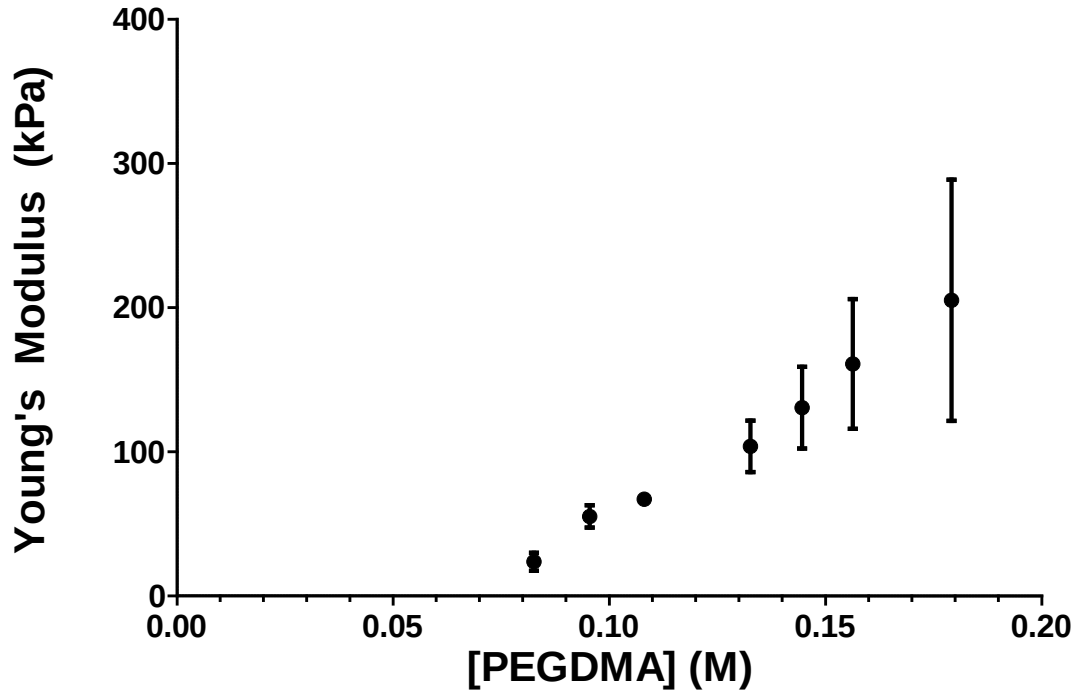

Figure 2.16 Young's modulus of PEG-PC at 0.3 M PC. Young's modulus, E, of PEG-PC hydrogels as a function of PEG cross-linker concentration from 83 mM to 179 mM. PC was held at 7.6 wt. % (0.3 M). Error bars are standard deviations.

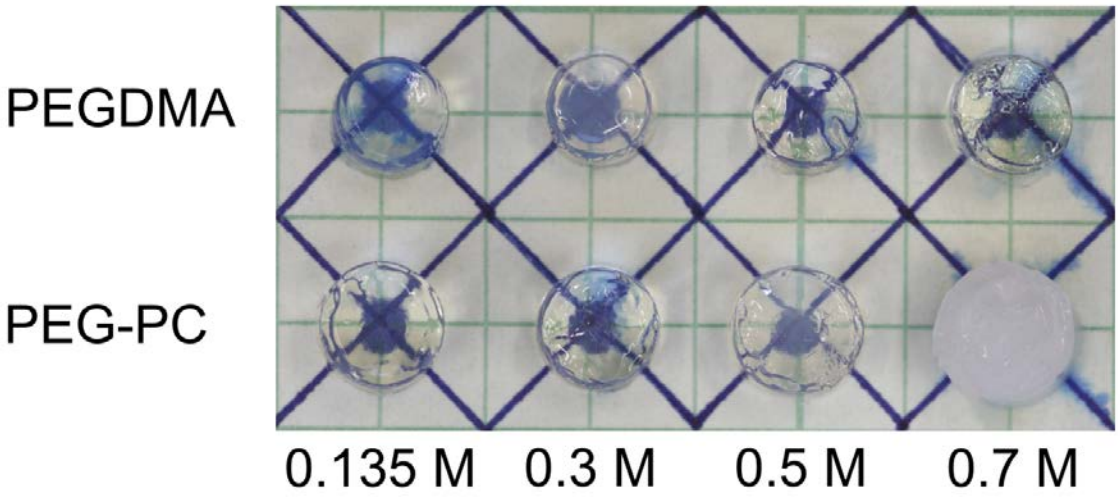

Figure 2.17 Images of PEG-PC hydrogels. PEG-PC hydrogels are optically transparent at low PEGDMA concentrations. The concentrations shown are of PEGDMA. PEG-PC hydrogels are 0.6 M PC. Figure adapted with permission from [9]. © 2013 American Chemical Society.

The range of stiffness of PEG-PC hydrogels is much wider than PEGDMA only hydrogels, and it covers the stiffness of many tissue types such as liver (5-55 kPa) [12–14], breast tumors (134-166 kPa) [15], articular cartilage (950 kPa), spinal cord (89 kPa), thyroid (9 kPa) [16]. PEGDMA hydrogels cannot polymerize at concentrations less than 70 mM (5 wt %), limiting the range of moduli obtainable. Incorporation of the PC polymer allows polymerization with as low as 7.4 mM PEGDMA (0.5wt %). This is likely due to the overall increase in polymer mass contributed from the PC. The 135 mM cross-linker hydrogels had mesh sizes half that of a 135 mM PEGDMA gel without PC, whereas the Young's modulus is nearly 10 times higher [17], implying the inherent structural changes when PC is incorporated. At concentrations of PEGDMA above 135 mM, there was a regime change within the hydrogel from a PC-domintated structure to a PEG-dominated structure. The changes in Young's modulus and mesh size are less dependent on cross-linker concentration as opposed to lower PEGDMA regime. However, the swelling behavior in this regime is still largely dependent on PEGDMA concentrations. Overall, the ability of PEG-PC to form two very different polymer structures may explain for its impressive mechanical range.

PEG-PC hydrogels allow independent tunability of stiffness and ligand density and have enhanced hydrophilicity for reduction of nonspecific protein adsorption while maintaining high optical clarity for modern quantitative microscopy techniques. PEG is a well characterized amphiphilic polymer, and PEG-based hydrogels are widely used in many biological applications due to its biocompatibility. PC molecules contain phospholipid groups, which are major components of biological membrane. Thus, combining PC and PEG to make PEG-PC results in highly biocompatible hydrogels. In

their studies, Ishihara et al. suggests that the state of water molecule around PC polymers is different from that of general amphiphilic polymers [7]. PC-incorporated polymers have large amount of free water in hydrated state, which is similar to the state water in aqueous solution. Thus, when a protein molecule in aqueous solution is in contact with the polymer surface, it does not need to release bound water molecules. This phenomena prevents the hyrophobic interactions between the protein molecule and the hydrophobic part of the polymer, which is a mechanism for protein adsorption. Protein molecules can contact PC-incorporated polymers reversibly without going through an irreversible conformational change in structure, which allows exposure of hydrophobic domains, leading to hydrophobic interactions [7]. This unique property of the PC groups imparts a highly anti-protein adsorption characteristic to PEG-PC hydrogels. Furthermore, PEG-PC hydrogels were experimentally shown to be more resistant to BSA adsorption compared to PEGDMA hydrogels of the same modulus, and the amount of adsorbed protein is inversely related to the PC content of the hydrogel (Figure 2.7). These results further confirm the non-fouling properties of PC. Another hydrophilic hydrogel system widely used is derived from hyaluronic acid [18–20]. However, hyaluronic acid can have bioactivity through interaction with CD44 receptors in certain cell types [18,20]. Thus, PC has the advantage of being biocompatible without interfering with cell behavior.

When HASMC, HEP3B, SkBr3, and MDA-MB-231 cell lines were cultured on PEG-PC gels from 18 to 400 kPa Young's moduli functionalized with collagen I, their focal adhesion properties corresponding to substrate modulus were cell-type dependent. These cell types originate from tissues that have different stiffnesses; thus their stiffness sensing can be different among cell type. Besides, the mechanotransduction machinery

depends on many factors such as integrins, proteins that make up adhesion complexes, proteins that regulate actin assembly at adhesion sites, and many more. For example, β_1 integrin is a major integrin that binds to collagen I [21], and SkBr3 cells inherently have lower β_1 intergin expression compared to MDA-MB-231 [22]. This partially helps to explain some observed differences in their focal adhesion properties between these two cell lines.

2.6 Conclusions

A new biomaterial platform, PEG-PC, was developed through copolymerization of PEGDMA polymers and PC monomers. This novel biomaterial has a much wider range of Young's modulus and more anti-adsorptive to non-specific protein bindings than PEGDMA hydrogels. Its impressive mechanical properties, which can be tuned over four orders of magnitude in Young's modulus, make it an ideal platform for mechanotransduction studies. It was demonstrated that different cell types can be cultured on PEG-PC surfaces and can sense different stiffnesses. In addition, PEG-PC is inexpensive and easy to synthesize, and these advantages will make it feasible for other labs to apply this system in their studies of cellular responses to ECM modulus.

2.7 References

[1] S.R. Peyton, C.B. Raub, V.P. Keschrumrus, A.J. Putnam. The use of poly(ethylene glycol) hydrogels to investigate the impact of ECM chemistry and mechanics on smooth muscle cells. Biomaterials. 2006. 27: 4881–93.

[2] J.S. Temenoff, K.A. Athanasiou, R.G. Lebaron, A.G. Mikos. Effect of poly (ethylene glycol) molecular weight on tensile and swelling properties of oligo (poly (ethylene glycol) fumarate) hydrogels for cartilage tissue engineering. 2001.

[3] S.P. Zustiak, J.B. Leach. Hydrolytically degradable poly(ethylene glycol) hydrogel scaffolds with tunable degradation and mechanical properties. Biomacromolecules. 2010. 11: 1348–57.

[4] A.T. Metters, K.S. Anseth, C.N. Bowman. Fundamental studies of a novel , biodegradable PEG- b -PLA hydrogel. 2000. 41: 3993–4004.

[5] G.P. Raeber, M.P. Lutolf, J. a Hubbell. Molecularly engineered PEG hydrogels: a novel model system for proteolytically mediated cell migration. Biophys. J. 2005. 89: 1374–88.

[6] Y. Iwasaki, K. Ishihara. Phosphorylcholine-containing polymers for biomedical applications. Anal. Bioanal. Chem. 2005. 381: 534–46.

[7] K. Ishihara, H. Nomura, T. Mihara, K. Kurita, Y. Iwasaki, N. Nakabayashi. Why do phospholipid polymers reduce protein adsorption? J. Biomed. Mater. Res. 1998. 39: 323–30.

[8] T. Goda, J. Watanabe, M. Takai, K. Ishihara. Water structure and improved mechanical properties of phospholipid polymer hydrogel with phosphorylcholine centered intermolecular cross-linker. Polymer (Guildf). 2006. 47: 1390–1396.

[9] W.G. Herrick, T. V Nguyen, M. Sleiman, S. McRae, T.S. Emrick, S.R. Peyton. PEG-phosphorylcholine hydrogels as tunable and versatile platforms for mechanobiology. Biomacromolecules. 2013. 14: 2294–304.

[10] S. McRae Page, S. Parelkar, A. Gerasimenko, D.Y. Shin, S.R. Peyton, T. Emrick. Promoting cell adhesion on slippery phosphorylcholine hydrogel surfaces. J. Mater. Chem. B. 2014. 2: 620.

[11] Y. Chang, Y.J. Shih, R.C. Ruaan, A. Higuchi, W.Y. Chen, J.Y. Lai. Preparation of poly(vinylidene fluoride) microfiltration membrane with uniform surface-copolymerized poly(ethylene glycol) methacrylate and improvement of blood compatibility. J. Memb. Sci. 2008. 309: 165–174.

[12] R. Masuzaki, R. Tateishi, H. Yoshida, T. Sato, T. Ohki, T. Goto, et al. Assessing liver tumor stiffness by transient elastography. Hepatol. Int. 2007. 1: 394–7.

[13] N. Ganne-Carrié, M. Ziol, V. de Ledinghen, C. Douvin, P. Marcellin, L. Castera, et al. Accuracy of liver stiffness measurement for the diagnosis of cirrhosis in patients with chronic liver diseases. Hepatology. 2006. 44: 1511–7.

[14] F. Vizzutti, U. Arena, R.G. Romanelli, L. Rega, M. Foschi, S. Colagrande, et al. Liver stiffness measurement predicts severe portal hypertension in patients with HCV-related cirrhosis. Hepatology. 2007. 45: 1290–7.

[15] J.M. Chang, I.A. Park, S.H. Lee, W.H. Kim, M.S. Bae, H.R. Koo, et al. Stiffness of tumours measured by shear-wave elastography correlated with subtypes of breast cancer. Eur. Radiol. 2013. 23: 2450–8.

[16] I. Levental, P.C. Georges, P. a. Janmey. Soft biological materials and their impact on cell function. Soft Matter. 2007. 3: 299.

[17] S.R. Peyton, Z.I. Kalcioglu, J.C. Cohen, A.P. Runkle, K.J. Van Vliet, D. a Lauffenburger, et al. Marrow-derived stem cell motility in 3D synthetic scaffold is governed by geometry along with adhesivity and stiffness. Biotechnol. Bioeng. 2011. 108: 1181–93.

[18] Y. Kim, S. Kumar. CD44-mediated Adhesion to Hyaluronic Acid Contributes to Mechanosensing and Invasive Motility. Mol. Cancer Res. 2014.

[19] B. Ananthanarayanan, Y. Kim, S. Kumar. Elucidating the mechanobiology of malignant brain tumors using a brain matrix-mimetic hyaluronic acid hydrogel platform. Biomaterials. 2011. 32: 7913–23.

[20] S. Khetan, M. Guvendiren, W.R. Legant, D.M. Cohen, C.S. Chen, J. a Burdick. Degradation-mediated cellular traction directs stem cell fate in covalently crosslinked three-dimensional hydrogels. Nat. Mater. 2013. 12: 458–65.

[21] J.D. Humphries, A. Byron, M.J. Humphries. Integrin ligands at a glance. J. Cell Sci. 2006. 119: 3901–3.

[22] C.C. Park, H. Zhang, M. Pallavicini, J.W. Gray, F. Baehner, C.J. Park, et al. Beta1 integrin inhibitory antibody induces apoptosis of breast cancer cells, inhibits growth, and distinguishes malignant from normal phenotype in three dimensional cultures and in vivo. Cancer Res. 2006. 66: 1526–35.

CHAPTER 3

THE ROLE OF THE EXTRACELLULAR MATRIX CUES IN CELL PROLIFERATION AND DRUG RESPONSE

3.1 Abstract

The tissue ECM has a crucial role in modulating the normal function of many cell types in the tissue, and deregulation of this matrix can cause different types of disease including cancers. The change from a normal ECM, which is the basement membrane ECM, to the cancerous ECM, which is rich in fibrillar collagens, induced some breast and liver cancer cells to be more resistant to sorafenib, and this trend is cell-type dependent. The proliferation of many cancer cell lines was regulated by the substrate modulus; however, the trend of proliferation with modulus also depends on the cell type. High-throughput platforms were developed from different types of hydrogels such as PAA, PEG, and PEG-PC. These platforms can be coupled with various types of ECM protein or cocktail of ECM protein. These platforms can allow multiple drugs to be tested with many cells on various moduli and proteins that capture the physicochemical properties of the tissue ECM.

3.2 Introduction

In drug development, multiple compounds are tested in plastic multi-well plates, followed by preclinical and clinical trials. This process costs over one billion dollars, and takes 11 to 15 years per drug on average [1]. The cost burden is partially caused by inefficiencies in high-throughput screening, as small molecule candidates often show efficacy in cells on plastic plates, but fail in animal or human trials. In order to improve high-throughput screening, compounds should be tested in cells on biomaterial platforms that have the ability to capture tissue properties. Traditionally, the cell-based high-throughput screening is usually done with cells plated on multi-well plastic plates such as 96- or 384- well plates. These plastic plates lack relevant chemical and physical cues, which are found in the ECM of native tissues. The tissue ECM is much softer than plastic plates, and it contains many growth factors and proteins that drive the cell biological functions through binding to cellular growth factor receptors and integrins [2,3]. Often, disruption in ECM homeostasis will lead to disorganized and deregulated ECM, resulting in cancer development and growth [2,4,5]. Hence, it is necessary to develop a new drug testing platform that not only includes human cell lines and appropriate growth factors but also allows a precise control over integrin-binding and substrate stiffness. Many groups are spurring the development of novel cell culture platforms for more rational and predictive drug discovery [6–8]; however, I found that existing systems are either cumbersome to use, or have limited adaptability. In response, I adapted the novel PEG-PC hydrogel system, an easy to use biomaterial, which is optically transparent, forms gels ranging from 1-10,000 kPa in Young's modulus, can be coupled with any protein or peptide of interest, and rapidly polymerizes within 96-well plates [9]. This novel platform

allowed me to quantify drug response in a high-throughput manner across a range of stiffness and integrin-binding conditions.

3.3 Materials And Methods

3.3.1 Cell culture

All supplies were purchased from Life Technologies (Carlsbad, CA) unless otherwise noted. Human breast cancer cell lines (MDA-MB-231, BT549, MCF7 and SkBr3) were generous gifts from Dr. Shannon Hughes at the Massachusetts Institute of Technology, and were cultured in Dulbecco's Modified Eagle's Medium (DMEM) supplemented with 10% fetal bovine serum (FBS) and 1% penicillin-streptomycin (P/S) at 37ºC and 5% CO_2. Human hepatocellular carcinoma (HCC) cells (HEP3Bs, American Type Culture Collection, Manassas, VA) were cultured in modified Eagle's medium (MEM) supplemented with 10% FBS and 1% P/S at 37ºC and 5% CO_2. Human breast cancer cell lines HCC38 and AU565 were generous gifts from Dr. Mario Niepel at the Harvard University, and they were cultured in Roswell Park Memorial Institute (RPMI) medium supplemented with 10% FBS and 1% P/S at 37ºC and 5% CO_2.

3.3.2 Protein coating and drug treatment on 96-well tissue culture plates

Sterile fibronectin protein solutions at different concentrations (0.5, 2.5, 5, 10 $\mu g/cm^2$) were made by mixing human plasma fibronectin (EMD Millipore, Billerica, MA) in a buffer solution (pH ~ 9.4 with acetic acid) that contains sodium carbonate (Thermo Fisher Scientific, Waltham, MA) and sodium bicarbonate (Thermo Fisher Scientific) at 15 mM and 35 mM, respectively. 100 µL of the fibronectin solution were added to each well of 96-well plates, and the plates were incubated overnight at 4ºC.

After incubation, the plates were washed 3 times with sterile phosphate buffered saline (PBS) and then incubated with sterile 10 mg/mL of pluronic F127 (Sigma-Aldrich, St. Louis, MO) dissolved in PBS. After a day of pluronic blocking at 4ºC, the plates were washed 3 times with sterile PBS, and 10,000 cells/well were seeded in serum-free medium. After 24 h, the medium was replaced with serum-free medium supplemented with 20 ng/mL of platelet-derived growth factor (PDGF-BB, eBioscience, San Diego, CA) and 20 ng/mL of epidermal growth factor (EGF, R&D Systems, Minneapolis, MN). After 24 h, cells were treated with sorafenib (LC Laboratories, Woburn, MA) from 0 to 30 μM, diluted in growth factor supplemented serum-free medium. After 24 h, cell proliferation was quantified with CellTiter 96 AQueous One Solution Cell Proliferation Assay (Promega, Madison, WI) (20 μL of assay per well and 4 hour incubation) and read at 490 nm (BioTek ELx800 microplate reader, BioTek, Winooski, VT). Cell apoptosis was quantified with propidium iodine (Life Technologies). When the propidium iodide was used, the medium in each well was aspirated and replaced with 200 μL of 4.5 μM propidium iodide in PBS. After 30 minute incubation at 37ºC, the plate was read at 530/620 nm wavelength (emission/excitation) with a fluorescent plate reader (Spectramax, Molecular Devices, Sunnyvale, CA). The inhibitory concentration at 50% (IC-50) was calculated with Prism v5.04 (GraphPad Software, La Jolla, CA).

For the collagen-rich ECM coating, the protein cocktail (5 $\mu g/cm^2$ total) was comprised of 65% type I collagen (rat tail, Life Technologies), 33% type III collagen (FibroGen, San Francisco, CA), and 2% fibronectin. The plates were incubated with both collagen I and III mixed in 0.02 M acetic acid for a day and then with fibronectin in sodium carbonate/bicarbonate buffer for another day before blocking with pluronic F127.

The plates were kept at 4ºC during the incubations and washed 3 times with PBS between each incubation. For the basement membrane ECM, the protein cocktail (0.5 μg/cm^2 total) was comprised of 46% collagen IV (Neuromics, Edina, MN), 46% fibronectin and 8% mouse laminin (Life Technologies). The procedure is similar to collagen-rich ECM coating with the exception that the plate was incubated with collagen IV in 0.02 M acetic acid for a day before incubating fibronectin and laminin mixed in sodium carbonate/bicarbonate buffer for another day. After blocking with pluronnic F127, the cell seeding and sorafenib treatment were similar to that described above.

3.3.3 Quantification of cell adhesion

HEP3B cells were seeded on a collagen-rich and basement membrane ECM-coated 96-well plate. After 24 h of adhesion, cells were washed with warm PBS, and 50 μL of 0.5 % (wt./v.) crystal violet (Thermo Fisher Scientific) in 20% (v./v.) methanol in water were added to each well. The plate was incubated for 10 min at room temperature. Then the plate was washed twice with PBS, and 100 uL of 1% (wt./v.) sodium dodecyl sulfate (SDS) in water was added to solubilize the stain. The plate was shaken on a plate shaker until all stains were dissolved, and then the absorbance was read at 570 nm on a plate reader (BioTek).

3.3.4 Real-time quantification of Caspase 7 activity

The plasmids that were used for expression of caspase-activable green fluorescent protein (CA-GFP) were a generous gift from Dr. Jeanne Hardy (Department of Chemistry, University of Massachusetts Amherst). The plasmids were inserted into E. Coli bacteria in a cuvette through electroporation with the Gene Pulser Xcell™ system (Bio-Rad Laboratories, Hercules, CA). After electroporation, 100 μL of Super Optimal

Broth (SOC) was added immediately into the cuvette, and the cuvette was incubated at 37ºC for 1 h. After incubation, 1 μL of bacterial solution was mixed with 99 μL of SOC medium, and the mixture was spread evenly on an agar plate. The agar plate was made with 1.5% wt./v. agar in Lysogeny Broth (LB) supplemented with 0.1 mg/mL ampicillin (Thermo Fisher Scientific) (prepared at 500x or 50 mg/mL in water). The plate was incubated at 37ºC for 16-20 h. After incubation, a colony was picked and incubated with 3 mL of LB medium, which is supplemented with 0.1 mg/mL ampicillin, for 16-20 h at 37ºC with shaking at 225 rpm. The plasmids were then purified using Pureyield™ Plasmid Miniprep System (Promega) following the manufacturer's protocol. The plasmid concentrations were determined with the NanoDrop (Thermo Fisher Scientific).

HEP3B cells were allowed to adhere to a 24 well plate. The cells were transfected with 1,000 ng of plasmid per well using Lipofectamine reagent (Life Technologies) following the manufacturer's protocol. Briefly, the plasmids were diluted in 100 μL Opti-Mem (Life Technologies). 0.5 μL of PLUS reagent was added into the mixture, and it was incubated for 15 min at room temperature. During the incubation, the cells were washed with Opti-MEM, and the medium was replaced with Opti-MEM. After a 15 min incubation, 2 μL of Lipofectamine reagent was added to the plasmid complex mixture, and the mixture was incubated for 25 min before being transferred to the well. After 5 h, the cells were washed and replaced with medium containing 10% FBS only. After 24 h, the cells were detached and seeded onto a glass-bottom 24-well plate (Mat Tek, Ashland, MA) coated with either collagen-rich or basement membrane ECM. After 24 h, the cells were treated with 4 μM sorafenib, and live-cell imaging was performed with a Zeiss Axio Observer Z1 microscope with a 63x oil immersion objective (Carl Zeiss AG,

Oberkochen, Germany). Images were analyzed in ImageJ (NIH, Bethesda, MD). The corrected total cell fluorescence (CTCF) was calculated from the following equation:

CTCF = Integrated Density - (area of selected cell x mean fluorescence of background readings)

3.3.5 96-well hydrogel platform

Glass-bottom 96-well plates (no. 1.5 coverslip glass; In Vitro Scientific, Sunnyvale, CA) were plasma treated (Harrick Plasma, Ithaca, NY) and subsequently methacrylate-silanized with 2 vol% 3-(trimethoxysilyl) propyl methacrylate (Sigma-Aldrich, St. Louis, MO) in 95% ethanol (adjusted to pH 5.0 with glacial acetic acid) for 5 min, washed 3 times with 100% ethanol, and dried at 40 °C for 30 min.

To make PEG-PC hydrogels, PEGDMA (Mn 750, Sigma-Aldrich), from 0.6-9.1 wt%, was combined with 17 wt% 2-methacryloyloxyethyl phosphorylcholine (PC) (Sigma-Aldrich) in phosphate buffered saline (PBS). These PEGDMA crosslinker concentrations tune the Young's moduli of the resulting gels from 6 to 400 kPa [9]. Solutions were sterilized using a 0.2 μm syringe filter (Thermo Fisher Scientific) and degassed by nitrogen sparging for 30s. Free-radical polymerization was induced by addition of 0.05 wt% ammonium persulfate (APS) and 0.125 vol% tetramethylethylenediamine (TEMED, Bio-Rad Laboratories). Hydrogels of 40 μL per well in the 96-well plates were polymerized under nitrogen for 10 min.

To make polyacryamide (PAA) hydrogels, acrylamide (40 wt % acrylamide solution) (A) and N, N'-methylenediacrylamide (2% bis solution) (B) are mixed together at different wt. % in 1X phosphate buffered saline (PBS, pH 7.0) in order to create hydrogels with various stiffnesses. Specifically, the combinations of 5%A/0.1%B,

8%A/0.2%B, 8%A/0.4%B, 8%A/0.6%B, 15%A/1.2%B (v./v.) create hydrogels that have these stiffnesses: 1, 22, 46, 52, and 308 kPa, respectively [10]. Solutions were sterile-filtered and degassed by nitrogen sparging. To induce polymerization in the 96-well plates, APS and TEMED were used at 0.02 wt% and 0.05 vol%, respectively.

To make PEG hydrogels, PEGDMA was mixed with PBS at different concentrations: 10, 15, 20, 25, 30 vol%. Solutions were sterile-filtered and degassed by nitrogen sparging. APS and TEMED were used at 0.1 wt% and 0.25 vol%, respectively.

Post-polymerization, hydrogels were allowed to swell for 24 h in PBS, then treated with 100 μL of sulfo-SANPAH (ProteoChem, Denver, CO; 0.6 mg/mL in pH 8.5 HEPES buffer) under UV light for 20 min, rinsed twice with HEPES buffer, and followed immediately by incubation with protein mixtures overnight. ECM protein mixtures defined as “bone” composed of 65% rat tail collagen I and 1% osteopontin (R&D Systems) at 5 $\mu g/cm^2$, "brain" composed of 50% fibronectin, 25% vitronectin (R&D Systems), 20% tenascin C (R&D Systems), and 5% mouse laminin at 1 $\mu g/cm^2$, or "lung" composed of 33% mouse laminin, 33% collagen IV, 15% collagen I, 15% fibronectin, 4% tenascin C at 2 $\mu g/cm^2$. When only collagen I was used, the concentration was 10 $\mu g/cm^2$. All proteins were mixed in pH 3.8 PBS. Post-protein coupling, the gels were rinsed twice with PBS, UV-sterilized for 1 h, and rinsed with sterile medium before cell seeding.

3.3.6 Proliferation of breast cancer cells

For the proliferation experiments on PEG-PC coupled with collagen I, SkBr3 and MDA-MB-231cells were seeded at 6,000 cells/well in serum-free DMEM with 1% P/S. HEP3B cells were seeded at 6,000 cells/well in MEM media with 10% FBS and 1% P/S.

After 24 h, the media was changed to 10% FBS media. Media was replenished every 2 days. Five days after seeding, the proliferation was measured with the CellTiter96 assay as described above.

For the proliferation experiments on PAA and PEG gels coupled with collagen I, 231s were seeded at 10,000 cells/well in DMEM with 10% FBS and 1% P/S. The proliferation was measured 2 days after seeding.

For the proliferation experiments on PEG-PC gels coupled with either "bone", "brain", or "lung" proteins, 231s and MCF7s were seeded at 6,000 cells/well in DMEM with 10% FBS and 1% P/S; HCC38 and AU565 were seeded at 6,000 cells/well in RPMI with 10% FBS and 1% P/S. The proliferation was measured 7 days after seeding.

3.3.7 Statistical Analysis

Statistical analysis was performed using Prism v5.04 (GraphPad Software, La Jolla, CA). Statistical significance was evaluated by either using unpaired Student's t tests (with Welch's correction as necessary) or one-way analysis of variance (ANOVA) with a Tukey post-test. Data are reported as mean ± standard deviation. $p \leq 0.05$ is denoted with *, ≤ 0.01 with **, and ≤ 0.001 with ***; $P > 0.05$ is considered not significant ("ns").

3.4 Results

3.4.1 The response of cancer cells to sorafenib depends on both ECM proteins and cell types

HEP3Bs were allowed to adhere to fibronectin coated on plastic plates at different protein concentrations and treated with sorafenib for 24 h. Both the IC-50s obtained from

the proliferation (Figure 3.1A) and apoptosis (Figure 3.1B) assays for sorafenib treatments indicate no significant difference across various protein concentrations. This result may suggest that the binding of HEP3Bs to fibronectin can be saturated at low protein concentration, and thus increasing the ligand density will not significantly alter HEP3Bs' responses to sorafenib. I also quantified the response of HEP3Bs to sorafenib in the presence of different protein cocktails that combined various proteins instead of just fibronectin. Similar to the results with fibronectin, the HEP3Bs' IC-50s were independent of protein concentration for both basement membrane ECM (collagen IV, laminin, and fibronectin) (Figure 3.2A) and collagen-rich ECM (collagen I, III, and fibronectin) (Figure 3.2B). Interestingly, the IC-50s on the collagen-rich ECM were higher than those on basement membrane ECM (4.6 vs. 3.1 μM). These results showed that the response of HEP3B to sorafenib is more dependent on the types of ligand binding than the ligand density.

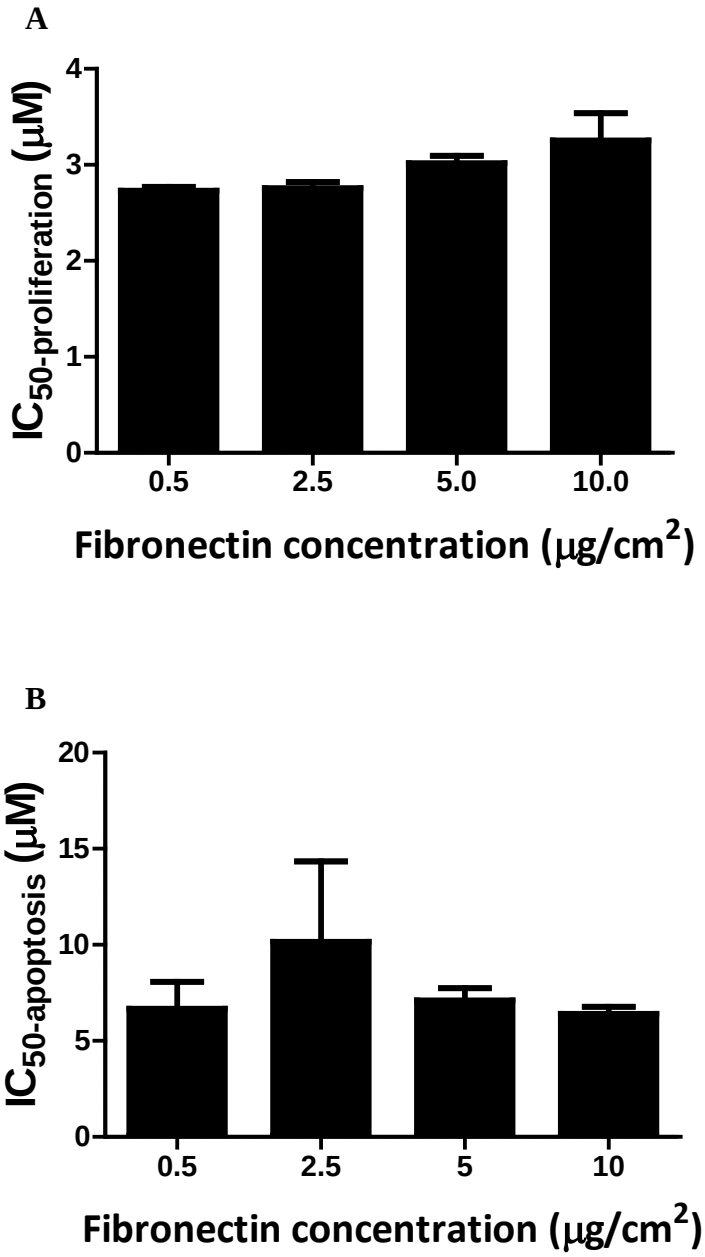

Figure 3.1 Sorafenib IC-50s of HEP3B cells across different fibronectin concentrations. The inhibitory concentrations at 50% (IC-50s) of HEP3Bs are not significantly different across different fibronectin concentrations. **(A)** IC-50s were calculated from the proliferation measurements with the CellTiter96 assay. **(B)** IC-50s were calculated from the apoptosis measurement with the propidium iodide assay.

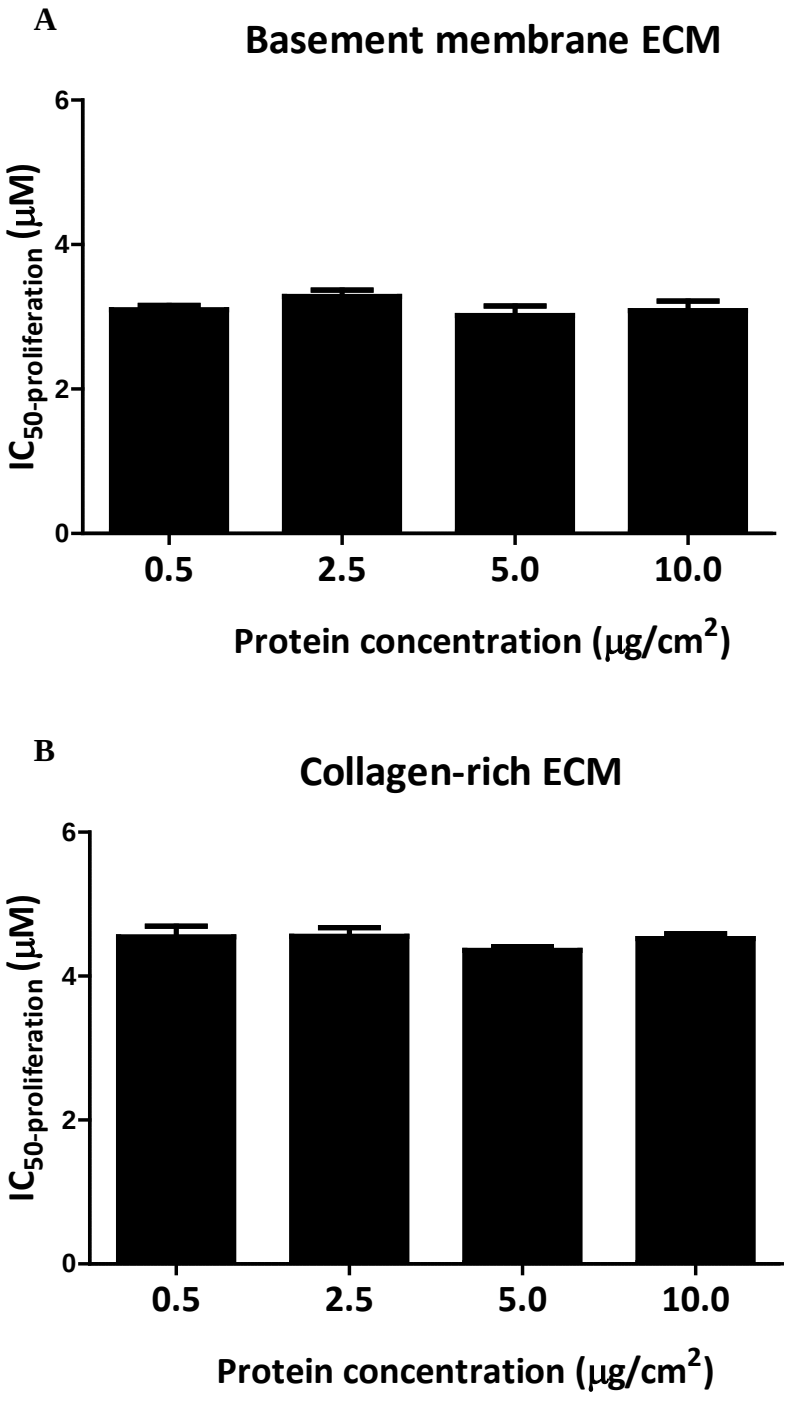

Figure 3.2 Sorafenib IC-50s of HEP3B cells across different protein mixture concentrations. The IC-50s of HEP3Bs are more dependent on protein types than protein concentrations. The IC-50s on **(A)** the basement membrane ECM (collagen IV, laminin, and fibronectin) are lower than those on **(B)** the collagen-rich (collagen I, III, and fibronectin), and the IC-50s on each ECM are similar across different concentrations.

Motivated by the interesting observations above, I quantified the IC-50s of the other cell lines in response to sorafenib when placed on 5 $\mu g/cm^2$ of collagen-rich ECM or 0.5 $\mu g/cm^2$ of basement membrane ECM (Figure 3.3). The IC-50s of HEP3Bs, MDA-MB-231s, and BT549s on collagen-rich ECM were 26%, 48%, and 54% higher than those on basement membrane ECM, respectively. However, the IC-50s of MCF7 and SkBr3 were not significantly different between the two ECMs. Therefore, the ability of cells to sense the differences in ECM binding was also cell type dependent. As a proof of concept, I used the crystal violet assay, which contains a DNA binding molecule, to quantify the HEP3B cell adhesion between the two ECMs. There was not any significant difference in the number of adherent cells between the collagen-rich and basement membrane ECMs (Figure 3.4). Thus, the difference in HEP3Bs' IC-50s between the two ECMs could not be caused by differences in cell adhesion.

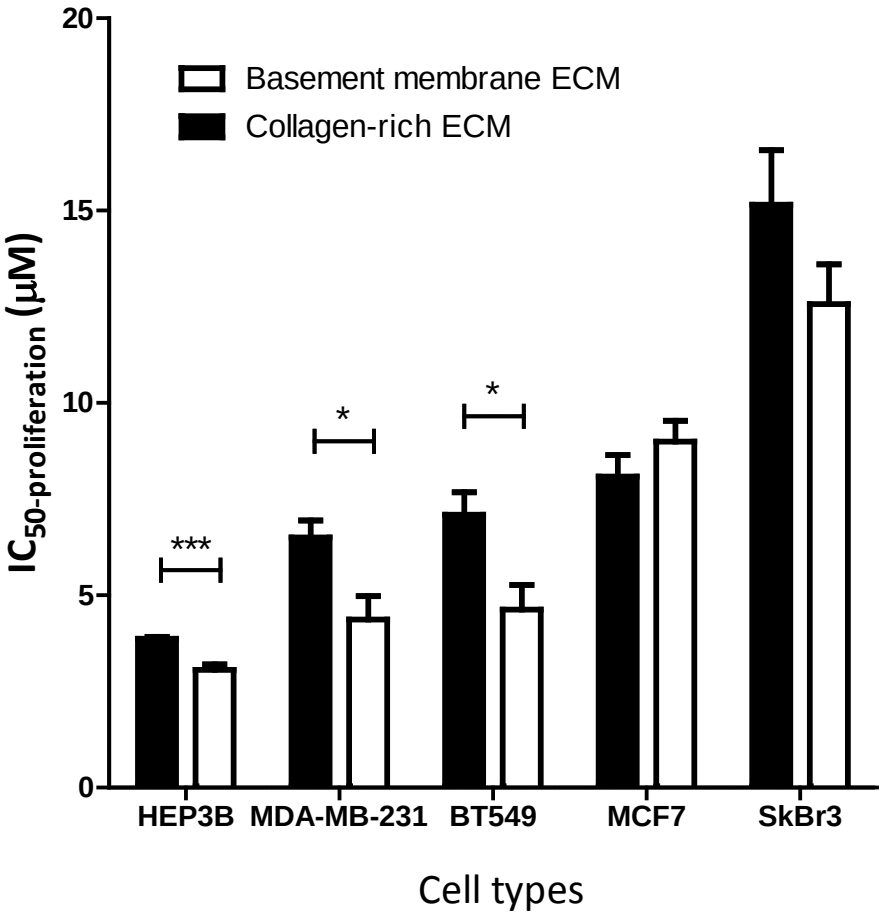

Figure 3.3 Sorafenib IC-50s multiple cell types across different protein mixture concentrations. Most of cell lines are more resistant to sorafenib when adhering collagen-rich ECM. HEP3B, MDA-MB-231, and BT549 are sensitive to the change in ECM, whereas SkBr3 and MCF7 are not.

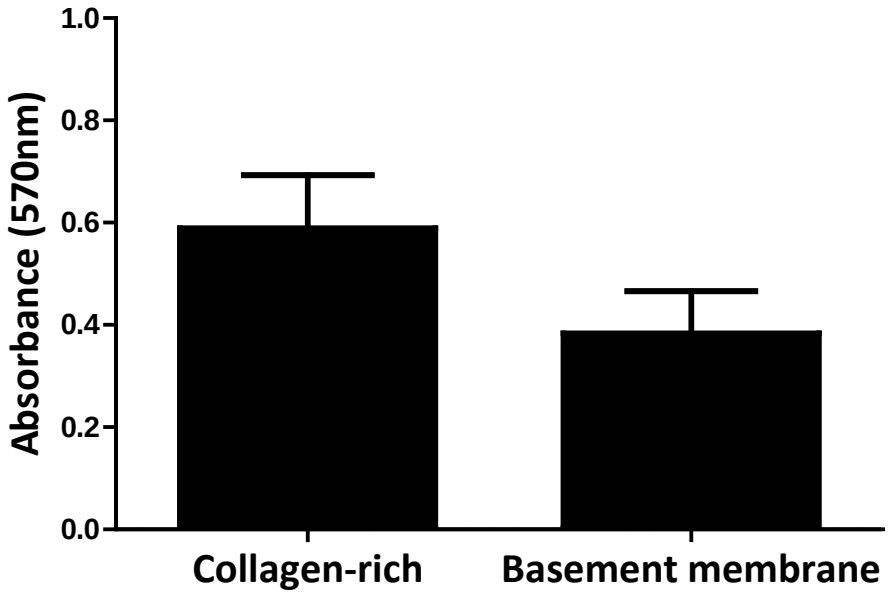

Figure 3.4 Adhesion quantification of HEP3B cells. The same amount of HEP3B cells adhere to both ECMs. Adhesion of HEP3Bs, which were quantified by crystal violet 24 h after cell seeding, is not significantly different between collagen-rich and basement membrane ECMs.

In addition, I quantified the response of HEP3B cells to sorafenib through the measurement of caspase-7 activity in real time. Caspase signaling plays an important role in regulating cellular apoptosis. Caspase-3/ -6/-7 are known to be the apoptosis executioners, which can cause cell shrinkage, membrane blebbing, and DNA fragmentation. These caspases can be activated by other upstream caspases such as caspase-2/-8/-9/-10 [11]. I transfected HEP3Bs with DNA plasmids that induced the expression of a green fluorescent protein (GFP). The GFP activity is fully quenched by a short peptide that contains the caspase-7 recognition site DEVA [12]. When caspase-7 is activated, it will cleave the quenching peptide to release the GFP. Therefore, the amount of GFP detected is correlated to the amount of caspase activation. Images of the GFP activation were taken in real time after HEP3Bs were treated with 4 μM of sorafenib

(Figure 3.5). However, the CTCF, which was quantified by imageJ, did not show any difference between the two ECMs (Figure 3.6).

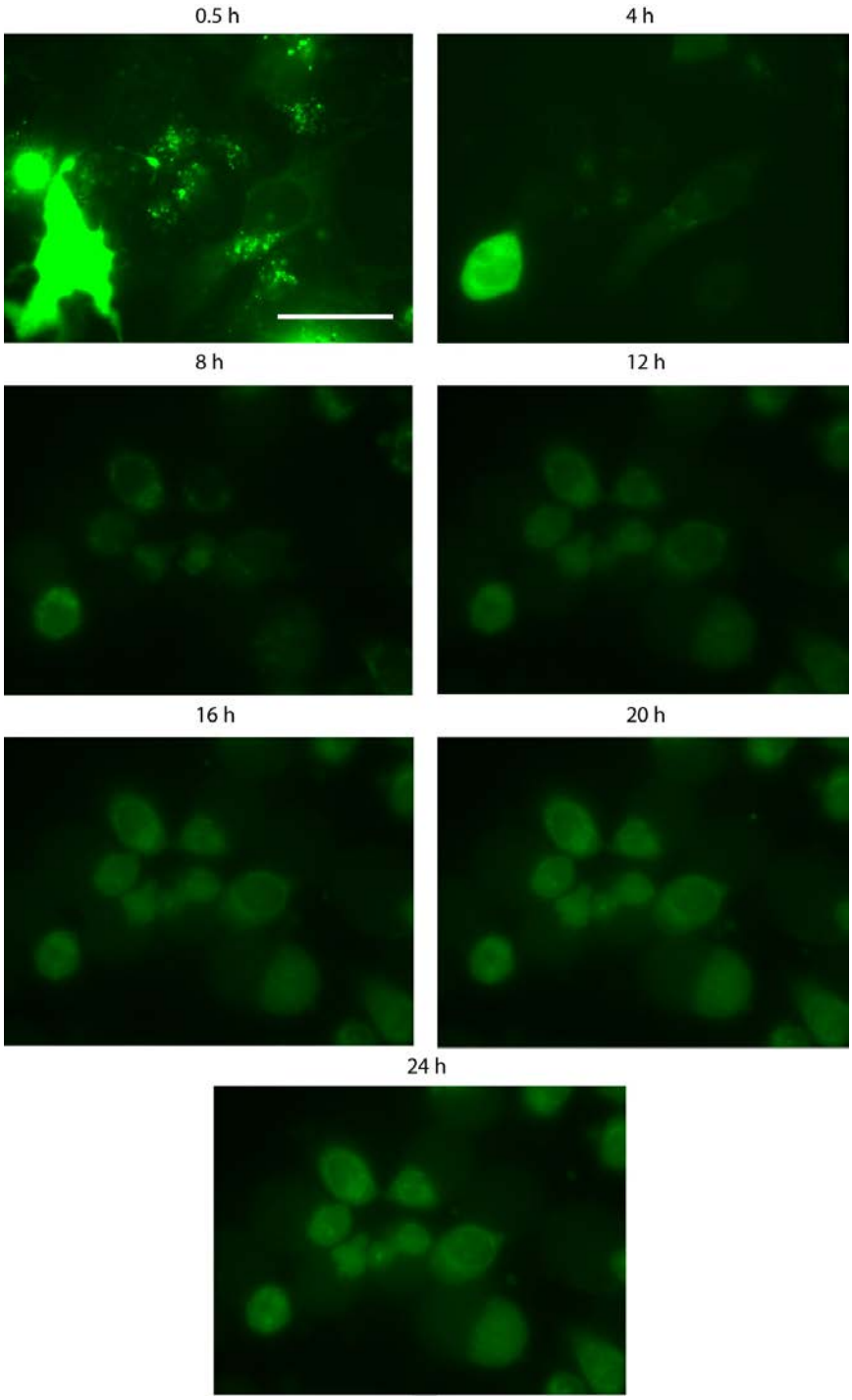

Figure 3.5 Expression of caspase-activable green fluorescent protein (CA-GFP) in HEP3B cells. HEP3Bs were transfected with plasmids that induced the expression of CA-GFP and allowed to adhere to the basement membrane ECM before treating with sorafenib. The GFP intensity keeps increasing over 24 hour under 4μM sorafenib treatment. Scale bar is 20 μm.

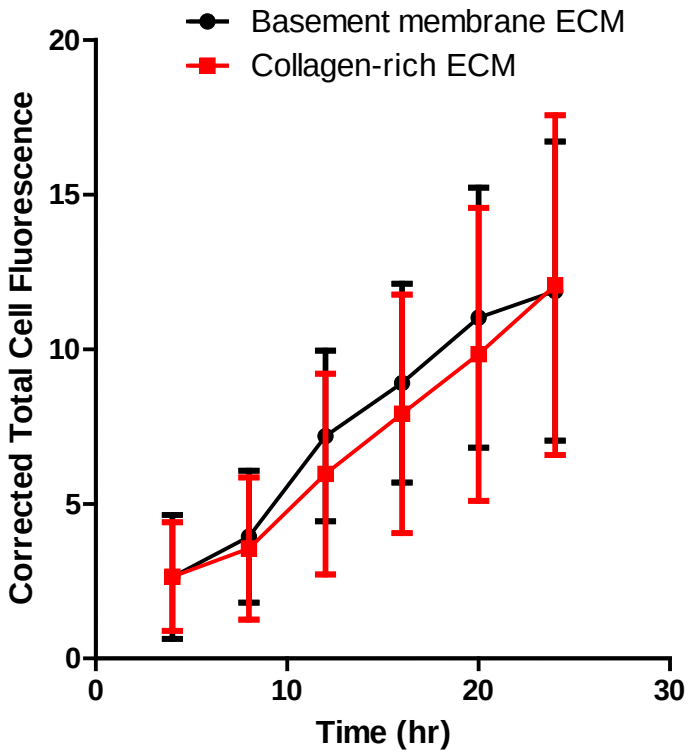

Figure 3.6 Fluorescent intensity of CA-GFP in HEP3B cells. The corrected total cell fluorescence increases over time and is similar between the two ECMs.

3.4.2 Substrate modulus affects cell proliferation

I adapted the PEG-PC, PAA, and PEG hydrogels into high-throughput platforms, which could be quickly used to study the relationship between mechanobiology and drug response. A representative image of PEG-PC gels in a 96-well plate is shown in Figure 3.7. The relationship between substrate modulus and cell proliferation was investigated with HEP3Bs, MDA-MB-231s, and SkBr3s. All cell lines were seeded on PEG-PC gels coupled with 10 $\mu g/cm^2$ collagen I. Both MDA-MB-231 and HEP3B cells showed an increase in proliferation with increasing PEG-PC modulus (Figure 3.8A and B). HEP3Bs were the most stiffness-sensitive cell line. Its proliferation increased nearly 3 fold between 18 and 165 kPa gels, whereas 231s showed a 26% increase in proliferation between 18 and 26 kPa gels before leveling off at higher stiffnesses. SkBr3 proliferation decreased approximately 50% between the softest and stiffest gel conditions (Figure 3.8C). MDA-MB-231s showed similar trends in increasing proliferation with increasing substrate modulus when placed on PAA gels (Figure 3.9) and PEG gels (Figure 3.10). While the proliferation on PAA gels showed a steady increase across the range of stiffness from 1 to 308 kPa, the proliferation trend on PEG-only gel was much more similar to PEG-PC gels with increasing proliferation at the lower stiffness range and saturating at higher stiffnesses (the modulus of 18.4% PEG-only gel was measured to be 174 ± 9.8 kPa).

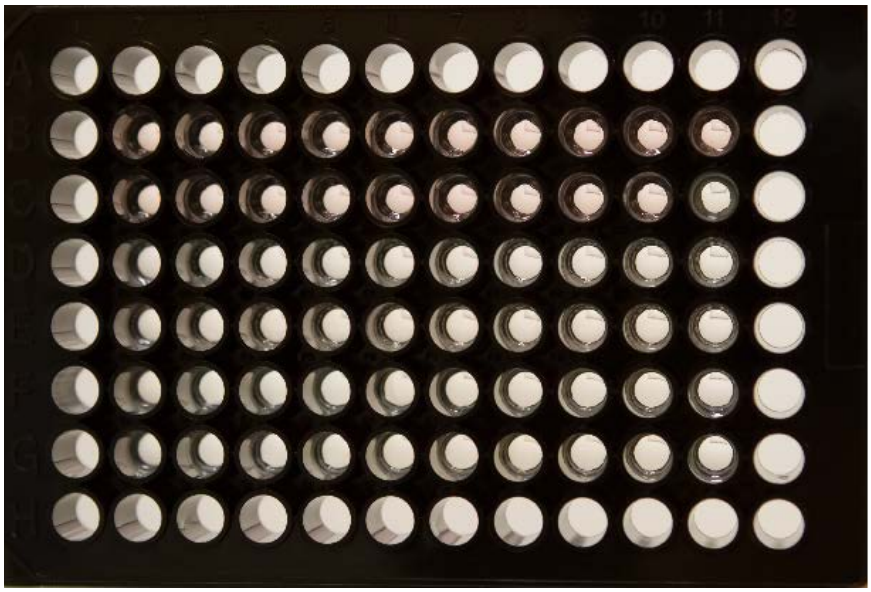

Figure 3.7 PEG-PC high-throughput platform. The high-throughput platform consists of a black-walled, glass bottom plate, with PEG-PC gels cast in each of the inner 6x10 wells.

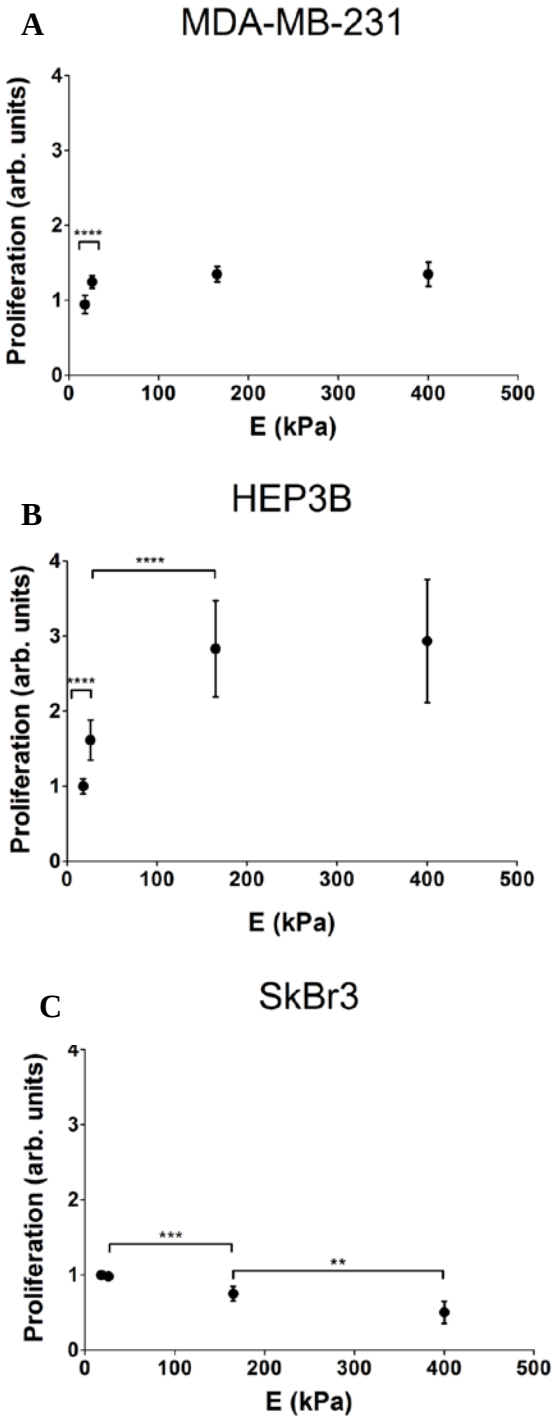

Figure 3.8 The proliferationof 231, HEP3B, and SkBr3 cells. The proliferation of **(A)** 231, **(B)** HEP3B, and **(C)** SkBr3 cells on PEG-PC, which is coupled with collagen I, from 18 to 400 kPa was quantified 5 days post-seeding. Results are the fold changes relative to the softest condition (18 kPa). HEP3Bs' proliferation is strongly dependent on substrate modulus whereas the proliferations of 231s and SkBr3s are less sensitive to substrate modulus and display opposing trends. Figure adapted with permission from [9]. © 2013 American Chemical Society.

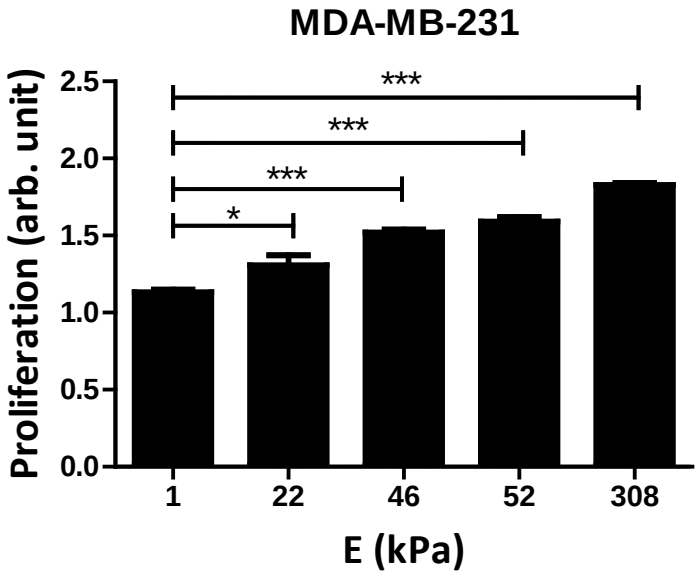

Figure 3.9 The proliferation of 231 cells on PAA gels. The proliferation of 231 cells on PAA gels coupled with collagen I increases with increasing substrate modulus. The proliferation was quantified 2 day post-seeding.

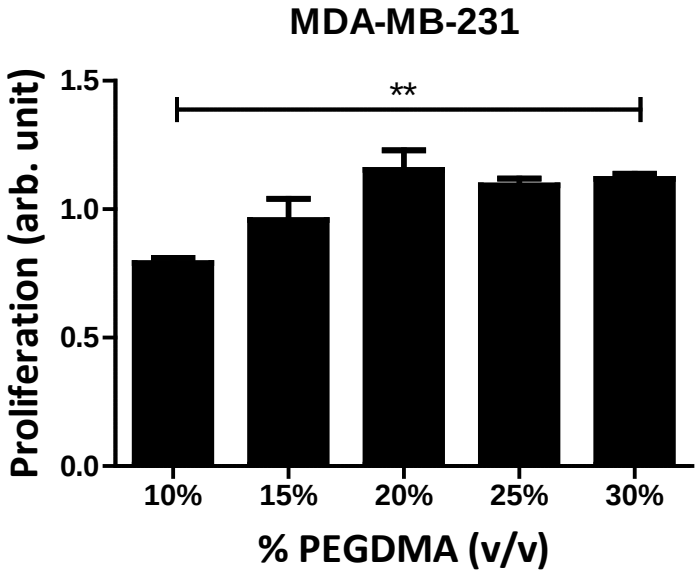

Figure 3.10 The proliferation of 231 cells on PEG-only gels. The proliferation of 231 cells on PEG-only gels coupled with collagen I increases with increasing PEGDMA concentrations at lower concentrations. The proliferation was quantified 2 day post-seeding.

3.4.3 Proliferation can be regulated by both substrate modulus and ECM proteins

MDA-MB-231s, MCF7s, HCC38s, and AU565s were placed on 6, 23, and 400 kPa PEG-PC gels that were coupled ECM proteins found in the brain (fibronectin, vitronectin, tenascin C, laminin), lung (laminin, collagen IV, collagen I, fibronectin, tenascin), and bone (collagen I and osteopontin). Both 231s and HCC38s proliferated more on lung and bone compared to brain, but there was not any significant difference between lung and bone (Figure 3.11A and B). However, AU565s were most proliferative on lung (Figure 3.11C), whereas MCF7s showed similar proliferation across the three different environments (Figure 3.11D).

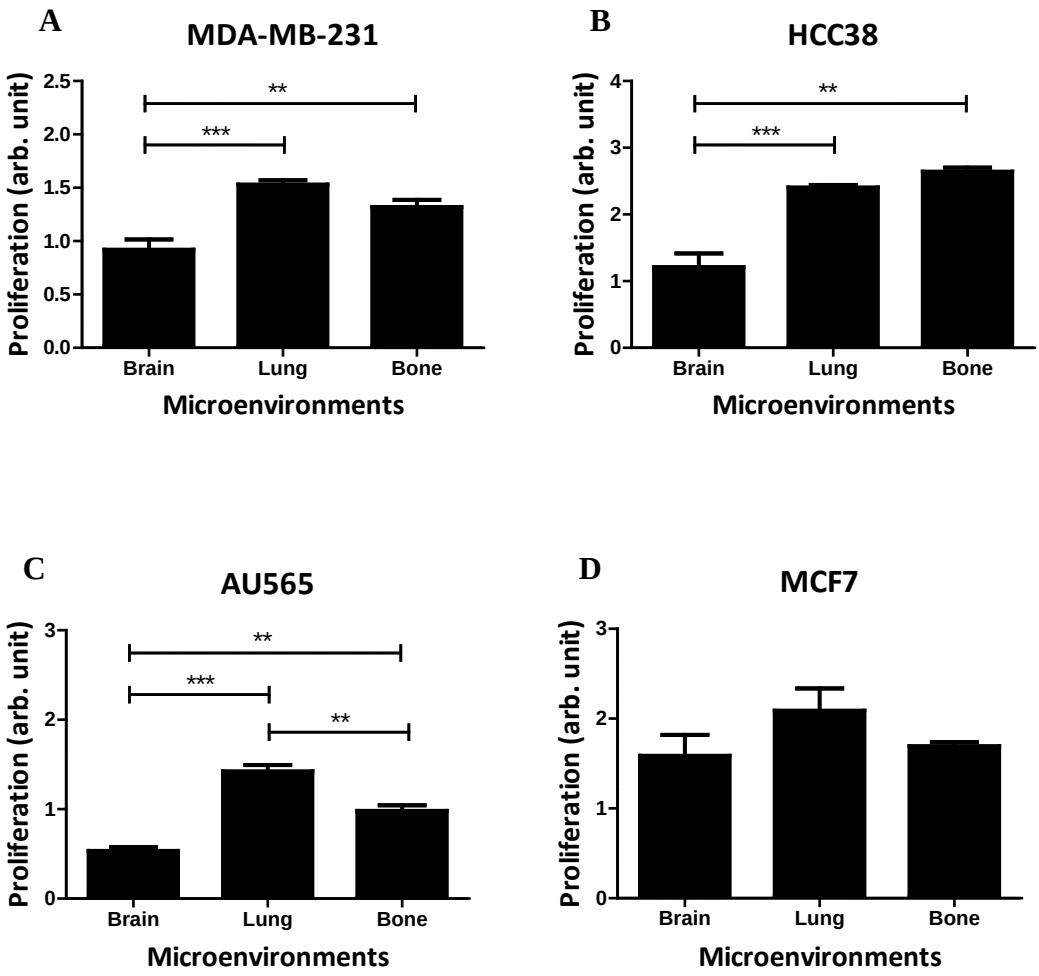

Figure 3.11 The proliferation of many cell types across different microenvironments. The proliferation on different microenvironments is cell-type dependent. Both **(A)** 231s and **(B)** HCC38s show similar trends in proliferation and are more proliferative on lung and bone compare to brain microenvironment. **(C)** AU565s' proliferation is strongly dependent on types of microenvironments, whereas **(D)** MCF7s are not sensitive to the changes in microenvironments.

3.5 Discussion

The tumor microenvironment plays an important role in mediating signals for cancer cells to grow, resist chemotherapies, and metastasize to distal tissues [13–16]. Cancer cells can receive biochemical signals from the tumor microenvironment through growth factors released in the tumor tissue or binding of their integrins to ECM proteins. Integrins are heterodimers composed of an α- and a β-subunits. Different heterodimerizations of α- and β-subunits are required when the cells bind to different types of ECM protein [17]. Binding of integrins to ECM proteins can mediate many different downstream signaling pathways such as PI3K/Akt and Ras/Raf/ERK to promote cell survival and proliferation or Rho/ROCK pathway to enhance cell motility [18], and integrin binding can also induce the drug resistance of cancer cells to other chemotherapeutic drugs [19]. Therefore, the switching of the basement membrane ECM, which is a representative of normal ECM [4], to the collagen-rich ECM, which is a representative of tumor ECM [4], can mediate resistance to sorafenib, which targets the Raf/ERK pathway [20]. The sorafenib resistance was observed in several cell lines such as HEP3Bs, 231s, and BT549s (Figure 3.3). Binding to collagen I was shown to mediate ERK signaling in T-Lymphocytes, whereas binding to laminin or fibronectin did not sustain ERK activation [21]. Thus, the presence of relevance ECM binding proteins is necessary for cell-based drug screening. Integrin structure, expression and downstream signaling was found to be heterogeneous across breast cancer cell lines [22]. Perhaps, this could be an explanation for the heterogeneous responses among different cell types toward the changes in ECM proteins (HEP3B, MDA-MB-231, and BT549 vs. MCF7 and SkBr3) and the insensitivity of HEP3Bs toward the changes in protein concentration.

Although HEP3B cells seeded on collagen-rich were more resistant to sorafenib, the caspase-7 activation was similar between the two ECMs (Figure 3.6). The GFP was only activated after the cells were already dead and round, from 8 h to 24 h (Figure 3.5). There was not any change in GFP detected between 0.5 h and 8 h during the transition from being alive to being dead. These results can be indicative of non-caspase induced death mechanism in HEP3B liver cancer cells. In two other liver cancer cell lines, sorafenib was shown to induce cell death via caspase-3 activation in HEPG2, but not in PCL/PRF/5 cells [20]. Sorafenib was also shown to induce apoptosis via nuclear translocation of apoptosis-inducing factor (AIF) in melanoma cells [23]. A few cells were found to have caspase-7 activated when sorafenib was added for just 0.5 h (cells in the bottom left corner of 0.5 h image, Figure 3.5). These cells could be dying via caspase-7 induced pathway due to natural causes before the addition of sorafenib since 0.5 h is too short for sorafenib to have any major effect.

As a proof of concept, cell proliferation was shown to be regulated by substrate modulus when cells were placed on PEG, PEG-PC, and PAA hydrogels coupled with collagen I (Figure 3.8, 3.9, 3.10). However, this modulus-regulated cell proliferation is cell-type dependent. Thus it is important to include relevant tissue modulus into the drug screening process since many drugs work by a mechanism of dampening cell proliferation.

When both substrate modulus and ECM proteins were varied, the substrate modulus and the ECM proteins synergistically regulate cell proliferation in certain cell type. MCF7 cell proliferation was insensitive to changes in microenvironments, and AU565 cells proliferated the most on the intermediate gel coupled with lung proteins

(Figure 3.11C). Thus, proliferation in this cell line is not a function of substrate modulus. Both MDA-MB-231 and HCC38 showed the similar proliferation trend as they proliferated the most on lung and bone gels. This could be due to the fact that lung and bone gels are stiffer than brain gels. 231s' proliferation saturated at gels that were stiffer than 26 kPa when they were seeded on collagen I (Figure 3.8A), and this trend is similar to the proliferation trend on brain (6 kPa), lung (23 kPa), and bone (400 kPa). This could infer that 231 proliferation is more strongly influenced by stiffness than the change in ECM proteins. Interesting, both 231s and HCC38s are triple negative, whereas AU565 and MCF7 are HER2+ and luminal, respectively. Therefore, the relationship between cell proliferation and microenvironments could be subtype-dependent.

3.6 Conclusions

I have shown that both ECM proteins and substrate modulus play an important role in regulating cell proliferation and response to drugs. The interactions between cells and these physicochemical cues are also dependent on cell types and subtype. Thus, both of these variables should be included in the cell-based high-throughput drug screening in order to bridge the gap between *in vitro* and *in vivo* models. The synthetic biomaterial platforms PEG-PC, PAA, and PEGDMA, which allow independent control of mechanical properties and ligand binding, were developed and proven to be useful for quantifying cell-matrix interactions in a high-throughput manner.

3.7 References

[1] M. Dickson, J.P. Gagnon. Key factors in the rising cost of new drug discovery and development. Nat. Rev. Drug Discov. 2004. 3: 417–29.

[2] C. Frantz, K.M. Stewart, V.M. Weaver. The extracellular matrix at a glance. J. Cell Sci. 2010. 123: 4195–200.

[3] M. a Glukhova, C.H. Streuli. How integrins control breast biology. Curr. Opin. Cell Biol. 2013. 25: 633–41.

[4] P. Lu, V.M. Weaver, Z. Werb. The extracellular matrix: a dynamic niche in cancer progression. J. Cell Biol. 2012. 196: 395–406.

[5] M.E. Blaauboer, F.R. Boeijen, C.L. Emson, S.M. Turner, B. Zandieh-Doulabi, R. Hanemaaijer, et al. Extracellular matrix proteins: A positive feedback loop in lung fibrosis? Matrix Biol. 2013.

[6] C.H. Kwon, I. Wheeldon, N.N. Kachouie, S.H. Lee, H. Bae, S. Sant, et al. Drug-Eluting Microarrays for Cell-Based Screening of Chemical-Induced Apoptosis. Anal. Chem. 2011.

[7] A. Skardal, L. Smith, S. Bharadwaj, A. Atala, S. Soker, Y. Zhang. Tissue specific synthetic ECM hydrogels for 3-D in vitro maintenance of hepatocyte function. Biomaterials. 2012. 33: 4565–75.

[8] D.M. Timm, J. Chen, D. Sing, J. a Gage, W.L. Haisler, S.K. Neeley, et al. A high-throughput three-dimensional cell migration assay for toxicity screening with mobile device-based macroscopic image analysis. Sci. Rep. 2013. 3: 3000.

[9] W.G. Herrick, T. V Nguyen, M. Sleiman, S. McRae, T.S. Emrick, S.R. Peyton. PEG-phosphorylcholine hydrogels as tunable and versatile platforms for mechanobiology. Biomacromolecules. 2013. 14: 2294–304.

[10] S.R. Peyton, A.J. Putnam. Extracellular matrix rigidity governs smooth muscle cell motility in a biphasic fashion. J. Cell. Physiol. 2005. 204: 198–209.

[11] T.-J. Fan, L.-H. Han, R.-S. Cong, J. Liang. Caspase Family Proteases and Apoptosis. Acta Biochim. Biophys. Sin. (Shanghai). 2005. 37: 719–727.

[12] S.B. Nicholls, J. Chu, G. Abbruzzese, K.D. Tremblay, J. a Hardy. Mechanism of a genetically encoded dark-to-bright reporter for caspase activity. J. Biol. Chem. 2011. 286: 24977–86.

[13] A.L. Correia, M.J. Bissell. The tumor microenvironment is a dominant force in multidrug resistance. Drug Resist. Updat. 2012. 15: 39–49.

[14] L. a Liotta, E.C. Kohn. The microenvironment of the tumour-host interface. Nature. 2001. 411: 375–9.

[15] K. Pietras, A. Ostman. Hallmarks of cancer: interactions with the tumor stroma. Exp. Cell Res. 2010. 316: 1324–31.

[16] T.L. Whiteside. The tumor microenvironment and its role in promoting tumor growth. Oncogene. 2008. 27: 5904–12.

[17] J.D. Humphries, A. Byron, M.J. Humphries. Integrin ligands at a glance. J. Cell Sci. 2006. 119: 3901–3.

[18] R.O. Hynes. Integrins : Bidirectional , Allosteric Signaling Machines In their roles as major adhesion receptors , integrins. 2002. 110: 673–687.

[19] A. E. Berman, N.I. Kozlova, G.E. Morozevich. Integrins as a potential target for targeted anticancer therapy. Biochem. Suppl. Ser. B Biomed. Chem. 2012. 6: 205–210.

[20] L. Liu, Y. Cao, C. Chen, X. Zhang, A. McNabola, D. Wilkie, et al. Sorafenib blocks the RAF/MEK/ERK pathway, inhibits tumor angiogenesis, and induces tumor cell apoptosis in hepatocellular carcinoma model PLC/PRF/5. Cancer Res. 2006. 66: 11851–8.

[21] S. Gendron, J. Couture, F. Aoudjit. Integrin α2β1 inhibits Fas-mediated apoptosis in T lymphocytes by protein phosphatase 2A-dependent activation of the MAPK/ERK pathway. J. Biol. Chem. 2003. 278: 48633–48643.

[22] A. Taherian, X. Li, Y. Liu, T. a Haas. Differences in integrin expression and signaling within human breast cancer cells. BMC Cancer. 2011. 11: 293.

[23] D.J. Panka. The Raf Inhibitor BAY 43-9006 (Sorafenib) Induces Caspase-Independent Apoptosis in Melanoma Cells. Cancer Res. 2006. 66: 1611–1619.

CHAPTER 4

SORAFENIB RESISTANCE AND JNK SIGNALING IN CARCINOMA DURING EXTRACELLULAR MATRIX STIFFENING

4.1 Abstract

Tumor progression is coincident with mechanochemical changes in the extracellular matrix (ECM). I hypothesized that tumor stroma stiffening, alongside a shift in the ECM composition from a basement membrane-like microenvironment toward a dense network of collagen-rich fibers during tumorigenesis, confers resistance to otherwise powerful chemotherapeutics. To test this hypothesis, I applied the high-throughput drug screening PEG-PC platform that I created as described in Chapter 3, and customized it to capture the stiffness and integrin-binding profile of *in vivo* tumors. I report that the efficacy of a Raf kinase inhibitor, sorafenib, is reduced on stiff, collagen-rich microenvironments, independent of ROCK activity. Instead, sustained activation of JNK mediated this resistance, and combining a JNK inhibitor with sorafenib eliminated stiffness-mediated resistance in triple negative breast cancer cells. Surprisingly, neither ERK nor p38 appears to mediate sorafenib resistance, and instead, either ERK or p38 inhibition rescued sorafenib resistance during JNK inhibition, suggesting negative crosstalk between these signaling pathways on stiff, collagen-rich environments. Overall, I discovered that β_1 integrin and its downstream effector JNK mediate sorafenib

resistance during tumor stiffening. These results also highlight the need for more advanced cell culture platforms, such as this high-throughput PEG-PC system, with which to screen chemotherapeutics.

4.2 Introduction

The tumor microenvironment plays an important role in providing a niche to nurture the growth of cancer cells [1]. Recently, stromal cells, growth factors, cytokines, and ECM proteins in the tumor microenvironment have been implicated in promoting resistance to chemotherapeutics as well [2, 3]. Specifically, certain stromal growth factors mediate cell proliferation in the presence of otherwise powerful chemotherapeutic drugs. For example, hepatocyte growth factor (HGF) imparts resistance to vemurafenib in melanoma [4, 5], and TGF-β induces the expansion of cancer stem-like cells, which are responsible for chemotherapy-resistance and relapses [6]. These growth factors are generally thought to be released by local stromal fibroblasts, which upon DNA-damage from treatments with a combination of mitoxantrone and docetaxel, or radiation stimulate prostate cancer cell proliferation and invasion through β-catenin signaling [7]. In addition to soluble growth factors, a change in adhesive ECM proteins in the tissue can confer resistance to chemotherapeutics via integrin-mediated signaling [8-11].

This evolution in the microenvironment during tumor progression is mediated by stromal fibroblasts, which differentiate into myofibroblasts [12] and cancer-associated fibroblasts (CAFs) [13], and remodel the ECM by breaking down the basement membrane and depositing fibril forming collagens [14-16]. The increase in crosslinked fibrous collagens results in tissue stiffening [17, 18], which stimulates cell proliferation

[17, 19], invasion and intravasation [20, 21], disrupts cell-cell adhesion [22], and alters cell sensitivity to growth factors [23], while simultaneously limiting the diffusion of therapeutic agents into the tumor [24].

I hypothesized that these mechanochemical changes in the ECM during tumor progression may induce drug resistance in carcinoma. Testing this hypothesis required a drug testing platform that included not only human cell lines and appropriate growth factors, but also tailored control over integrin-binding and ECM stiffness. Therefore, I applied the high-throughput PEG-PC platform, which was described in chapter 3, as a tool for the study to validate this hypothesis.

The role of stiffness in regulating drug response was explored by Schrader et al., who observed a reduction in apoptosis of cells on stiff substrates when treated with cisplatin [25]. Also, Zustiak et al. reported cell line-dependent stiffness sensitivity to paclitaxel [26]. Sorafenib was developed as a Raf kinase inhibitor [27], and unlike these previously tested drugs, there is no obvious link between this signaling pathway and ECM stiffness. Phosphorylation of ERK, a downstream effector of Raf kinase, has been implicated in controlling cell proliferation during ECM stiffening [19, 28], so I hypothesized that sorafenib efficacy could be hampered in stiff environments, contributing at least partially to sorafenib's modest clinical efficacy [29].

To capture the evolution of the tumor microenvironment during disease progression, I formed hydrogel environments with a range of stiffnesses, including either basement membrane-like ECM proteins [30], or a collagen-rich inflammatory ECM [21]. I examined whether stiff environments protected carcinoma cells from sorafenib treatment, and if this drug resistance was mediated by the canonical Rho-ROCK and β_1

integrin signaling pathways. Motivated by a targeted phospho-proteomic screen, I also quantified the role of ERK, Akt, JNK and p38 signaling during cell response to sorafenib on stiff substrates. The results demonstrate the utility of the tunable, high-throughput PEG-PC biomaterial platform in drug screening, and identify an exciting new mechanism to increase the efficacy of sorafenib in stiff tumor environments.

4.3 Materials And Methods

4.3.1 Cell culture

All supplies were purchased from Life Technologies (Carlsbad, CA) unless otherwise noted. Human breast cancer cell lines (MDA-MB-231, BT549, and SkBr3) were generous gifts from Dr. Shannon Hughes at the Massachusetts Institute of Technology, and were cultured in Dulbecco's Modified Eagle's Medium (DMEM) supplemented with 10% fetal bovine serum (FBS) and 1% penicillin-streptomycin (P/S) at 37ºC and 5% CO_2. Human hepatocellular carcinoma (HCC) cells (HEP3Bs, American Type Culture Collection, Manassas, VA) were cultured in modified Eagle's medium (MEM) supplemented with 10% FBS and 1% P/S at 37ºC and 5% CO_2. MDA-MB-231 expressing DsRed and DsRed-let7c-sensor were generous gifts from Dr. D. Joseph Jerry at the Department of Veterinary and Animal Science, University of Massachusetts Amherst. These two cell lines were cultured in DMEM:F12 supplemented with 14 mM sodium bicarbonate, 10 mM HEPES, and 10% FBS, 10 μg/mL Insulin, 1x antibiotic/antimycotic, 15 μg/mL gentamicin, and 2 mM L-Glutamine.

4.3.2 96-well hydrogel platform

Glass-bottom 96-well plates (no. 1.5 coverslip glass; In Vitro Scientific, Sunnyvale, CA) were plasma treated (Harrick Plasma, Ithaca, NY) and subsequently methacrylate-silanized with 2 vol% 3-(trimethoxysilyl) propyl methacrylate (Sigma-Aldrich, St. Louis, MO) in 95% ethanol (adjusted to pH 5.0 with glacial acetic acid) for 5 min, washed 3 times with 100% ethanol, and dried at 40 °C for 30 min. PEGDMA (Mn 750, Sigma-Aldrich), from 0.6-9.1 wt%, was combined with 17 wt% 2-methacryloyloxyethyl phosphorylcholine (PC) (Sigma-Aldrich) in phosphate buffered saline (PBS). These PEGDMA crosslinker concentrations tune the Young's moduli of the resulting gels from 6 to 400 kPa [31]. Solutions were sterilized with a 0.2 μm syringe filter (Thermo Fisher Scientific, Waltham, MA) and degassed by nitrogen sparging for 30s. Free-radical polymerization was induced by addition of 0.05 wt% ammonium persulfate (APS) and 0.125 vol% tetramethylethylenediamine (TEMED, Bio-Rad Laboratories, Hercules, CA). Hydrogels of 40 μL per well in the 96-well plates were polymerized under nitrogen for 10 min.

Post-polymerization, hydrogels were allowed to swell for 24 hours in PBS, then treated with 100 μL of sulfo-SANPAH (ProteoChem, Denver, CO; 0.6 mg/mL in pH 8.5 HEPES buffer) under UV light for 20 min, rinsed twice with HEPES buffer, and followed immediately by incubation with protein mixtures overnight. ECM protein mixtures were defined as either “basement membrane” composed of 46% human collagen IV (Neuromics, Edina, MN), 46% human fibronectin (EMD Millipore, Billerica, MA), and 8% mouse laminin at 5 $\mu g/cm^2$, buffered in pH 7.0 PBS, or “collagen rich” composed of 65% rat tail collagen I, 33% human collagen III (FibroGen, San Francisco, CA), and 2%

fibronectin at 5 μg/cm^2, buffered in pH 3.8 PBS. Post-protein coupling, the gels were rinsed twice with PBS, UV-sterilized for 1 h, and rinsed with sterile medium before cell seeding.

4.3.3 Quantification of drug resistance

Cells were seeded onto gel surfaces at a density of 31,000 cells/cm^2 in serum-free medium supplemented with 20 ng/mL of platelet-derived growth factor (PDGF-BB, eBioscience, San Diego, CA) and 20 ng/mL of epidermal growth factor (EGF, R&D Systems, Minneapolis, MN). After 24 h, cells were treated with sorafenib (LC Laboratories, Woburn, MA) from 0 to 120 μM, diluted in growth factor-supplemented serum-free medium. After 24 h, I measured cell proliferation with CellTiter 96 AQueous One Solution Cell Proliferation Assay (Promega, Madison, WI) at 490 nm (BioTek ELx800 microplate reader, BioTek, Winooski, VT). The concentration of sorafenib that reduced cell proliferation by 50% (IC-50) was calculated with Prism v5.04 (GraphPad Software, La Jolla, CA). In some experiments, sorafenib was also co-administered with: an anti-β_1 integrin antibody (clone P5D2, R&D Systems, 0.5 μg/mL), p160ROCK inhibitor (Y-27632, R&D Systems, 10 μM), EGF receptor (EGFR) inhibitor (AG1478, AG Scientific, San Diego, CA, 1 μM), JNK inhibitor (SP600125, LC Laboratories, 20 μM), p38 inhibitor (BIRB796, LC Laboratories, 1 μM), or ERK inhibitor (FR180204, Sigma-Aldrich, 20 μM). Dimethyl sulfoxide (Sigma-Aldrich) was used as a vehicle control in all experiments. I also verified that cell proliferation measurements approximately linearly correlated to cell count (Figure 4.1).

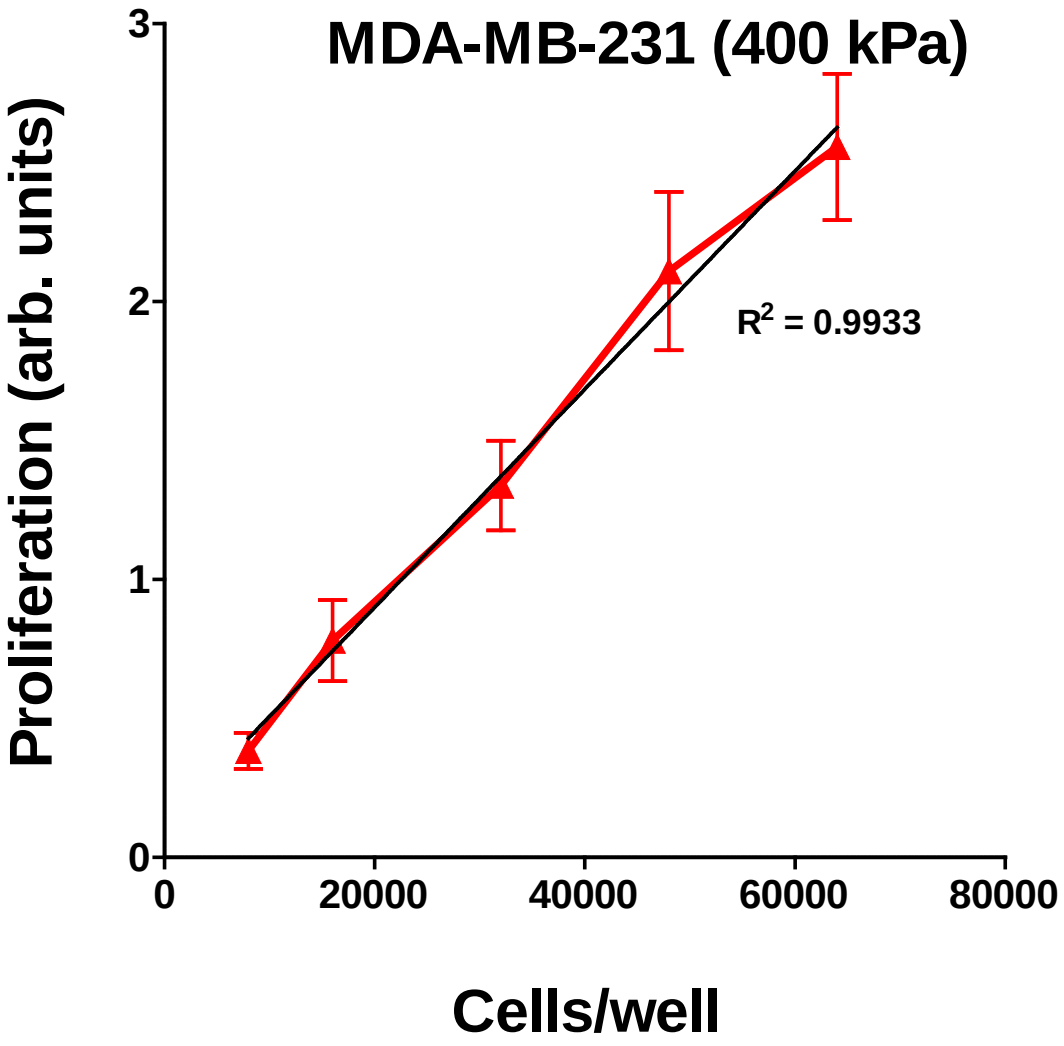

Figure 4.1 MTS assay linearly correlates with raw cell counts. 231 cells were seeded at different cell densities on 400 kPa gels, and the MTS assay was run 24-hour post-seeding. The resulting absorbance (proliferation, y-axis) linearly correlates with initial cell number (x-axis) with a R^2 of 0.9933. Figure adapted with permission from [74]. © 2014 Elsevier, Inc.

4.3.4 Immunofluorescent imaging

18 mm glass coverslips (Thermo Fisher Scientific, Waltham, MA) were plasma treated, methacrylate-silanized, and dried at 120 °C for 15 min. 80 μL PEG-PC hydrogels were polymerized with APS and TEMED between a methacrylated-silanized coverslip and an untreated coverslip for 20 min on the bench. After polymerization, the hydrogels were allowed to swell in PBS, and the non-treated coverslips were removed easily with fine forceps. Swollen gels on coverslips were transferred to 12-well tissue culture dishes, coupled with protein mixtures as described above, rinsed 3 times with PBS, and UV-sterilized for 1 h prior to cell seeding.

Cells were seeded at a density of 10,000 cells/cm^2 in growth factor-supplemented serum-free medium and allowed to adhere for 24 hours. Cells were rinsed three times with warm PBS, fixed with 4% formaldehyde, permeabilized with Tris-buffered saline (TBS) containing 0.5% Triton X-100 (Promega), and blocked with AbDil (2 wt.% BSA in TBS with 0.1% Triton X-100, TBS-T). F-actin was labeled with Alexa Fluor 555-conjugated phalloidin for 1 h. Vinculin was labeled with a monoclonal mouse anti-vinculin antibody (Sigma-Aldrich) for 1 h, followed by an anti-mouse FITC secondary antibody (Jackson ImmunoResearch Laboratories, West Grove, PA) for 1 h. Cell nuclei were labeled with DAPI (MP Biomedicals, Santa Ana, CA) for 5 min. Each sample was treated with ProLong Gold antifade reagent for 5 min before imaging on a Zeiss Axio Observer Z1 microscope with a 63x oil immersion objective (Carl Zeiss AG, Oberkochen, Germany), and images were compiled in ImageJ (NIH, Bethesda, MD).

4.3.5 Multiplex phospho-protein quantification

MDA-MB-231 cells ('231s') were seeded at 50,000 cells/cm^2 on 6 and 400 kPa 18 mm diameter coverslip-mounted gels in 12-well plates. Immediately after seeding, at 0 min, 30 min, 1 h, 2 h, 4 h, 6 h, and 24 h time points, coverslips were transferred to a new 12-well plate on ice, the gels were washed once with ice-cold Bioplex cell wash buffer (Bio-Rad, Hercules, CA), and lysed with ice-cold lysis buffer (Bioplex cell lysis buffer, Bio-Rad) containing protease (EDTA-free Protease Inhibitor Cocktail Tablets, Roche, Indianapolis, IN) and phosphatase (2x phosphatase inhibitors cocktail-II, Boston Bioproducts, Boston, MA) inhibitors. Separately, cells were allowed to adhere for 24 hours, treated with sorafenib, and lysates were collected at 0 min, 1 h, 5 h, 15 h, and 24 h time points after sorafenib treatment. Total protein concentration was quantified with a BCA protein assay (Thermo Scientific, Rockford, IL). Lysate concentrations were adjusted to 100 μg/mL, and the phosphorylation levels of ERK1/2, Akt, JNK, and p38 were quantified with a MAGPIX (Luminex, Austin, TX) with Bio-Plex Pro™ phospho-ERK1/2, phospho-Akt, phospho-JNK, and phopho-p38 magnetic beads (Bio-Rad), according to the manufacturer instructions.

4.3.6 Quantification of mammary stem/progenitor cells

MDA-MB-231s expressing DsRed-let7c-sensor were seeded at 3,100 cells/cm^2 on 18-mm gel-laden coverslips, which were coupled with collagen-rich ECM, in the same cell-culture medium. The medium was replenished every other day, and the gels were imaged at day 1, 3, 5, and 7. Then the number of red cells was manually counted from the images.

When flow cytometry was used to quantify the number of progenitor cells, cells were collected from the gels on day 7 and resuspended in 1x PBS supplemented with 0.5 wt. % of BSA and 1 mM Ethylenediaminetetraacetic acid (EDTA). The cell suspension was filtered with a cell strainer (Thermo Fisher Scientific) to eliminate large cell clumps. The Fluorescence-Activated Cell Sorting (FACS) data were collected with a total of 100,000 events using LSRII (BD Biosciences, San Jose, CA) and analyzed with BD FACSDiva Software (BD Biosciences).

4.3.7 Statistical analysis

A one-way analysis of variance (ANOVA) with a Tukey post-test was performed with Prism v5.04 (GraphPad Software). Data are reported as mean ± standard error. $p \leq 0.05$ is denoted with *, ≤ 0.01 with **, and ≤ 0.001 with ***; $P > 0.05$ is considered not significant ("ns").

4.4 Results

4.4.1 Carcinoma cell response to sorafenib on PEG-PC hydrogels

I created a high-throughput biomaterial platform to rapidly assay cell responses to chemotherapeutic drugs in different mechanochemical environments (Figure 4.2). In particular, I focused on how these changes perturbed the efficacy of sorafenib, a Raf kinase inhibitor approved for thyroid, kidney and liver cancer, but which has had limited clinical success [29, 32, 33]. One potential cause of drug resistance by carcinoma cells might be the stiffening of the tumor environment itself, and so I quantified the responses of a liver cancer cell line and three breast cancer cell lines to sorafenib on PEG-PC of increasing stiffness (Figure 4.3).

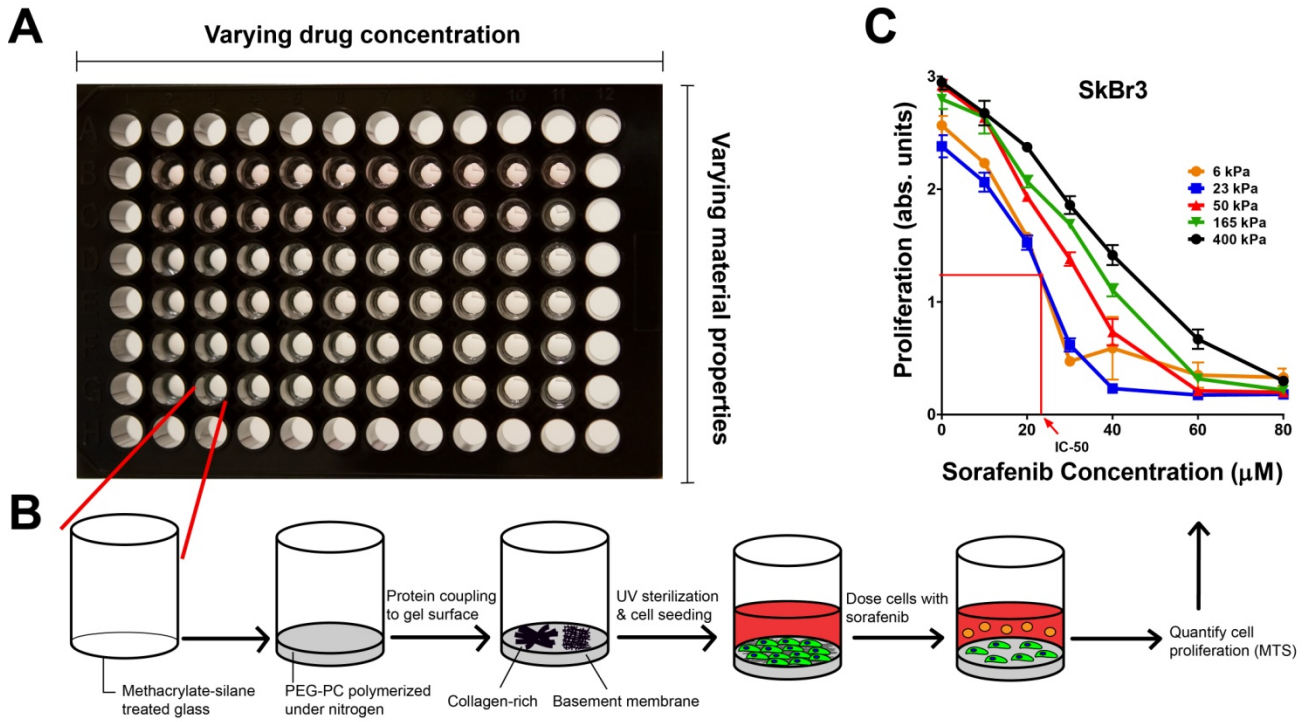

Figure 4.2 High-throughput biomaterial platform for drug screening. **(A)** The high-throughput platform consists of a black-walled, glass bottom plate, with PEG-PC gels cast in each of the inner 6x10 wells. **(B)** Gels can be functionalized with any protein or peptide of interest, and they support the adhesion and growth of carcinoma cells. I used this platform to test carcinoma cell response to a kinase inhibitor (sorafenib) as a function of underlying gel stiffness and ECM adhesive protein cocktail. **(C)** A representative graph of SkBr3 proliferation (y-axis) in response to sorafenib (x-axis) across a range of gel stiffness (colors) demonstrates the IC-50 calculation. Figure adapted with permission from [74]. © 2014 Elsevier, Inc.

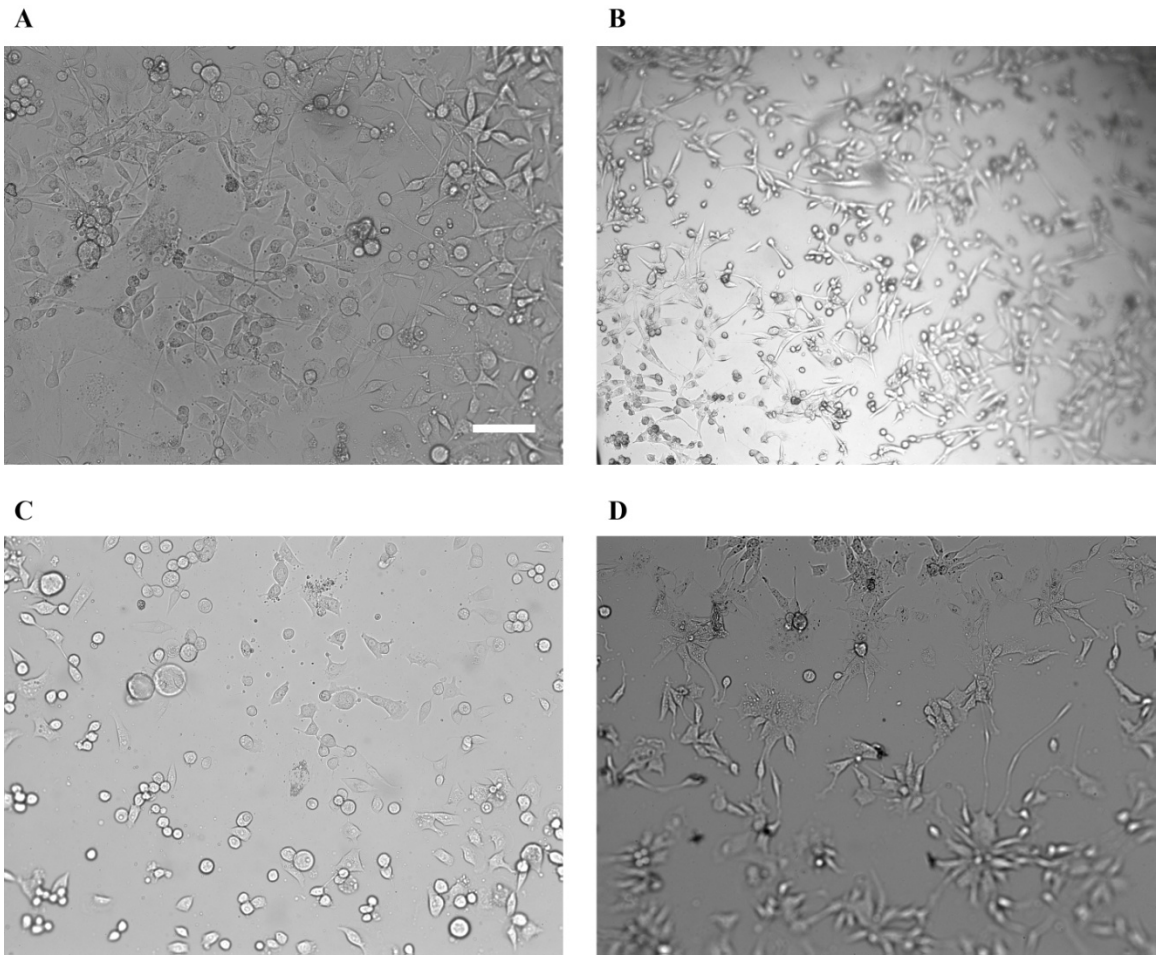

Figure 4.3 Representative images of cells adhering on 165 kPa gels coupled with collagen-rich ECM in 96-well plate. **(A)** MDA-MB-231 **(B)** BT549 **(C)**SkBr3 **(D)** HEP3B. Scale bar is 100 μm.

In all cell lines, I consistently observed a significant increase in sorafenib IC-50, the concentration at which the proliferation was dampened by half, with increasing substrate stiffness (Figures 4.4A-B). I observed this phenomenon on both the basement membrane-like ECM (Figure 4.4A), and the collagen-rich ECM (Figure 4.4B), demonstrating that this stiffness-induced drug resistance is maintained even with alterations in integrin binding. Two of the breast cancer cell lines I tested, the SkBr3s and 231s, were the most drug resistant cell lines on the basement membrane ECM (Figure 4.4A). When I normalized the IC-50s within each cell line to the softest condition, I observed that these two cell lines also showed the most stiffness-induced resistance to sorafenib, with 3.7 and 3 fold increases in IC-50 on the stiffest gels when compared to the softest condition, respectively (Figure 4.5A). On the collagen-rich mixture, again the 231 and SkBr3s were the most drug resistant cell lines (Figure 4.4B), but, interestingly, the HEP3B cell line was the most stiffness sensitive (Figure 4.5B). Altogether, on the collagen-rich ECM, the SkBr3 and 231 cell lines are more sorafenib resistant across all gel conditions. Stiffness increases their sorafenib resistance, but they appear less stiffness sensitive than the HEP3Bs because the HEP3Bs are, overall, less resistant to sorafenib.

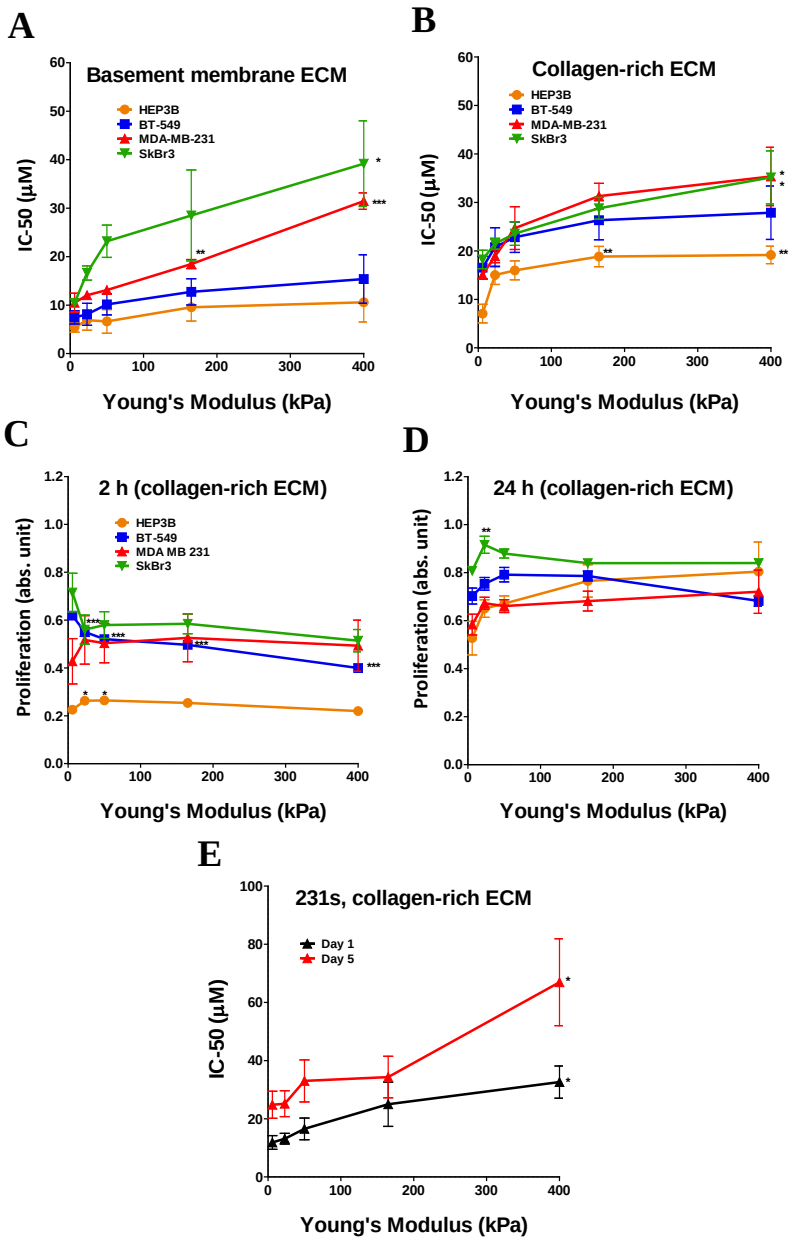

Figure 4.4 Cells on stiff substrates resist sorafenib. The IC-50 (from proliferation measurements) of HEP3B (orange), BT-549 (blue), MDA-MB-231 (red), and SkBr3 (green) cells increases with stiffness on both **(A)** basement membrane ECM proteins and **(B)** collagen-rich ECM proteins. On the collagen-rich ECM, the same proliferation assay without sorafenib at **(C)** 2 hours and **(D)** 24 hours post-seeding demonstrates that differences in initial cell adhesion or proliferation do not explain the results in A and B for each cell line. **(E)** Resistance to sorafenib of 231 cells is heightened and maintained at longer (5 days, red) culture times on the gels. Statistics shown are with respect to the softest gel condition, with the exception of the BT549 cells in D which were significantly different when comparing 50 and 400 kPa gels. N ≥ 3 independent biological replicates, and N = 3 technical replicates. Figure adapted with permission from [74]. © 2014 Elsevier, Inc.

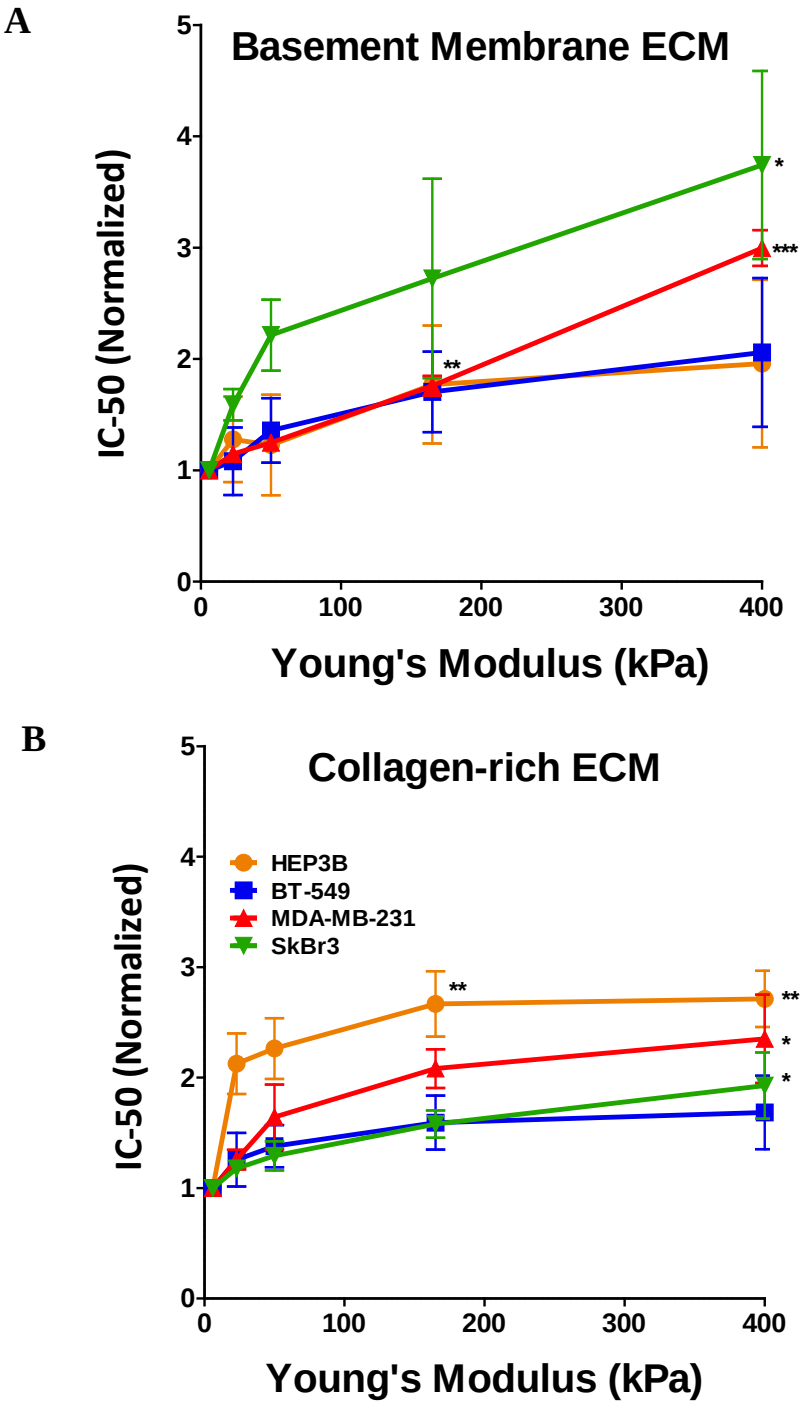

Figure 4.5 Normalized cell proliferation in response to stiffness. **(A)** and **(B)** are the data from Figure 2, re-drawn with each cell line internally normalized to the softest gel condition. **(A)** On the basement membrane proteins, SkBr3 cells were the most stiffness sensitive cell line, whereas **(B)** HEP3B cells were the most stiffness sensitive cell line on collagen-rich proteins. Statistics are relative to the soft gel conditions. Figure adapted with permission from [74]. © 2014 Elsevier, Inc.

Neither initial cell adhesion to the gels, nor proliferation at 24 hours showed the same consistent trends as drug resistance, ruling them out as significant contributors to sorafenib resistance (Figures 4.4C-D and Figure 4.6). I also cultured the 231 cells for five days prior to sorafenib treatment and found that the cells responded to sorafenib in the same manner as compared to dosing 24 hours post-seeding, but with larger IC-50s due to cell proliferation in the days prior to drug treatment (Figure 4.4E). This result demonstrates that the observed stiffness-mediated drug resistance is maintained at longer time points of culture.

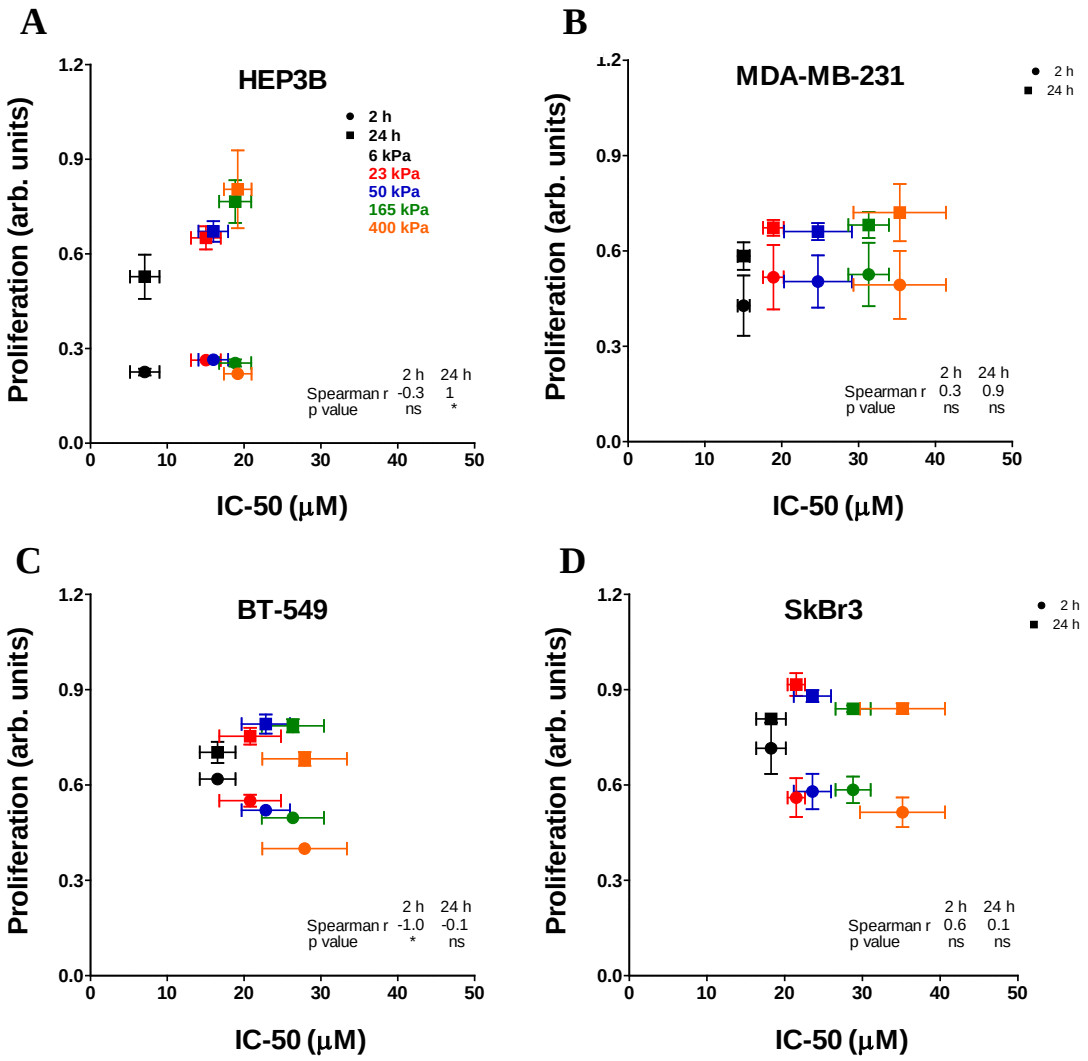

Figure 4.6 Spearman correlation between proliferation and IC-50s. Early cell adhesion does not correlate with stiffness-mediated sorafenib resistance. **(A)** HEP3B, **(B)** MDA-MB-231, **(C)** BT549, **(D)** SkBr3. With the exception of the HEP3B cell line (**A**, 24 hours only), no cell lines showed a positive Spearman correlation between the MTS reading (y-axis) at 2 (circles) or 24-hours (squares) post seeding and the observed IC-50 value of sorafenib treatment (x-axis). Different colors represent the values at the different stiffness gels. Figure adapted with permission from [74]. © 2014 Elsevier, Inc.

4.4.2 Cytoskeletal tension and sorafenib resistance

Given the known role of substrate stiffness in influencing cell proliferation via the canonical Rho-ROCK pathway [19, 28], I hypothesized that intracellular tension was the most probable mechanism by which increasing stiffness protected cells from sorafenib. I quantified cell area and imaged F-actin organization in response to increasing substrate stiffness for the two most drug resistant cell lines (231 and SkBr3, Figure 4.7A-D). Interestingly, on the collagen-rich ECM, cell spread area had a biphasic dependence on substrate stiffness, whereas cell spread area increased with stiffness on the basement membrane proteins. This result does not match the observed drug resistance results (compare Figures 4.7B and D with Figures 4.4A-B), and implies that intracellular tension does not exclusively explain the observed stiffness-mediated resistance on collagen-rich ECM. Figures 4.7A-D also demonstrate that integrin binding (via ECM proteins) influences the sensitivity of cell area to substrate stiffness.

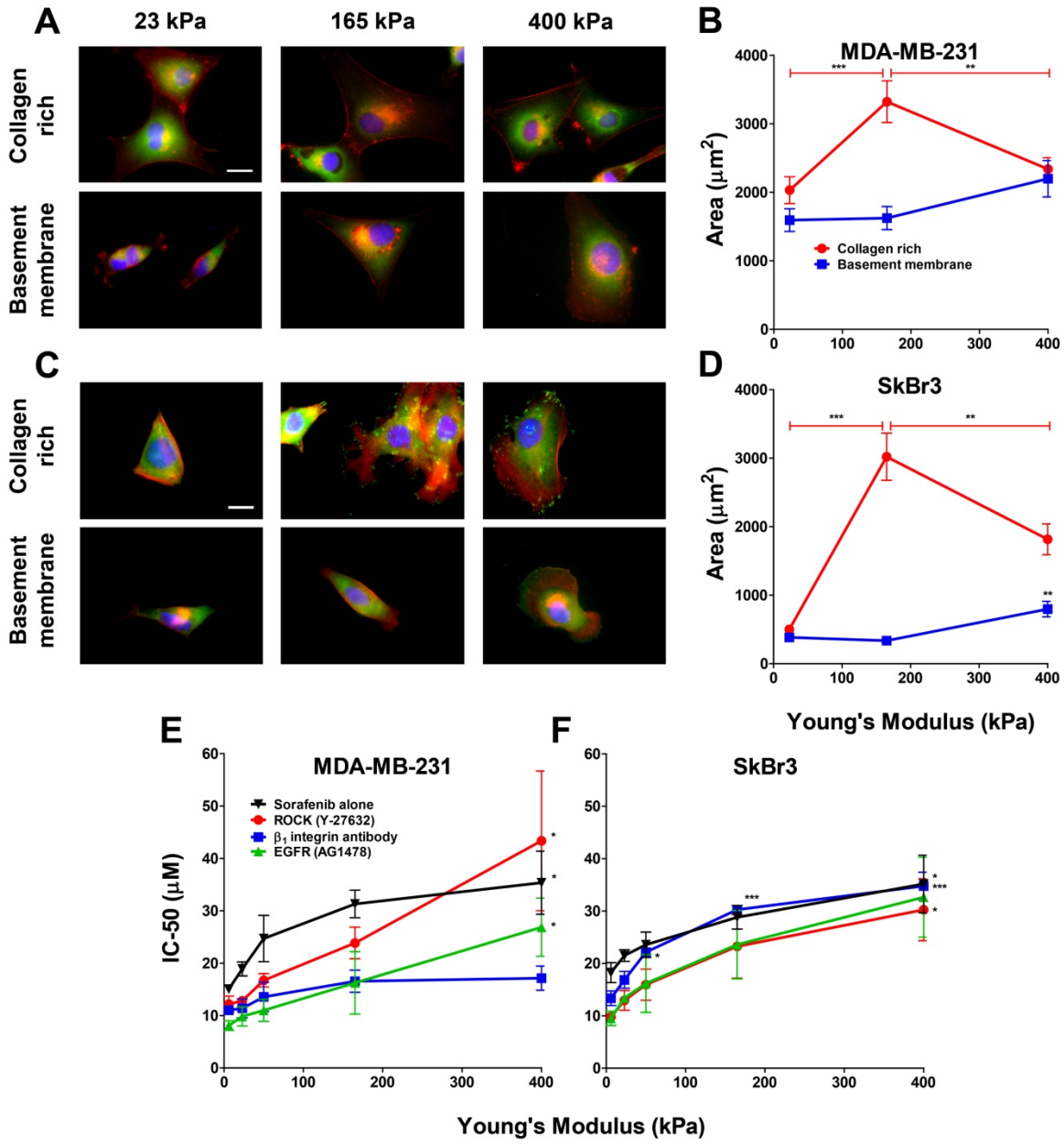

Figure 4.7 Sorafenib resistance is not mediated by cytoskeletal tension. Both MDA-MB-231s **(A-B)** and SkBr3s **(C-D)** show a biphasic relationship between cell spread area and stiffness on the collagen-rich ECM, and increasing spread areas on the basement membrane ECM. In A and C, cells were fixed and stained for F-actin (red), vinculin (green), and the nucleus (DAPI, blue). **(E)** MDA-MB-231 stiffness-induced drug resistance is significantly reduced when sorafenib is co-administered with an antibody to β_1 integrin (compare black and blue lines), whereas inhibitors to ROCK (red) and EGFR (green) do not affect the stiffness-induced sorafenib resistance. **(F)** Neither the ROCK nor EGFR inhibitors, nor the β_1 integrin antibody effectively altered the response to sorafenib in the SkBr3s. Statistics are with respect to the softest gel condition. $N \geq 3$ independent biological replicates, and $N = 3$ technical replicates. Scale bar is 20 μm. Figure adapted with permission from [74]. © 2014 Elsevier, Inc.

I further examined the potential role of intracellular tension in mediating stiffness-induced sorafenib resistance via ROCK activity. ROCK is a downstream effector of RhoA, a GTPase that regulates cell contractility and actin stress fiber formation [34]. I co-administered sorafenib with a ROCK inhibitor (Y27632) in both the 231 and SkBr3 cell lines on the collagen-rich ECM (Figures 4.7E-F). When compared to the sorafenib alone condition (black lines), ROCK inhibition (red lines) dampened sorafenib resistance across all moduli, except for the stiffest condition; however, even in the presence of ROCK inhibitor, the IC-50s still increased with stiffness in both cell lines. Going further, I attempted to block cell adhesion to the collagen-rich ECM by co-administering sorafenib with a blocking antibody to the β_1 integrin subunit (blue lines). Blocking β_1 integrin was significantly effective in the 231 cells at all stiffnesses, but had no effect on sorafenib resistance in the SkBr3s, perhaps implying that SkBr3s can survive sorafenib treatment in low adhesive environments. Finally, I treated cells with an inhibitor to EGFR, given the known role EGFR activation in promoting resistance of several HCC cell lines to sorafenib [35], and given the fact that all these experiments are supplemented with EGF. EGFR inhibition (green lines) increased the efficacy of sorafenib modestly in both cell lines, but the trend of stiffness-induced drug resistance remained. Taken together, neither ROCK nor EGFR appears to regulate stiffness-mediated sorafenib resistance; however, β_1 integrin antibody may be a candidate for co-treatment with sorafenib in triple negative breast cancer (the subtype of the 231 cell line), but not HER2 overexpressing breast cancer (SkBr3 subtype).

4.4.3 Signaling pathways activated during ECM stiffening

Given that β_1 integrin antibody was the only effective co-treatment with sorafenib in the 231 cells, I investigated a subset of candidate signaling pathways, downstream of β_1, which might be interfering with sorafenib efficacy. I used a multi-plex MAGPix system to quantify the phosphorylation of three members of the MAPK family (ERK1/2, JNK, p38), and Akt of the PI3K pathway at multiple time points post-adhesion to the softest and stiffest substrates tested in the 231 cell line (Figures 4.8A-D). On both the collagen-rich and basement membrane ECMs, I observed an early peak in phosphorylation of ERK1/2 and Akt post-adhesion, but there was no difference when comparing between the soft and stiff gel conditions. JNK phosphorylation was delayed on the basement membrane ECM when compared to the collagen rich ECM, and the activity of JNK and p38 was higher on the stiffer gel at all time points on the collagen-rich ECM. Therefore, changes in JNK signaling could partially explain differences in cell behavior on the two protein mixtures, and both JNK and p38 are promising candidates to explain sorafenib resistance on stiff substrates.

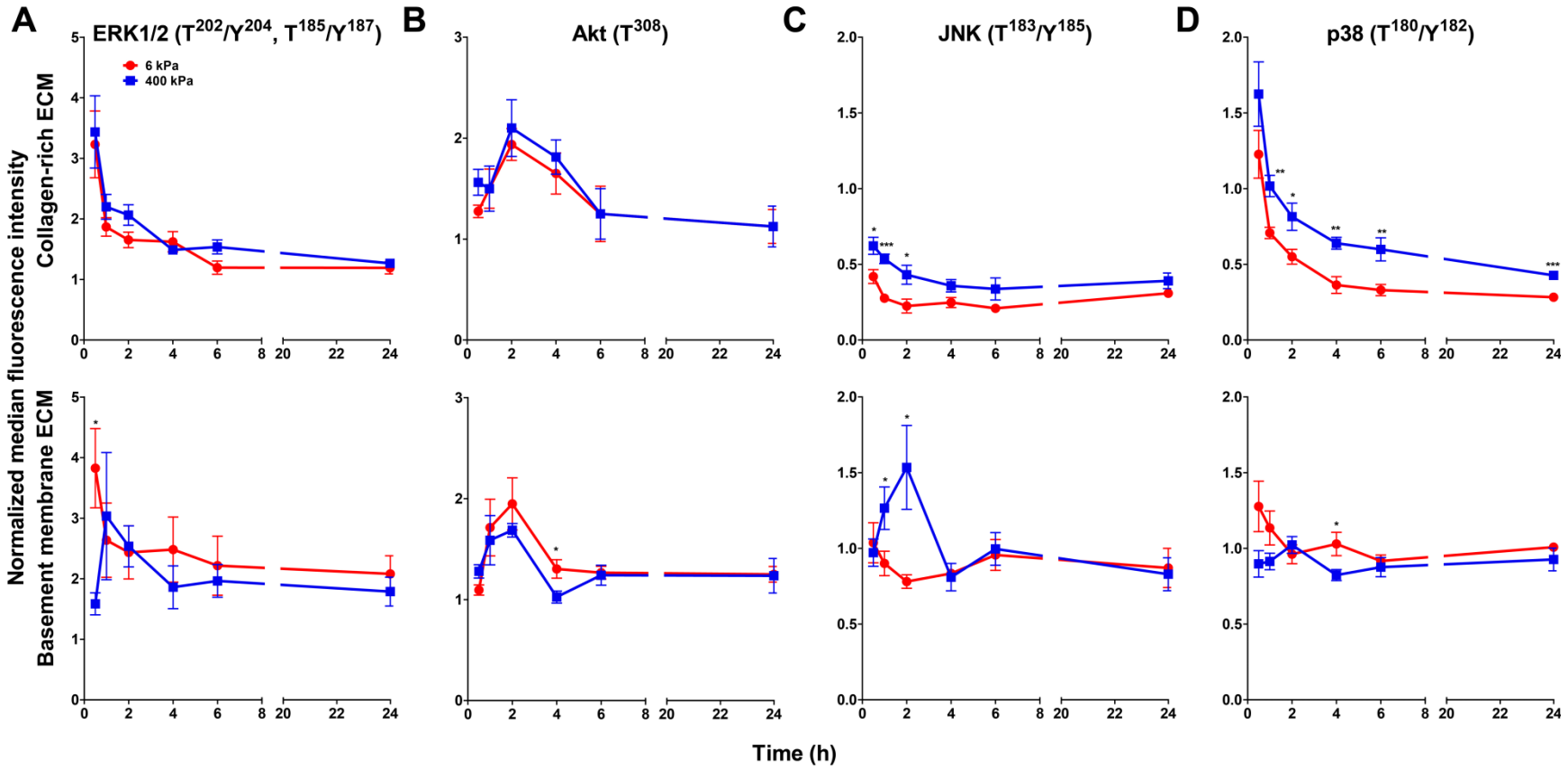

Figure 4.8 JNK and p38 phosphorylation increases on stiff substrates. Phosphorylation levels of ERK1/2 **(A)** and Akt **(B)** over time (x-axis) as cells adhered to the gel surface are not sensitive to the change in stiffness (red = 6kPa, blue = 400kPa) for both collagen-rich (top row) and basement membrane (bottom row) ECMs, as determined by a MAGPix assay. **(C)** JNK activity is higher on the stiff substrate with both protein mixtures, and p38 phosphorylation **(D)** is higher on the stiff substrate on the collagen-rich ECM. Statistics are with respect to the soft gel condition at the same time point. N ≥ 2 independent biological replicates, and N = 3 technical replicates. Figure adapted with permission from [74].

4.4.4 Combinatorial treatment of a JNK inhibitor and sorafenib on stiff substrates

To determine whether sorafenib treatment perturbed the activity of these signaling proteins, I allowed 231 cells to adhere to the two stiffness gels coupled with collagen-rich ECM for 24 hours, and performed the MAGPix assay at various time points directly following a 15 μM sorafenib treatment. Upon sorafenib treatment, ERK1/2 phosphorylation on the stiff substrate remained significantly higher than that on the softer gel at early time points post-dosing (Figure 4.9A). Akt phosphorylation also peaked in the first hour after sorafenib treatment; however, there was no difference in Akt phosphorylation between the soft and stiff substrates, which further confirmed that Akt signaling was not involved in stiffness-mediated drug resistance (Figure 4.9B). The observed peak in Akt might be due to the ability of Ras to mediate signaling through PI3K/Akt pathway [36], while sorafenib inhibits the Ras/Raf/MEK/ERK pathway. JNK phosphorylation was highest on the stiff substrate, and, unlike ERK and Akt, did not change over time (Figure 4.9C). Sorafenib treatment also reduced the stiffness sensitivity of p38 phosphorylation (Figure 4.9D).

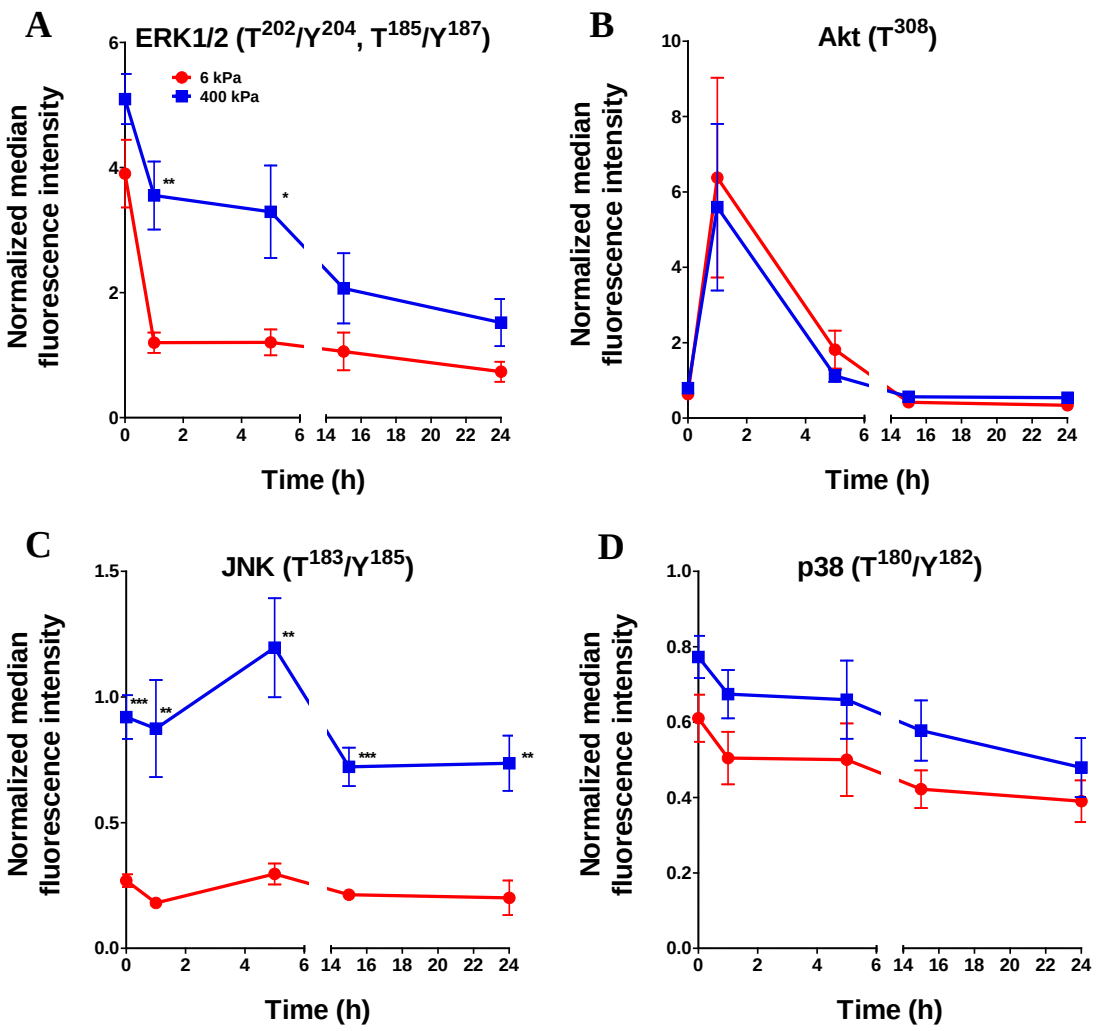

Figure 4.9 Stiffness-induced sorafenib resistance is mediated by JNK activity. 231 cells on collagen-rich ECM were treated with 15 μM sorafenib, and subsequent phosphorylation of ERK1/2, Akt, JNK, and p38 was quantified with a MAGPix assay. **(A)** ERK phosphorylation remained high on stiffer substrate (blue) at early time points (x-axis) when treated with sorafenib. **(B)** Akt phosphorylation peaked at 1 hour post-sorafenib treatment, but did not vary with stiffness. **(C)** Sustained phosphorylation of JNK was unaffected by sorafenib treatment, and high levels were maintained on the stiff substrate. **(D)** Phosphorylation of p38 in the presence of sorafenib was not significantly different between soft and stiff substrates. N ≥ 2 independent biological replicates, and N = 3 technical replicates. Statistics are relative to the soft gel condition. Figure adapted with permission from [74]. © 2014 Elsevier, Inc.

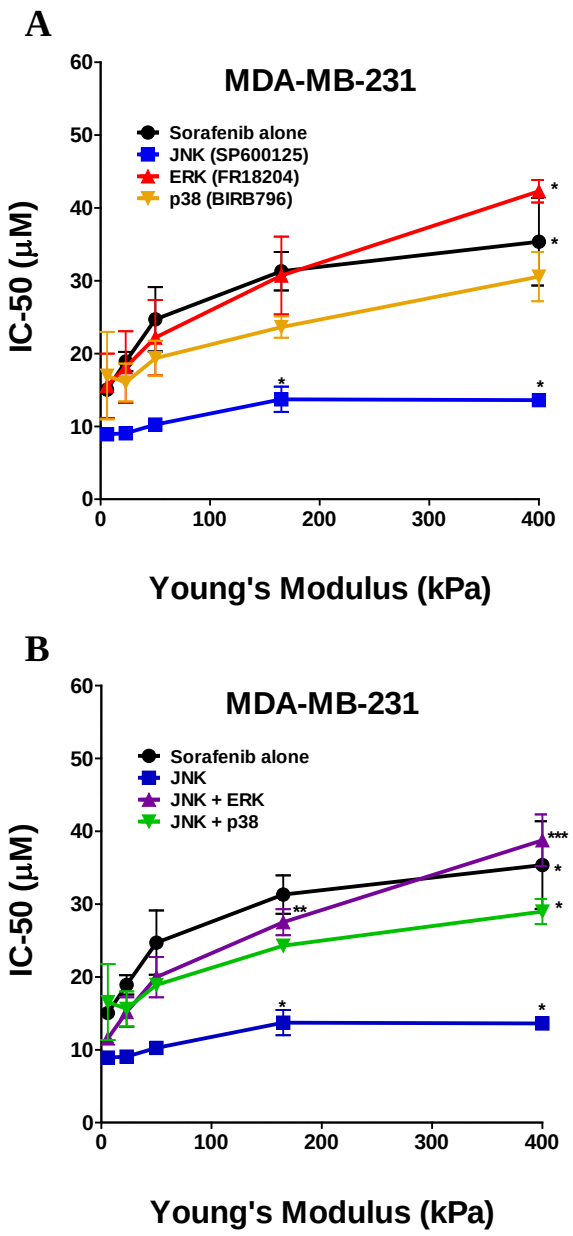

Figure 4.10 Co-administering sorafenib with a JNK inhibitor reduces the stiffness-induced drug resistance. **(A)** MTS assays were performed on 231 cells on collagen-rich ECM in the presence of sorafenib alone (black), sorafenib plus a pharmacological JNK inhibitor (blue, SP600125), sorafenib plus an ERK inhibitor (red, FR18204), or sorafenib plus p38 inhibitor (yellow, BIRB796). The sorafenib dose was varied (resulting in an IC-50, y-axis), while inhibitor concentrations were constant. JNK inhibition reduced both the overall sorafenib resistance and stiffness-induced resistance (compare the blue and black lines), whereas p38 and ERK inhibitors did not affect sorafenib efficacy. **(B)** Combining either ERK (purple) or p38 (green) inhibitors with JNK inhibitor and sorafenib reversed the previously observed effect of inhibiting JNK alone (blue). N ≥ 3 independent biological replicates, and N = 3 technical replicates. Statistics are relative to the soft gel condition. Figure adapted with permission from [74]. © 2014 Elsevier, Inc.

When considering the results in Figures 4.8 and 4.9 together, ERK, p38, and JNK were all potential candidates for involvement in stiffness-mediated sorafenib resistance. I co-administered sorafenib with inhibitors to each of these molecules (Figure 4.10A), and found that JNK inhibition (blue line) both significantly increased sorafenib efficacy, and eliminated the impact of substrate stiffness. In hindsight, this result could have been anticipated, as JNK was the only signaling molecule both enhanced by substrate stiffness during cell adhesion (Figure 4.8C), and unaffected by sorafenib treatment (Figure 4.9C). With an expected synergistic effect in mind, I then co-administered sorafenib with JNK inhibitor, and either ERK or p38 inhibitors (Figure 4.10B). Strikingly, I found that combining either p38 or ERK inhibitors alongside the JNK inhibitor and sorafenib treatment reversed the effect of co-administering the JNK inhibitor alone.

4.4.5 Enrichment of mammary stem/progenitor cells on stiff substrates

Cancer stem/progenitor cells (CSC) are notoriously resistant to chemotherapeutics, and exposure to chemotherapy can lead to an increase of CSCs population [37]. The stemness of cancer cells was also found to be modulated by the tumor microenvironment in colon cancer [38]. Therefore, I investigated whether the observed drug resistance on stiffer substrates could be caused by an increase in the CSC population. Since let-7 microRNAs are present in differentiated cells, but depleted in mammary progenitor cells [39], MDA-MB-231s expressing DsRed-let7c-sensor were cultured on varying-modulus gels, which were coupled with collagen-rich proteins, for 7 days. The number of DsRed expressing cells were observed to increase over time, indicating an increase in the number of progenitor cells, but there was not any difference across stiffnesses (Figure 4.11). The increase in progenitor cells could be due to an

increase in the total cell population, as the cells were proliferating. To be more precise, flow cytometry was performed to quantitatively measure the fraction of the DsRed population (Figures 4.12A-F). The fraction of DsRed cells were similar across all stiffnesses, and accounted for approximately 0.2% of the entire population. Thus it can be concluded that the stiffness-induced sorafenib resistance was not caused by an increase in number of progenitor cells on stiff substrates.

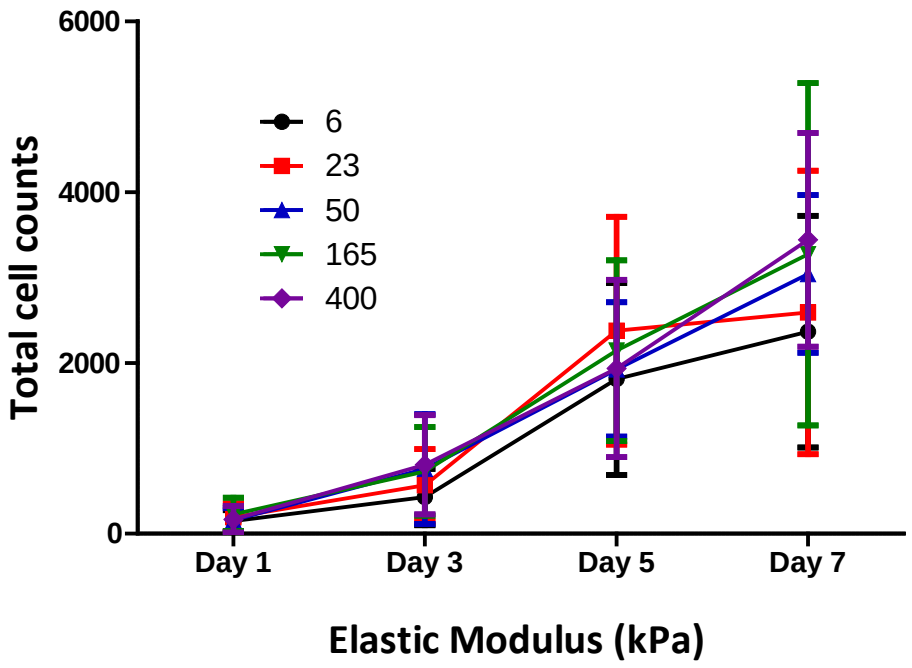

Figure 4.11 The number of progenitor cells over time. The total number of mammary stem/progenitor cells increases over time, but not regulated by substrate modulus.

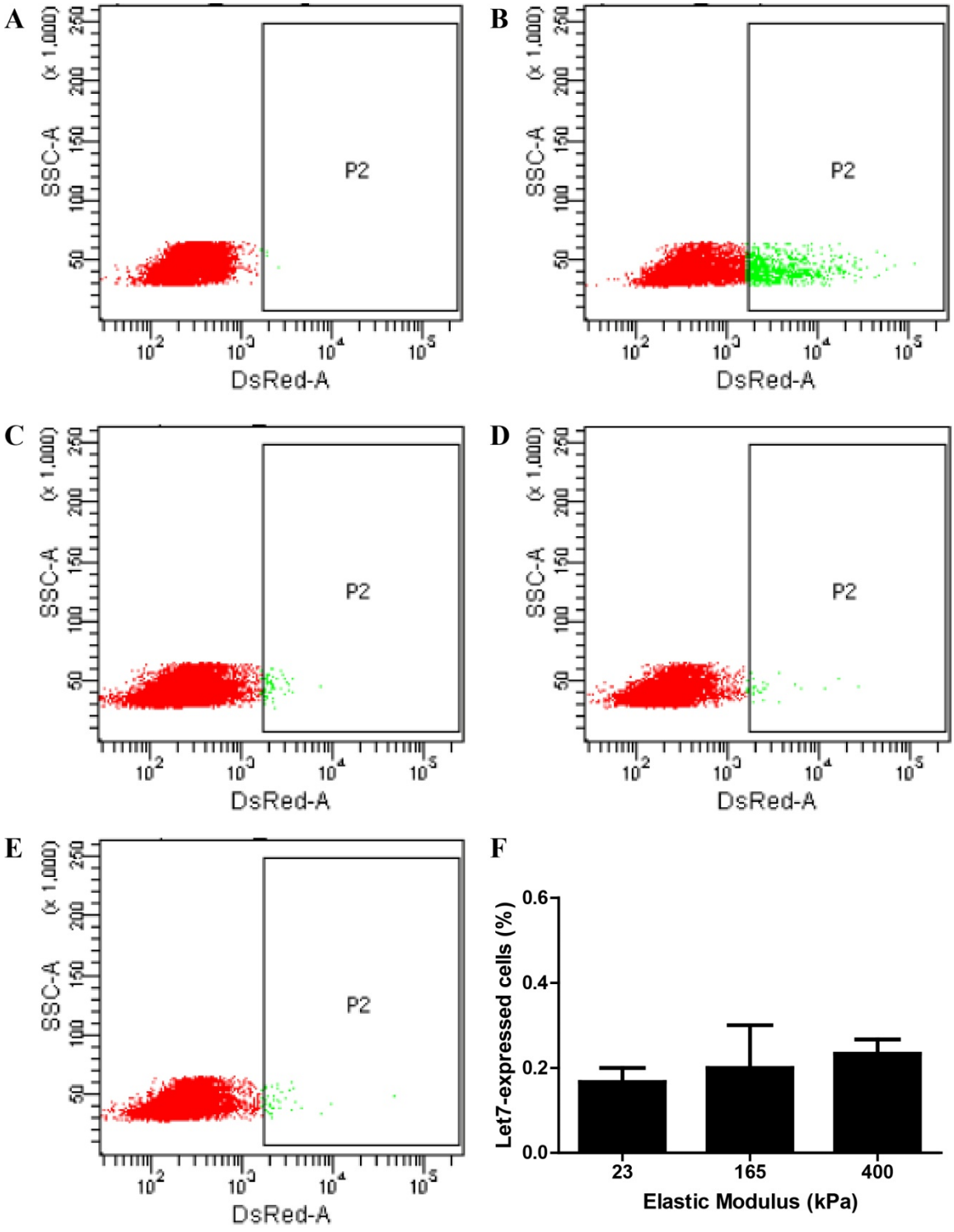

Figure 4.12 The enrichment of mammary stem/progenitor cells are independent of substrate modulus. **(A)** non-DsRed expressing cells were used as a negative control. **(B)** DsRed expressing cells were used as a positive control. An increase in substrate modulus with **(C)** 23kPa, **(D)** 165 kPa, and **(E)** 400 kPa does not significantly change the population of stem/progenitor cells **(F)**. Abbreviations: SSC-A: side scatter-area.

4.5 Discussion

Several groups have demonstrated a link between substrate stiffness and cell proliferation across a variety of cell types [26, 40-43], and many of these studies have linked stiffness sensing, the actin and microtubule cytoskeleton, and the classic Rho-ROCK pathway. This foundation of work has propelled me and others to determine if this pathway, which is known to control cell growth and survival, might also be responsible for drug resistance in stiff tumor environments. For instance, Zustiak et al found that paclitaxel, a cytotoxic microtubule stabilizing agent, eliminated stiffness-induced drug resistance in most tested cell lines [26]. However, chemotherapies that induce apoptosis via non-cytoskeletal pathways, are also affected by substrate stiffness. Schrader et al. showed that stiff substrates reduced HCC cell apoptosis when treated with cisplatin, which causes apoptosis by crosslinking cellular DNA [25]. These studies motivated me to look at how stiffness might perturb the efficacy of a common chemotherapeutic within another class of drugs, specifically, sorafenib, a Raf kinase inhibitor that targets the Raf/MEK/ERK pathway. I also observed a clear stiffness-induced resistance to sorafenib across multiple cell lines. Consistent with Schrader et al., the HCC cell line (HEP3B) was the most stiffness-sensitive cell line tested, and showed a positive correlation between cell proliferation (at 24 hours) and drug resistance (Figure 4.6A). However, cell proliferation did not correlate with drug resistance in any of the other cell lines tested, which were all from breast carcinoma; thus the simplest explanation for the results in Figure 4.4, that cell proliferation on high stiffnesses was responsible for sorafenib resistance, does not hold. The IC-50s for most cell lines are higher on collagen-rich proteins than on basement membrane proteins, with the exception of the SkBr3 cell line,

which has similar IC-50s on both protein mixtures (Figure 4.4A-B). Yang et al. also found that binding of SkBr3 cells to laminin, which is a component in the basement membrane mixture, causes substantial resistance to anti-ErbB2 agents [11], possibly agreeing with the results in the SkBr3 cells. These results point to maximum possible sorafenib resistance in stiff, collagen-rich microenvironments, which represent highly progressed tumors. These results implicate tumor stiffening as a cause for the lack of success for sorafenib, which boasts a paltry 3-month survival increase in comparison to placebo in HCC [29].

Integrin binding can mediate cellular responses to substrate stiffness via RhoA activity, leading to stress fiber formation, focal adhesion assembly, actomyosin contractility, and cell spreading [34, 44, 45]. Although I did observe cell spread area changes in response to both stiffness and ECM protein (Figure 4.7A-D), I quantified no change in stiffness-induced resistance trend when co-administered sorafenib with ROCK inhibitor. Instead, I examined whether integrin-binding mediated this stiffness-induced drug response via some other pathway. β_1 integrin has a high affinity for collagen [46], and increased signaling through β_1 integrin binding protects cancer cells (MDA-MB-231 and MDA-MB-435) against paclitaxel [8] and small cell lung cancer cells against doxorubicin, cyclophosphamide, and etoposide [47]. Reducing β_1 integrin binding with an antibody sensitized the 231 cells to sorafenib, but did not affect the SkBr3s (Figure 4.7E-F). Park et al. also observed that SkBr3 cells were not responsive to β_1 integrin inhibition as compared to MDA-MB-231, likely because of their inherently low β_1 integrin expression [9].

Ezzoukhry et al. observed that inhibiting EGFR sensitized several HCC cell lines to sorafenib treatment [35]; however, I found that co-treatment of a pharmacological EGFR inhibitor with sorafenib in both MDA-MB-231 and SkBr3 cells only affected sorafenib efficacy on soft gels (Figure 4.7E-F). Given that integrin binding to the ECM can enhance EGFR phosphorylation in the absence of ligand binding [48], it is possible that, at lower stiffnesses, β_1 integrin predominantly mediates signaling through EGFR phosphorylation in the absence of ligand binding [49], but not at higher stiffness.

I found that JNK was the key mediator of sorafenib resistance on stiff substrates (Figures 4.8-4.10). Activation of JNK has been reported to mediate either pro-apoptotic or anti-apoptotic signaling pathways depending on stimuli [50, 51], with parallel contradictory roles *in vivo*, either supporting tumor growth [52-55] or suppressing tumorigenesis [56-59]. My results indicate a role for JNK in enhancing cell survival during sorafenib treatment, and for the first time I show that JNK activation is regulated by substrate stiffness. The high activity of JNK on stiff substrates implicates high Rac1 activity and low RhoA activity [49, 60], and low RhoA activity is consistent with the overall lack of stress fiber formation observed in 231 cells [61], regardless of stiffness (Figure 4.7A). Further, ROCK inhibition did not affect the stiffness-induced drug resistance. Finally, RhoA/ROCK can activate ERK [28], and indirectly activates PI3K-Akt pathway [62], supporting my observations of a lack of stiffness-dependent ERK or Akt phosphorylation (Figures 4.8A-B).

Conversely, when we quantified phospho-protein activity in the presence of sorafenib and PDGF and EGF, we observed that ERK phosphorylation was higher on the stiff substrate. This is consistent with other observations that cells on stiff substrates are

more sensitive to EGF stimulation in comparison to those on soft substrates (Figures 4.9A-B) [19, 23]. However, this transient ERK activation on stiff substrates did not prolong cell survival in the presence of sorafenib treatment (Figure 4.10A). Combining both p38 and JNK inhibitors alongside sorafenib reversed the effect of inhibiting JNK alone, suggesting negative crosstalk between JNK and p38. Other studies have reported this antagonism between p38 and JNK before [63, 64]. I observed this same rescue of stiffness-mediated sorafenib resistance when I co-administered JNK and ERK inhibitors, which is also supported by reports of JNK and ERK antagonism [65, 66].

Overall, these results elucidate a role for JNK in mediating resistance to sorafenib through β_1 integrin binding to collagen-rich environments (Figure 4.13). β_1 integrin activation leads to Src-mediated phosphorylation of EGFR [49, 67], which activates Ras/Raf/MEK/ERK and PI3K/Vav2/Rac1/JNK. Inhibiting EGFR improved the efficacy of sorafenib on soft gels (Figure 4.7E), which I attribute to low β_1 integrin affinity [49]. At high stiffness, however, EGFR inhibition had no effect, as integrin clustering increases, recruiting the FAK-Cas complex and activating Ras/Rac1/JNK [68-70].

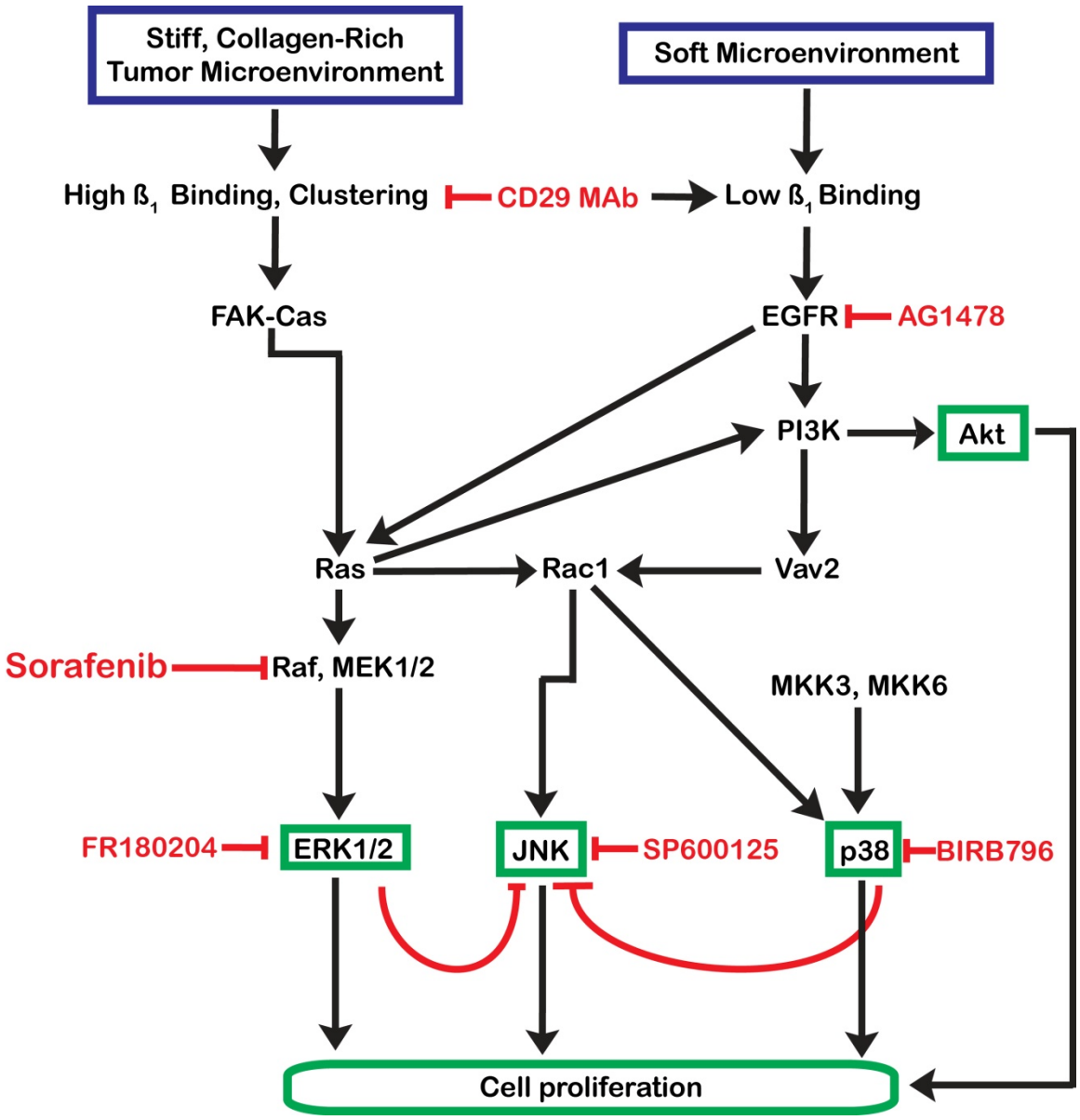

Figure 4.13 Proposed role for JNK in stiffness-mediated sorafenib resistance. I propose that stiff gels increase β_1 clustering when bound to ECM, increasing the activation of the Ras-Raf-MEK pathways, which is targeted by sorafenib, but also Rac1 and downstream JNK activation, offering increased cell proliferation and anti-apoptosis signaling, protecting cells from sorafenib. Inhibiting ERK and p38 are known to block JNK inhibition, providing a reversal of the observed ability of JNK inhibition to improve sorafenib efficacy on stiff substrates. Blue boxes indicate the microenvironment changes that are controlled, green boxes indicate the biological responses that are measured, and red letters indicates inhibitors used to perturb the signaling pathways. Figure adapted with permission from [74]. © 2014 Elsevier, Inc.

In sum, the ability to capture the cell-matrix interactions present in the *in vivo* tumor microenvironment could profoundly influence our ability to understand true drug efficacy *in vitro.* Others have created similar high-throughput biomaterial platforms including ECM microarrays [71], contact-printed microarrays [72], PEG microwells [73], and 2D biomaterials in 96-well plates [26, 41]. The most promising of these approaches have each used polyacryamide (PAA) gels, but require either a complicated plate insert [41], or manually placing gels into individual wells [26]. My method of casting PEG-PC gels allowed me to quickly make multiple uniform gels of varying stiffnesses in multiple 96-well plates at the same time, and does not require fabrication of any special devices (Figure 4.2). My high-throughput PEG-PC platform allowed me to identify β_1 integrin, and its downstream effector, JNK, as mediators of tissue stiffening-induced drug resistance. Co-administering sorafenib with inhibitors to either of these targets equally eliminated stiffness-induced resistance in the 231 cells (Figure 4.14). However, when co-administering sorafenib with inhibitor to JNK, p38, and ERK in SkbR3 cells, the IC-50s were dampend, but the stiffness-induced drug resistance trend remained (Figure 4.15). This results were further supported with the measurement of phosphorylation levels of these molecules on soft and stiff substrates (Figure 4.16).

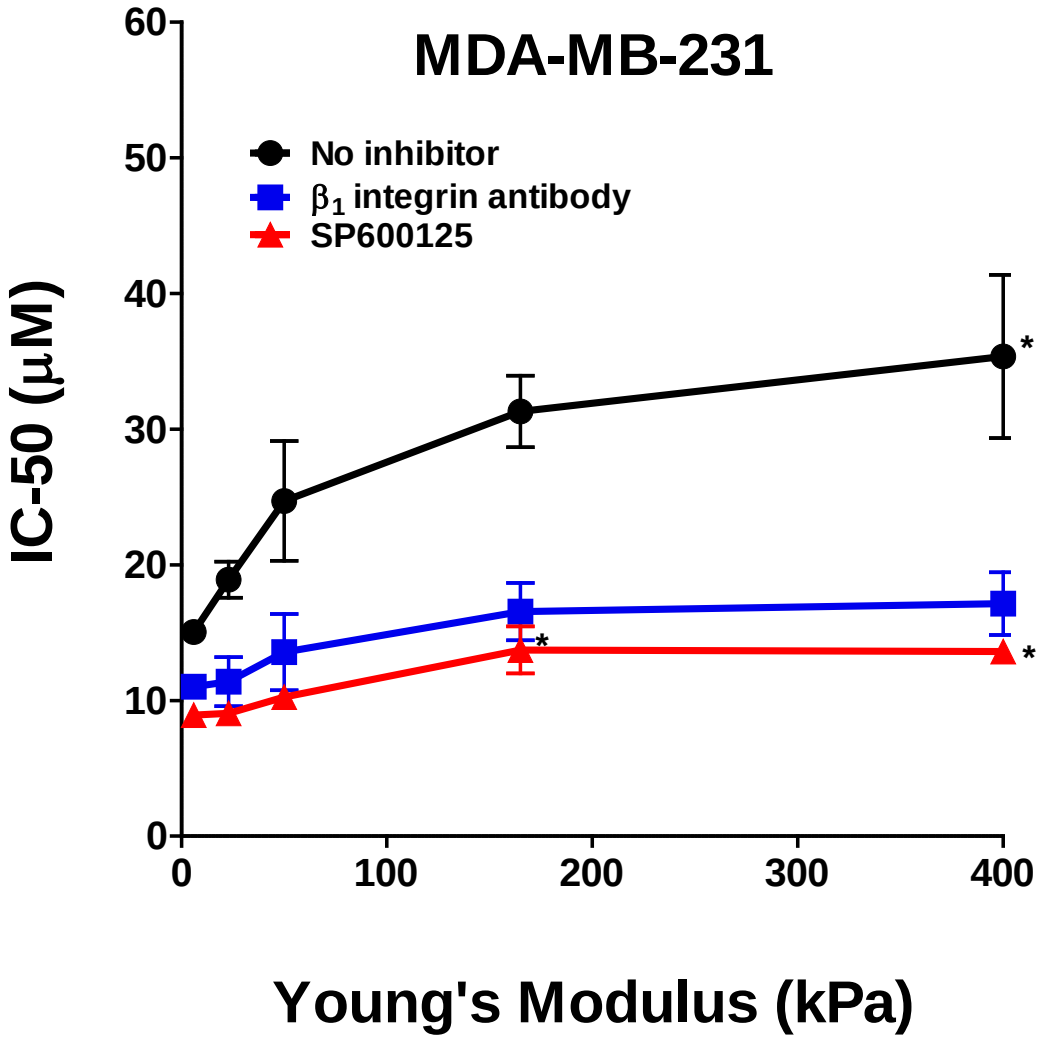

Figure 4.14 Inhibition of JNK shows similar results to treating with a β1 integrin antibody. Inhibition of β_1 integrin or its downstream effector JNK reduces the overall IC-50 and eliminates the stiffness-mediated drug resistance trend. Statistics shown are with respect to the softest gel condition. Figure adapted with permission from [74]. © 2014 Elsevier, Inc.

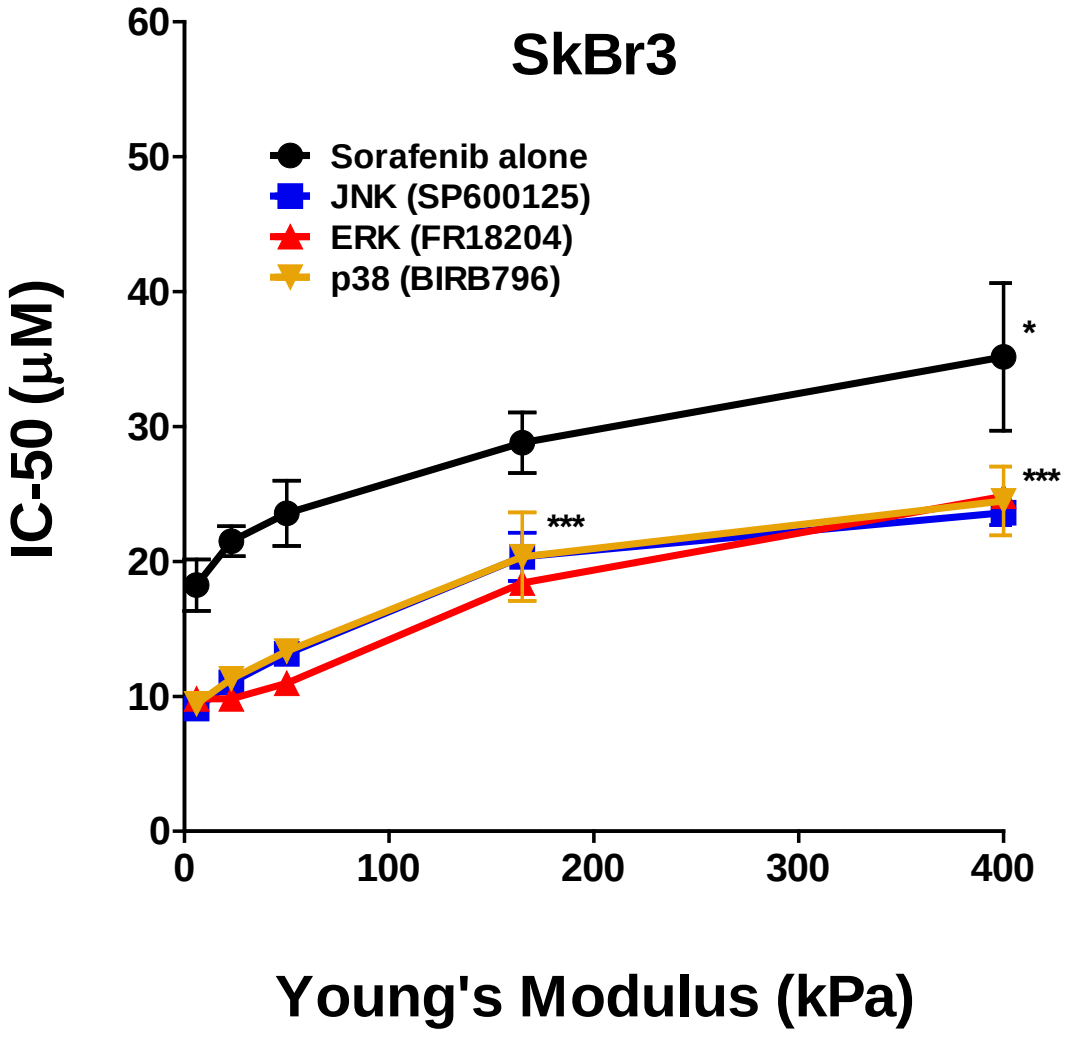

Figure 4.15 Inhibitions of JNK, ERK, and p38 do not dampen the stiffness induced drug resistance in SkBr3 cells. Inhibition of these molecule enhance the effectiveness of sorafenib at all conditions, but does not eliminate the stiffness-induced sorafenib resistance.

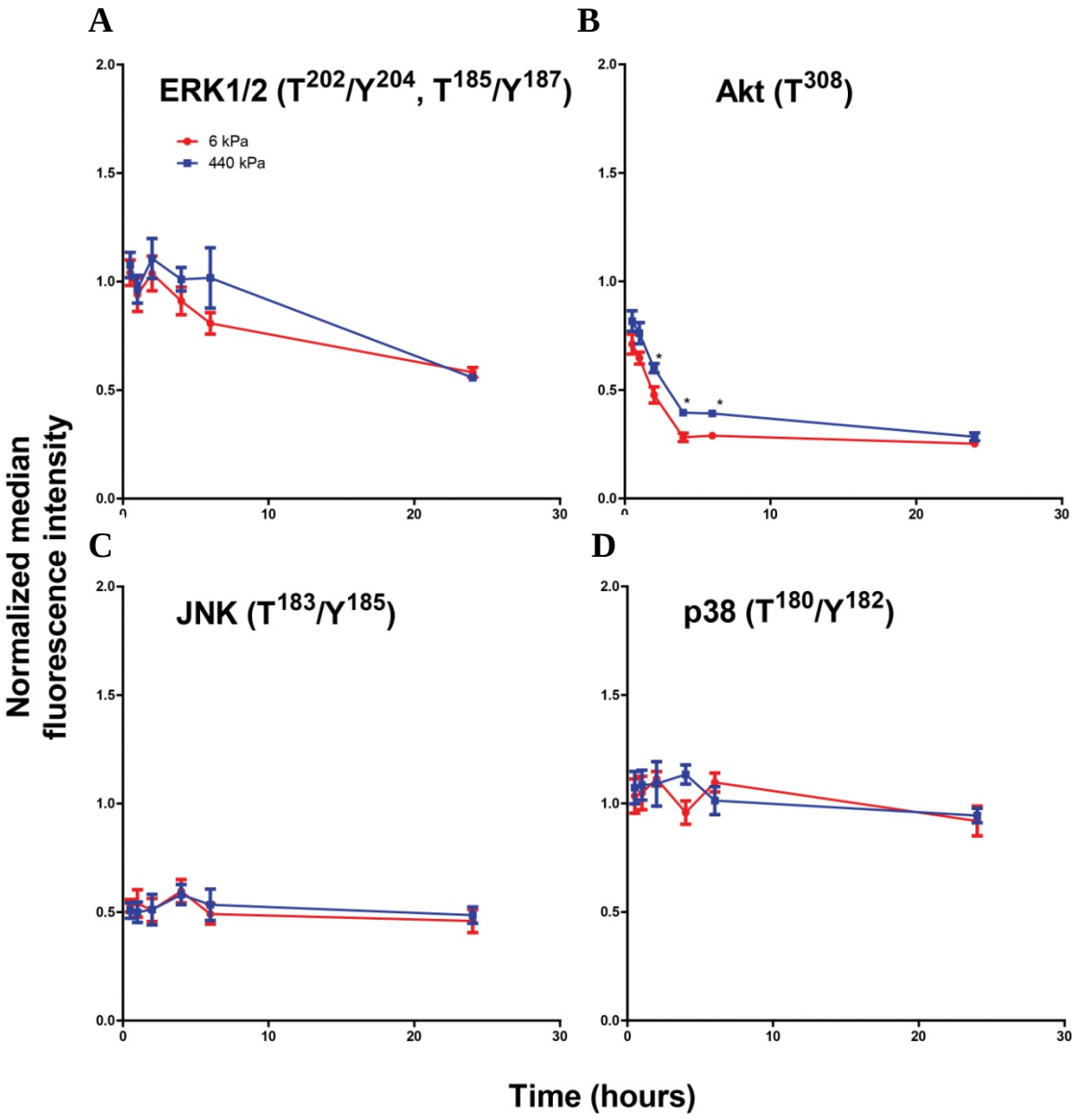

Figure 4.16 SkBr3s' Akt phosphorylation is increased on stiff subtrate. **(B)** Akt is the only signaling molecule that shows a modest increase in phosphorylation on stiff gels whereas the phosphorylation of **(A)** ERK, **(C)** JNK, **(D)** p38 are similar between soft and stiff substrates.

4.6 Conclusions

I propose that systems like my high-throughput PEG-PC hydrogel platform are critical for future screening of potential chemotherapeutics, as well as for discovery of possible mechanisms for failed efficacy of previously promising targets. With my platform, I discovered that the efficacy of sorafenib in carcinoma could potentially be increased by co-administering inhibitors to β_1 integrin or JNK, which could not have been appreciated on traditional tissue culture plastic plates. My results highlight the importance of incorporating relevant tissue stiffness and integrin binding ligands into the high-throughput drug screening process to increase the success of drugs in the development pipeline.

4.7 References

[1] Lu P, Weaver VM, Werb Z. The extracellular matrix: a dynamic niche in cancer progression. J Cell Biol 2012;196:395-406.

[2] Pietras K, Ostman A. Hallmarks of cancer: interactions with the tumor stroma. Exp Cell Res 2010;316:1324-31.

[3] Ostman A. The tumor microenvironment controls drug sensitivity. Nat Med 2012;18:1332-4.

[4] Wilson TR, Fridlyand J, Yan Y, Penuel E, Burton L, Chan E, et al. Widespread potential for growth-factor-driven resistance to anticancer kinase inhibitors. Nature 2012;487:505-9.

[5] Straussman R, Morikawa T, Shee K, Barzily-Rokni M, Qian ZR, Du J, et al. Tumour micro-environment elicits innate resistance to RAF inhibitors through HGF secretion. Nature 2012;487:500-4.

[6] Bhola NE, Balko JM, Dugger TC, Kuba MG, Sanchez V, Sanders M, et al. TGF-β inhibition enhances chemotherapy action against triple-negative breast cancer. J Clin Invest 2013;123:1348-58.

[7] Sun Y, Campisi J, Higano C, Beer TM, Porter P, Coleman I, et al. Treatment-induced damage to the tumor microenvironment promotes prostate cancer therapy resistance through WNT16B. Nat Med 2012;18:1359-68.

[8] Aoudjit F, Vuori K. Integrin signaling inhibits paclitaxel-induced apoptosis in breast cancer cells. Oncogene 2001;20:4995-5004.

[9] Park CC, Zhang H, Pallavicini M, Gray JW, Baehner F, Park CJ, et al. Beta1 integrin inhibitory antibody induces apoptosis of breast cancer cells, inhibits growth, and distinguishes malignant from normal phenotype in three dimensional cultures and in vivo. Cancer Res 2006;66:1526-35.

[10] Liu S, Wang J, Niu W, Liu E, Wang J, Peng C, et al. The beta6-integrin-ERK/MAP kinase pathway contributes to chemo resistance in colon cancer. Cancer Lett 2013;328:325-34.

[11] Yang XH, Flores LM, Li Q, Zhou P, Xu F, Krop IE, et al. Disruption of laminin-integrin-CD151-focal adhesion kinase axis sensitizes breast cancer cells to ErbB2 antagonists. Cancer Res 2010;70:2256-63.

[12] Rdnnov-jessen L, Petersen OW, Koteliansky V, Bissell MJ. The origin of the myofibroblasts in breast cancer. J Clin Invest 1995;95:859-73.

[13] Paraiso KH, Smalley KS. Fibroblast-mediated drug resistance in cancer. Biochem Pharmacol 2013;85:1033-41.

[14] Vong S, Kalluri R. The role of stromal myofibroblast and extracellular matrix in tumor angiogenesis. Genes Cancer 2011;2:1139-45.

[15] Otranto M, Sarrazy V, Bonte F, Hinz B, Gabbiani G, Desmouliere A. The role of the myofibroblast in tumor stroma remodeling. Cell Adh Migr 2012;6:203-19.

[16] Yang JD, Nakamura I, Roberts LR. The tumor microenvironment in hepatocellular carcinoma: current status and therapeutic targets. Semin Cancer Biol 2011;21:35-43.

[17] Levental KR, Yu H, Kass L, Lakins JN, Egeblad M, Erler JT, et al. Matrix crosslinking forces tumor progression by enhancing integrin signaling. Cell 2009;139:891-906.

[18] Samani A, Zubovits J, Plewes D. Elastic moduli of normal and pathological human breast tissues: an inversion-technique-based investigation of 169 samples. Phys Med Biol 2007;52:1565-76.

[19] Paszek MJ, Zahir N, Johnson KR, Lakins JN, Rozenberg GI, Gefen A, et al. Tensional homeostasis and the malignant phenotype. Cancer Cell 2005;8:241-54.

[20] Condeelis J, Pollard JW. Macrophages: obligate partners for tumor cell migration, invasion, and metastasis. Cell 2006;124:263-6.

[21] Egeblad M, Rasch MG, Weaver VM. Dynamic interplay between the collagen scaffold and tumor evolution. Curr Opin Cell Biol 2010;22:697-706.

[22] Kumar S, Weaver VM. Mechanics, malignancy, and metastasis: the force journey of a tumor cell. Cancer Metastasis Rev 2009;28:113-27.

[23] Kim J, Asthagiri AR. Matrix stiffening sensitizes epithelial cells to EGF and enables the loss of contact inhibition of proliferation. J Cell Sci 2011;124:1280-7.

[24] Netti PA, Berk DA, Swartz MA, Grodzinsky AJ, Jain RK. Role of extracellular matrix assembly in interstitial transport in solid tumors. Cancer Res 2000;60:2497-503.

[25] Schrader J, Gordon-Walker TT, Aucott RL, van Deemter M, Quaas A, Walsh S, et al. Matrix stiffness modulates proliferation, chemotherapeutic response, and dormancy in hepatocellular carcinoma cells. Hepatology 2011;53:1192-205.

[26] Zustiak S, Nossal R, Sackett DL. Multiwell stiffness assay for the study of cell responsiveness to cytotoxic drugss. Biotechnol Bioeng 2013;9999:1-8.

[27] Liu L, Cao Y, Chen C, Zhang X, McNabola A, Wilkie D, et al. Sorafenib blocks the RAF/MEK/ERK pathway, inhibits tumor angiogenesis, and induces tumor cell apoptosis in hepatocellular carcinoma model PLC/PRF/5. Cancer Res 2006;66:11851-8.

[28] Khatiwala CB, Kim PD, Peyton SR, Putnam AJ. ECM compliance regulates osteogenesis by influencing MAPK signaling downstream of RhoA and ROCK. J Bone Miner Res 2009;24:886-98.

[29] Xie B, Wang DH, Spechler SJ. Sorafenib for treatment of hepatocellular carcinoma: a systematic review. Dig Dis Sci 2012;57:1122-9.

[30] Tian B, Li Y, Ji XN, Chen J, Xue Q, Ye SL, et al. Basement membrane proteins play an active role in the invasive process of human hepatocellular carcinoma cells with high metastasis potential. J Cancer Res Clin Oncol 2005;131:80-6.

[31] Herrick WG, Nguyen TV, Sleiman M, McRae S, Emrick TS, Peyton SR. PEG-phosphorylcholine hydrogels as tunable and versatile platforms for mechanobiology. Biomacromolecules 2013;14:2294-304.

[32] Escudier B, Eisen T, Stadler WM, Szczylik C, Oudard S, Staehler M, et al. Sorafenib for treatment of renal cell carcinoma: Final efficacy and safety results of the phase III treatment approaches in renal cancer global evaluation trial. J Clin Oncol 2009;27:3312-8.

[33] Gupta-Abramson V, Troxel AB, Nellore A, Puttaswamy K, Redlinger M, Ransone K, et al. Phase II trial of sorafenib in advanced thyroid cancer. J Clin Oncol 2008;26:4714-9.

[34] Ridley AJ. Rho GTPases and cell migration. J Cell Sci 2001;114:2713-22.

[35] Ezzoukhry Z, Louandre C, Trecherel E, Godin C, Chauffert B, Dupont S, et al. EGFR activation is a potential determinant of primary resistance of hepatocellular carcinoma cells to sorafenib. Int J Cancer 2012;131:2961-9.

[36] Mendoza MC, Er EE, Blenis J. The Ras-ERK and PI3K-mTOR pathways: cross-talk and compensation. Trends Biochem Sci 2011;36:320-8.

[37] Singh A, Settleman J. EMT, cancer stem cells and drug resistance: an emerging axis of evil in the war on cancer. Oncogene 2010;29:4741-51.

[38] Vermeulen L, De Sousa EMF, van der Heijden M, Cameron K, de Jong JH, Borovski T, et al. Wnt activity defines colon cancer stem cells and is regulated by the microenvironment. Nat Cell Biol 2010;12:468-76.

[39] Tao L, Roberts AL, Dunphy KA, Bigelow C, Yan H, Jerry DJ. Repression of mammary stem/progenitor cells by p53 is mediated by Notch and separable from apoptotic activity. Stem Cells 2011;29:119-27.

[40] Klein EA, Yin L, Kothapalli D, Castagnino P, Byfield FJ, Xu T, et al. Cell-cycle control by physiological matrix elasticity and in vivo tissue stiffening. Curr Biol 2009;19:1511-8.

[41] Mih JD, Sharif AS, Liu F, Marinkovic A, Symer MM, Tschumperlin DJ. A multiwell platform for studying stiffness-dependent cell biology. PLoS One 2011;6:e19929.

[42] Tilghman RW, Cowan CR, Mih JD, Koryakina Y, Gioeli D, Slack-Davis JK, et al. Matrix rigidity regulates cancer cell growth and cellular phenotype. PLoS One 2010;5:e12905.

[43] Ulrich TA, de Juan Pardo EM, Kumar S. The mechanical rigidity of the extracellular matrix regulates the structure, motility, and proliferation of glioma cells. Cancer Res 2009;69:4167-74.

[44] Geiger B, Spatz JP, Bershadsky AD. Environmental sensing through focal adhesions. Nat Rev Mol Cell Biol 2009;10:21-33.

[45] Wang HB, Dembo M, Hanks SK, Wang Y. Focal adhesion kinase is involved in mechanosensing during fibroblast migration. Proc Natl Acad Sci U S A 2001;98:11295-300.

[46] Humphries JD, Byron A, Humphries MJ. Integrin ligands at a glance. J Cell Sci 2006;119:3901-3.

[47] Sethi T, Rintoul RC, Moore SM, MacKinnon AC, Salter D, Choo C, et al. Extracellular matrix proteins protect small cell lung cancer cells against apoptosis: a mechanism for small cell lung cancer growth and drug resistance in vivo. Nat Med 1999;5:662-8.

[48] Cabodi S, Moro L, Bergatto E, Boeri Erba E, Di Stefano P, Turco E, et al. Integrin regulation of epidermal growth factor (EGF) receptor and of EGF-dependent responses. Biochem Society Transactions 2004;32:438-42.

[49] Huveneers S, Danen EHJ. Adhesion signaling - crosstalk between integrins, Src and Rho. J Cell Sci 2009;122:1059-69.

[50] Manning AM, Davis RJ. Targeting JNK for therapeutic benefit: from junk to gold? Nat Rev Drug Discov 2003;2:554-65.

[51] Tournier C. The 2 faces of JNK signaling in cancer. Genes Cancer 2013;4:397-400.

[52] Cellurale C, Sabio G, Kennedy NJ, Das M, Barlow M, Sandy P, et al. Requirement of c-Jun NH(2)-terminal kinase for Ras-initiated tumor formation. Mol Cell Biol 2011;31:1565-76.

[53] Hess P, Pihan G, Sawyers CL, Flavell RA, Davis RJ. Survival signaling mediated by c-Jun NH(2)-terminal kinase in transformed B lymphoblasts. Nat Genet 2002;32:201-5.

[54] Sakurai T, Maeda S, Chang L, Karin M. Loss of hepatic NF-kappa B activity enhances chemical hepatocarcinogenesis through sustained c-Jun N-terminal kinase 1 activation. Proc Natl Acad Sci U S A 2006;103:10544-51.

[55] Wang J, Kuiatse I, Lee AV, Pan J, Giuliano A, Cui X. Sustained c-Jun-NH2-kinase activity promotes epithelial-mesenchymal transition, invasion, and survival of breast cancer cells by regulating extracellular signal-regulated kinase activation. Mol Cancer Res 2010;8:266-77.

[56] Cellurale C, Girnius N, Jiang F, Cavanagh-Kyros J, Lu S, Garlick DS, et al. Role of JNK in mammary gland development and breast cancer. Cancer Res 2012;72:472-81.

[57] Cellurale C, Weston CR, Reilly J, Garlick DS, Jerry DJ, Sluss HK, et al. Role of JNK in a Trp53-dependent mouse model of breast cancer. PLoS One 2010;5:e12469.

[58] Das M, Garlick DS, Greiner DL, Davis RJ. The role of JNK in the development of hepatocellular carcinoma. Genes Dev 2011;25:634-45.

[59] Hübner A, Mulholland DJ, Standen CL, Karasarides M, Cavanagh-kyros J. JNK and PTEN cooperatively control the development of invasive adenocarcinoma of the prostate. Proc Natl Acad Sci U S A 2012;109:12046-51.

[60] Coso OA, Chiariello M, Yu JC, Teramoto H, Crespo P, Xu N, et al. The small GTP-binding proteins Rac1 and Cdc42 regulate the activity of the JNK/SAPK signaling pathway. Cell 1995;81:1137-46.

[61] Hall A. Rho GTPases and the actin cytoskeleton. Science 1998;279:509-14.

[62] Yu H, Mouw JK, Weaver VM. Forcing form and function: biomechanical regulation of tumor evolution. Trends Cell Biol 2011;21:47-56.

[63] Hui L, Bakiri L, Mairhorfer A, Schweifer N, Haslinger C, Kenner L, et al. p38alpha suppresses normal and cancer cell proliferation by antagonizing the JNK-c-Jun pathway. Nat Genet 2007;39:741-9.

[64] Wada T, Stepniak E, Hui L, Leibbrandt A, Katada T, Nishina H, et al. Antagonistic control of cell fates by JNK and p38-MAPK signaling. Cell Death Differ 2008;15:89-93.

[65] Junttila MR, Li SP, Westermarck J. Phosphatase-mediated crosstalk between MAPK signaling pathways in the regulation of cell survival. FASEB J 2008;22:954-65.

[66] Shen YH, Godlewski J, Zhu J, Sathyanarayana P, Leaner V, Birrer MJ, et al. Cross-talk between JNK/SAPK and ERK/MAPK pathways: sustained activation of JNK blocks ERK activation by mitogenic factors. J Biol Chem 2003;278:26715-21.

[67] Meng F, Lowell CA. A beta 1 integrin signaling pathway involving Src-family kinases, Cbl and PI-3 kinase is required for macrophage spreading and migration. The EMBO Journal 1998;17:4391-403.

[68] Hirsch E, Barberis L, Brancaccio M, Azzolino O, Xu D, Kyriakis JM, et al. Defective Rac-mediated proliferation and survival after targeted mutation of the beta1 integrin cytodomain. J Cell Biol 2002;157:481-92.

[69] Almeida EA, Ilić D, Han Q, Hauck CR, Jin F, Kawakatsu H, et al. Matrix survival signaling from fibronectin via focal adhesion kinase to c-Jun NH(2)-terminal kinase. J Cell Biol 2000;149:741-54.

[70] Hsia DA, Mitra SK, Hauck CR, Streblow DN, Nelson JA, Ilic D, et al. Differential regulation of cell motility and invasion by FAK. J Cell Biol 2003;160:753-67.

[71] Flaim CJ, Chien S, Bhatia SN. An extracellular matrix microarray for probing cellular differentiation. Nat Methods 2005;2:119-25.

[72] Anderson DG, Putnam D, Lavik EB, Mahmood TA, Langer R. Biomaterial microarrays: rapid, microscale screening of polymer-cell interaction. Biomaterials 2005;26:4892-7.

[73] Khademhosseini A, Langer R, Borenstein J, Vacanti JP. Microscale technologies for tissue engineering and biology. Proc Natl Acad Sci U S A 2006;103:2480-7.

[74] Nguyen TV, Sleiman M, Moriarty T, Herrick WG, Peyton SR. Sorafenib resistance and JNK signaling in carcinoma during extracellular matrix stiffening. Biomaterials 2014;35:5749-5759.

CHAPTER 5

A COMPARISON BETWEEN 2D AND 3D PLATFORMS FOR CANCER DRUG SCREENING

5.1 Abstract

The tumor microenvironment plays an important role in providing a niche to nurture tumor growth and promote drug resistance. Various platforms have been developed to recapitulate many key features of the tumor ECM. I have taken a holistic approach to compare the drug response of the MDA-MB-231, an EGFR overexpressing cell line, and SkBr3, a HER2 overexpressing cell line, across different types of two and three dimensional (2D and 3D) platforms. I have tested sorafenib (a Raf inhibitor), lapatinib (an EGFR/HER2 inhibitor), temsirolimus (a mTOR inhibitor), and doxorubicin (a cytotoxic drug), and observed that the sensitivity of cell-drug interaction to microenvironment is dependent on both drug type and cell type. The IC-50s of SkBr3s when treated with sorafenib and temsirolimus were most sensitive to the change in platform, whereas those of 231s were sensitive to the platform type when treated with sorafenib and lapatinib. The IC-50 of both cell lines, when treated with doxorubicin, were not sensitive to the type of platform. Both HER3 and EGFR phosphorylation in SkBr3s were found to be sensitive to the change in the surrounding microenvironment whereas HER2 phosphorylation was not. Long-term culture of SkBr3 cells with lapatinib induced an upregulation of Insulin Receptor (IR) and its downstream effector ERK in 2D, but not

in 3D. These results provide insights into how the interaction between cell and microenvironment influences their response to drug and may guide future development of biomaterial platforms for drug screening.

5.2 Introduction

Many groups have developed various cell culture platforms in both 2D and 3D that are capable of capturing the key features of the tumor microenvironment to study cellular response to chemotherapeutics. For example, I have previously developed a high-through put drug screening tool based on PEG-PC hydrogel system, whereas others have done so with PAA hydrogels [1,2], and all of these systems can be easily integrated with the traditional high-throughput screening of drug compounds in 96- or 384-well plates. Other high-throughput systems, which are more complicated to fabricate, have also been developed such as PEG microwells [3] and microarray for cell-based drug screening [4]. In addition, cell-drug interaction can be studied in 3D biomaterial scaffolds such as PEG-based hydrogels that encapsulated single cell [5] or spheroids [6,7], or gelatin hydrogel encapsulating spheroids [8]. Other 3D spheroid models include various methods that induce spheroid formation through allowing aggregation of non-adherent cells such as agarose [9] or PDMS [10] coated plates.

Each type of these models has advantages and drawbacks with respect to recapitulation of the complex biology, ease of fabrication and use, cost, etc. As compared with 3D models, the 2D platforms are easier to fabricate and scale up for high-throughput screening; however, these models can only capture the tissue mechanical properties and allow highly-controlled bioconjugation of integrin binding sites. They cannot recapitulate

the 3D microenvironment that cells experience *in vivo*. Some 3D models can capture the three dimensional geometry, modulus, integrin binding sites, and MMP degradable sites that allow cells to remodel the environment. For instance, Leight et al. developed a 3D PEG-based platform with MMP-degradable and MMP sensor peptides to study the relationship between RAF inhibitors and MMP activity of metastatic melanoma cells [5]. However, single cells encapsulated in these 3D materials lack the *in vivo* cell-cell contact. Cadherins, which mediate cell-cell contact, can crosstalk with other growth factors receptors such as EGFR [11], HGFR, and FGFR [12] followed by activation of downstream signaling pathways such as Wnt signaling [12] or MAPK [13] that can promote survival in the presence of chemotherapeutics [14]. Thus, the spheroid models allow cells to establish complex cell-cell and cell matrix interactions and capture certain features of human *in vivo* tissues such as histomorphology, function, and microenvironments [15]; therefore, they are usually touted as an ideal model for preanimal and preclinical drug screening to identify promising drug candidates [9]. However, it takes time for spheroid culture, and it is also hard to scale-up for high-throughput screening.

To identify an appropriate model for drug screening, I investigated cell-drug interaction across multiple platforms: the common tissue culture plastic plate, 2D hydrogel platform, 3D platform that encapsulates single cell or spheroid. Since variation in modulus is known to affect cellular response to drugs [1,16,17], I considered two different moduli for each platform. I applied the previously developed 2D PEG-PC platform [16,18] and the 3D PEG-Maleimide (PEG-MAL) system, which is well-characterized by Phelps et al. [19]. PEG-MAL can be crosslinked by thiol containing

crosslinker following Micheal-type addition, which requires a nucleophilic buffering reagent such as TEOA or HEPES instead of using toxic free-radicals and UV light [19]. I tested 3 targeted drugs, which target the two most common cell proliferation pathways (temsirolimus - Akt/mTOR and sorafenib - Raf/MEK/ERK) and two of the most well-characterized receptor tyrosine kinases (lapatinib - EGFR and HER2), and one cytotoxic drug (doxorubicin). I also examined the sensitivity of RTK receptors to modulus in 3D under growth factor stimulation and the influence of 2D and 3D platforms to RTKs' phosphorylation and downstream signaling in drug-treated cells.

5.3 Materials And Methods

5.3.1 Cell culture

All supplies were purchased from Life Technologies (Carlsbad, CA) unless otherwise noted. Human breast cancer cell lines (MDA-MB-231 and SkBr3) were generous gifts from Dr. Shannon Hughes at the Massachusetts Institute of Technology, and were cultured in Dulbecco's Modified Eagle's Medium (DMEM) supplemented with 10% fetal bovine serum (FBS) and 1% penicillin-streptomycin (P/S) at 37ºC and 5% CO_2.

5.3.2 Spheroids culture

The lyophilized poly(N-isopropylacryamide)-poly(ethylene glycol) (PNIPAAm-PEG, Cosmo Bio, Carlsbad, CA) was reconstituted in cell culture medium for a day and kept in the refrigerator for long-term storage. All cell suspensions were prepared at a density between 1-1.5 million cells per mL. An appropriate volume of cell suspension was added into PNIPAAm-PEG solutions to make 100,000 cells/mL for SkBr3s and

167,000 cells/mL for 231s. The gel solution was kept on ice to prevent early gelation. Gels with 150 μL volume were pipetted into a 6-well plate, and the plates were incubated in the incubator for 10-15 minutes to induce gelation. After gelation, cell culture medium was added to the wells. Cells were cultured to grow into spheroids for 14 days, and the medium was replenished every other day.

5.3.3 Hydrogel mechanical characterization

Hydrogels polymerized from 4-arm PEG-maleimide (20 kDa, PEG-MAL, Jenkem Technology USA, Plano, TX) were used as a platform to study the response of cells to drugs in 3D. PEG-MAL solutions were prepared at 10 wt % and 20 wt %, and PEG dithiol (average Mn 1000, Sigma-Aldrich, St. Louis, MO) was dissolved in triethanolamine (TEA, pH ~ 7.4) at concentrations of 100 and 200 mg/mL. Polymerization of PEG-MAL gels were induced by combining 10 and 20 wt % PEG-MAL with 100 and 200 mg/mL of PEG dithiol, respectively (9:1 PEG-MAL:PEG dithiol by volume). Hydrogel cylinders for mechanical compression testing were formed in 5-mm Teflon molds and swelled in PBS for 24 h. Post swelling, hydrogel dimensions were measured with a digital caliper, and mechanical compression tests were performed with a TA Instruments (New Castle, DE) AR-2000 rheometer at a 2 μm/s strain rate. The Young's modulus (E) for each hydrogel was calculated by plotting the measured normal force between 0 and 4% strain and dividing the slope of the best-fit linear regression by the hydrogel cross-sectional area.

5.3.4 Quantification of drug response

5.3.4.1 Spheroids in 3D PEG-MAL hydrogels

The medium in the 6-well plate that had spheroids cultured in PNIPAAm-PEG was removed. 4 mL of cold serum-free DMEM supplemented with 1% pen/strep were added to each of the well, and the plate was kept on ice for 5 minutes to ensure the complete dissolution of PNIPAAm gels. The spheroids in suspension were transferred into 2 15-mL tubes with equal volume in each, and cut pipette tips were used to handle the spheroids in order to reduce the shear stress. The tubes were kept on ice for 30 minutes to allow the spheroids to settle at the bottom. After 30 minutes, the medium was carefully removed so that the spheroids were not disturbed. Then the spheroids in each tube were resuspended in 10 wt % and 20 wt % PEG-MAL dissolved in serum-free DMEM. Cell binding peptide CRGD (Genscript, Piscataway, NJ) was added to the PEG-MAL solutions to make 2 mM final concentration. The gels were made in a 48-well plate by combining 9 μL of PEG-MAL with 1 μL of PEG dithiol in TEOA. The gel was allowed to polymerize for 5 minutes before addition of either serum-free DMEM supplemented with 1% P/S, 20 ng/mL of epidermal growth factor (EGF, R&D Systems, Minneapolis, MN) and 20 ng/mL of platelet-derived growth factor (PDGF-BB, eBioscience, San Diego, CA) or DMEM with 1% P/S and 10% FBS. To ensure the consistency among experiments, the amount of spheroids collected from 1 PNIPAAm gels were consistently transfered to 9 PEG-MAL gels. After 24 h, spheroids were treated with lapatinib (0-80 μM, LC Laboratories, Woburn, MA), sorafenib (0-64 μM, LC Laboratories), temsirolimus (0-80 μM, Selleckchem, Houston, TX), or doxorubicin (0-20 μM, LC Laboratories). All drugs were dissolved in the same type of medium as the

spheroids prior to drug treatment. Dimethyl sulfoxide (DMSO, Sigma-Aldrich) was used as a vehicle control in all experiments. After 48 h of drug treatment, cell viability was quantified by CellTiter Glo® Luminescent Cell Viability Assay (Promega, Madison, WI), which measured the amount of ATP in the cells. After 40 minutes of incubation, the plate were read with the Synergy 2 Multi-Mode Reader (BioTek, Winooski, VT). The IC-50s were calculated by using the Excel's non-linear curve fitting of the data.

5.3.4.2 Single cells in 3D PEG-MAL hydrogels

Cells cultured on tissue culture flask were collected and resuspended in PEG-MAL solutions at the concentration of 555,556 cells/mL (5,000 cells per gel). PEG-MAL gels including 2 mM RGD were made as described above and kept in serum-free DMEM with growth factors. After 24 h, the cells were treated with similar drugs described above.

5.3.4.3 Cells on 2D PEG-PC hydrogels

2D PEG-PC hydrogels in the 96-well plate and protein coupling were prepared as described previously [16]. PC was used at 17 wt % (0.6M), and PEG was used at 1.1 wt % (0.015 M) and 3.2 wt % (0.043 M) to make 10 and 33 kPa gels, respectively. Collagen I was coupled to the gel surface at 3.3 $\mu g/cm^2$. Cells were seeded at 10,000 cells per well in serum-free DMEM with growth factors. After 24 h, the cells were treated with similar drugs described above.

5.3.4.4 Cells on tissue culture plastic plate

Cells were seeded at 5,000 cells per well in serum containing medium. After 24 h, the medium was replaced with serum-free medium supplemented with EGF and PDGF growth factors. After 24 h, cells were treated with similar drugs.

5.3.5 Quantification of cell number in spheroids in PEG-MAL gels

In order to quantify the total number of cells in each of the PEG-MAL gel encapsulating spheroids, the total amount of DNA in spheroids was quantified with CyQUANT Cell Proliferation Assay Kit (Life Technologies). The assay was prepared by mixing the 1X cell lysis buffer with the Cyquant GR Dye (1:400, Dye:Lysis buffer). The gels were removed from the plate with a spatula and placed in 1.5 mL microcentrifuge tubes. All tubes were flash-frozen with liquid nitrogen. 200 μL of the assay were added to the tube. The hand-held biovortexer (Research Products International, Mt Prospect, IL) was used to mechanically break down the gels and enhanced the release of the dye into the solution. The solutions were transfer to a 96-well plate, and the fluorescent intensity was read at 480/520 excitation/emission with the Synergy 2 plate reader.

5.3.6 EGF stimulation of spheroids in PEG-MAL gels

Spheroids were encapsulated in 10 and 20 wt % PEG-MAL with RGD binding peptides and serum-starved for 24 h. Then spheroids were stimulated with 100 ng/mL of EGF, and cell lysates were collect at 10, 30, and 60 min. After 1 h, EGF medium was replaced with serum-free medium, and cell lysates were collected at 7 and 24 h time points. Cell lysis buffer (MILLIPLEX® MAP Phospho Mitogenesis RTK Magnetic Bead, EMD Millipore, Billerica, MA) was supplemented with protease (EDTA-free Protease Inhibitor Cocktail Tablets, 1 tablet in 3 mL, Roche, Indianapolis, IN) and phosphatase (2x phosphatase inhibitors cocktail-II, Boston Bioproducts, Boston, MA) inhibitors, 1 mM of phenylmethylsulfonyl fluoride (PMSF, Thermo Scientific, Rockford, IL), 5 μg/mL of pepstatin (Thermo Fisher Scientific, Waltham, MA), 10 μg/mL of leupeptin (Thermo Fisher Scientific), 1 mM of sodium pyrophosphate (Thermo Fisher

Scientific), 25 mM of β-glycerophosphate (Santa Cruz, Dallas, TX), 1 mM of sodium orthovanadate (MP Biomedicals, Solon, OH). At each time point, the gels were washed with ice-cold 1X PBS, transfered to the tubes, frozen with liquid nitrogen, and stored at -80ºC. Multiple gels were combined in order to collect enough proteins for each of the condition. When collecting lysates, samples were allowed to thaw on ice for 20 minutes before addition of cell lysis buffer. A biovortexer was used to enhance the release of the proteins to the solution. Total protein concentration was quantified with a BCA protein assay (Thermo Scientific). Lysate concentrations were adjusted to 120 μg/mL, and the phosphorylation levels of c-MET/HGFR, EGFR, ErbB2/HER2, ErbB3/HER3, ErbB4/HER4, IGF-1R, IR were quantified with a MAGPIX (Luminex, Austin, TX) with the MILLIPLEX® MAP Phospho Mitogenesis RTK Magnetic Bead (EMD Millipore) according to the manufacturer instructions.

5.3.7 Long-term lapatinib treatment on 2D and in 3D

SkBr3 single cells were either encapsulated in PNIPAAm-PEG gels or seeded on a plastic 6-well plate. Post encapsulation/seeding, cells were kept in cell culture medium with either 1.25 μM of Lapatinib or DMSO control. After 14 days, both cells on plastic plate and in gels were serum-starved for 24 h. Then cells were stimulated with 10% serum medium for 15 min, and cell lysates were collected. The phosphorylation levels of similar RTKs and downstream signaling molecules (ERK1/2, Akt, JNK, Bio-Plex Pro™ phospho-ERK1/2, phospho-Akt, phospho-JNK, Bio-Rad Laboratories, Hercules, CA) were quantified.

5.3.8 Statistical Analysis

Prism v5.04 (GraphPad Software) was used to perform unpaired Student's t-test, a one-way analysis of variance (ANOVA) with a Tukey post-test, and a two-way ANOVA. Data are reported as mean ± standard error. $p \leq 0.05$ is denoted with *, ≤ 0.01 with **, and ≤ 0.001 with ***; $P > 0.05$ is considered not significant ("ns").

5.4 Results

5.4.1 The influence of platform to the IC-50 is drug-type dependent

I have evaluated drug response across 4 different classes of drugs with two cell lines on classic plastic surfaces, 2D gel surfaces, and within 3D gels (either as single cells or spheroids in serum or serum-free medium) to identify the appropriate model for each type of drug mechanism (Figure 5.1A). The drugs include sorafenib, which targets Raf kinase in the Raf/MEK/ERK pathway, lapatinib, which targets EGFR/HER2 receptor tyrosine kinases (RTK), temsirolimus, which targets mTOR in the PK3K/Akt pathway, and doxorubicin, which causes cell death by DNA intercalation. All of the experiments were done with serum-free DMEM supplemented with P/S and 20 ng/mL of EGF and PDGF except for some experiments with spheroid in 10% FBS medium as indicated. For 3D platform, single cells were encapsulated in PNIPAAm-PEG hydrogels and cultured for 14 days to induce spheroid formation (Figure 5.1B-E). Spheroids were then transferred to PEG-MAL gels of 10 and 20 wt. %, which were measured to be 3 and 5 kPa (Figure 5.2). The similar fluorescent signals, which were determined by the fluorescent DNA-binding dye, between 3 and 5 kPa PEG-MAL gels indicate that the total amount of spheroids were evenly distributed (Figure 5.3).

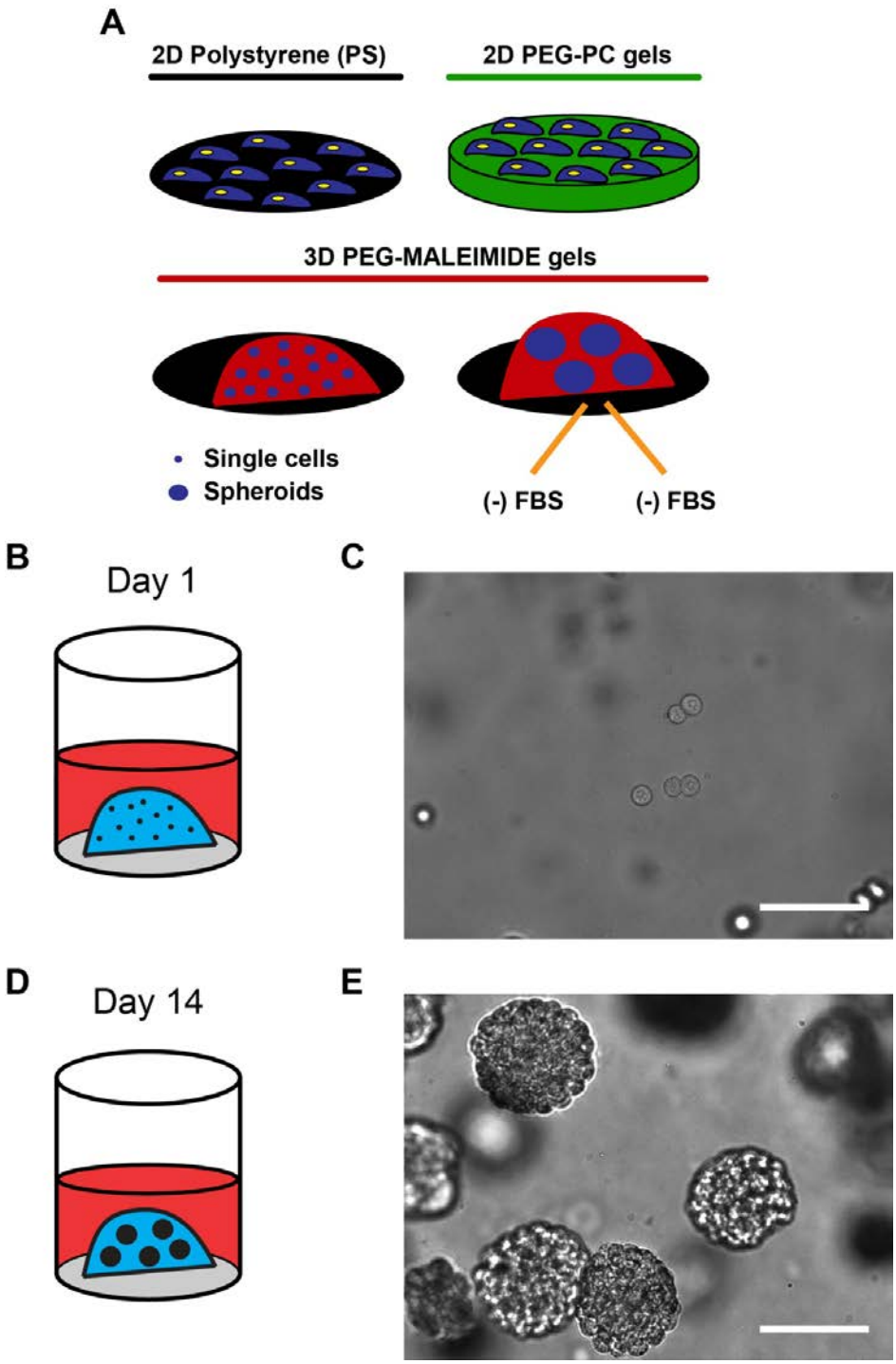

Figure 5.1 Schematic of different types of platforms for drug screening. **(A)** Cells were laid on polystyrene 96-well plates and PEG-PC gels of different stiffnesses in 96-well plate, or encapsulated in PEG-MAL gels of different stiffnesses as single cells or spheroids. Spheroids were treated with either serum medium or no-serum medium. Scale bars are 100 μm. Representative images of SkBr3 cells encapsulated in PNIPAAm-PEG hydrogel on day 1 **(B)** - **(C)** and day 14 **(D)** - **(E)**.

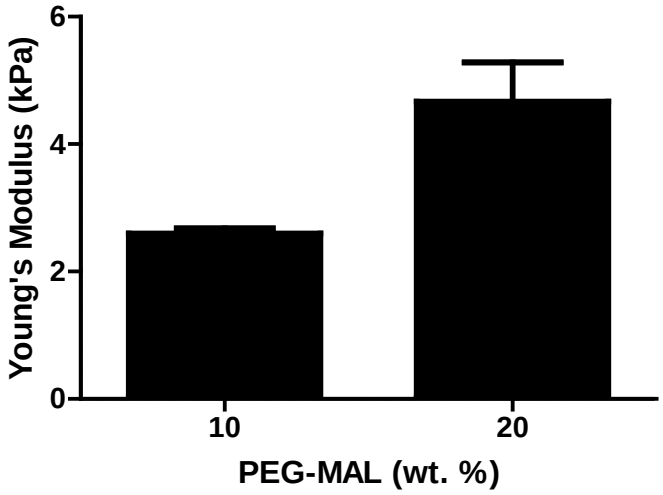

Figure 5.2 Young's modulus of 10 and 20 wt % PEG-MAL hydrogels.

A

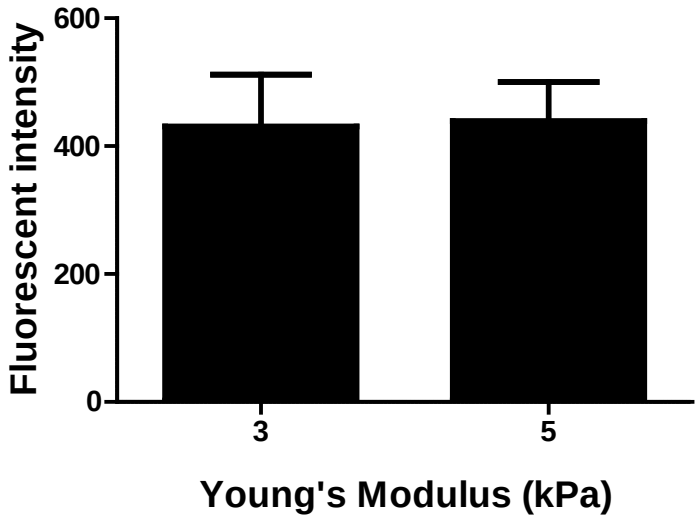

B

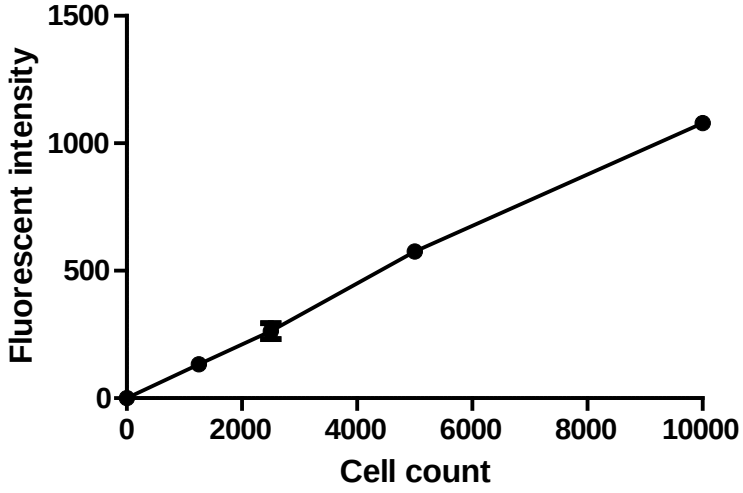

Figure 5.3 The amount of spheroids are similar between 3 and 5 kPa PEG-MAL gels. **(A)** The fluorescent intensity, which correlates with the amount of DNA, are the same. **(B)** The fluorescent intensity is linearly correlated with cell number.

Drug resistance in spheroids can be mediated by the limitation of drug diffusion into the spheroids [20], and drug and oxygen diffusion can decrease significantly for tumor cells that were more than 60 μm from blood vessels [21]. Therefore, all spheroids were harvested when their size were around 100-150 μm in diameter (Figure 5.1E) to eliminate this possibility. For both cell lines, proliferation was quantified at the same time point as drug treatment. When analyzing the proliferation of SkBr3 across all platforms, the students' t-test, which was used to compare the proliferation between soft and stiff gels within the same platform, shows a significant increase in proliferation of monolayer cells on stiff 2D PEG-PC gels and a decrease in proliferation of single cell and spheroids in stiff 3D PEG-MAL gels as compared with the other modulus condition (Figure 5.4A). This observed opposite trend in proliferation between 2D and 3D platforms is consistent with other observations that cells proliferate more on 2D stiffer substrate [22,23] and in 3D softer gels [24,25]. When comparing between 2D and 3D platforms (2D gels, 3D single cell and spheroids), two-way ANOVA analysis found that the change in platform was the larger driver of proliferation (35% of total variance, $p < 0.0001$), followed by modulus (10%, $p < 0.0001$) (Table 5.1). Proliferation on plastic could not be included in two-way ANOVA analysis because it had only one stiffness condition. When comparing the effect between medium and modulus (3D spheroids with and without FBS), two-way ANOVA analysis showed that the change in medium had a larger effect on total variance (56%, $p < 0.0001$)) than the change in modulus (3%, $p = 0.064$). When two-way ANOVA analysis was performed to the IC-50s of all 4 drugs in the same manner with proliferation data, both sorafenib (Figure 5.4B) and temsirolimus (Figure 5.4D) are strongly sensitive to platform (51% ($p = 0.0018$) and 80% ($p = 0.0007$) of total variance as opposed to 3%

($p = 0.2898$ and 0.2404) from modulus for both sorafenib and tesmirolimus, respectively) and medium condition (81% ($p < 0.0001$)and 87% ($p = 0.0006$) of total variance as opposed to 2% ($p = 0.168$) and 0.3% ($p = 0.7101$) from modulus for sorafenib and temsirolimus, respectively). For both lapatinib (Figure 5.4C) and doxorubicin (Figure 5.4E), although none of these three variables cause a significant difference in the IC-50s, the platform was found to affect the results more than modulus (35% ($p = 0.0995$) vs. 10% ($p = 0.2241$) and 8% ($p = 0.6956$) vs. 2 % ($p = 0.6735$) of total variance for lapatinib and doxorubicin, respectively). Similarly, medium effected to results more than modulus (28% ($p = 0.1688$) vs. 0.08% ($p = 0.9351$) and 49% ($p = 0.0526$) vs. 0.01% ($p = 0.9764$) of total variance for lapatinib and doxorubicin, respectively). Overall, variations in platform and medium strongly affected how SkBr3s responded to sorafenib and temsirolimus, but not to lapatinib and doxorubicin. In addition, when one-way ANOVA was performed to compared the IC-50s across all conditions for all 4 drugs, spheroids in serum-supplemented medium were found to be most resistant to sorafenib and temsirolimus, but not to lapatinib and doxorubicin. Surprisingly, all variations with IC-50s across all conditions were not correlated with proliferation (Figures 5.5A-D).

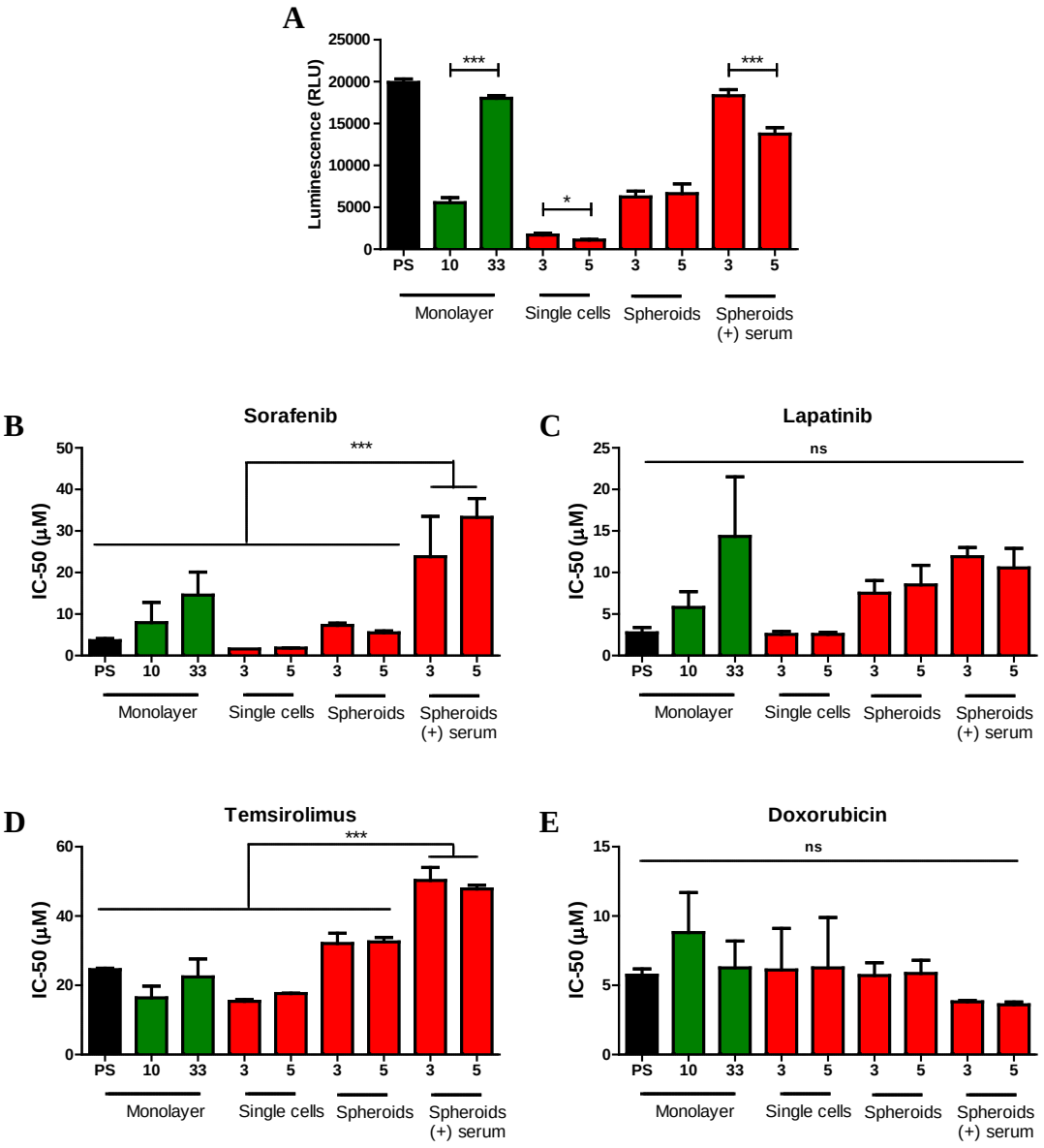

Figure 5.4 The responses of SkBr3 cells to drugs are dependent on drug types, platform, and medium condition. **(A)** The proliferation was quantified across multiple platforms. The students' t-test showed cells proliferated more on stiffer substrate in 2D and in softer substrate in 3D. One-way ANOVA analysis across all conditions showed the IC-50s of spheroids in serum medium were highest with **(B)** sorafenib and **(D)** temsirolimus, but did not change much with **(C)** lapatinib and **(E)** doxorubicin.

	Sensitivity to platform (%) (2D and 3D)	Sensitivity to modulus (%) (2D and 3D)	Sensitivity to medium (%) (spheroid only)	Sensitivity to modulus (%) (spheroid only)
Proliferation	35 (*)	10 (*)	57 (*)	3
Sorafenib	51 (*)	3	81 (*)	2
Lapatinib	35	10	28	0.08
Temsirolimus	80 (*)	3	87 (*)	0.3
Doxorubicin	8	2	49	0.01

Table 5.1 Two-way ANOVA analysis of SkBr3 cells. Summary of two-way ANOVA analysis of SkBr3s' IC-50s for sensitivity to platform, medium, and modulus.

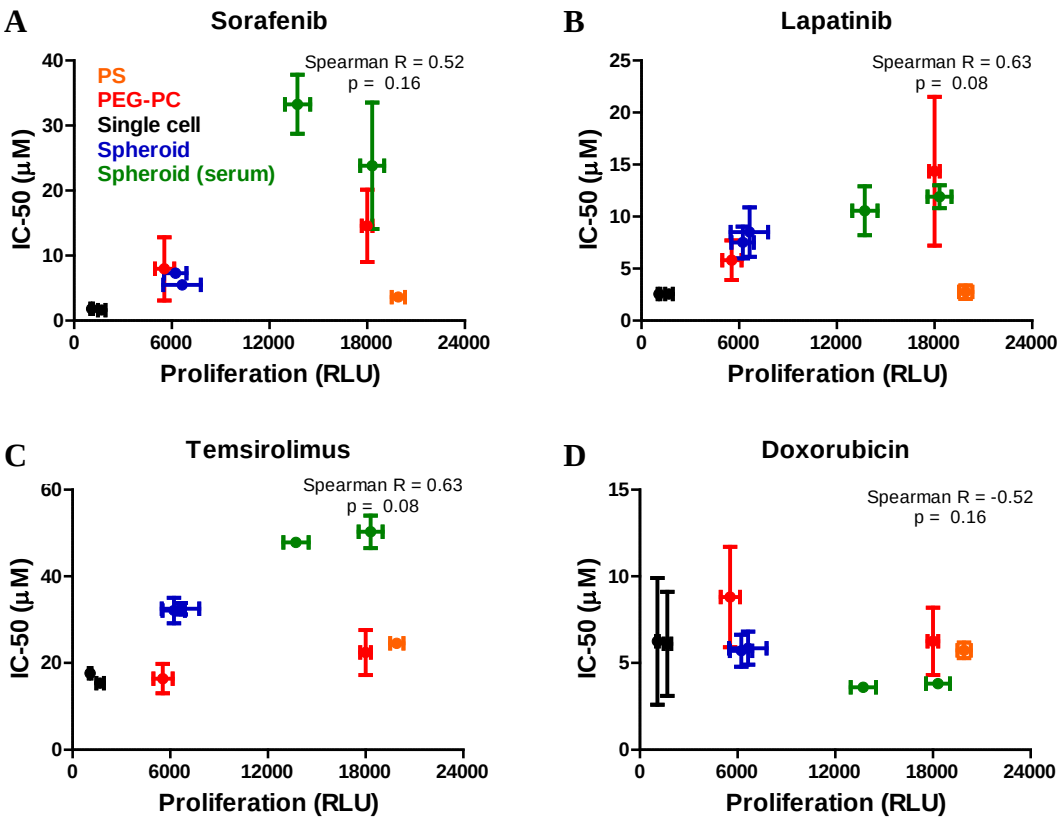

Figure 5.5 Spearman correlation between IC-50s and proliferation of SkBr3s. There is not any significant correlation between the IC-50s and proliferation for all drugs: **(A)** sorafenib, **(B)** lapatinib, **(C)** temsirolimus, and **(D)** doxorubicin.

Interestingly, the proliferation of MDA-MB-231 cells also showed a similar modulus-dependent trend as SkBr3 cells, with cells proliferating more on 2D stiffer gels, and in 3D softer gels, as indicated by the student's t-test (Figure 5.6A). However, when a two-way ANOVA was performed as described above, both platform and medium appeared to affect the proliferation more than modulus (49% ($p < 0.0001$) vs. 0.8% ($p = 0.1329$) and 59% ($p < 0.0001$) vs. 28% ($p < 0.0001$) of total variance for both platform and medium, respectively). For sorafenib (Figure 5.6B) and lapatinib (Figure 5.6C), platform, medium, and modulus significantly contributed to the variation in IC-50s (with the exception of modulus when compared with platform for sorafenib); however, platform and medium had a much larger effect on total variance than modulus (Table 5.2). For temsirolimus (Figure 5.6D) and doxorubicin (Figure 5.6E), none of these parameters significantly affected the outcome of the IC-50; nevertheless, the modulus had a slightly larger effect on total variance than the platform and medium (with the exception of modulus when compared with medium for temsirolimus) (Table 5.2). One-way ANOVA analysis of all IC-50s for 4 drugs indicated that spheroids in serum-supplemented medium were most resistant to sorafenib and lapatinib, but not to temsirolimus and doxorubicin. Overall, platform, medium, and modulus significantly affected the 231s' IC-50s of sorafenib and lapatinib, but none of these had any impact on the IC-50s of temsirolimus and doxorubicin. In contrast to the SkBr3s, the variations in IC-50s of the 231s were positively correlated with the change in proliferation across different platforms for sorafenib, lapatinib, and temsirolimus (Figures 5.7A-C); however, similar to the SkBr3s, there was not a correlation between the IC-50 and proliferation for doxorubicin (Figure 5.7D).

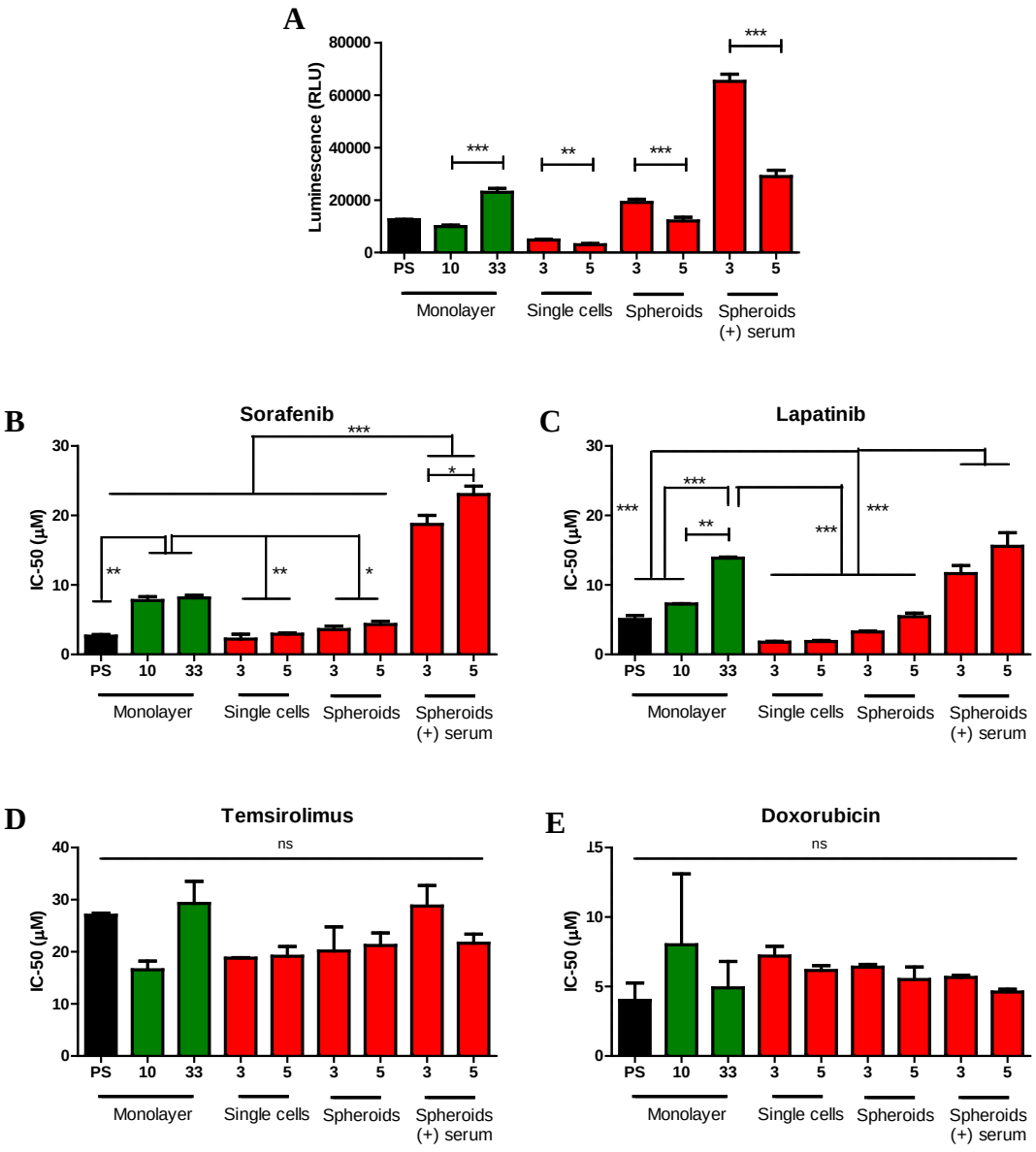

Figure 5.6 The responses of MDA-MB-231 cells to drugs are dependent on drug types, platform, medium, and modulus conditions. **(A)** The proliferation was quantified across multiple platforms. The students' t-test showed cells proliferated more on stiffer substrate in 2D and in softer substrate in 3D. One-way ANOVA analysis across all conditions showed the IC-50s were strongly sensitive to platform and medium condition with **(B)** sorafenib and **(C)** lapatinib, but did not change much with **(D)** temsirolimus and **(E)** doxorubicin.

	Sensitivity to platform (%) (2D and 3D)	Sensitivity to modulus (%) (2D and 3D)	Sensitivity to medium (%) (spheroid only)	Sensitivity to modulus (%) (spheroid only)
Proliferation	49 (*)	0.8	59 (*)	28 (*)
Sorafenib	91 (*)	2	96 (*)	2 (*)
Lapatinib	76 (*)	14 (*)	86 (*)	9 (*)
Temsirolimus	11	22	22	10
Doxorubicin	1	11	27	37

Table 5.2 Two-way ANOVA analysis of MDA-MB-231 cells. Summary of two-way ANOVA analysis of MDA-MB-231s' IC-50s for sensitivity to platform, medium, and modulus.

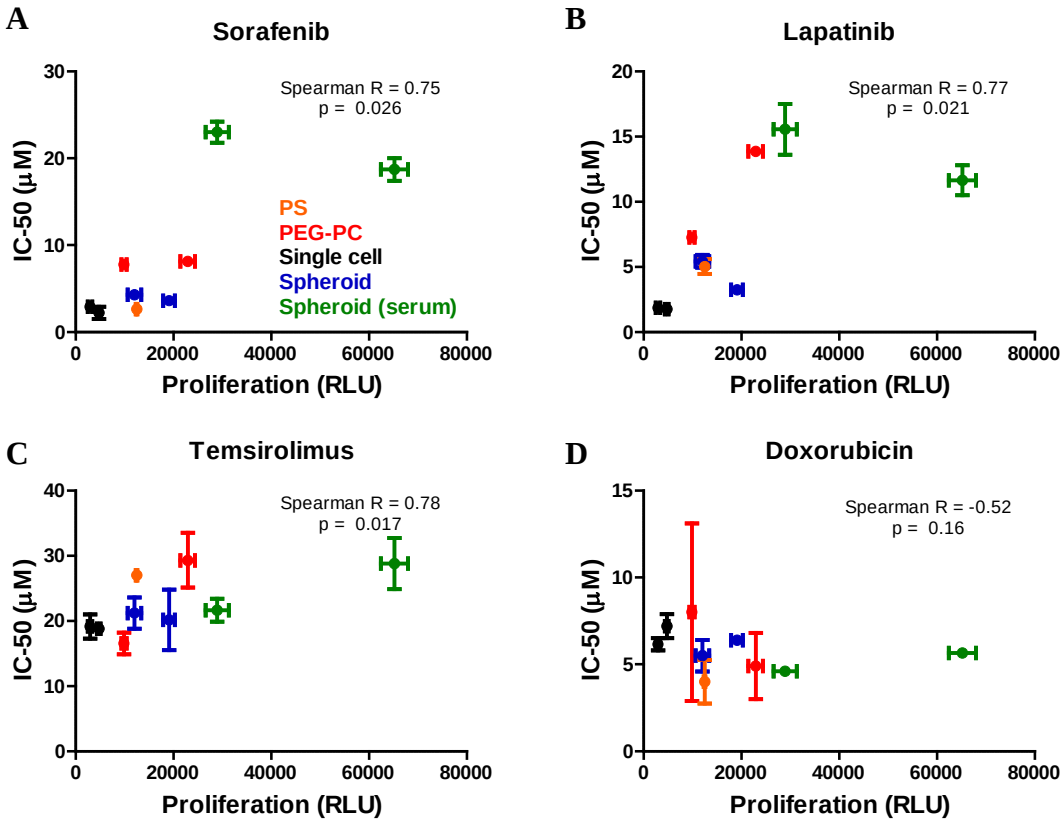

Figure 5.7 Spearman correlation between IC-50s and proliferation of MDA-MB-231s. There is a significant positive correlation between the IC-50s and proliferation for **(A)** sorafenib, **(B)** lapatinib, and **(C)** temsirolimus, but not with **(D)** doxorubicin.

5.4.2 Varying in IC-50 is dictated by cell-microenvironment interaction

Since the change in platform significantly affected how cells responded to certain types of drug, I quantified the difference in drug response between cells cultured in 3D and 2D to see if long-term culture in 3D could possibly cause a significant change in cell behavior that ultimately led to the results above. After 14 days of culture in PNIPAAm, SkBr3 and MDA-MB-231 spheroids were dissociated, placed on the plastic 96-well plate, and treated with drugs. The IC-50s were then compared to cells cultured in tissue culture flasks (Figure 5.8A). Strikingly, only SkBr3 cultured in 3D was 50% more resistant to sorafenib as opposed to cells cultured in 2D, and the rest of the IC-50s do not show any significant difference in drug response between cells cultured in 2D and 3D (Figures 5.8B and C). These results suggested that cell-drug interaction is strongly regulated by the immediate change in microenvironment/platform not long-term culture condition.

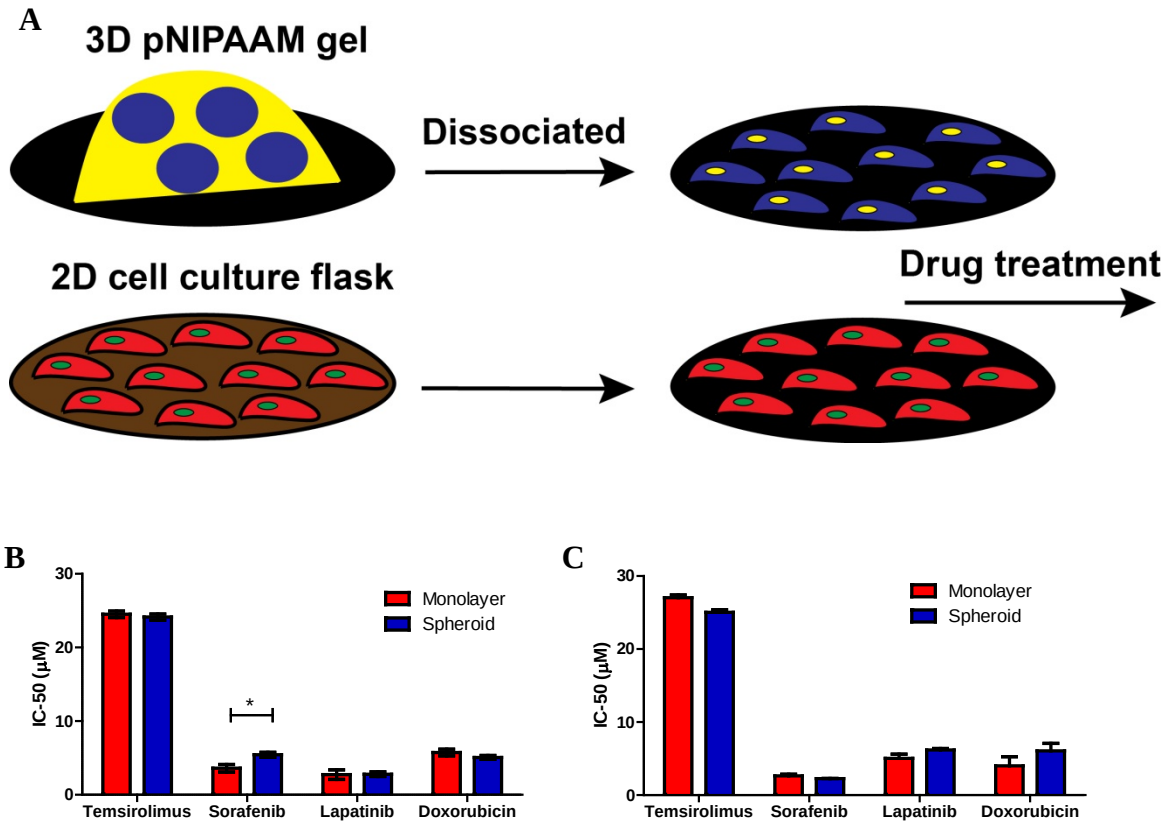

Figure 5.8 Long-term culture of spheroids in 3D PNIPAAm does not significantly change the nature of the cells. **(A)** Cells were cultured to form spheroids for 14 days, then the spheroids were removed from the gels, dissociated and seeded on the 96-well plates similarly to cells cultured in the tissue culture flask. Both SkBr3s **(B)** and MDA-MB-231s **(C)** responded to drugs in a similar manner regardless of culture methods, except for that SkBr3 cells cultured in 3D were more resistant to sorafenib.

5.4.3 SkBr3's response to EGF in 3D is independent of stiffness

Cells on stiff 2D substrates were not only more proliferative, but also previously shown to be more sensitive to EGF stimulation by me [16] and others [26,27]. Since serum medium contains EGF and many other growth factors, and SkBr3 spheroids proliferated significantly more in softer gels with serum (Figure 5.4A), I quantified the response of spheroids to EGF at different stiffness conditions to see if growth factor stimulation was responsible for the observed difference in proliferation. Encapsulated SkBr3 spheroids in 3 and 5 kPa gels were stimulated with EGF for an hour, then the EGF medium was replaced with serum-free medium (Figure 5.9A). The phosphorylation of 7 different RTK receptors (HGFR, EGFR, HER2, HER3, HER4, IGF1R, IR) were quantified by using a multi-plex MAGPix system; however, only signals from phosphorylated EGFR, HER2, HER3 were detected. In contrast to observations on 2D substrates, phosphorylation of EGFR was similar between the two stiffnesses. The phosphorylation peaked at 10 min after stimulation, then decreased over time (Figure 5.9B). The phosphorylation of HER2 reduced to a minimum at 30 min and 60 min for 3 and 5 kPa gels, respectively (Figure 5.9C). Similar to this trend, the phosphorylation of HER3 in the 3 kPa gels decreased to a minimum at 60 min and remained low (Figure 5.9D); however, HER3 phosphorylation in the 5 kPa gels did not change significantly across all time points. Although there were minor differences in phosphorylation of HER2 at 24 h and HER 3 at 7 h time points, the phosphorylation levels of HER2 and HER3 across other time points were similar between the soft and stiff gels. When comparing the phosphorylation of similar RTK receptors between the encapsulated spheroids in PEG-MAL gel and the unencapsulated spheroids, only signals from

phosphorylated EGFR, HER2 and HER3 were detected. Strikingly, the encapsulation significantly reduced the phosphorylation of EGFR and HER3 (Figure 5.9E-F), whereas HER2 phosphorylation remained unchanged (Figure 5.9G). This result emphasized the role of the surrounding microenvironment in influencing the activity of certain RTK receptor such as EGFR and HER3.

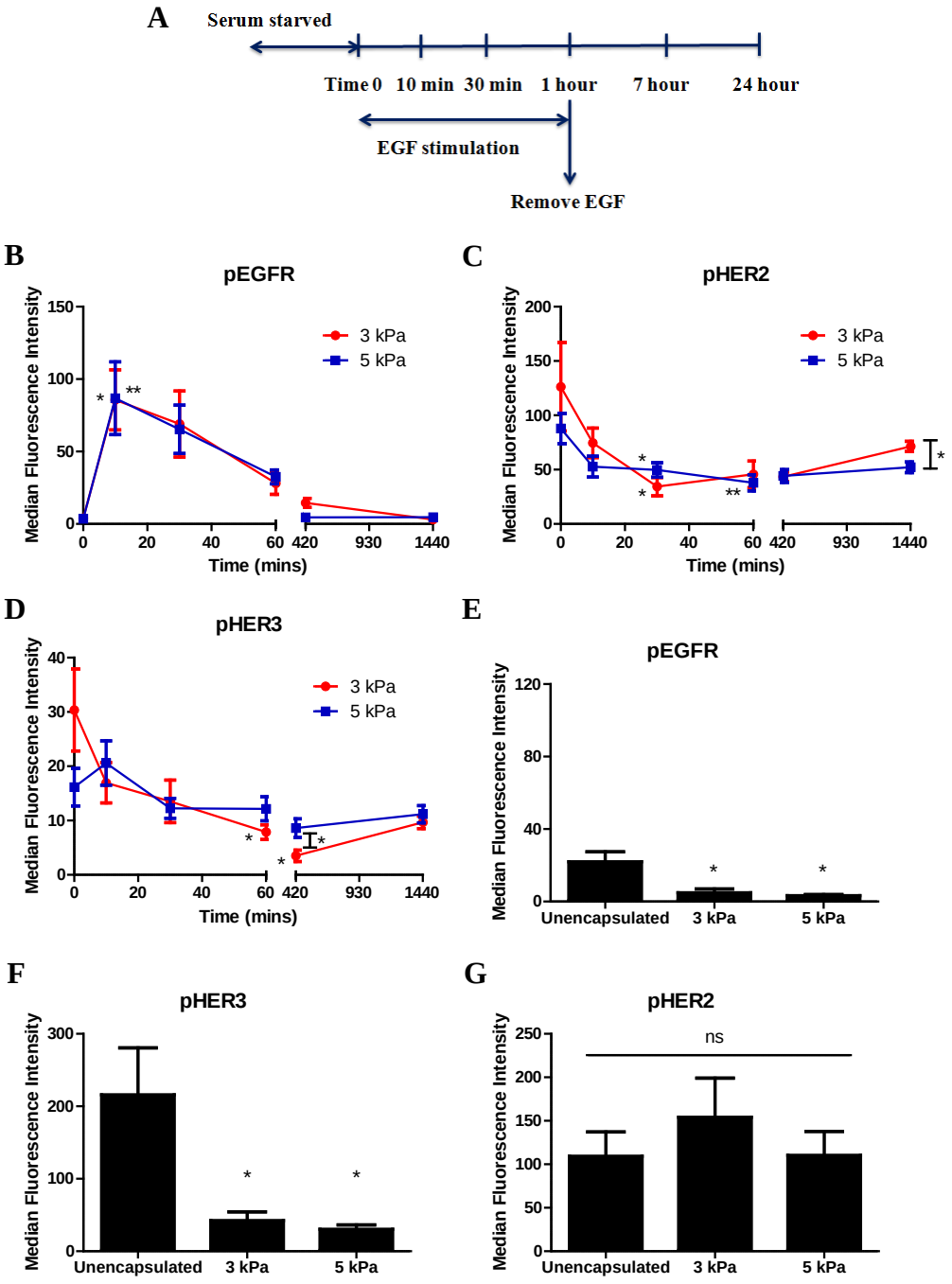

Figure 5.9 The response of SkBr3 spheroids to EGF in 3D is stiffness independent. **(A)** Encapsulated spheroids in PEG-MAL gels were serum-starved for 24 h before stimulating with 100 ng/mL of EGF. After 1 h, EGF medium was replaced with serum-free medium. **(B)** EGFR phosphorylation peaked at 10 min and decreased over time. Both **(C)** HER2 and **(D)** HER3 phosphorylation decreased during the EGF stimulation and remained low even after EGF removal. Although there was a significant decrease in **(E)** EGFR and **(F)** HER3 phosphorylation post encapsulation, there was not any significant change in **(G)** HER2 phosphorylation due to encapsulation. Statistics are with respect to time 0.

5.4.4 Long-term exposure of SkBr3 to lapatinib results in different signaling pathways activated in 2D and 3D

Since there was not any significant change in IC-50s across all platforms after short term exposure of SkBr3s to lapatinib (Figure 5.4C), this motivated me to investigate the influence 2D and 3D platforms on SkBr3s after being treated with lapatinib over a long time period. SkBr3s were seeded on 2D plastic plates or encapsulated in PNIPAAm, and then treated with lapatinib or DMSO control over 14 days. They were serum-starved before being simulated with 10% FBS medium for 15 minutes. Phosphorylation of EGFR, HER2, HER3, HER4, IGF1R, and IR were detected, whereas HGFR phosphorylation was equal to the blank. Interestingly, lapatinib treated cells had significantly lower phosphorylation of EGFR, HER2 and HER3 in both 2D and 3D as compared with the control (Figures 5.10A-C). However, the IR phosphorylation of lapatinib treated cells was significantly higher than the control in 2D, but similar to the control in 3D (Figure 5.10D). The phosphorylation of HER4 and IGF1R were the same between the control and treated cells for both 2D and 3D (Figures 5.10E-F). When quantifying the downstream signaling molecules ERK, JNK, and Akt for the same samples, strikingly, the phophorylation pattern of JNK (Figure 5.11A) was similar to that of EGFR (compare Figures 5.10A and 5.11A). Both had a significant higher phophorylation level of 2D control cells as opposed to the rest of the conditions (one-way ANOVA). JNK phosphorylation was lower for lapatinib treated cells in 2D, but it was not significantly different between the control and treated cells in 3D. ERK phosphorylation displayed an opposite trend with lapatinib treated cells higher in 2D and lower in 3D (Figure 5.11B), and there was not any difference in Akt phosphorylation between the

control and treated cells in both 2D and 3D. Although the change in platfrom did not cause any significant difference in SkBr3 response to lapatinib for a short-term exposure, the type of platform did influence the activity of several signaling molecules (IR and ERK) in SkBr3 cells after long-term exposure to lapatinib.

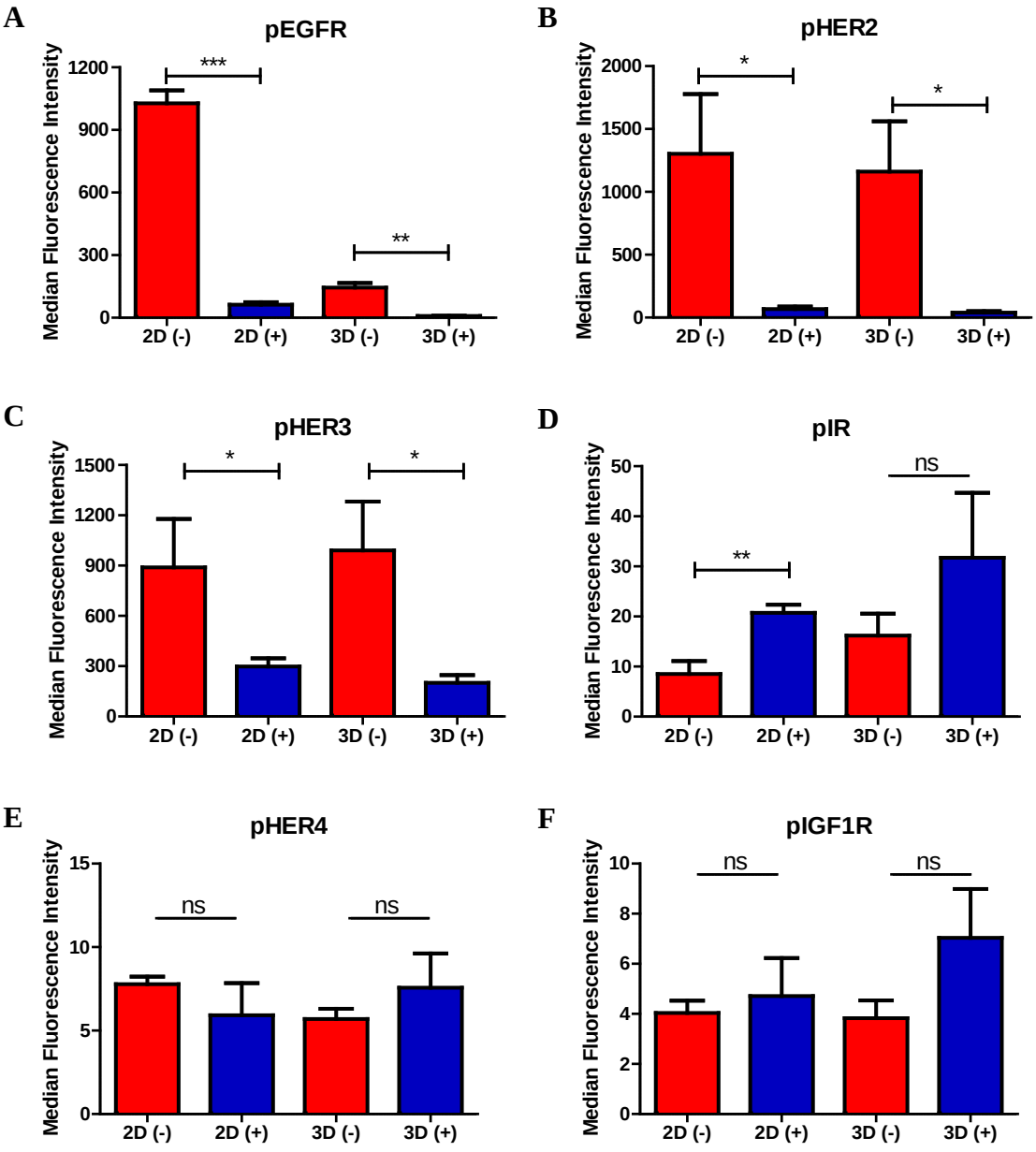

Figure 5.10 Phosphorylation of RTK receptors of SkBr3 cells under serum stimulation. Cells were cultured in 2D plastic plate or encapsulated in 3D PNIPAAm. Cells were treated with 1.25 uM of lapatinib or DMSO control for 14 days followed by serum-starvation and serum-stimulation. Phosphorylation level of **(A)** EGFR, **(B)** HER2, and **(C)** HER3 in lapatinib treated cells decreased in both 2D and 3D as compared with the control. Lapatinib treated cells had increased **(D)** IR phosphorylation in 2D but not in 3D, and there was not any significant difference in phosphorylation between lapatinib treated cells and the control in both 2D and 3D for **(E)** IGF1R and **(F)** HER4.

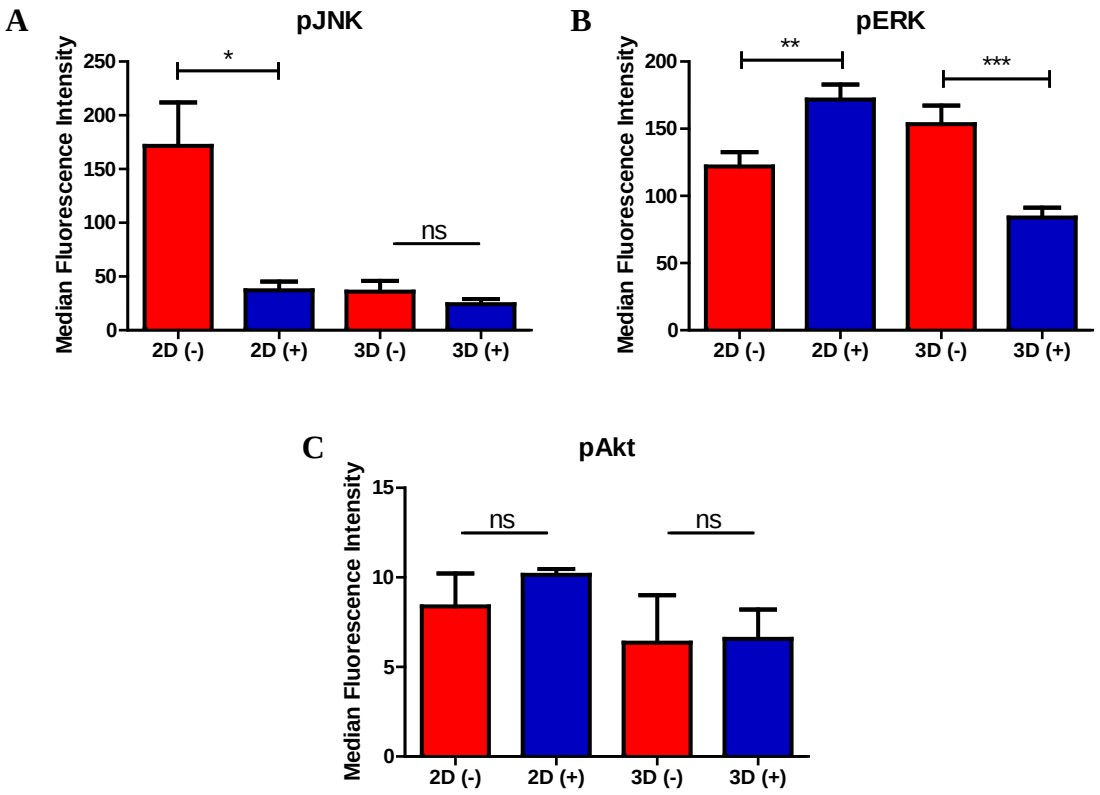

Figure 5.11 Signaling of ERK, JNK, and Akt in SkBr3 cells under serum stimulation. **(A)** phosphorylation of JNK significantly decreased in lapatinib treated cells in 2D, but not in 3D, as compared with the control. **(B)** ERK phosphorylation increased in 2D and decreased in 3D for lapatinib treated cells, whereas **(C)** Akt phosphorylation did not change.

5.5 Discussion

I have identified that the IC-50s of SkBr3s treated with either sorafenib or temsirolimus and 231s treated with either sorafenib or lapatinib were sensitive to the change in platform and medium. The IC-50s of both cell lines were insensitive to the change in platform or medium when treated with doxorubicin, which induces cell death by DNA intercalation and topoisomerase II inhibition. Although spheroids can capture many microenvironmental features of an *in vivo* tumor [28], cells in spheroids are not neccessarily more drug resistant than cells cultured on monolayers. Ewing sarcoma tumor cells cultured to form spheroids in 3D PCL scaffolds were 228-fold more resistant to doxorubicin than 2D monolayer cells, and this is not due to poor drug penetration into the innermost cell layer [29]. However, ovarian cancer spheroids grown in PEG-based hydrogels were approximately 2.5-fold more resistant to cisplatin than 2D monolayer, which causes apoptosis by crosslinking DNA [6]. Camptothecin (inhibitor to topoisomerase I), fluorouracil (inhibitor to DNA synthesis) [30], and some derivatives of imidazoacridinone (inhibitor to topoisomerase II) [31] were found to have similar cytotoxic effects to cells cultured as monolayers or as spheroids. Thus, multiple different drugs, which share similar targets (DNA intercalation or topoisomerase inhibition), can have different or similar cytotoxic effects to cells in monolayer or spheroid. In my case, I observed that doxorubicin had a similar effect on both cell types across all testing platforms.

Interestingly, variations in both platform and medium were found to have large effects on both cell lines when treated with sorafenib. ERK signaling, which is targeted by sorafenib, was implicated in ECM stiffening in both 2D and 3D [26,32,33], and cancer

cells on stiffer substrates were more resistant to sorafenib [16]. This suggests that the Raf/MEK/ERK pathway could be sensitive to the change in microenvironment. Indeed, both cell lines' response to sorafenib were highly sensitive to the type of platform. The Raf/MEK/ERK pathway is also one of the key downstream signaling pathways of RTK receptors [34], which can be activated by growth factors in serum. This could be an explanation for the sensitivity of both cell lines to medium when treated with sorafenib.

Although PI3K/Akt/mTOR is another major signaling pathway downstream of RTK activation [34], only SkBr3 spheroids showed higher IC-50s when treated with temsirolimus, which inhibits mTOR, in serum supplemented medium (Figure 5.4D). Moreover, the temsirolimus IC-50s of SkBr3 cells were more sensitive to variation in platform than 231 cells. Both Raf/MEK/ERK and PI3K/Akt/mTOR pathways are responsible for proliferation of HER2-overexpressing cells [35], whereas Ras/Raf/MEK/ERK could be the main driver of 231 cell proliferation due to its B-Raf and K-Ras mutation [36,37]. In the basal signaling protein profiles identified by Niepel et al., phosphorylated Akt in the SkBr3s is nearly 40-fold higher than the 231s, whereas phosphorylated ERK is similar for both cell types [38]. SkBr3 cells were shown to switch from PI3K/Akt signaling to MEK/ERK signaling in 3D Matrigel, whereas both pathways were activated in 2D [39], and inhibition of PI3K resulted in enhanced MEK/ERK signaling [40]. These reports support my observation that inhibition of Akt/mTOR signaling in SkBr3s, but not 231s, was sensitive to the change in platform.

When treating with lapatinib, which targets both HER2 and EGFR, 231s' IC-50s were sensitive to variations in both platform and medium. Since 231 cells overexpress EGFR [41,42], it can be implied that EGFR signaling in 231 cells is sensitive to the type

of platform and medium. Luca et al. also found that many colorectal cancer cell lines had lower EGFR gene expression when cultured in 3D laminin-rich ECM [43]. SkBr3 response to lapatinib was insensitive to the change in both platform and medium. Thus, it can be implied that the activities of EGFR and HER2 in SkBr3s were not sensitive to the change in platform and medium. Further experiments confirmed that HER2 phosphorylation was not sensitive to modulus (Figure 5.9C), nor encapsulation (Figure 5.9 F), nor platform (2D vs. 3D in Figure 5.10B). EGFR phosphorylation of SkBr3 in 3D was not affected by stiffness (Figure 5.9B), whereas EGFR phosphorylation was higher on stiffer substrates [26], its phosphorylation on 2D plastic surface was 7-fold higher than in 3D gels (Figure 5.10A). However, in SkBr3 cells, EGFR protein expression was much lower than 231 cells, and their HER2 protein expression was very high [42]. Thus, the signaling from HER2 may outweigh the effect from EGFR signaling in SkBr3s. As a result, the IC-50s of lapatinib treated SkBr3 were less sensitive to the change in microenvironment as opposed to those of 231 cells, which express only EGFR.

Unlike HER2 phosphorylation, which was not sensitive to the change in the surrounding microenvironment, HER3 phosphorylation in SkBr3 spheroids decreased significantly upon encapsulation (Figure 5.9E). Among the HER-family, HER3 is the only member that does not have tyrosine kinase activity upon binding its ligand heregulin, and it needs to heterodimerize with the other HER-family members in order to be activated [44]. In 2D, HER3 was found to heterodimerize with HER2 as an oncogenic unit to drive tumor cell proliferation [45]. It is possible that encapsulation could disrupt the heterodimerization of HER3 and lead to a decrease in its phosphorylation, and this

could cause an attenuation of the downstream PI3K/Akt signaling. In fact, Weigelt et al. found that Akt phosphorylation of SkBr3s in 3D Matrigel was abolished [39].

Reduction of EGFR and HER3 phosphorylation during cell encapsulation may have a profound impact on future research of HER-family receptors. Various methods has been developed to induce 3D spheroid formation by allowing cell aggregation on non-adherent surfaces such as the hanging drop method [46], agarose [9] or PDMS [10] coated plates, or thin film PDMS micropatterning [15]. An encapsulation model may be more relevant because tumor cells are tightly packed within the tumor microenvironment, and encapsulation status could affect the activity of certain RTK receptors such as EGFR and HER3.

Interestingly, during EGF stimulation, both HER2 and HER3 phosphorylation decreased concurrently with EGFR activation. It is common that EGFR, upon EGF binding, will heterodimerize with HER2 and subsequently lead to phosphorylation in both receptors that results in activation of PI3K/Akt and Ras/Raf/MEK/ERK pathways [35]. What I observed here suggests a mechanism of EGFR homodimerization and possibly a disruption of HER2-HER3 complexes, which leads to a reduction in phosphorylation level of both receptors. Similarly, after EGF stimulation in 2D, Brockhoff et al. found a formation of EGFR-HER2 receptors complexes with BT474 cells, but not with SkBr3 cells, and the authors suggested an EGFR-EGFR homodimerization mechanism in SkBr3 cells due to the higher number of available EGFRs on the surface of these cells [47]. However, the authors observed a high amount of HER2-HER3 heterodimers and constitutively activated Akt regardless of stimulation. Taken together, these results also support my previous conclusion regarding the

sensitivity of HER2-HER3 interaction to the surrounding encapsulating microenvironment. Although the phosphorylation of SkBr3 spheroids under EGF stimulation is independent of modulus, SkBr3 spheroids in the soft gels proliferated significantly more than those in stiffer gels, and this trend was consistent with the 231s, and from others [24,25]. This effect can be attributed to the larger solid stress in stiffer gels, and this stress on the spheroids can limit the spheroid proliferation [48–50]. The *in vivo* tumor is also subjected to solid stress induced by stiff collagen fibers, which provide tensile strength to the tissue, and hyaluronic acid, which provides the compressive resistance due to its ability to hold water [51]. Thus, it is necessary to take into account the effect from the solid stress as this can influence cell response to drug treatment, and this solid stress is lacking from unencapsulated spheroid models.

Although short term exposure to lapatinib across various 2D and 3D platforms did not show any significant variation in IC-50, long-term exposure to lapatinib showed some differences in phosphorylation of certain signaling molecules across 2D plastic plate and 3D PNIPAAm. Upon serum stimulation, phosphorylation levels of EGFR, HER2, and HER3 in lapatinib treated cells were significantly lower than the control for both platforms, and Jegg et al. also observed similar phenomena with long-term lapatinib-treated SkBr3 on 2D [52]. However, IR phosphorylation of lapatinib-treated cells in 2D increased significantly compared with the control but not in 3D (Figure 5.10D). Since IR is capable of activating downstream signaling pathways such as Ras/Raf/MEK/ERK and PI3K/Akt/mTOR [53], this corresponds with the increase in downstream ERK activation in lapatinib treated cells in 2D (Figure 5.11B). Liu et al. identified the activation of Akt and ERK due to an upregulation of the upstream AXL receptor as a mechanism for

survival of lapatinib resistance BT474 cells in 2D [54], whereas Jegg et al. identified the activation of mTOR independent of PI3K/Akt signaling as a mechanism for lapatinib resistance in SkBr3 cells. However, the methods of creating lapatinib resistant cells between the authors were also really different. In my case, exposure to lapatinib for 14 days was not long enough to create an established lapatinib resistant cell line (Figure 5.12) despite similar observable trends, which EGFR, HER2, and HER3 was down-regulated in long-term lapatinib treated cells, with both Liu et al. and Jegg et al.. Nevertheless, 14 days of lapatinib exposure was enough for me to see a different pattern of SkBr3 response between 2D and 3D with IR and ERK activation. The pattern of EGFR activation was similar to JNK activation with very high phosphorylation on 2D and low phosphorylation in 3D. This could be indicative of EGFR activating JNK under EGF stimulation since EGF stimulation is known to activate PI3K/Akt and Ras/Raf/MEK/ERK [55] as well as JNK through Ras/Rac1 pathway [56,57].

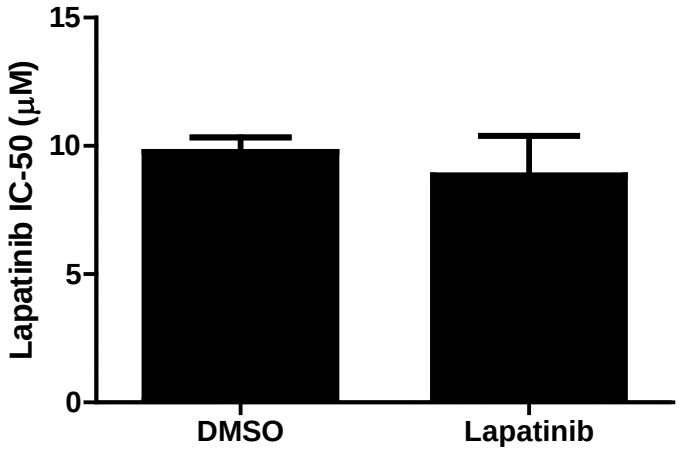

Figure 5.12 Lapatinib treated and DMSO control SkBr3 spheroids have similar IC-50s. SkBr3s were cultured in PNIPAAm for 6 days (DMSO) and 14 days (lapatinib) to create spheroids of similar sizes since cells cultured with lapatinib grew at a slower rate. Spheroids were transfered to 3 kPa gels and treated with laptinib.

5.6 Conclusions

Overall, through testing 3 targeted drugs and 1 cytotoxic drug with 2 cell lines across multiple platforms, I found that the sensitivity of cell-drug interaction to the platform or medium is dependent on both drug type and cell type. The IC-50s of SkBr3s were sensitive to platform type when treated with temsirolimus and sorafenib. The IC-50s of 231s were sensitive to platform type when treated with sorafenib and lapatinib. Variation in platform did not matter for both 231s and SkB3s when treated with doxorubicin. I also found that HER3 and EGFR activation were sensitive to the surrounding microenvironment, whereas HER2 phosphorylation is not. Long-term exposure of SkBr3 to lapatinib caused distinct patterns of IR and ERK signaling observed in 2D, but not in 3D. My results highlight the importance of understanding the cell type and drug mechanism in choosing the relevant biomaterial system for studying of cell response to drugs.

5.7 References

[1] S. Zustiak, R. Nossal, D.L. Sackett. Multiwell stiffness assay for the study of cell responsiveness to cytotoxic drugss. Biotechnol. Bioeng. 2013. 9999: 1–8.

[2] J.D. Mih, A.S. Sharif, F. Liu, A. Marinkovic, M.M. Symer, D.J. Tschumperlin. A multiwell platform for studying stiffness-dependent cell biology. PLoS One. 2011. 6: e19929.

[3] A. Khademhosseini, R. Langer, J. Borenstein, J.P. Vacanti. Microscale technologies for tissue engineering and biology. Proc. Natl. Acad. Sci. U. S. A. 2006. 103: 2480–7.

[4] C.H. Kwon, I. Wheeldon, N.N. Kachouie, S.H. Lee, H. Bae, S. Sant, et al. Drug-Eluting Microarrays for Cell-Based Screening of Chemical-Induced Apoptosis. Anal. Chem. 2011.

[5] J.L. Leight, E.Y. Tokuda, C.E. Jones, A.J. Lin, K.S. Anseth. Multifunctional bioscaffolds for 3D culture of melanoma cells reveal increased MMP activity and migration with BRAF kinase inhibition. Proc. Natl. Acad. Sci. 2015. 112: 201505662.

[6] D. Loessner, K.S. Stok, M.P. Lutolf, D.W. Hutmacher, J. a Clements, S.C. Rizzi. Bioengineered 3D platform to explore cell-ECM interactions and drug resistance of epithelial ovarian cancer cells. Biomaterials. 2010. 31: 8494–506.

[7] C.S. Ki, T.-Y. Lin, M. Korc, C.-C. Lin. Thiol-ene hydrogels as desmoplasia-mimetic matrices for modeling pancreatic cancer cell growth, invasion, and drug resistance. Biomaterials. 2014. 35: 9668–77.

[8] J.Y. Fang, S.-J. Tan, Z. Yang, C. Tayag, B. Han. Tumor bioengineering using a transglutaminase crosslinked hydrogel. PLoS One. 2014. 9: e105616.

[9] J. Friedrich, C. Seidel, R. Ebner, L. a Kunz-Schughart. Spheroid-based drug screen: considerations and practical approach. Nat. Protoc. 2009. 4: 309–24.

[10] S. Chandrasekaran, J.R. Marshall, J. a Messing, J.-W. Hsu, M.R. King. TRAIL-mediated apoptosis in breast cancer cells cultured as 3D spheroids. PLoS One. 2014. 9: e111487.

[11] S. Pece, J.S. Gutkind. Signaling from E-cadherins to the MAPK pathway by the recruitment and activation of epidermal growth factor receptors upon cell-cell contact formation. J. Biol. Chem. 2000. 275: 41227–33.

[12] M. Conacci-sorrell, J. Zhurinsky, A. Ben-ze. The cadherin-catenin adhesion system in signaling and cancer. 2002. 109: 987–991.

[13] M. Yilmaz, G. Christofori. Mechanisms of motility in metastasizing cells. Mol. Cancer Res. 2010. 8: 629–42.

[14] H.-G. Kang, J.M. Jenabi, J. Zhang, N. Keshelava, H. Shimada, W. a May, et al. E-cadherin cell-cell adhesion in ewing tumor cells mediates suppression of anoikis through activation of the ErbB4 tyrosine kinase. Cancer Res. 2007. 67: 3094–105.

[15] F. Hirschhaeuser, H. Menne, C. Dittfeld, J. West, W. Mueller-Klieser, L. a Kunz-Schughart. Multicellular tumor spheroids: an underestimated tool is catching up again. J. Biotechnol. 2010. 148: 3–15.

[16] T. V. Nguyen, M. Sleiman, T. Moriarty, W.G. Herrick, S.R. Peyton. Sorafenib resistance and JNK signaling in carcinoma during extracellular matrix stiffening. Biomaterials. 2014. 35: 5749–59.

[17] E.Y. Tokuda, J.L. Leight, K.S. Anseth. Modulation of matrix elasticity with PEG hydrogels to study melanoma drug responsiveness. Biomaterials. 2014. 35: 4310–4318.

[18] W.G. Herrick, T. V Nguyen, M. Sleiman, S. McRae, T.S. Emrick, S.R. Peyton. PEG-phosphorylcholine hydrogels as tunable and versatile platforms for mechanobiology. Biomacromolecules. 2013. 14: 2294–304.

[19] E. a Phelps, N.O. Enemchukwu, V.F. Fiore, J.C. Sy, N. Murthy, T. a Sulchek, et al. Maleimide cross-linked bioactive PEG hydrogel exhibits improved reaction kinetics and cross-linking for cell encapsulation and in situ delivery. Adv. Mater. 2012. 24: 64–70, 2.

[20] O. Trédan, C.M. Galmarini, K. Patel, I.F. Tannock. Drug resistance and the solid tumor microenvironment. J. Natl. Cancer Inst. 2007. 99: 1441–54.

[21] J.M. Brown, A.J. Giaccia. The Unique Physiology of Solid Tumors : Opportunities (and Problems) for Cancer Therapy The Unique Physiology of Solid Tumors : Opportunities (and Problems) for Cancer Therapy1. 1998. 1408–1416.

[22] V. Umesh, A.D. Rape, T. a Ulrich, S. Kumar. Microenvironmental stiffness enhances glioma cell proliferation by stimulating epidermal growth factor receptor signaling. PLoS One. 2014. 9: e101771.

[23] J.D. Mih, A. Marinkovic, F. Liu, A.S. Sharif, D.J. Tschumperlin. Matrix stiffness reverses the effect of actomyosin tension on cell proliferation. J. Cell Sci. 2012. 125: 5974–83.

[24] Y. Liang, J. Jeong, R.J. DeVolder, C. Cha, F. Wang, Y.W. Tong, et al. A cell-instructive hydrogel to regulate malignancy of 3D tumor spheroids with matrix rigidity. Biomaterials. 2011. 32: 9308–15.

[25] C. Wang, X. Tong, F. Yang. Bioengineered 3D Brain Tumor Model To Elucidate the Effects of Matrix Stiffness on Glioblastoma Cell Behavior Using PEG-Based Hydrogels. 2014.

[26] M.J. Paszek, N. Zahir, K.R. Johnson, J.N. Lakins, G.I. Rozenberg, A. Gefen, et al. Tensional homeostasis and the malignant phenotype. Cancer Cell. 2005. 8: 241–54.

[27] J.-H. Kim, A.R. Asthagiri. Matrix stiffening sensitizes epithelial cells to EGF and enables the loss of contact inhibition of proliferation. J. Cell Sci. 2011. 124: 1280–7.

[28] C.R. Thoma, M. Zimmermann, I. Agarkova, J.M. Kelm, W. Krek. 3D cell culture systems modeling tumor growth determinants in cancer target discovery. Adv. Drug Deliv. Rev. 2014. 69-70: 29–41.

[29] E.L.S. Fong, S.-E. Lamhamedi-Cherradi, E. Burdett, V. Ramamoorthy, A.J. Lazar, F.K. Kasper, et al. Modeling Ewing sarcoma tumors in vitro with 3D scaffolds. Proc. Natl. Acad. Sci. U. S. A. 2013. 110: 6500–5.

[30] B. Desoize, J. Jardillier. Multicellular resistance: a paradigm for clinical resistance? Crit. Rev. Oncol. Hematol. 2000. 36: 193–207.

[31] a Skladanowski, S.Y. Plisov, J. Konopa, a K. Larsen. Inhibition of DNA topoisomerase II by imidazoacridinones, new antineoplastic agents with strong activity against solid tumors. Mol. Pharmacol. 1996. 49: 772–780.

[32] C.B. Khatiwala, P.D. Kim, S.R. Peyton, A.J. Putnam. Signaling Downstream of RhoA and ROCK. J. Bone Miner. Res. 2009. 24: 886–898.

[33] P.P. Provenzano, D.R. Inman, K.W. Eliceiri, P.J. Keely. Matrix density-induced mechanoregulation of breast cell phenotype, signaling and gene expression through a FAK-ERK linkage. Oncogene. 2009. 28: 4326–4343.

[34] M.A. Arslan, O. Kutuk, H. Basaga. Protein kinases as drug targets in cancer. Curr. Cancer Drug Targets. 2006. 6: 623–34.

[35] A.T. Baker, A. Zlobin, C. Osipo. Notch-EGFR/HER2 Bidirectional Crosstalk in Breast Cancer. Front. Oncol. 2014. 4: 360.

[36] J.T. Price, T. Tiganis, A. Agarwal, D. Djakiew, E.W. Thompson. Epidermal Growth Factor Promotes MDA-MB-231 Breast Cancer Cell Migration through a Phosphatidylinositol 3*-Kinase and Phospholipase C-dependent Mechanism. Cancer Res. 1999. 59: 5475–5478.

[37] S.M. Wilhelm, C. Carter, L. Tang, D. Wilkie, A. Mcnabola, H. Rong, et al. BAY 43-9006 Exhibits Broad Spectrum Oral Antitumor Activity and Targets the RAF / MEK / ERK Pathway and Receptor Tyrosine Kinases Involved in Tumor Progression and Angiogenesis BAY 43-9006 Exhibits Broad Spectrum Oral Antitumor Activity and Targets the Pr. 2004.

[38] M. Niepel, M. Hafner, E.A. Pace, M. Chung, D.H. Chai, L. Zhou, et al. Profiles of Basal and Stimulated Receptor Signaling Networks Predict Drug Response in Breast Cancer Lines. 2013. 6: 1–12.

[39] B. Weigelt, A.T. Lo, C.C. Park, J.W. Gray, M.J. Bissell. HER2 signaling pathway activation and response of breast cancer cells to HER2-targeting agents is dependent strongly on the 3D microenvironment. Breast Cancer Res. Treat. 2010. 122: 35–43.

[40] V. Serra, M. Scaltriti, L. Prudkin, P.J. a Eichhorn, Y.H. Ibrahim, S. Chandarlapaty, et al. PI3K inhibition results in enhanced HER signaling and acquired ERK dependency in HER2-overexpressing breast cancer. Oncogene. 2011. 30: 2547–2557.

[41] B. Corkery, J. Crown, M. Clynes, N. O'Donovan. Epidermal growth factor receptor as a potential therapeutic target in triple-negative breast cancer. Ann. Oncol. 2009. 20: 862–867.

[42] C. Knuefermann, Y. Lu, B. Liu, W. Jin, K. Liang, L. Wu, et al. HER2/PI-3K/Akt activation leads to a multidrug resistance in human breast adenocarcinoma cells. Oncogene. 2003. 22: 3205–12.

[43] A.C. Luca, S. Mersch, R. Deenen, S. Schmidt, I. Messner, K.L. Schäfer, et al. Impact of the 3D Microenvironment on Phenotype, Gene Expression, and EGFR Inhibition of Colorectal Cancer Cell Lines. PLoS One. 2013. 8.:

[44] C. Gutierrez, R. Schiff. HER2: biology, detection, and clinical implications. Arch. Pathol. Lab. Med. 2011. 135: 55–62.

[45] T. Holbro, R.R. Beerli, F. Maurer, M. Koziczak, C.F.B. Iii, N.E. Hynes. The ErbB2 ¯ErbB3 heterodimer functions as an oncogenic unit : ErbB2 requires ErbB3 to drive breast tumor cell proliferation. 2003. 100.:

[46] J.M. Kelm, N.E. Timmins, C.J. Brown, M. Fussenegger, L.K. Nielsen. Method for generation of homogeneous multicellular tumor spheroids applicable to a wide variety of cell types. Biotechnol. Bioeng. 2003. 83: 173–80.

[47] G. Brockhoff, P. Heiss, J. Schlegel, F. Hofstaedter, R. Knuechel. Epidermal growth factor receptor, c-erbB2 and c-erbB3 receptor interaction, and related cell cycle kinetics of SK-BR-3 and BT474 breast carcinoma cells. Cytometry. 2001. 44: 338–348.

[48] G. Cheng, J. Tse, R.K. Jain, L.L. Munn. Micro-environmental mechanical stress controls tumor spheroid size and morphology by suppressing proliferation and inducing apoptosis in cancer cells. PLoS One. 2009. 4: e4632.

[49] G. Helmlinger, P. a. Netti, H. c. Lichtenbeld, R. j. Melder, R. k. Jain. Solid stress inhibits the growth of multicellular tumor spheroids. Nat. Biotechnol. 1997.

[50] D. Loessner, J. a Flegg, H.M. Byrne, J. a Clements, D.W. Hutmacher. Growth of confined cancer spheroids: a combined experimental and mathematical modelling approach. Integr. Biol. (Camb). 2013. 5: 597–605.

[51] R.K. Jain, J.D. Martin, T. Stylianopoulos. The role of mechanical forces in tumor growth and therapy. Annu. Rev. Biomed. Eng. 2014. 16: 321–46.

[52] A.M. Jegg, T.M. Ward, E. Iorns, N. Hoe, J. Zhou, X. Liu, et al. PI3K independent activation of mTORC1 as a target in lapatinib-resistant ERBB2+ breast cancer cells. Breast Cancer Res. Treat. 2012. 136: 683–692.

[53] P. Singh, J. Marin, F. Bast. Insulin receptor (IR) and insulin-like growth factor receptor 1 (IGF-1R) signaling systems : novel treatment strategies for cancer. 2014. 1.:

[54] L. Liu, J. Greger, H. Shi, Y. Liu, J. Greshock, R. Annan, et al. Novel Mechanism of Lapatinib Resistance in HER2-Positive Breast Tumor Cells : Activation of AXL. 2009. 1363089: 6871–6879.

[55] F. Ciardiello, G. Tortora. EGFR antagonists in cancer treatment. N. Engl. J. Med. 2008. 358: 1160–74.

[56] E. a Almeida, D. Ilić, Q. Han, C.R. Hauck, F. Jin, H. Kawakatsu, et al. Matrix survival signaling: from fibronectin via focal adhesion kinase to c-Jun NH(2)-terminal kinase. J. Cell Biol. 2000. 149: 741–54.

[57] A. Minden, A. Lin, M. McMahon, C. Lange-Carter, B. Dérijard, R.J. Davis, et al. Differential activation of ERK and JNK mitogen-activated protein kinases by Raf-1 and MEKK. Science. 1994. 266: 1719–23.

CHAPTER 6

SUMMARY AND CONCLUSIONS

6.1 Summary

Throughout this thesis, the hypothesis that the physicochemical cues from the ECM can promote drug resistance in cancer cells has been tested. First, various 2D and 3D biomaterial systems were developed and applied to test the hypothesis. Second, cancer cells' response to sorafenib on 2D biomaterials with varying material and integrin binding properties were probed. Finally, cancer cells were tested with different drugs across various types of 2D and 3D microenvironments.

6.1.1 Biomaterial platforms

In Chapter 2, a novel hydrophilic material, PEG-PC, was developed, and its properties were characterized. The hydrogel system was shown to have a tunable mechanical range from 1 to 10,000 kPa and more hydrophilic than PEG alone. Different methods were utilized to couple full-length matrix proteins to the gel surface. Chapter 3 described the adaptation of PEG-PC, PEG, and PAA hydrogels to the 96-well plate format for high-throughput applications. Matrix proteins were coupled to these hydrogels in the 96-well plate by using a heterobifunctional crosslinker. The gels' moduli were 6, 23, 50, 165, and 400 kPa. Chapter 5 detailed the adaptation of 3D biomaterial systems. PNIPAAm-PEG is a thermal-reversible gel which was used to support the long-term culture and formation of 3D spheroids. Cell-drug interaction in 3D was studied with cells

or spheroids encapsulated in the PEG-MAL gels. The mechanical property of this 3D gel system was tunable, and two different moduli being used were 3 and 5 kPa. Short bioactive peptide sequence CRGD was also incorporated into the PEG-MAL gel system.

6.1.2 Matrix stiffness and integrin binding regulate the drug response in 2D

As described in chapter 3 and 4, most of cell lines were more resistant to sorafenib when binding to collagen-rich matrix as compared with binding to basement membrane matrix. Chapter 4 detailed the response of similar cell lines to sorafenib when placed on 2D high-throughput platforms coupled with either collagen-rich or basement membrane ECM. Cells on stiffer gels were more resistant to sorafenib than those on softer gels. Although cells on stiffer gels are known to be more proliferative, this stiffness-induced drug resistance was found to be independent of proliferation and not related to the canonical Rho-ROCK pathway. Instead, this drug resistance was mediated by β_1 integrin and JNK activation, and co-administering sorafenib with inhibitor to either of β_1 integrin or JNK abolished the stiffness-induced drug resistance.

6.1.3 The role of biomaterial platforms in controlling cellular response to drugs

Chapter 5 described the studying of cell-drug interaction across varying types of 2D and 3D platforms and identified that the sensitivity of cell-drug interaction to microenvironment is dependent on both drug type and cell type. Although cell response to drug was found to be strongly regulated by material modulus in 2D, the effect on the IC-50s from changing platforms and medium outweighed the effect from varying modulus when comparing across different types of platform, medium, and modulus. Changing in platform and medium affects how SkBr3 cells' response to sorafenib and temsirolimus, and 231 cells' response to sorafenib and lapatinib, whereas both cell types'

response to doxorubicin are independent of platform, medium, and modulus conditions. Both HER3 and EGFR receptors were found to be sensitive to the microenvironment, but not HER2 receptor.

6.2 Conclusions

The results presented in this dissertation support the hypothesis that the interaction between cancer cells and the microenvironment can mediate survival signals to cancer cells in the presence of chemotherapeutics. The stiffness-induced sorafenib resistance on 2D substrates is independent of the change in cytoskeletal networks that could influence the canonical Rho/ROCK signaling, but instead depending on β_1 integrin and JNK activation. This finding elucidates a new mechanism through which 2D matrix stiffness can modulate cell behavior through pathways that are not related to those that regulate cytoskeletal assembly. In 3D, matrix stiffness does not affect the drug response as much as other factors such as cell-cell contact or medium condition, and the influence of these factors to drug response is also dependent on drug type and cell type.

The results from this dissertation can have a great impact on future research regarding developing preclinical models for cancer drug discovery. First, a better understanding of how biomaterial platforms regulate drug response in cancer cells may guide future effort in designing better model for preclinical drug development, and having the relevant preclinical model that is more predictive of *in vivo* outcome will save both time and money. Secondly, this research has created and applied separate *in vitro* model systems including a novel biomaterial with an extremely wide mechanical range that is suitable for many other applications, various 2D high-throughput biomaterial

platforms for studies of cell-drug interaction and mechanobiology, a 3D biomaterial system to culture multi-cellular spheroids, and a 3D spheroid model which can be easily tunable for mechanical, integrin binding, and MMP-degradable properties.

6.3 Future Considerations

6.3.1 Matrix stiffening and inflammation

As shown previously in Chapter 4, matrix stiffening triggers higher JNK phosphorylation. Activation of JNK in hepatocyte is known to stimulate its production of high-mobility group box 1 protein (HMGB1), S100 calcium binding proteins, heat-shock proteins, and purine metabolites that can activate IKK-β and NF-κB of local Kuffer cells and trigger these cells to produce pro-inflammatory cytokines [1]. Activation of JNK in macrophages can inhibit the function of glucocorticoid receptors, thereby allowing NF-κB to be activated and enhancing the production of proinflammatory cytokines and chemokines by these cells [2]. The pro-inflammatory cytokines can promote the tumor cell growth and attract the infiltration of other immune cells, and this infiltration in turn makes the tumor microenvironment more inflammatory, which could exacerbate the disease [3,4]. It is proposed here that activation of JNK in 231s on stiff substrate can make these cells produce more pro-inflammatory cytokines and other factors. Examination of condition medium of these cells cultured on stiff substrates may provide insights into this phenomena.

6.3.2 Apoptotic signaling on stiffen matrix

In Chapter 4, cells on stiff substrates were shown to be more resistant to sorafenib, and this was found to be independent of Rho/ROCK signaling and

proliferation. JNK activation was found to be responsible for the survival of 231s, but not SkBr3s. Both MAPK and Akt signaling in SkBr3 was not responsible for this cell line's resistance to sorafenib. It is proposed that the down regulation of apoptotic signals instead of activation of survival pathways could be responsible for sorafenib resistance of SkBr3s on stiff substrates. Caspases are known to mediate intracellular apoptosis. Caspases-8 and -10 are activated upon binding of death-inducing ligands such as FasL and TNF [5], but in my case, these ligands were not included in the experiment. Thus, down regulation of intrisic death pathway mediated by caspase-9 and downstream caspase-3/-6/-7 [5] could be responsible for promoting sorafenib resistance. Growth arrest could be another mechanism for survival of drug resistance cells. Activation of CDK1 is important for cells to enter into M phase, which includes mitosis and cytokinesis, from G2 phase [6]. Therefore, activity of CDK1 also should be probed in order to truly understand the mechanism of sorafenib resistance.

6.3.3 Cadherin-mediated cell-cell contact and drug resistance

In Chapter 5, SkBr3 spheroids were observed to be much more resistant to sorafenib, lapatinib, and temsirolimus than SkBr3 single cells. However, 231 spheroids's IC-50s do not show a profound difference with single cells' IC-50s as much as those of SkBr3 cells . It is proposed that cadherin-mediated cell-cell contact can promote a stronger drug resistance in SkBr3 cells than in 231s cells. 231 is a more aggressive cell type that can invade local tissue and metastasize distal organs; thus it could be infer that survival of these cells can be less dependent on cell-cell contact as opposed to the less aggressive SkBr3s. SkBr3s on monolayer do not express any of the major cadherins such as E-cadherin, N-cadherin, P-cadherin, cadherin-11, whereas 231s only express cadherin-

11 [7]. However, SkBr3s were capable of forming tight spheroids in my 3D culture system. Thus, the expression of cadherin in 3D and 2D can be different depending on the microenvironment. Quantifying the expression of cadherins of these two cell types under conditions as monolayer, single cell in 3D, and spheroid can provide insights into how microenvironment regulates cadherin expression. Ligation of cadherins can mediate β-catenin signaling, and cadherins can also interact with other RTKs and subsequently trigger survival pathways such as PI3K/Akt or MAPK [8]. These downstream signaling pathways should be quantified to understand how microenvironment induces cadherin expression and its downstream signaling.

6.3.4 Cell-cell communication and drug resistance

The interaction between tumor cells and other factors released by different cell types can impart resistance to chemotherapeutics such as HGF is known to mediate vemurafenib resistance [9,10]. Cancer associated fibroblasts also play a role in promoting the growth of tumor cells [11]. Thus, it is important to identify the influence of fibroblast in the spheroid formation. The 3D PNIPAAm culture system allows tumor cells to be co-cultured with fibroblasts, which can be seeded on the plate surface. Tumor spheroids can be collected separately from fibroblasts. A thorough examination of spheroids from co-culture and mono-culture would include a gene expression analysis via reverse transcription polymerase chain reaction (RT-PCR) or real-time quantitative reverse transcription PCR (qRT-PCR), and their drug response should also be tested. Conditioned medium of the co-culture system should be quantified with the Luminex assays and compared with the mono-culture of spheroid and fibroblast alone. The drug response of spheroids from the co-culture and mono-culture systems should also be tested and related

to the gene expression results in order to identify the molecular targets that could be responsible for the differences.

6.3.5 Nuclear shape and drug resistance

The enlargement of the nucleus was found to be associated with poorer prognosis in breast cancer as the nuclear area increased with disease progression [12]. The change in nuclear shape allows different rearrangements of chromatins, which may allow or prohibit the accessibility of transcription factors to certain locations of the chromatins for gene transcription. Thus, certain genes can be upregulated or downregulated, and this results in different cell behaviors, and perhaps their response to drugs. Indeed, the increase in nuclear volume and chromatin decondensation were found to be highly correlated with DNA synthesis in endothelial cells [13], and smooth muscle cells that had larger nuclear area were found to proliferate more [14]. Since cells in advanced stage of breast cancer tend to be more drug resistant than those in earlier stage, it is proposed that cells with larger nuclear areas can be more resistant to chemotherapeutics than those with smaller areas. Preliminary data showed that the nuclear area and perimeter of cells are changed when treating with doxorubicin (Figure 6.1A-D) and sorafenib (Figure 6.2A-D). However, the trend was different between the two cell types, and the nuclei of cells treated with doxorubicin had larger changes than those of cells treated with sorafenib partially due to different drug's mechanisms. Doxorubicin is a chemotherapeutic drug that can cause cell death by DNA intercalation and has to be localized in the nucleus to be effective, whereas sorafenib is a kinase inhibitor that can inhibit Raf kinase in the cytoplasm. Based upon these observations, drug treatment can cause a change in cellular nucleus, thus, it is possible to infer the reverse that the change in the nucleus can also

affect the effectiveness of drug treatment, especially the drugs that have to localize in the nucleus to be effective. Micro-contact printing can be employed to pattern glass surface with square or circular shapes that have different areas to control cell spreading, which in turn controls the nuclear area. The change in cell spreading can alter the ratio of lamin A and B, thereby affecting the nuclear mechanics, shape, and area; these changes play an important role in cell proliferation and differentiation [15]. Thus, the relative of amount lamin A and B of cells with different spreading area should be quantified. A partial knock-down of lamin A (with siRNA) of cells with the same spreading area can also be done to eliminate the effect of changing the cytoskeleton outside of the nucleus due to the change in cell shape.

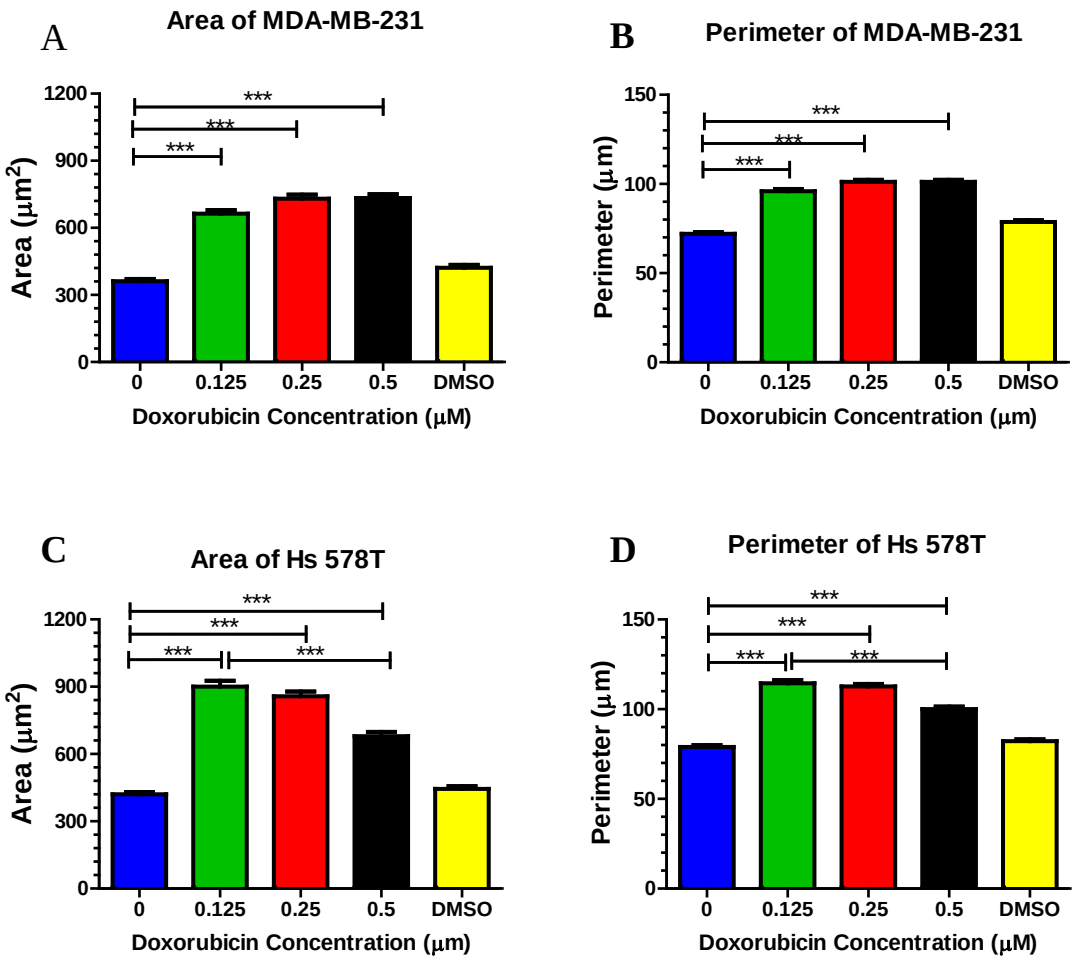

Figure 6.1 The change in nuclear shape and area as a function of doxorubicin treatment. Increasing in doxorubicin concentration increases 231s' **(A)** nuclear area and **(B)** perimeter while decreasing Hs-578Ts' **(C)** nuclear area and **(D)** perimeter.

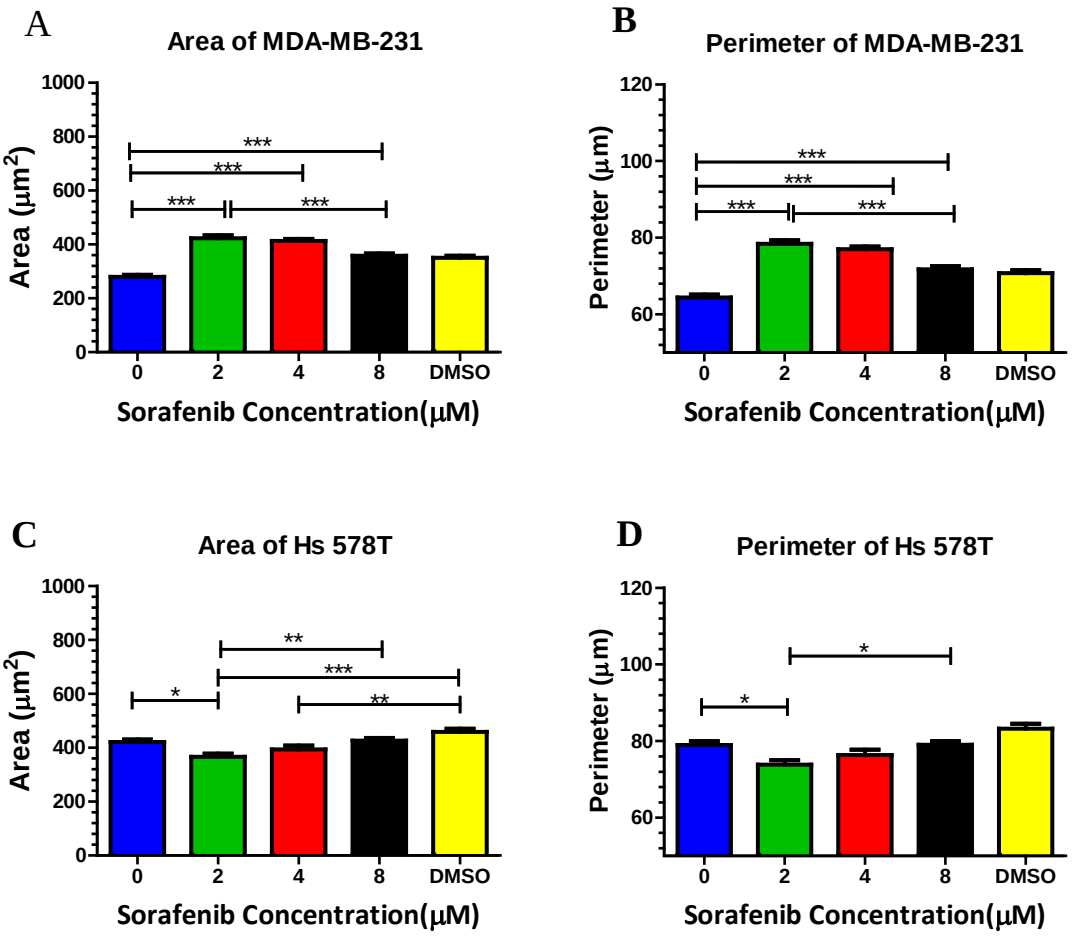

Figure 6.2 The change in nuclear shape and area as a function of sorafenib treatment. Increasing in sorafenib concentration slightly decreases 231s' **(A)** nuclear area and **(B)** perimeter while slightly increasing Hs-578Ts' **(C)** nuclear area and **(D)** perimeter.

6.4 References

[1] M. Karin, F.R. Greten. NF-kappaB: linking inflammation and immunity to cancer development and progression. Nat. Rev. Immunol. 2005. 5: 749–759.

[2] C.L. Raison, L. Capuron, A.H. Miller. Cytokines sing the blues: Inflammation and the pathogenesis of depression. Trends Immunol. 2006. 27: 24–31.

[3] L.M. Coussens, Z. Werb. Inflammation and cancer. Nature. 2002. 420: 860–867.

[4] F. Balkwill, A. Mantovani. Inflammation and cancer: Back to Virchow? Lancet. 2001. 357: 539–545.

[5] T.-J. Fan, L.-H. Han, R.-S. Cong, J. Liang. Caspase Family Proteases and Apoptosis. Acta Biochim. Biophys. Sin. (Shanghai). 2005. 37: 719–727.

[6] H. Okada, T.W. Mak. Pathways of apoptotic and non-apoptotic death in tumour cells. Nat. Rev. Cancer. 2004. 4: 592–603.

[7] M.T. Nieman, R.S. Prudoff, K.R. Johnson, M.J. Wheelock. N-Cadherin Promotes Motility in Human Breast Cancer Cells Regardless of their E-Cadherin Expression. J. Cell Biol. 1999. 147: 631–643.

[8] M. Yilmaz, G. Christofori. Mechanisms of motility in metastasizing cells. Mol. Cancer Res. 2010. 8: 629–42.

[9] T.R. Wilson, J. Fridlyand, Y. Yan, E. Penuel, L. Burton, E. Chan, et al. Widespread potential for growth-factor-driven resistance to anticancer kinase inhibitors. Nature. 2012. 487: 505–9.

[10] R. Straussman, T. Morikawa, K. Shee, M. Barzily-Rokni, Z.R. Qian, J. Du, et al. Tumour micro-environment elicits innate resistance to RAF inhibitors through HGF secretion. Nature. 2012. 487: 500–4.

[11] K.H.T. Paraiso, K.S.M. Smalley. Fibroblast-mediated drug resistance in cancer. Biochem. Pharmacol. 2013. 85: 1033–41.

[12] K.J. Pienta, D.S. Coffey. Correlation of Nuclear Morphometry With Progression of Breast Cancer. Cancer. 1991. 68: 2012–2016.

[13] P. Roca-Cusachs, J. Alcaraz, R. Sunyer, J. Samitier, R. Farré, D. Navajas. Micropatterning of single endothelial cell shape reveals a tight coupling between nuclear volume in G1 and proliferation. Biophys. J. 2008. 94: 4984–95.

[14] R.G. Thakar, Q. Cheng, S. Patel, J. Chu, M. Nasir, D. Liepmann, et al. Cell-shape regulation of smooth muscle cell proliferation. Biophys. J. 2009. 96: 3423–32.

[15] J. Swift, I.L. Ivanovska, A. Buxboim, T. Harada, P.C.D.P. Dingal, J. Pinter, et al. Nuclear lamin-A scales with tissue stiffness and enhances matrix-directed differentiation. Science. 2013. 341: 1240104.

BIBLIOGRAPHY

[1] U.S.C.S.W. Group. United States Cancer Statistics: 1999-2011 Incidence and Mortality Web-based Report. Atlanta U.S. Dep. Heal. Hum. Serv. Centers Dis. Control Prev. Natl. Cancer Inst. 2014.

[2] R.L. Siegel, K.D. Miller, A. Jemal. Cancer Statistics, 2015. CA Cancer J Clin. 2015. 65: 5–29.

[3] L. Rahib, B.D. Smith, R. Aizenberg, A.B. Rosenzweig, J.M. Fleshman, L.M. Matrisian. Projecting cancer incidence and deaths to 2030: The unexpected burden of thyroid, liver, and pancreas cancers in the united states. Cancer Res. 2014. 74: 2913–2921.

[4] A.B. Mariotto, K. Robin Yabroff, Y. Shao, E.J. Feuer, M.L. Brown. Projections of the cost of cancer care in the United States: 2010-2020. J. Natl. Cancer Inst. 2011. 103: 117–128.

[5] R. Siegel, C. Desantis, K. Virgo, K. Stein, A. Mariotto, T. Smith, et al. Cancer Treatment and Survivorship Statistics , 2012. CA. Cancer J. Clin. 2012. 62: 220–241.

[6] J. V. Crist, E. a. Grunfeld. Factors reported to influence fear of recurrence in cancer patients: A systematic review. Psychooncology. 2013. 22: 978–986.

[7] S. Simard, B. Thewes, G. Humphris, M. Dixon, C. Hayden, S. Mireskandari, et al. Fear of cancer recurrence in adult cancer survivors: A systematic review of quantitative studies. J. Cancer Surviv. 2013. 7: 300–322.

[8] D. Hanahan, R.A. Weinberg. The Hallmarks of Cancer. Cell. 2000. 100: 57–70.

[9] D. Hanahan, R. a Weinberg. Hallmarks of cancer: the next generation. Cell. 2011. 144: 646–74.

[10] E. Levy-Lahad, E. Friedman. Cancer risks among BRCA1 and BRCA2 mutation carriers. Br. J. Cancer. 2007. 96: 11–15.

[11] C.D. Heinen. Genotype to phenotype: Analyzing the effects of inherited mutations in colorectal cancer families. Mutat. Res. - Fundam. Mol. Mech. Mutagen. 2010. 693: 32–45.

[12] E.R. Fearon, B. Vogelstein. A genetic model for colorectal tumorigenesis. Cell. 1990. 61: 759–767.

[13] K. Kawada, S. Hasegawa, T. Murakami, Y. Itatani, H. Hosogi, M. Sonoshita, et al. Molecular mechanisms of liver metastasis. Int. J. Clin. Oncol. 2011. 16: 464–72.

[14] Z. Kan, B.S. Jaiswal, J. Stinson, V. Janakiraman, D. Bhatt, H.M. Stern, et al. Diverse somatic mutation patterns and pathway alterations in human cancers. Nature. 2010. 466: 869–873.

[15] C. Greenman, P. Stephens, R. Smith, G.L. Dalgliesh, C. Hunter, G. Bignell, et al. Patterns of somatic mutation in human cancer genomes. Nature. 2007. 446: 153–158.

[16] L.M. Coussens, Z. Werb. Inflammation and cancer. Nature. 2002. 420: 860–867.

[17] M.L. Gillison, T. Broutian, R.K.L. Pickard, Z. Tong, W. Xiao, L. Kahle, et al. Prevalence of Oral HPV Infection in the United States, 2009-2010. Yearb. Pediatr. 2013. 2013: 10–12.

[18] M.L. Gillison, X. Castellsagué, A. Chaturvedi, M.T. Goodman, P. Snijders, M. Tommasino, et al. Eurogin Roadmap: Comparative epidemiology of HPV infection and associated cancers of the head and neck and cervix. Int. J. Cancer. 2013. 134: 497–507.

[19] J.R. Carter, Z. Ding, B.R. Rose. HPV infection and cervical disease: A review. Aust. New Zeal. J. Obstet. Gynaecol. 2011. 51: 103–108.

[20] L. Castéra, J. Vergniol, J. Foucher, B. Le Bail, E. Chanteloup, M. Haaser, et al. Prospective comparison of transient elastography, Fibrotest, APRI, and liver biopsy for the assessment of fibrosis in chronic hepatitis C. Gastroenterology. 2005. 128: 343–350.

[21] F. Vizzutti, U. Arena, R.G. Romanelli, L. Rega, M. Foschi, S. Colagrande, et al. Liver stiffness measurement predicts severe portal hypertension in patients with HCV-related cirrhosis. Hepatology. 2007. 45: 1290–7.

[22] S. Lotersztajn, B. Julien, F. Teixeira-Clerc, P. Grenard, A. Mallat. Hepatic fibrosis: molecular mechanisms and drug targets. Annu. Rev. Pharmacol. Toxicol. 2005. 45: 605–28.

[23] C. Cha, R.P. Dematteo. Molecular mechanisms in hepatocellular carcinoma development. Best Pract. Res. Clin. Gastroenterol. 2005. 19: 25–37.

[24] S.I. Grivennikov, F.R. Greten, M. Karin. Immunity, Inflammation, and Cancer. Cell. 2010. 140: 883–899.

[25] F. Balkwill, A. Mantovani. Inflammation and cancer: Back to Virchow? Lancet. 2001. 357: 539–545.

[26] A.Y. Hui, S.L. Friedman. Molecular basis of hepatic fibrosis. Expert Rev. Mol. Med. 2004. 5: 1–23.

[27] J.D. Yang, I. Nakamura, L.R. Roberts. The tumor microenvironment in hepatocellular carcinoma: current status and therapeutic targets. Semin. Cancer Biol. 2011. 21: 35–43.

[28] C. Holohan, S. Van Schaeybroeck, D.B. Longley, P.G. Johnston. Cancer drug resistance: an evolving paradigm. Nat. Rev. Cancer. 2013. 13: 714–26.

[29] M.M. Gottesman. Mechanism of Cancer Drug Resistance. 2002.

[30] J. Zhang, P.L. Yang, N.S. Gray. Targeting cancer with small molecule kinase inhibitors. Nat. Rev. Cancer. 2009. 9: 28–39.

[31] D.L. Shattuck, J.K. Miller, K.L.C. Iii, C. Sweeney. Met Receptor Contributes to Trastuzumab Resistance of Her2-Overexpressing Breast Cancer Cells. 2008. 1471–1478.

[32] L. Liu, J. Greger, H. Shi, Y. Liu, J. Greshock, R. Annan, et al. Novel Mechanism of Lapatinib Resistance in HER2-Positive Breast Tumor Cells : Activation of AXL. 2009. 1363089: 6871–6879.

[33] Z. Ezzoukhry, C. Louandre, E. Trécherel, C. Godin, B. Chauffert, S. Dupont, et al. EGFR activation is a potential determinant of primary resistance of hepatocellular carcinoma cells to sorafenib. Int. J. Cancer. 2012. 131: 2961–9.

[34] K. Chen, H. Chen, W. Tai, W. Feng, C. Hsu, P. Chen, et al. Activation of Phosphatidylinositol 3-Kinase / Akt Signaling Pathway Mediates Acquired Resistance to Sorafenib in Hepatocellular Carcinoma Cells. 2011. 337: 155–161.

[35] J.S. Duncan, M.C. Whittle, K. Nakamura, A.N. Abell, A. a Midland, J.S. Zawistowski, et al. Dynamic reprogramming of the kinome in response to targeted MEK inhibition in triple-negative breast cancer. Cell. 2012. 149: 307–21.

[36] D. Perna, F.A. Karreth, A.G. Rust, P.A. Perez-mancera, M. Rashid. BRAF inhibitor resistance mediated by the AKT pathway in an oncogenic BRAF mouse melanoma model. 2014. 1–10.

[37] M. Guix, A.C. Faber, S.E. Wang, M.G. Olivares, Y. Song, S. Qu, et al. Acquired resistance to EGFR tyrosine kinase inhibitors in cancer cells is mediated by loss of IGF-binding proteins. 2008. 2609–2619.

[38] H. Daub, K. Specht, A. Ullrich. Strategies to overcome resistance to targeted protein kinase inhibitors. Nat. Rev. Drug Discov. 2004. 3: 1001–10.

[39] U. Sartorius, P. Krammer. Upregulation of BCL-2 is involved in the mediation of chemotherapy resistance in human small cell lung cancer cell lines. 2002. 592: 584–592.

[40] D. Decaudin, S. Geley, T. Hirsch, M. Castedo, P. Marchetti, A. Macho, et al. Bcl-2 and Bcl-X L Antagonize the Mitochondrial Dysfunction Preceding Nuclear Apoptosis Induced by Chemotherapeutic Agents Bcl-2 and Bcl-XL Antagonizethe Mitochondrial DysfunctionPrecedingNuclear Apoptosis Induced by Chemotherapeutic Agents1. 1997. 62–67.

[41] W. Qian, J. Salamoun, J. Wang, V. Roginskaya, B. Van Houten, P. Wipf. The combination of thioxodihydroquinazolinones and platinum drugs reverses platinum resistance in tumor cells by inducing mitochondrial apoptosis independent of Bax and Bak. Bioorg. Med. Chem. Lett. 2015. 25: 856–863.

[42] Y. Pommier, O. Sordet, S. Antony, R.L. Hayward, K.W. Kohn. Apoptosis defects and chemotherapy resistance: molecular interaction maps and networks. Oncogene. 2004. 23: 2934–49.

[43] a Singh, J. Settleman. EMT, cancer stem cells and drug resistance: an emerging axis of evil in the war on cancer. Oncogene. 2010. 29: 4741–51.

[44] L. a Hazlehurst, T.H. Landowski, W.S. Dalton. Role of the tumor microenvironment in mediating de novo resistance to drugs and physiological mediators of cell death. Oncogene. 2003. 22: 7396–402.

[45] A.L. Correia, M.J. Bissell. The tumor microenvironment is a dominant force in multidrug resistance. Drug Resist. Updat. 2012. 15: 39–49.

[46] L. Rdnnov-jessen, O.W. Petersen, V.E. Koteliansky, M.J. Bissell. The Origin of the Myofibroblasts in Breast Cancer. 1995. 95: 859–873.

[47] K.H.T. Paraiso, K.S.M. Smalley. Fibroblast-mediated drug resistance in cancer. Biochem. Pharmacol. 2013. 85: 1033–41.

[48] E.S. Radisky, D.C. Radisky. Stromal induction of breast cancer: inflammation and invasion. Rev. Endocr. Metab. Disord. 2007. 8: 279–87.

[49] S. Faouzi, B. Le Bail, V. Neaud, L. Boussarie, J. Saric, P. Bioulac-sage, et al. Myofibroblasts are responsible for collagen synthesis in the stroma of human hepatocellular carcinoma: an in vivo and in vitro study. 1999. 275–284.

[50] M.F. Insana, C. Pellot-Barakat, M. Sridhar, K.K. Lindfors. Viscoelastic imaging of breast tumor microenvironment with ultrasound. J. Mammary Gland Biol. Neoplasia. 2004. 9: 393–404.

[51] A. Samani, J. Zubovits, D. Plewes. Elastic moduli of normal and pathological human breast tissues: an inversion-technique-based investigation of 169 samples. Phys. Med. Biol. 2007. 52: 1565–76.

[52] K.R. Levental, H. Yu, L. Kass, J.N. Lakins, M. Egeblad, J.T. Erler, et al. Matrix crosslinking forces tumor progression by enhancing integrin signaling. Cell. 2009. 139: 891–906.

[53] M.J. Paszek, N. Zahir, K.R. Johnson, J.N. Lakins, G.I. Rozenberg, A. Gefen, et al. Tensional homeostasis and the malignant phenotype. Cancer Cell. 2005. 8: 241–54.

[54] M. Egeblad, M.G. Rasch, V.M. Weaver. Dynamic interplay between the collagen scaffold and tumor evolution. Curr. Opin. Cell Biol. 2010. 22: 697–706.

[55] J. Condeelis, J.W. Pollard. Macrophages: obligate partners for tumor cell migration, invasion, and metastasis. Cell. 2006. 124: 263–6.

[56] A. Haage, I.C. Schneider. Cellular contractility and extracellular matrix stiffness regulate matrix metalloproteinase activity in pancreatic cancer cells. FASEB J. 2014. 1–11.

[57] S. Kumar, V.M. Weaver. Mechanics, malignancy, and metastasis: the force journey of a tumor cell. Cancer Metastasis Rev. 2009. 28: 113–27.

[58] J.-H. Kim, A.R. Asthagiri. Matrix stiffening sensitizes epithelial cells to EGF and enables the loss of contact inhibition of proliferation. J. Cell Sci. 2011. 124: 1280–7.

[59] P.A. Netti, D.A. Berk, M.A. Swartz, A.J. Grodzinsky, R.K. Jain. Role of Extracellular Matrix Assembly in Interstitial Transport in Solid Tumors Role of Extracellular Matrix Assembly in Interstitial Transport in Solid Tumors 1. 2000. 2497–2503.

[60] J.D. Humphries, A. Byron, M.J. Humphries. Integrin ligands at a glance. J. Cell Sci. 2006. 119: 3901–3.

[61] R.O. Hynes. Integrins : Bidirectional , Allosteric Signaling Machines In their roles as major adhesion receptors , integrins. 2002. 110: 673–687.

[62] a. E. Berman, N.I. Kozlova, G.E. Morozevich. Integrins as a potential target for targeted anticancer therapy. Biochem. Suppl. Ser. B Biomed. Chem. 2012. 6: 205–210.

[63] X.H. Yang, L.M. Flores, Q. Li, P. Zhou, F. Xu, I.E. Krop, et al. Disruption of laminin-integrin-CD151-focal adhesion kinase axis sensitizes breast cancer cells to ErbB2 antagonists. Cancer Res. 2010. 70: 2256–63.

[64] F. Aoudjit, K. Vuori. Integrin signaling inhibits paclitaxel-induced apoptosis in breast cancer cells. Oncogene. 2001. 20: 4995–5004.

[65] N. Cordes, C.C. Park. Beta1 Integrin As a Molecular Therapeutic Target. Int. J. Radiat. Biol. 2007. 83: 753–60.

[66] C.C. Park, H. Zhang, M. Pallavicini, J.W. Gray, F. Baehner, C.J. Park, et al. Beta1 integrin inhibitory antibody induces apoptosis of breast cancer cells, inhibits growth, and distinguishes malignant from normal phenotype in three dimensional cultures and in vivo. Cancer Res. 2006. 66: 1526–35.

[67] E.S. Yao, H. Zhang, Y.-Y. Chen, B. Lee, K. Chew, D. Moore, et al. Increased beta1 integrin is associated with decreased survival in invasive breast cancer. Cancer Res. 2007. 67: 659–64.

[68] P.B. dos Santos, J.S. Zanetti, A. Ribeiro-Silva, E.I.C. Beltrão. Beta 1 integrin predicts survival in breast cancer: a clinicopathological and immunohistochemical study. Diagn. Pathol. 2012. 7: 104.

[69] S. Liu, J. Wang, W. Niu, E. Liu, J. Wang, C. Peng, et al. The β6-integrin-ERK/MAP kinase pathway contributes to chemo resistance in colon cancer. Cancer Lett. 2013. 328: 325–34.

[70] H. Yu, J.K. Mouw, V.M. Weaver. Forcing form and function: biomechanical regulation of tumor evolution. Trends Cell Biol. 2011. 21: 47–56.

[71] T. Geiger, R. Zaidel-Bar. Opening the floodgates: proteomics and the integrin adhesome. Curr. Opin. Cell Biol. 2012. 24: 562–8.

[72] a. Hall. Rho GTPases and the Actin Cytoskeleton. Science (80-.). 1998. 279: 509–514.

[73] N. a Hotchin, a Hall. The assembly of integrin adhesion complexes requires both extracellular matrix and intracellular rho/rac GTPases. J. Cell Biol. 1995. 131: 1857–65.

[74] C.T. Mierke. The role of focal adhesion kinase in the regulation of cellular mechanical properties. Phys. Biol. 2013. 10: 065005.

[75] R.K. Jain, J.D. Martin, T. Stylianopoulos. The role of mechanical forces in tumor growth and therapy. Annu. Rev. Biomed. Eng. 2014. 16: 321–46.

[76] W.R. Wilson, M.P. Hay. Targeting hypoxia in cancer therapy. Nat. Rev. Cancer. 2011. 11: 393–410.

[77] P. Carmeliet, R.K. Jain. Molecular mechanisms and clinical applications of angiogenesis. Nature. 2011. 473: 298–307.

[78] L. a Liotta, E.C. Kohn. The microenvironment of the tumour-host interface. Nature. 2001. 411: 375–9.

[79] T.L. Whiteside. The tumor microenvironment and its role in promoting tumor growth. Oncogene. 2008. 27: 5904–12.

[80] K. Pietras, A. Ostman. Hallmarks of cancer: interactions with the tumor stroma. Exp. Cell Res. 2010. 316: 1324–31.

[81] T.R. Wilson, J. Fridlyand, Y. Yan, E. Penuel, L. Burton, E. Chan, et al. Widespread potential for growth-factor-driven resistance to anticancer kinase inhibitors. Nature. 2012. 487: 505–9.

[82] R. Straussman, T. Morikawa, K. Shee, M. Barzily-Rokni, Z.R. Qian, J. Du, et al. Tumour micro-environment elicits innate resistance to RAF inhibitors through HGF secretion. Nature. 2012. 487: 500–4.

[83] N.E. Bhola, J.M. Balko, T.C. Dugger, M.G. Kuba, V. Sánchez, M. Sanders, et al. TGF- β inhibition enhances chemotherapy action against triple-negative breast cancer. 2013. 123.:

[84] Y. Sun, J. Campisi, C. Higano, T.M. Beer, P. Porter, I. Coleman, et al. Treatment-induced damage to the tumor microenvironment promotes prostate cancer therapy resistance through WNT16B. Nat. Med. 2012. 18: 1359–68.

[85] M.J. Duffy, T.M. Maguire, A. Hill, E. Mcdermott, N.O. Higgins, S. Vincent. Metalloproteinases : role in breast carcinogenesis , invasion and metastasis. 2000.

[86] A. Köhrmann, U. Kammerer, M. Kapp, J. Dietl, J. Anacker. Expression of matrix metalloproteinases (MMPs) in primary human breast cancer and breast cancer cell lines: New findings and review of the literature. BMC Cancer. 2009. 9: 188.

[87] W. Lin, M. Karin. A cytokine-mediated link between innate immunity , inflammation , and cancer. J. Clin. Investig. 2007. 117: 1175–1183.

[88] G. Dranoff. Cytokines in cancer pathogenesis and cancer therapy. Nat. Rev. Cancer. 2004. 4: 11–22.

[89] S.-H. Park, J.-H. Kim, D.-H. Lee, J.-W. Kang, H.-H. Song, S.-R. Oh, et al. Luteolin 8-C-β-fucopyranoside inhibits invasion and suppresses TPA-induced MMP-9 and IL-8 via ERK/AP-1 and ERK/NF-κB signaling in MCF-7 breast cancer cells. Biochimie. 2013. 95: 2082–2090.

[90] K. Wu, S. Katiyar, A. Li, M. Liu, X. Ju, V.M. Popov, et al. Dachshund inhibits oncogene-induced breast cancer cellular migration and invasion through suppression of interleukin-8. Proc. Natl. Acad. Sci. U. S. A. 2008. 105: 6924–6929.

[91] S. Desai, S. Laskar, B.N. Pandey. Autocrine IL-8 and VEGF mediate epithelial-mesenchymal transition and invasiveness via p38/JNK-ATF-2 signalling in A549 lung cancer cells. Cell. Signal. 2013. 25: 1780–91.

[92] M. Todaro, M.P. Alea, A. Scopelliti, J.P. Medema, G. Stassi. IL-4-mediated drug resistance in colon cancer stem cells. Cell Cycle. 2008. 7: 309–313.

[93] V. Levina, A.M. Marrangoni, R. DeMarco, E. Gorelik, A.E. Lokshin. Drug-selected human lung cancer stem cells: Cytokine network, tumorigenic and metastatic properties. PLoS One. 2008. 3.:

[94] W.N. Hait. Anticancer drug development: the grand challenges. Nat. Rev. Drug Discov. 2010. 9: 253–254.

[95] M. Dickson, J.P. Gagnon. Key factors in the rising cost of new drug discovery and development. Nat. Rev. Drug Discov. 2004. 3: 417–29.

[96] a S. Hoffman. Hydrogels for biomedical applications. Ann. N. Y. Acad. Sci. 2001. 944: 62–73.

[97] A.J. Engler, S. Sen, H.L. Sweeney, D.E. Discher. Matrix elasticity directs stem cell lineage specification. Cell. 2006. 126: 677–89.

[98] T.P. Kraehenbuehl, P. Zammaretti, A.J. Van der Vlies, R.G. Schoenmakers, M.P. Lutolf, M.E. Jaconi, et al. Three-dimensional extracellular matrix-directed cardioprogenitor differentiation: systematic modulation of a synthetic cell-responsive PEG-hydrogel. Biomaterials. 2008. 29: 2757–66.

[99] H.-D. Kim, S.R. Peyton. Bio-inspired materials for parsing matrix physicochemical control of cell migration: a review. Integr. Biol. (Camb). 2012. 4: 37–52.

[100] S.R. Peyton, A.J. Putnam. Extracellular matrix rigidity governs smooth muscle cell motility in a biphasic fashion. J. Cell. Physiol. 2005. 204: 198–209.

[101] W.G. Herrick, S. Rattan, T. V. Nguyen, M.S. Grunwald, C.W. Barney, A.J. Crosby, et al. Smooth Muscle Stiffness Sensitivity is Driven by Soluble and Insoluble ECM Chemistry. Cell. Mol. Bioeng. 2015.

[102] G. Maheshwari, G. Brown, D. a Lauffenburger, a Wells, L.G. Griffith. Cell adhesion and motility depend on nanoscale RGD clustering. J. Cell Sci. 2000. 113 (Pt 1: 1677–86.

[103] S.R. Peyton, C.B. Raub, V.P. Keschrumrus, A.J. Putnam. The use of poly(ethylene glycol) hydrogels to investigate the impact of ECM chemistry and mechanics on smooth muscle cells. Biomaterials. 2006. 27: 4881–93.

[104] J.E. Leslie-Barbick, J.J. Moon, J.L. West. Covalently-immobilized vascular endothelial growth factor promotes endothelial cell tubulogenesis in poly(ethylene glycol) diacrylate hydrogels. J. Biomater. Sci. Polym. Ed. 2009. 20: 1763–79.

[105] C.M. Kraning-Rush, S.P. Carey, M.C. Lampi, C. a Reinhart-King. Microfabricated collagen tracks facilitate single cell metastatic invasion in 3D. Integr. Biol. (Camb). 2013. 5: 606–16.

[106] D. Loessner, K.S. Stok, M.P. Lutolf, D.W. Hutmacher, J. a Clements, S.C. Rizzi. Bioengineered 3D platform to explore cell-ECM interactions and drug resistance of epithelial ovarian cancer cells. Biomaterials. 2010. 31: 8494–506.

[107] E.Y. Tokuda, J.L. Leight, K.S. Anseth. Modulation of matrix elasticity with PEG hydrogels to study melanoma drug responsiveness. Biomaterials. 2014. 35: 4310–4318.

[108] N. a. Peppas, J.Z. Hilt, a. Khademhosseini, R. Langer. Hydrogels in Biology and Medicine: From Molecular Principles to Bionanotechnology. Adv. Mater. 2006. 18: 1345–1360.

[109] S.R. Khetani, S.N. Bhatia. Engineering tissues for in vitro applications. Curr. Opin. Biotechnol. 2006. 17: 524–31.

[110] B. Ananthanarayanan, Y. Kim, S. Kumar. Elucidating the mechanobiology of malignant brain tumors using a brain matrix-mimetic hyaluronic acid hydrogel platform. Biomaterials. 2011. 32: 7913–23.

[111] J. Patterson, M.M. Martino, J. a. Hubbell. Biomimetic materials in tissue engineering. Mater. Today. 2010. 13: 14–22.

[112] J.F. Lutz, Z. Zarafshani. Efficient construction of therapeutics, bioconjugates, biomaterials and bioactive surfaces using azide-alkyne “click” chemistry. Adv. Drug Deliv. Rev. 2008. 60: 958–970.

[113] G.H. Underhill, P. Galie, C.S. Chen, S.N. Bhatia. Bioengineering methods for analysis of cells in vitro. Annu. Rev. Cell Dev. Biol. 2012. 28: 385–410.

[114] L.G. Griffith. Emerging design principles in biomaterials and scaffolds for tissue engineering. Ann. N. Y. Acad. Sci. 2002. 961: 83–95.

[115] C. Wang, X. Tong, F. Yang. Bioengineered 3D Brain Tumor Model To Elucidate the Effects of Matrix Stiffness on Glioblastoma Cell Behavior Using PEG-Based Hydrogels. 2014.

[116] J.L. Leight, E.Y. Tokuda, C.E. Jones, A.J. Lin, K.S. Anseth. Multifunctional bioscaffolds for 3D culture of melanoma cells reveal increased MMP activity and migration with BRAF kinase inhibition. Proc. Natl. Acad. Sci. 2015. 112: 201505662.

[117] A.N. Stachowiak, D.J. Irvine. Inverse opal hydrogel-collagen composite scaffolds as a supportive microenvironment for immune cell migration. J. Biomed. Mater. Res. A. 2008. 85: 815–28.

[118] C.S. Ki, T.-Y. Lin, M. Korc, C.-C. Lin. Thiol-ene hydrogels as desmoplasia-mimetic matrices for modeling pancreatic cancer cell growth, invasion, and drug resistance. Biomaterials. 2014. 35: 9668–77.

[119] S.C. Rizzi, J. a Hubbell. Recombinant protein-co-PEG networks as cell-adhesive and proteolytically degradable hydrogel matrixes. Part I: Development and physicochemical characteristics. Biomacromolecules. 2005. 6: 1226–38.

[120] J.S. Temenoff, K.A. Athanasiou, R.G. Lebaron, A.G. Mikos. Effect of poly (ethylene glycol) molecular weight on tensile and swelling properties of oligo (poly (ethylene glycol) fumarate) hydrogels for cartilage tissue engineering. 2001.

[121] S.P. Zustiak, J.B. Leach. Hydrolytically degradable poly(ethylene glycol) hydrogel scaffolds with tunable degradation and mechanical properties. Biomacromolecules. 2010. 11: 1348–57.

[122] A.T. Metters, K.S. Anseth, C.N. Bowman. Fundamental studies of a novel , biodegradable PEG- b -PLA hydrogel. 2000. 41: 3993–4004.

[123] G.P. Raeber, M.P. Lutolf, J. a Hubbell. Molecularly engineered PEG hydrogels: a novel model system for proteolytically mediated cell migration. Biophys. J. 2005. 89: 1374–88.

[124] Y. Iwasaki, K. Ishihara. Phosphorylcholine-containing polymers for biomedical applications. Anal. Bioanal. Chem. 2005. 381: 534–46.

[125] K. Ishihara, H. Nomura, T. Mihara, K. Kurita, Y. Iwasaki, N. Nakabayashi. Why do phospholipid polymers reduce protein adsorption? J. Biomed. Mater. Res. 1998. 39: 323–30.

[126] T. Goda, J. Watanabe, M. Takai, K. Ishihara. Water structure and improved mechanical properties of phospholipid polymer hydrogel with phosphorylcholine centered intermolecular cross-linker. Polymer (Guildf). 2006. 47: 1390–1396.

[127] W.G. Herrick, T. V Nguyen, M. Sleiman, S. McRae, T.S. Emrick, S.R. Peyton. PEG-phosphorylcholine hydrogels as tunable and versatile platforms for mechanobiology. Biomacromolecules. 2013. 14: 2294–304.

[128] S. McRae Page, S. Parelkar, A. Gerasimenko, D.Y. Shin, S.R. Peyton, T. Emrick. Promoting cell adhesion on slippery phosphorylcholine hydrogel surfaces. J. Mater. Chem. B. 2014. 2: 620.

[129] Y. Chang, Y.J. Shih, R.C. Ruaan, A. Higuchi, W.Y. Chen, J.Y. Lai. Preparation of poly(vinylidene fluoride) microfiltration membrane with uniform surface-copolymerized poly(ethylene glycol) methacrylate and improvement of blood compatibility. J. Memb. Sci. 2008. 309: 165–174.

[130] R. Masuzaki, R. Tateishi, H. Yoshida, T. Sato, T. Ohki, T. Goto, et al. Assessing liver tumor stiffness by transient elastography. Hepatol. Int. 2007. 1: 394–7.

[131] N. Ganne-Carrié, M. Ziol, V. de Ledinghen, C. Douvin, P. Marcellin, L. Castera, et al. Accuracy of liver stiffness measurement for the diagnosis of cirrhosis in patients with chronic liver diseases. Hepatology. 2006. 44: 1511–7.

[132] J.M. Chang, I.A. Park, S.H. Lee, W.H. Kim, M.S. Bae, H.R. Koo, et al. Stiffness of tumours measured by shear-wave elastography correlated with subtypes of breast cancer. Eur. Radiol. 2013. 23: 2450–8.

[133] I. Levental, P.C. Georges, P. a. Janmey. Soft biological materials and their impact on cell function. Soft Matter. 2007. 3: 299.

[134] S.R. Peyton, Z.I. Kalcioglu, J.C. Cohen, A.P. Runkle, K.J. Van Vliet, D. a Lauffenburger, et al. Marrow-derived stem cell motility in 3D synthetic scaffold is governed by geometry along with adhesivity and stiffness. Biotechnol. Bioeng. 2011. 108: 1181–93.

[135] Y. Kim, S. Kumar. CD44-mediated Adhesion to Hyaluronic Acid Contributes to Mechanosensing and Invasive Motility. Mol. Cancer Res. 2014.

[136] S. Khetan, M. Guvendiren, W.R. Legant, D.M. Cohen, C.S. Chen, J. a Burdick. Degradation-mediated cellular traction directs stem cell fate in covalently crosslinked three-dimensional hydrogels. Nat. Mater. 2013. 12: 458–65.

[137] C. Frantz, K.M. Stewart, V.M. Weaver. The extracellular matrix at a glance. J. Cell Sci. 2010. 123: 4195–200.

[138] M. a Glukhova, C.H. Streuli. How integrins control breast biology. Curr. Opin. Cell Biol. 2013. 25: 633–41.

[139] P. Lu, V.M. Weaver, Z. Werb. The extracellular matrix: a dynamic niche in cancer progression. J. Cell Biol. 2012. 196: 395–406.

[140] M.E. Blaauboer, F.R. Boeijen, C.L. Emson, S.M. Turner, B. Zandieh-Doulabi, R. Hanemaaijer, et al. Extracellular matrix proteins: A positive feedback loop in lung fibrosis? Matrix Biol. 2013.

[141] C.H. Kwon, I. Wheeldon, N.N. Kachouie, S.H. Lee, H. Bae, S. Sant, et al. Drug-Eluting Microarrays for Cell-Based Screening of Chemical-Induced Apoptosis. Anal. Chem. 2011.

[142] A. Skardal, L. Smith, S. Bharadwaj, A. Atala, S. Soker, Y. Zhang. Tissue specific synthetic ECM hydrogels for 3-D in vitro maintenance of hepatocyte function. Biomaterials. 2012. 33: 4565–75.

[143] D.M. Timm, J. Chen, D. Sing, J. a Gage, W.L. Haisler, S.K. Neeley, et al. A high-throughput three-dimensional cell migration assay for toxicity screening with mobile device-based macroscopic image analysis. Sci. Rep. 2013. 3: 3000.

[144] T.-J. Fan, L.-H. Han, R.-S. Cong, J. Liang. Caspase Family Proteases and Apoptosis. Acta Biochim. Biophys. Sin. (Shanghai). 2005. 37: 719–727.

[145] S.B. Nicholls, J. Chu, G. Abbruzzese, K.D. Tremblay, J. a Hardy. Mechanism of a genetically encoded dark-to-bright reporter for caspase activity. J. Biol. Chem. 2011. 286: 24977–86.

[146] L. Liu, Y. Cao, C. Chen, X. Zhang, A. McNabola, D. Wilkie, et al. Sorafenib blocks the RAF/MEK/ERK pathway, inhibits tumor angiogenesis, and induces tumor cell apoptosis in hepatocellular carcinoma model PLC/PRF/5. Cancer Res. 2006. 66: 11851–8.

[147] S. Gendron, J. Couture, F. Aoudjit. Integrin α2β1 inhibits Fas-mediated apoptosis in T lymphocytes by protein phosphatase 2A-dependent activation of the MAPK/ERK pathway. J. Biol. Chem. 2003. 278: 48633–48643.

[148] A. Taherian, X. Li, Y. Liu, T. a Haas. Differences in integrin expression and signaling within human breast cancer cells. BMC Cancer. 2011. 11: 293.

[149] D.J. Panka. The Raf Inhibitor BAY 43-9006 (Sorafenib) Induces Caspase-Independent Apoptosis in Melanoma Cells. Cancer Res. 2006. 66: 1611–1619.

[150] S. Zustiak, R. Nossal, D.L. Sackett. Multiwell stiffness assay for the study of cell responsiveness to cytotoxic drugss. Biotechnol. Bioeng. 2013. 9999: 1–8.

[151] J.D. Mih, A.S. Sharif, F. Liu, A. Marinkovic, M.M. Symer, D.J. Tschumperlin. A multiwell platform for studying stiffness-dependent cell biology. PLoS One. 2011. 6: e19929.

[152] A. Khademhosseini, R. Langer, J. Borenstein, J.P. Vacanti. Microscale technologies for tissue engineering and biology. Proc. Natl. Acad. Sci. U. S. A. 2006. 103: 2480–7.

[153] J.Y. Fang, S.-J. Tan, Z. Yang, C. Tayag, B. Han. Tumor bioengineering using a transglutaminase crosslinked hydrogel. PLoS One. 2014. 9: e105616.

[154] J. Friedrich, C. Seidel, R. Ebner, L. a Kunz-Schughart. Spheroid-based drug screen: considerations and practical approach. Nat. Protoc. 2009. 4: 309–24.

[155] S. Chandrasekaran, J.R. Marshall, J. a Messing, J.-W. Hsu, M.R. King. TRAIL-mediated apoptosis in breast cancer cells cultured as 3D spheroids. PLoS One. 2014. 9: e111487.

[156] S. Pece, J.S. Gutkind. Signaling from E-cadherins to the MAPK pathway by the recruitment and activation of epidermal growth factor receptors upon cell-cell contact formation. J. Biol. Chem. 2000. 275: 41227–33.

[157] M. Conacci-sorrell, J. Zhurinsky, A. Ben-ze. The cadherin-catenin adhesion system in signaling and cancer. 2002. 109: 987–991.

[158] M. Yilmaz, G. Christofori. Mechanisms of motility in metastasizing cells. Mol. Cancer Res. 2010. 8: 629–42.

[159] H.-G. Kang, J.M. Jenabi, J. Zhang, N. Keshelava, H. Shimada, W. a May, et al. E-cadherin cell-cell adhesion in ewing tumor cells mediates suppression of anoikis through activation of the ErbB4 tyrosine kinase. Cancer Res. 2007. 67: 3094–105.

[160] F. Hirschhaeuser, H. Menne, C. Dittfeld, J. West, W. Mueller-Klieser, L. a Kunz-Schughart. Multicellular tumor spheroids: an underestimated tool is catching up again. J. Biotechnol. 2010. 148: 3–15.

[161] T. V. Nguyen, M. Sleiman, T. Moriarty, W.G. Herrick, S.R. Peyton. Sorafenib resistance and JNK signaling in carcinoma during extracellular matrix stiffening. Biomaterials. 2014. 35: 5749–59.

[162] E. a Phelps, N.O. Enemchukwu, V.F. Fiore, J.C. Sy, N. Murthy, T. a Sulchek, et al. Maleimide cross-linked bioactive PEG hydrogel exhibits improved reaction kinetics and cross-linking for cell encapsulation and in situ delivery. Adv. Mater. 2012. 24: 64–70, 2.

[163] O. Trédan, C.M. Galmarini, K. Patel, I.F. Tannock. Drug resistance and the solid tumor microenvironment. J. Natl. Cancer Inst. 2007. 99: 1441–54.

[164] J.M. Brown, A.J. Giaccia. The Unique Physiology of Solid Tumors : Opportunities (and Problems) for Cancer Therapy The Unique Physiology of Solid Tumors : Opportunities (and Problems) for Cancer Therapy1. 1998. 1408–1416.

[165] V. Umesh, A.D. Rape, T. a Ulrich, S. Kumar. Microenvironmental stiffness enhances glioma cell proliferation by stimulating epidermal growth factor receptor signaling. PLoS One. 2014. 9: e101771.

[166] J.D. Mih, A. Marinkovic, F. Liu, A.S. Sharif, D.J. Tschumperlin. Matrix stiffness reverses the effect of actomyosin tension on cell proliferation. J. Cell Sci. 2012. 125: 5974–83.

[167] Y. Liang, J. Jeong, R.J. DeVolder, C. Cha, F. Wang, Y.W. Tong, et al. A cell-instructive hydrogel to regulate malignancy of 3D tumor spheroids with matrix rigidity. Biomaterials. 2011. 32: 9308–15.

[168] C.R. Thoma, M. Zimmermann, I. Agarkova, J.M. Kelm, W. Krek. 3D cell culture systems modeling tumor growth determinants in cancer target discovery. Adv. Drug Deliv. Rev. 2014. 69-70: 29–41.

[169] E.L.S. Fong, S.-E. Lamhamedi-Cherradi, E. Burdett, V. Ramamoorthy, A.J. Lazar, F.K. Kasper, et al. Modeling Ewing sarcoma tumors in vitro with 3D scaffolds. Proc. Natl. Acad. Sci. U. S. A. 2013. 110: 6500–5.

[170] B. Desoize, J. Jardillier. Multicellular resistance: a paradigm for clinical resistance? Crit. Rev. Oncol. Hematol. 2000. 36: 193–207.

[171] a Skladanowski, S.Y. Plisov, J. Konopa, a K. Larsen. Inhibition of DNA topoisomerase II by imidazoacridinones, new antineoplastic agents with strong activity against solid tumors. Mol. Pharmacol. 1996. 49: 772–780.

[172] C.B. Khatiwala, P.D. Kim, S.R. Peyton, A.J. Putnam. Signaling Downstream of RhoA and ROCK. J. Bone Miner. Res. 2009. 24: 886–898.

[173] P.P. Provenzano, D.R. Inman, K.W. Eliceiri, P.J. Keely. Matrix density-induced mechanoregulation of breast cell phenotype, signaling and gene expression through a FAK-ERK linkage. Oncogene. 2009. 28: 4326–4343.

[174] M.A. Arslan, O. Kutuk, H. Basaga. Protein kinases as drug targets in cancer. Curr. Cancer Drug Targets. 2006. 6: 623–34.

[175] A.T. Baker, A. Zlobin, C. Osipo. Notch-EGFR/HER2 Bidirectional Crosstalk in Breast Cancer. Front. Oncol. 2014. 4: 360.

[176] J.T. Price, T. Tiganis, A. Agarwal, D. Djakiew, E.W. Thompson. Epidermal Growth Factor Promotes MDA-MB-231 Breast Cancer Cell Migration through a Phosphatidylinositol 3*-Kinase and Phospholipase C-dependent Mechanism. Cancer Res. 1999. 59: 5475–5478.

[177] S.M. Wilhelm, C. Carter, L. Tang, D. Wilkie, A. Mcnabola, H. Rong, et al. BAY 43-9006 Exhibits Broad Spectrum Oral Antitumor Activity and Targets the RAF / MEK / ERK Pathway and Receptor Tyrosine Kinases Involved in Tumor Progression and Angiogenesis BAY 43-9006 Exhibits Broad Spectrum Oral Antitumor Activity and Targets the Pr. 2004.

[178] M. Niepel, M. Hafner, E.A. Pace, M. Chung, D.H. Chai, L. Zhou, et al. Profiles of Basal and Stimulated Receptor Signaling Networks Predict Drug Response in Breast Cancer Lines. 2013. 6: 1–12.

[179] B. Weigelt, A.T. Lo, C.C. Park, J.W. Gray, M.J. Bissell. HER2 signaling pathway activation and response of breast cancer cells to HER2-targeting agents is dependent strongly on the 3D microenvironment. Breast Cancer Res. Treat. 2010. 122: 35–43.

[180] V. Serra, M. Scaltriti, L. Prudkin, P.J. a Eichhorn, Y.H. Ibrahim, S. Chandarlapaty, et al. PI3K inhibition results in enhanced HER signaling and acquired ERK dependency in HER2-overexpressing breast cancer. Oncogene. 2011. 30: 2547–2557.

[181] B. Corkery, J. Crown, M. Clynes, N. O'Donovan. Epidermal growth factor receptor as a potential therapeutic target in triple-negative breast cancer. Ann. Oncol. 2009. 20: 862–867.

[182] C. Knuefermann, Y. Lu, B. Liu, W. Jin, K. Liang, L. Wu, et al. HER2/PI-3K/Akt activation leads to a multidrug resistance in human breast adenocarcinoma cells. Oncogene. 2003. 22: 3205–12.

[183] A.C. Luca, S. Mersch, R. Deenen, S. Schmidt, I. Messner, K.L. Schäfer, et al. Impact of the 3D Microenvironment on Phenotype, Gene Expression, and EGFR Inhibition of Colorectal Cancer Cell Lines. PLoS One. 2013. 8.:

[184] C. Gutierrez, R. Schiff. HER2: biology, detection, and clinical implications. Arch. Pathol. Lab. Med. 2011. 135: 55–62.

[185] T. Holbro, R.R. Beerli, F. Maurer, M. Koziczak, C.F.B. Iii, N.E. Hynes. The ErbB2 ¯ErbB3 heterodimer functions as an oncogenic unit : ErbB2 requires ErbB3 to drive breast tumor cell proliferation. 2003. 100.:

[186] J.M. Kelm, N.E. Timmins, C.J. Brown, M. Fussenegger, L.K. Nielsen. Method for generation of homogeneous multicellular tumor spheroids applicable to a wide variety of cell types. Biotechnol. Bioeng. 2003. 83: 173–80.

[187] G. Brockhoff, P. Heiss, J. Schlegel, F. Hofstaedter, R. Knuechel. Epidermal growth factor receptor, c-erbB2 and c-erbB3 receptor interaction, and related cell cycle kinetics of SK-BR-3 and BT474 breast carcinoma cells. Cytometry. 2001. 44: 338–348.

[188] G. Cheng, J. Tse, R.K. Jain, L.L. Munn. Micro-environmental mechanical stress controls tumor spheroid size and morphology by suppressing proliferation and inducing apoptosis in cancer cells. PLoS One. 2009. 4: e4632.

[189] G. Helmlinger, P. a. Netti, H. c. Lichtenbeld, R. j. Melder, R. k. Jain. Solid stress inhibits the growth of multicellular tumor spheroids. Nat. Biotechnol. 1997.

[190] D. Loessner, J. a Flegg, H.M. Byrne, J. a Clements, D.W. Hutmacher. Growth of confined cancer spheroids: a combined experimental and mathematical modelling approach. Integr. Biol. (Camb). 2013. 5: 597–605.

[191] A.M. Jegg, T.M. Ward, E. Iorns, N. Hoe, J. Zhou, X. Liu, et al. PI3K independent activation of mTORC1 as a target in lapatinib-resistant ERBB2+ breast cancer cells. Breast Cancer Res. Treat. 2012. 136: 683–692.

[192] P. Singh, J. Marin, F. Bast. Insulin receptor (IR) and insulin-like growth factor receptor 1 (IGF-1R) signaling systems : novel treatment strategies for cancer. 2014. 1.:

[193] F. Ciardiello, G. Tortora. EGFR antagonists in cancer treatment. N. Engl. J. Med. 2008. 358: 1160–74.

[194] E. a Almeida, D. Ilić, Q. Han, C.R. Hauck, F. Jin, H. Kawakatsu, et al. Matrix survival signaling: from fibronectin via focal adhesion kinase to c-Jun NH(2)-terminal kinase. J. Cell Biol. 2000. 149: 741–54.

[195] A. Minden, A. Lin, M. McMahon, C. Lange-Carter, B. Dérijard, R.J. Davis, et al. Differential activation of ERK and JNK mitogen-activated protein kinases by Raf-1 and MEKK. Science. 1994. 266: 1719–23.

[196] M. Karin, F.R. Greten. NF-kappaB: linking inflammation and immunity to cancer development and progression. Nat. Rev. Immunol. 2005. 5: 749–759.

[197] C.L. Raison, L. Capuron, A.H. Miller. Cytokines sing the blues: Inflammation and the pathogenesis of depression. Trends Immunol. 2006. 27: 24–31.

[198] H. Okada, T.W. Mak. Pathways of apoptotic and non-apoptotic death in tumour cells. Nat. Rev. Cancer. 2004. 4: 592–603.

[199] M.T. Nieman, R.S. Prudoff, K.R. Johnson, M.J. Wheelock. N-Cadherin Promotes Motility in Human Breast Cancer Cells Regardless of their E-Cadherin Expression. J. Cell Biol. 1999. 147: 631–643.

[200] K.J. Pienta, D.S. Coffey. Correlation of Nuclear Morphometry With Progression of Breast Cancer. Cancer. 1991. 68: 2012–2016.

[201] P. Roca-Cusachs, J. Alcaraz, R. Sunyer, J. Samitier, R. Farré, D. Navajas. Micropatterning of single endothelial cell shape reveals a tight coupling between nuclear volume in G1 and proliferation. Biophys. J. 2008. 94: 4984–95.

[202] R.G. Thakar, Q. Cheng, S. Patel, J. Chu, M. Nasir, D. Liepmann, et al. Cell-shape regulation of smooth muscle cell proliferation. Biophys. J. 2009. 96: 3423–32.

[203] J. Swift, I.L. Ivanovska, A. Buxboim, T. Harada, P.C.D.P. Dingal, J. Pinter, et al. Nuclear lamin-A scales with tissue stiffness and enhances matrix-directed differentiation. Science. 2013. 341: 1240104.